THESE

Présentée par:

Alfonso GARCIA MARQUEZ

Pour obtenir le titre de

DOCTEUR DE L'UNIVERSITE DE STRASBOURG

Domaine: **Chimie Organique Moléculaire et Chimie des Matériaux**

SYNTHESE ET CARACTERISATION D'ELASTOMERES ET DE RESEAUX FONCTIONNELS

Soutenue le 28 avril de 2009 devant la commission d'examen:

Pr. Gero DECHER	Rapporteur interne
Pr. André-Jean ATTIAS	Rapporteur externe
Pr. Heino FINKELMANN	Rapporteur externe
Dr. Daniel GUILLON	Directeur de thèse
Dr. Bertrand DONNIO	Co-encadrant

Remerciements

Cette thèse a été le fruit de trois ans et demie de recherche en collaboration avec plusieurs laboratoires et je tiens à remercier toutes les personnes qui ont contribué, de près ou de loin, à sa réalisation.

Je voudrais d'abord remercier Prof. Gero Decher, Prof. Heino Finkelmann et Prof. André-Jean Attias pour avoir accepté d'évaluer ce manuscrit et de faire partie du jury.

Je tiens particulièrement à remercier Dr. Daniel Guillon de m'avoir offert ce sujet de thèse et de suivre de très près l'avance ce cette recherche et de son soutien inconditionnel lors de ces 3 ans. Merci de cette opportunité.

Je tiens à remercier également Dr. Bertrand Donnio pour son soutien, son encadrement exemplaire, son intérêt enthousiaste pour ce sujet si complexe et particulièrement les mots d'encouragement dans les moments difficiles et une liberté absolue pour développer ce projet. Ces qualités m'ont permis d'aller toujours plus loin dans mon travail de recherche.

Tout au long de cette thèse, J'ai bénéficié d'un support administratif et technique exemplaire. Du côté administratif Je tiens à remercier très sincèrement Mme Agnès Bouet et Mme Rose-Marie Weller pour leur aide efficace et leur patience infinie pour les tâches administratives. Du coté technique, Mlle Laurence Oswald qui m'a montré de façon détaillée les procédures, la gestion et le maintien des laboratoires du département, pour pouvoir réaliser mon travail de façon propre et efficace. Mlle Emilie Couzigné, qui a géré de façon impeccable la commande, livraison et disposition des produits. Et finalement Mlle Emilie Voirin, qui a contribué dans la synthèse de certains produits à la dernière partie de ce travail. Mes remerciements les plus sincères.

La caractérisation des élastomères cristaux liquides faits à Strasbourg repose sur deux grands piliers, chargés de la construction et de la maintenance des dispositifs de rayons-X, DSC et thermoélastiques. Ces deux piliers sont M. Nicolas Beyer et Dr. Benoît Heinrich. Merci beaucoup de votre implication, de votre disponibilité et de vos qualités. Grâce à vous il est maintenant possible d'étudier les élastomères au sein de l'institut.

Je remercie aussi le groupe du Prof. Heino Finkelmann pour m'avoir donné libre accès aux techniques de préparation d'elastomères. Les discussions au sein de son groupe, m'ont permis de surmonter les difficultés que ce type de matériaux présentent. Merci Laura, Simon, Dominic, Frank, Patrick, Natalia and Felicitas.

La pluridisciplinarité de ce sujet a permis de créer une nouvelle collaboration avec le Prof. Guy Schlatter au LIPHT de Strasbourg. Son intérêt et enthousiasme nous ont permis de chercher des nouvelles études de rhéologie pour les élastomères qui ouvriront une nouvelle ligne de recherche. Merci beaucoup.

Concernant à la rhéologie des élastomères cristaux liquides, j'ai eu l'honneur de collaborer avec les spécialistes du domaine : Dr. Phillippe Martinoty et Dr. Daniel Rogez. Merci de votre intérêt et pour l'étude judicieuse de certains systèmes.

Une partie des réseaux magnétiques fonctionnels a aussi été issu d'une collaboration DCMI-DMO, Je tiens à remercier Prof. Sylvie Bégin-Collin et Dr. Arnaud Démortière pour la préparation de nanoparticules de ferrite ; Dr. Guillaume Rogez pour les études de SQUID et la lecture critique du cinquième chapitre ; au Dr. Jean-Louis Gallani des discussions sur le magnétisme et la rhéologie et au Dr. Emmanuel Terazzi pour la synthèse et discussions sur les systèmes d'oxyde de manganèse (Mn12), également, de son amitié.

Je remercie très spécialement Dr. Antoni Sánchez Ferrer. Tony, gracias a todas las discusiones que tuvimos, he podido llegar hasta aquí sin perder la rienda. Gracias de todo corazón.

J'associe à mes remerciements tous les chercheurs du DMO (ex-GMO) avec qui j'ai partagé cette étape de ma vie. Merci Sylvestre, et la connaissance de la grotte le hand et de Bazbat ; Merci Jerôme, le gars le plus cool de la planète ; Merci Will, si cette feuille suffisait pour tout dire…., amitié en or solide ; Merci pour tout Hind, et mon admiration pour gérer le temps entre recherche et Lina ; Merci Stéphane pour toutes les discussions sur polymères et le Bagad ; Merci très spécialement à toi Cyril, pour les concerts, les sorties et ton amitié inconditionnelle ; Merci Dr. Laurent Douce, Alexandre, Jean, Julien, Pierre, Dr. Patrick Masson, Virginie, Dr. Delphine Felder-Flesch, Giusseppe, Julieta, Prof. Yves Galerne, Jean-Baptiste, Nathan, Romain.

Avant moi, le Dr. Miguel Bispo a été le pionnier du sujet au sein du département. Grâce à sa contribution, nous avons pu aller au niveau suivant. Muito obrigado Miguel.

Finalement, je remercie du fond de mon cœur mes supporteurs inconditionnels : Ma famille, mes amis et Anaïs.

Dédiée à Francisco et à Didier.

Ce travail a été financé par la bourse CONACyT Nº dossier 185485.

Résumé de la thèse.

1. Introduction.

Depuis longtemps l'homme essaie de créer des outils pour reproduire et amplifier l'action mécanique de ses membres. L'évolution de ces outils par l'amélioration des qualités de ses composants (comme la dureté, la résistance, la rapidité et l'efficacité) lui ont permis de s'adapter et de mieux appréhender son environnement. Un des systèmes le plus difficile à obtenir est le muscle artificiel, tant du point de vue de sa réalisation que de sa performance. Par définition, il doit être capable de répondre d'une façon rapide et efficace à un effort ou stimulus extérieur. L'ensemble de ce travail de recherche est une petite contribution au développement de ces systèmes.

Depuis leur découverte, les cristaux liquides ont été utilisés dans diverses applications en particulier dans le domaine des écrans plats. Ils présentent plusieurs mésophases telles que les phases nématiques, smectiques, colonnaires ou les phases cubiques (arrangements tridimensionnels complexes). Avec l'induction de la chiralité, certaines de ces mésophases présentent des propriétés intéressantes de ferroélectricité ou antiferroelectricité. Récemment celles-ci ont été obtenues avec quelques molécules présentant une structure coudée (ressemblant aux bananes).

Dans le domaine des polymères et elastomères, Kuhn *et al.*[i] ont observé qu'un polymère gel réticulé, peut agir comme un muscle artificiel en soulevant une charge au moment d'être gonflé par un solvant. De plus, de Gennes[ii] a décrit un modèle de nouveau matériau, produit par la combinaison d'un polymère réticulé amorphe (alterné en blocs) et d'un autre polymère qui présente des propriétés mésomorphes.

[i] Kuhn,W., Hargilay, B.,Katchalsky, A., Eisenberg, H,. *Nature* , **1950**, 165, 514.
[ii] De Gennes, P.G. *C. R. Acad Sci. Paris serie B*, **1975**, t 281, 343.

Celui-ci présente la caractéristique d'être déformable sous contrainte mécanique. Enfin H. Finkelmann[iii] s'est inspiré de ces précédents travaux et a synthétisé le premier élastomère cristal liquide en réticulant des chaînes de polymères. L'obtention de ces nouveaux matériaux a ouvert la voie à de nombreuses applications (actuateurs mécaniques, matériaux photosensibles, etc.

Il existe deux classes principales d'élastomères cristaux liquides qui se différencient par des notions de topologie: 1) les élastomères à chaînes latérales où les mésogènes sont greffés latéralement sur la chaîne flexible du polymère, lequel est réticulé par des molécules polyfonctionnalisées (figure 1) et, 2) les élastomères cristaux liquides à chaîne principale où les unités mésogènes sont insérées dans les chaînes de polymères, lesquelles sont ensuite reliées par des agents de réticulation (Figure 2).

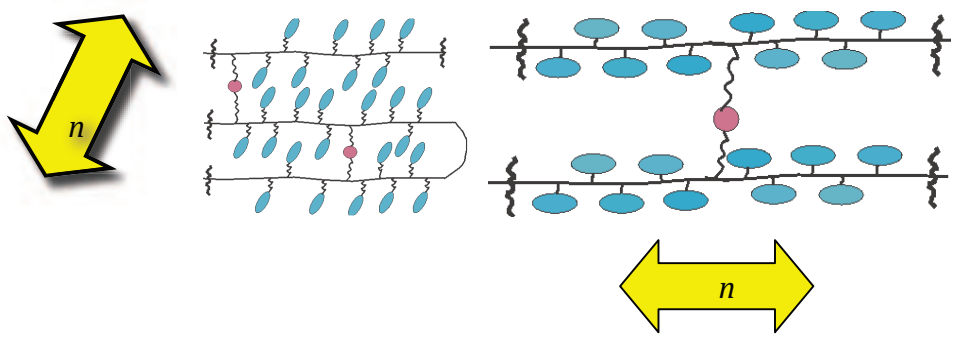

Figure 1. Elastomères cristaux liquides à chaîne latérale « en peigne » (gauche) et « en haltère » (droite). La flèche indique la direction moyenne du directeur.

Dans le cas des élastomères élastomères à chaînes principales, la capacité d'élongation élastique dépasse largement celle des analogues à chaînes latérales. Cela est dû principalement au fait que le vecteur directeur moyen des mésogènes est aligné parallèlement aux chaînes résultantes de polymères, et aussi à un couplage très fort

[iii] Finkelmann, H, Kock, H., Rehage, G., *Makromol. Rapid Commun.,* **1981**, 2, 317.

polymère-mésogène, au contraire du cas des systèmes à chaînes latérales où il existe un découplage prononcé polymère mésogène.

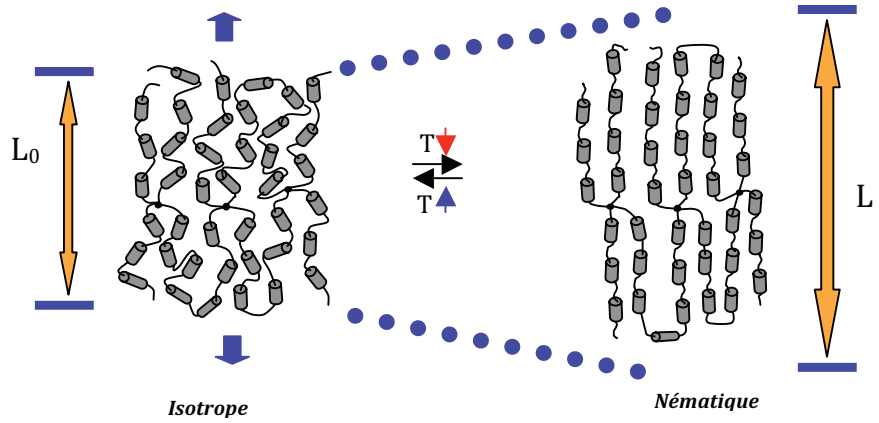

Figure 2. Elongation d'un élastomère cristal liquide à chaîne principale à la transition Nématique-Isotrope.

L'obtention de ce type d'élastomères est depuis le début un grand challenge, au niveau de la synthèse. Depuis la première publication[iv], deux méthodes différentes ont été employées: d'une part, la réticulation d'un polymère à chaîne principale[v] et d'autre part, la réaction en une étape[vi] qui combine simultanément les étapes de polymérisation et de réticulation. Cette dernière est considérée comme la plus efficace.

Objectifs.

Les différents objectifs de cette thèse concernent la préparation d'élastomères à chaînes principales et l'étude des propriétés physico-chimiques notamment celles

[iv] Bergmann,G., Finkelmann, H., Percec, V., Zhao, M., *Macromolecular Rapid Comm.* **1997**, 18, (5) 353.
[v] a) Di Maio, L., Iannelli, P., Pragolia, S., Roviello, A., Sirigu, A., *J. Polym. Phys.* **1998**, 36, 433 ; b) Caruso, U., Hatfull, L., Roviello, A., Sirigu. A., *Polymer* **1999**, 40, 6753 ; c) Acierno, D., Fresa, R. Iannelli, P., Roviello, A., Vacca, P., *Polymer* **2000**, 41, 4179.
[vi] Donnio, B., Wermter, H., Finkelmann, H., *Macromolecules,* (**2000**) 33, 7724.

reliées au couplage mésomorphisme-élasticité. Différents types de systèmes ont été élaborés afin de mener à bien ce projet.

Pour une élongation maximale à la transition nématique-isotrope, il est souhaitable d'obtenir des élastomères présentant une phase nématique sur un grand domaine de température avec une isotropisation à basse température. L'utilisation d'un mélange de mésogènes peut être une approche intéressante pour produire des systèmes nématiques à basse température. Dans une première partie, nous avons décidé d'étudier des copolymères et coélastomères composés de 2 mésogènes différents (**N1** et **N2**) afin d'évaluer les propriétés mésomorphes en fonction de leur proportion respective. Le diagramme de phase des deux monomères en fonction de la proportion relative a été réalisé (copolymères et coelastomères). Deux longueurs de "l'extenseur" siloxane ont été utilisées (tetraméthyledisiloxane et hexaméthyletrisiloxane). L'agent de réticulation est le pentamethylecyclopentasiloxane, et la densité de réticulation est maintenue constante (4 % mol).

Dans une deuxième partie, nous avons cherché à développer de nouveaux systèmes élastomèriques dont la déformation pourrait être induite par d'autres stimuli que la température. Par exemple, des systèmes activés par la lumière ont été réalisés[vii] en insérant dans les chaînes polymères les dérivés du type azobenzène. Dans cette étude, nous avons utilisé des monomères dits "banane" connus pour leurs propriétés ferroélectriques et leur sensibilité au champ électrique. Nous avons ainsi préparé plusieurs élastomères à base de "bananes" ainsi que des systèmes coélastomères à base de "bananes" et de mésogènes calamitiques. Il était anticipé que ce type de

[vii] a) Y. Yanlei, T.Ikeda, *Angew Chem Int. Ed. Eng.* 2006, **45**, 5416-5418. b) A. Sanchez-Ferrer. H. Finkelmann. *in Press*, 2008. c) M. Camacho López, H. Finkelmann, P. Palffy Muhoray, M. Shelley *Nature Mat.* 2004, **3**, 307–310.

système puisse se déformer sous l'action d'un champ électrique, mais également d'abaisser l'ordre des mésophases et les températures de transition.

Dans la dernière partie de la thèse, nous avons utilisé l'élastomère comme moyen d'organiser des nanoparticules ou clusters magnétiques. En effet, l'obtention d'élastomères cristaux liquides à l'aide d'une molécule qui présente à elle seule des propriétés d'aimant moléculaire, nous permettra de contrôler leur organisation dans le volume et avoir en même temps, un actuateur magnétique.

2. Synthèse.

Tous les monomères, polymères et élastomères ont été caractérisés par les techniques classiques, et leurs propriétés mésomorphes par DSC et diffraction des rayons X ainsi que les études thermoélastiques et viscoélastiques pour quelques uns d'entre eux.

Le chapitre 2 décrit et discute les diverses méthodes de synthèse implicant les réactions de Steglich, Williamson et Mitsunobu qui ont été utilisées pour l'obtention des différents monomères employés avec de bons rendements dans la plupart des cas, conduisant à deux monomères mésomorphes à chaînes éther vinylique **N1** et **N2** (Schéma 1) et 6 composés bent-core (**B1**- **B6**, Figure 3).

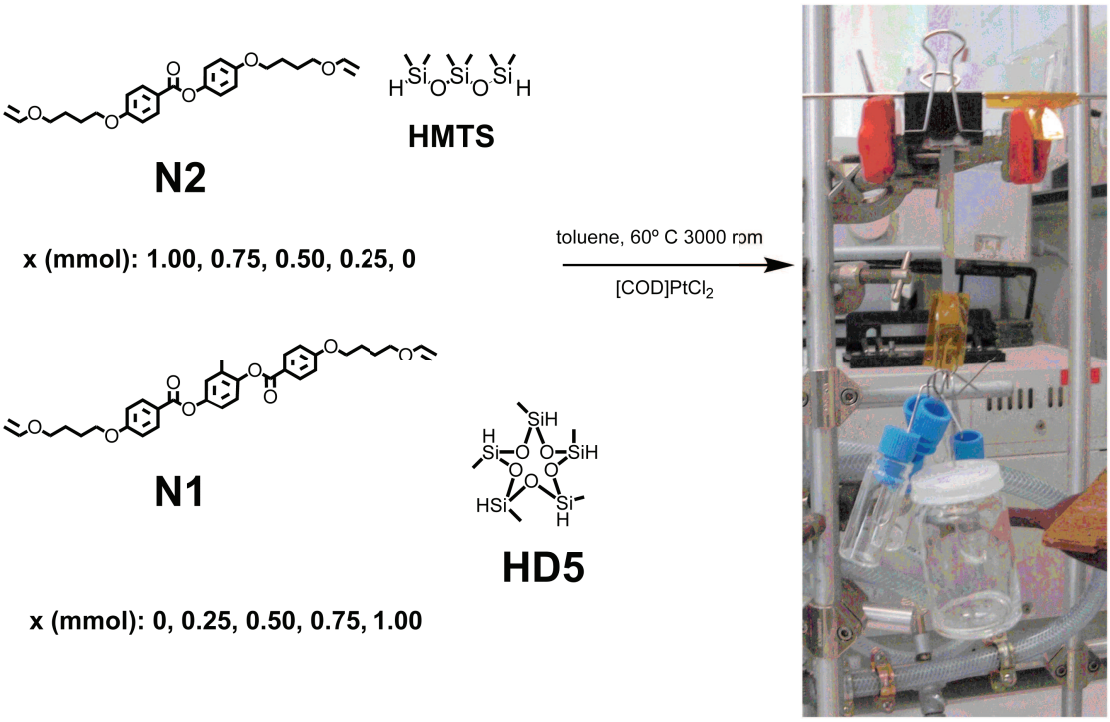

Schéma 1. Représentation schématique de la synthèse des coélastomères cristaux liquides comportant **HMTS** comme extenseur de chaîne (les analogues portant TMDS ne sont pas montrés).

La synthèse des polymères a été réalisée par hydrosilylation des bisoléfines catalysée par le platine (0), avec de bons degrés de polymérisation.

En utilisant des chaînes éthers vinyliques à la place des oléfines terminales lors de la synthèse, nous avons optimisé les conditions de polymérisation des monomères (DPn élevés) mais la polydispérsité s'est révélé élevée également. Nous avons synthétisé les élastomères correspondants des copolymères réalisés par ajout de l'agent de réticulation HD5 dans le mélange réactionnel, suivant la même méthode d'hydrosililation. Le processus d'élaboration des élastomères a été largement optimisé pour obtenir un pourcentage de matière soluble faible soit 3% dans le meilleur des cas.

3. Propriétés Mesomorphes.

Le diagramme de phases du système à deux mésogènes montre une dépendance de la température d'isotropisation, avec la proportion relative de chacun des monomères. L'augmentation de cette transition est corrélée avec l'augmentation de la proportion du monomère ayant la température de transition la plus élevée (**N1**). Cette observation nous a permis de concevoir des systèmes thermorégulables. Les élastomères précédents présentent une phase smectique C, identifiée par diffraction de rayons X. L'ordre observé dans nos systèmes est vraisemblablement dû à la ségrégation provoquée par les espaceurs (**HMTS**), optimisant par là même les interactions entre les parties rigides des unités mésomorphes. Le diagramme de phase des systèmes portant des extenseurs de chaîne **HMTS** est montré dans le graphique 1.

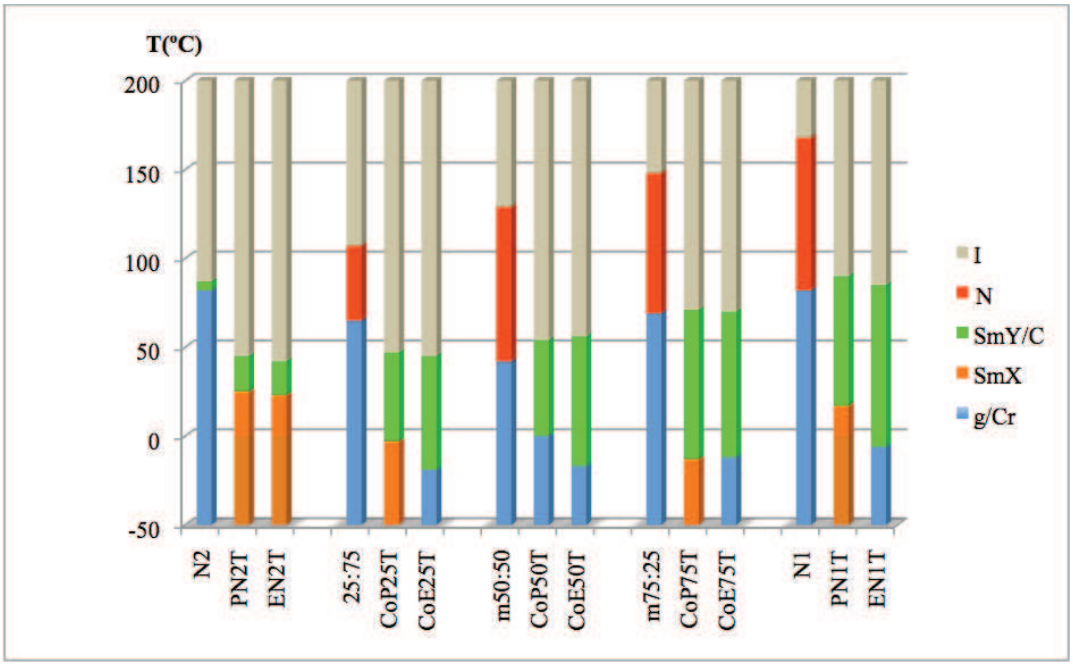

Graphique 1. Diagramme de phase obtenu pour des différents mélanges de monomères ainsi que les polymères et élastomères synthétisés avec le hexaméthyletrisiloxane.

Nous avons alors synthétisé une autre série de coélastomères en utilisant le tetraméthyldisiloxane pour étudier son impact sur la nature et la stabilité des

mésophases obtenues. Les élastomères ainsi obtenus présentent tous une phase nématique dont la stabilité dépend d'une manière assez remarquable de la proportion entre les monomères mésogènes (graphique 2).

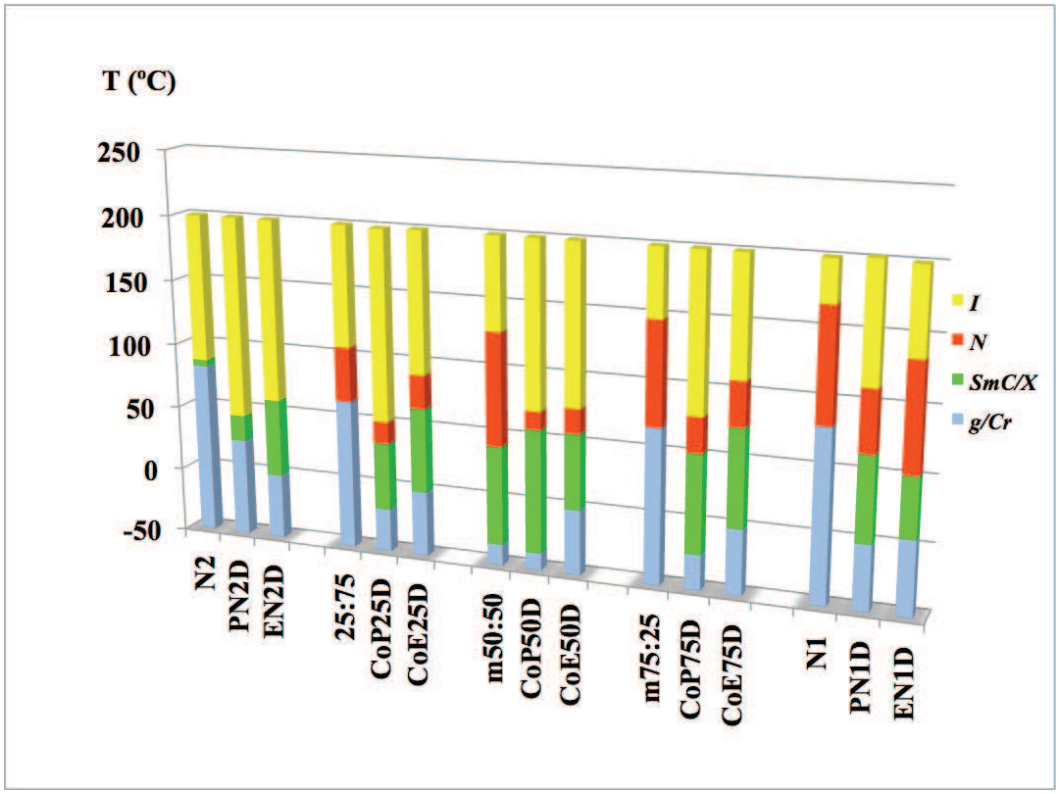

Graphique 2. Diagramme de phase obtenu pour les élastomères synthétisés avec le tetraméthyldisiloxane.

Cette étude nous a montré que l'utilisation de mélanges était une solution intéressante pour obtenir des systèmes nématiques avec des transitions d'isotropisation à basse température, pouvant faciliter l'étude de leurs propriétés physico-chimiques. Cependant nous n'avons pas pu nous affranchir de la présence de la phase smectique C, néfaste pour des élongations réversibles.

Pour la deuxième étude, nous avons synthétisé des monomères "bananes" pour l'élaboration de nouveaux élastomères cristaux liquides à chaînes principales présentant des phases à propriétés potentiellement ferroélectriques. Partant de l'idée

d'obtenir des systèmes qui présentent des phases Bx[viii] orientables sous un champ électrique, donc capables d'induire des déformations, nous avons conçu des coelastomères avec des molécules analogues à celles étudiées par Tschierske.[ix] Nous avons synthétisé plusieurs molécules coudées en variant certains paramètres structuraux (figure 3) afin d'évaluer les relations structure-activité.

A part le monomère **B3**, aucun monomère ne possède de propriétés mésomorphes, ainsi que les polymères obtenus. Sur la base de ces résultats, nous avons utilisé, en les combinant respectivement avec **N1** ou **N2**, deux de ces monomères (**B4** et **B6**) en petites quantités pour la préparation de six coélastomères, et étudier ainsi l'influence sur l'organisation du réseau.

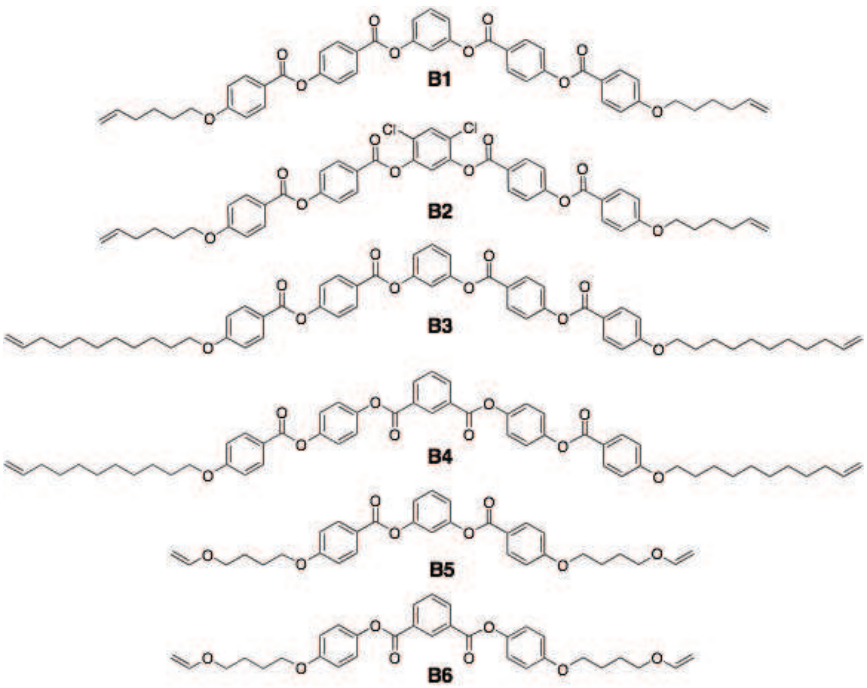

Figure 3: Monomères "bent-core" synthétisés.

[viii] Takezoe, H., Takanishi, Y., *Jpn. J. Appl. Phys.***2006,** 45, 597.

[ix] Dantlgraber, G., Diele, S., Tschierske, C., *Chem. Commun*, **2002**, 2768 ; Amaranatha Reddy, R., Baumeister, U., Keith, C., Hahn, H., Lang, H., Tschierske, C., *Soft Matter*, **2007**, 3, 558.

Pour les coélastomères à faible proportion de molécules “bananes”, le comportement thermique ressemble à celui des élastomères sans molécules “bananes”. La seule différence se trouvant au niveau de la stabilité de la phase cristal-liquide. En effet, la température de transition nématique-isotrope est plus basse ce qui est un avantage pour nos études rhéologiques. Par contre, aucune phase dite “banane” n’a été induite.

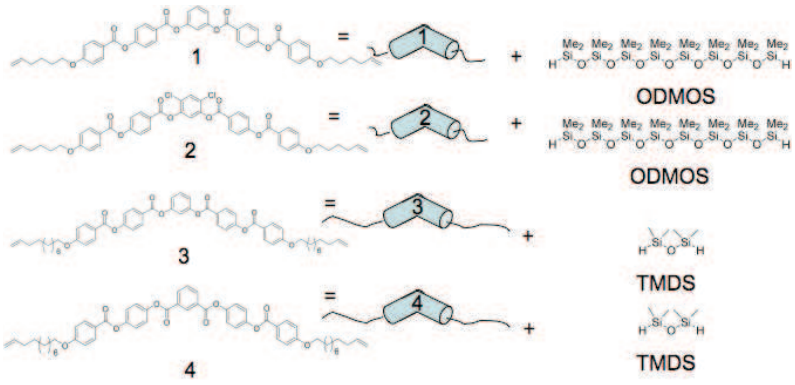

Schéma 3. Produits de départ des polymères synthétisés, mêmes conditions de réaction que dans le schéma 2.

Quand la quantité de monomère “bent-core” est augmentée, l’ordre du réseau est perturbé, cette perte d’ordre est observée en DRX par l’élargissement des signaux aux petits angles, en accord avec la faible valeur de l’anisotropie de gonflement. Dans la série de coélastomères **CoEN2B6D** (figure 4), une concentration à laquelle les propriétés anisotropes du système sont perdues a été déterminée (25 mol% de **B6)**.

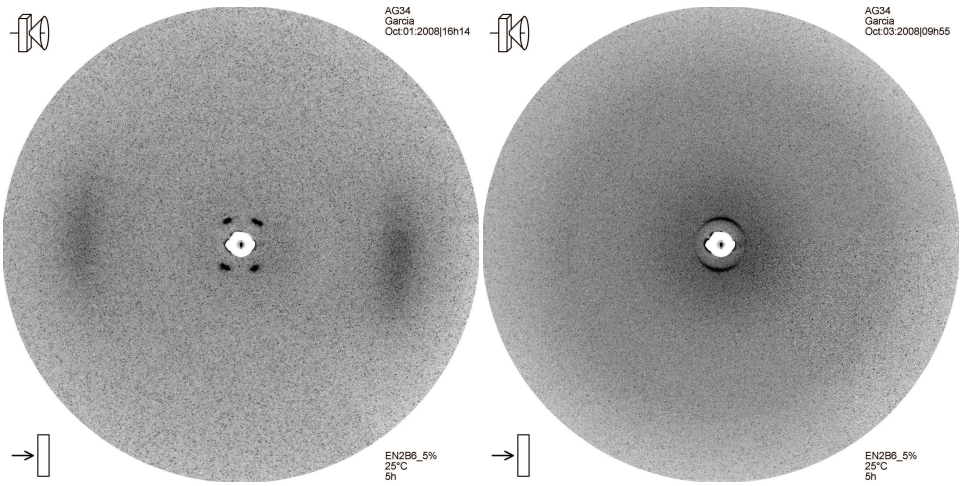

Figure 4 : Clichés de rayons X pris à températures ambiante des coelastomères **CoEN2B6D 5%** (gauche) ; et **CoEN2B6D 25%** (droite).

Le coelastomère **CoEN1B4D 5%** a présenté un comportement mésomorphe assez particulier. Il s'agissait d'une transition graduelle SmC-N qui dépendait du temps de relaxation aux températures en dessous de la température de transition. Suite aux études calorimétriques et de DRX spécifiques, cet effet a été attribué au réarrangement subi par les molécules **B4** dans la phase nématique qui restent piégées dans la structure, lors du refroidissement à l'intervalle du domaine d'existence de la phase smectique C, ce qui empêche le réarrangement des molécules cristal-liquides dans les couches propres de la phase SmC. Ce phénomène est dépendant du temps (cinétique) et pas de la température (thermodynamique).

4. Propriétés Thermoélastiques et Mécaniques.

Un avant-dernier chapitre de cette thèse traite des études mécaniques et thermoélastiques effectuées sur quelques échantillons répresentatifs. Nous avons observé leur comportement sous contrainte uniaxiale dynamique (rhéologie) et leurs capacités d'élongation avec un appareil de thérmoelasticité. Les études rhéologiques

ont des différences dans les valeurs du module de stockage (E') (graphique 3). On a pu s'apercevoir que tous les élastomères comportant des monomères calamitiques ont un comportement similaire de point de vue rhéologique. Cette observation est confirmée par les valeurs du module E' (dans la phase isotrope et en phase nématique) entre les coelastomères contenant trisiloxane (**HMTS**) et ceux portant des motifs disiloxane (**TMDS**).

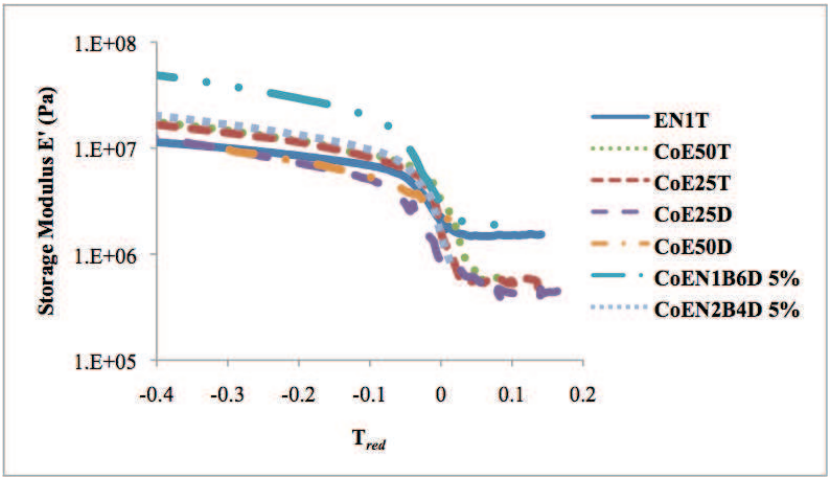

Graphique 3. Module de stockage en fonction de la température des films de coelastomères cristaux liquides.

Les études thermoelastiques réalisées avec les coélastomères **CoE25D** et **CoE75D** nous ont permis de connaître le taux d'élongation maximale ($L/L_{iso\ max}$ entre 200 et 300%) et ainsi d'estimer le coefficient d'expansion (Λ^T).

5. Réseaux Magnétiques Fonctionnels.

Dans la dernière partie, nous avons mis à profit notre expérience pour élaborer des élastomères magnétiques. Nous avons envisagé de créer une nouvelle famille d'actuateurs présentant une réponse sous champ magnétique. En s'appuyant sur un

travail récent de notre groupe[x], nous avons synthétisé de nouveaux matériaux en utilisant de trois façons différentes un dérivé du cluster d'oxyde de manganèse **Mn12Ac** décrit par Lis [xi], et des nanoparticules de ferrite de 3 nm:

a) Comme monomère polyfonctionnel.

b) Comme coagent de réticulation (film et masse).

Dans ce domaine, peu de publications font référence à l'utilisation de particules ou de molécules magnétiques dans les élastomères.[xii] Ce travail est le premier qui combine un réseau à chaîne principale et un cluster comme agent de réticulation. Les propriétés magnétiques de nos systèmes ont montré un comportement classique d'aimant moléculaire et un comportement superparamagnétique simple pour l'élastomère réticulé par des dérivés de ferrite. Les propriétés de ces matériaux s'avèrent prometteuses.

6. Conclusions et Perspectives.

Toute une nouvelle série d'élastomères présentant des propriétés physico-chimiques intéressantes a été synthétisée par la méthode «one-pot améliorée ». Leur préparation a impliqué plusieurs étapes de mise au point de la méthodologie originale utilisée dans le cadre de ce travail. La pureté des monomères et les bonnes conditions de réaction de polymérisation et la technique de spin casting ont permis d'obtenir bons

[x] Terazzi, E., Bourgogne, C., Welter, R., Gallani, J.L., Guillon, D., Rogez, G., Donnio. B., *Angew. Chem. Int. Ed.* **2008**, 47, 490.
[xi] Lis, T. , *Acta Crystallogr. Sect. B,* **1980**, 36, 2042.
[xii] a) Song, H. M., Kim, J. C., Hong, J. H., Lee, Y. B., Choi, J., Lee, J. I., Kim, W. S., Kim, J.H., Hur, N.H., *Adv. Funct. Mater.* **2007**, 17, 2070; b) Kaiser, A.; Winkler, M.; Krause, S.; Finkelmann, H., Schmidt, A. M. *J. Mater. Chem.* **2009**, 19, 538.

degrés de polymérisation dans le cas des polymères et des copolymères, et de faibles pourcentages de matière soluble dans le cas des élastomères et coélastomères. Les avantages presentés par cette méthode nous ont aussi permis d'insérer de façon systématique des molécules bent-core dans les réseaux calamitiques et obtenir des nouveaux matériaux avec un comportement et des propriétés intéressantes.

Grâce à la caractérisation thermique et la diffraction de rayons-X nous avons aussi confirmé les différentes mésophases et les températures de transition de nos produits. Cela nous permet de considérer nos systèmes comme des matériaux à forme thermocontrolée en variant la proportion de chacun des monomères. Dans le cas des élastomères et coelastomères contenant **HMTS** nous avons réussi à diminuer la température de transition de la phase isotrope tout en favorisant l'induction de la phase SmC au profit de la phase N. De même, nous avons aussi réussi à augmenter la largeur du domaine la phase nématique pour les coélastomères portant **TMDS** sans toutefois s'affranchir de la présence de la phase SmC. Concernant les coélastomères avec des monomères bent-core, nous avons remarqué dans quelques cas des perturbations de l'organisation et des transitions cinétiques dépendantes.

Un échantillonnage sélectif de nos films a été analysé du point de vue rhéologique. Cela nous a permis d'observer leur comportement viscoélastique. Malheureusement, ces études sont longues et demandent une quantité considérable d'échantillon. Nous n'avons présenté que des résultats préliminaires. Les études thermoélastiques réalisées sur deux échantillons ont permis de déterminer le coefficient d'élongation égal à 280% dans le meilleur de cas.

Finalement, il a aussi été possible d'obtenir des réseaux cristaux liquide contenant des agents de réticulation autres que les molécules organiques et des cyclosiloxanes.

Ces nouveaux matériaux hybrides peuvent être activés sous l'effet d'autres stimuli que la température comme par exemple le champ électrique ou le champ magnétique. De toute façon, des études approfondies sont encore nécessaires pour arriver à un bon contrôle du système. Les exemples montrés (réseaux Mn12 et l'elastomère réticulé avec des nanoparticules de ferrite) seront étudiés ultérieurement, ouvrant une nouvelle thématique de recherche dans notre groupe.

Les perspectives de ce travail se centrent dans la synthèse de coélastomères portant d'autres proportions de monomères **N1**/**N2.** Les études rhéologiques devraient permettre, si possible, d'établir la relation entre le module de Young et la proportion de monomères utilisée, les études thermoélastiques pourraient permettre d'établir de façon analogue, leur taux d'elongation par rapport à la proportion des monomères. Dans le cas des élastomères bent-core calamitiques, les investigations préliminaires se sont avérées prometteuses et un développement des actionneurs à réponse électrique peut être envisagé.

Index

Chapter 1

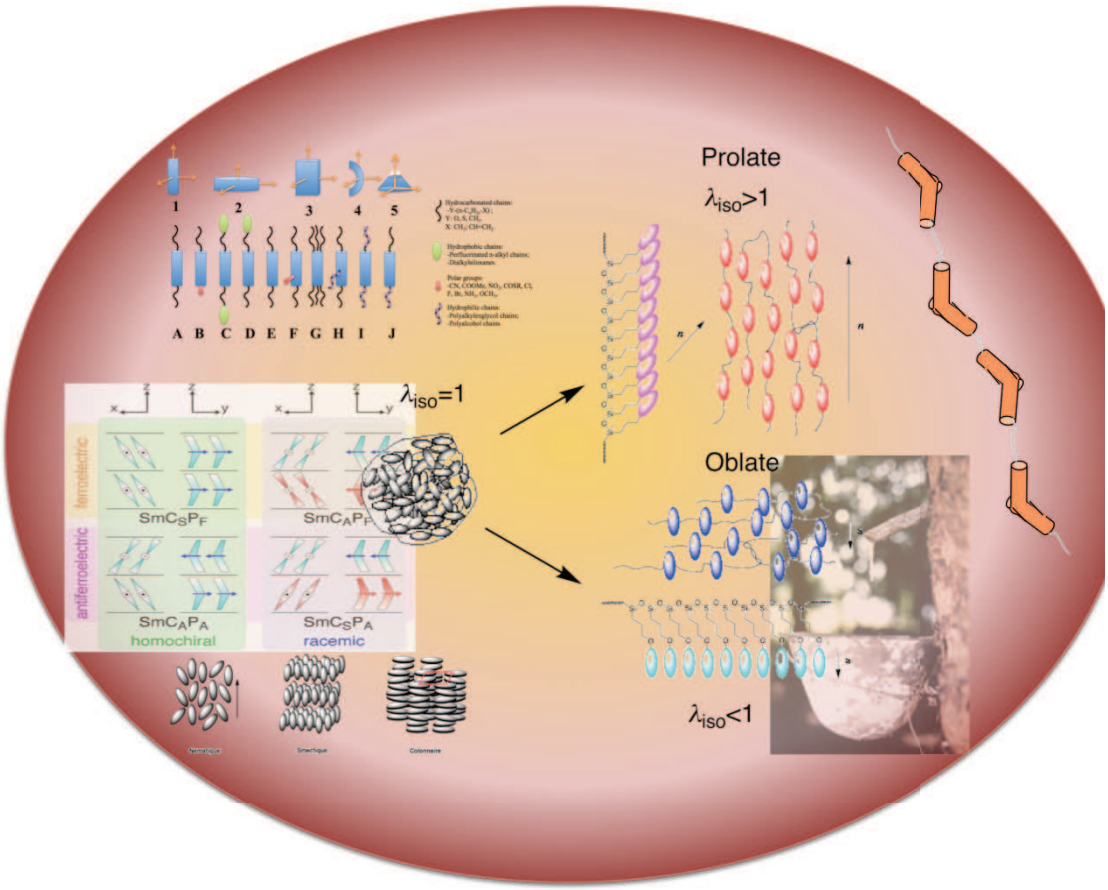

Introduction

1. Introduction.

Mankind has always been able to apprehend his environment by learning to use and control the power of his hands. In the course of evolution, Man started to simplify and facilitate life by making tools and machines that allowed him to be more efficient and to make life more comfortable. This research to improve his capability has allowed mankind to evolve for a long time.

One of the systems that has taken most of attention to imitate is the muscle, *alma mater* of movement and force. It is one of the most difficult systems to elaborate and replicate because of its complexity, resistance and reaction speed. The study presented here is one small contribution to this ensemble of works that contribute to enrich the subject.

1.1. Liquid Crystals.

Some crystalline compounds, instead of melting directly into fluid amorphous liquids, suffer one or several transitions into intermediate states whose short-range positional and orientational orders give some remarkable properties at the micro and macroscopic scale.

In 1888, Reinitzer[1] noticed that a derivative of cholesterol molecule had two melting temperatures; he first supposed that product impurities were responsible for the formation of a white fluid before complete melting. This white and opaque liquid between these two temperatures turned into a transparent one as it reached the second melting temperature. Reinitzer discussed his observations with Otto Lehmann who

[1] Mitov, M. "Les cristaux liquides" Que sais Je?, **2000**.

studied this material by using a microscope, which allowed to polarize the incident light. Since the initial work of these two pioneers, this particular behavior has been called "flüssigkristalle" i.e. "liquid crystal". In order to characterize and classify this novel "intermediate state of matter", Friedel[2] published a detailed classification of the liquid crystalline phases depending on the type of order presented in relation to the molecular shape.

Depending on the system induction of mesophases, the liquid crystalline state is divided in two main families: *thermotropic* liquid crystals, in which the LC phase is generated as an effect of the temperature where order is gradually lost as temperature increases, and *lyotropic* liquid crystals in which the phase transitions depend on the concentration of the LC in a solvent. An additional family of LC compounds in which the liquid crystalline depends on both temperature and solvent concentration is denominated *amphotropic* liquid crystals[3]. Due to the scope of the present work the introduction will focus exclusively on *thermotropic* liqud crystals.

1.1.1. *Molecular Shape*

Molecular architecture and shape play a crucial role in mesophase genesis. Mesomorphic molecules are conceived with specific molecular criteria. They must present a dichotomic molecular structure, which is seen as at least two portions of contrasting structural character consisting generally of a rigid anisotropic polarizable core, equipped with one or various peripheral segments (*i.e.* amphipatic character). The rigid anisotropic moiety leads to a parallel organization of these units (orientational order) and the aliphatic chains provide mobility, preventing these

[2] Friedel, G. *Ann. Phys.* **1922**, 18, 273-475.
[3] Ringsdorf, H. , Schlarb, B., Venzmer, J., *Angew. Chem., Int. Ed.*, **1998**, 27, 113; Tschierske, C., *Prog. Polym. Sci.,* **1996**, 21, 775.

systems for crystallizing. Amphipatic character generates the liquid crystalline intermediate state, which can also be seen as a multiple step melting process[4] leading to believe that mesophase formation results from a phase separation process.[5] Supramolecular interactions such as dipolar, electrostatic, hydrogen bond and van der Waals, also contribute to the mesophase stabilization in thermotropic mesophases. These interactions result from the anisometry of the molecules; repulsive forces will result from the amphipatic character. The most common liquid crystalline materials have the rod-like (calamitic) and the disk-like (discotic) shapes. Considering both kind of molecules as a cylinder, calamitic molecules have a longer axis perpendicular to their bases ($z > r$) (figure 1.1. structure **1**) whereas for discotics the largest distance is the radius ($z < r$) as illustrated in figure 1.1.(structure **2**). The chemical structure of these molecules consists of specific arrangements of linked phenyl, cyclic or heterocyclic derivatives through single, double, or triple bonds as well as ester, amide, imine, azo, or even metals (known also as metalomesogens),[6] whereas the flexible moieties, often hydrocarbon chains, oligoaliphatic ethers, siloxanes, etc., are connected at one or several sections of the rigid core (ends or sides).

Polar functionalities such as nitriles, amines or halogens can be incorporated within the structures (both rigid and flexible counterparts) to modify some physical properties.[7] The last level of mesogen conception respecting to the mesogens is H-

---

[4] Skoulios A., Guillon, D., *Mol. Cryst. Liq. Cryst.*, **1988**, 165, 317.
[5] Tschierske, C. , *J. Mater. Chem.*, **1998**, 8, 1485.
[6] B. Donnio, D. Guillon, D. W. Bruce, R. Deschenaux. Metallomesogens In *Comprehensive Coordination Chemistry II: From Biology to Nanotechnology*/. Ed. McCleverty J. A., Meyer, T. J., Elsevier, Oxford, **2003**. Volume 7: From the Molecular to the Nanoscale: Synthesis, Structure, and Properties, pp. 357-627; Donnio, B., Guillon, D., Bruce, D. W., Deschenaux, R., Metallomesogens In *Comprehensive Organometallic Chemistry III: From Fundamentals to Applications*. Ed. Crabtree, R. H., Mingos, D. M. P., Elsevier, Oxford, **2006**, Volume 12: Applications III: Functional Materials, Environmental and Biological Applications, pp. 195-294.
[7] Hird M., Toyne, K. J., *Mol. Cryst. Liq. Cryst.*, **1998**, 323, 1.

bonding supramolecular chemistry, that allows to obtain LC molecules without molecular linking.[8]

Liquid crystallinity is not restricted to cylindrical molecules and using the previously described strategies, sanidic mesogens,[9] bent-core[22,23] and bowlic[10] considered as polar mesogens as well as polycatenar[19] mesogens can be obtained. A schematic representation of all these structures is illustrated in figure 1.1.

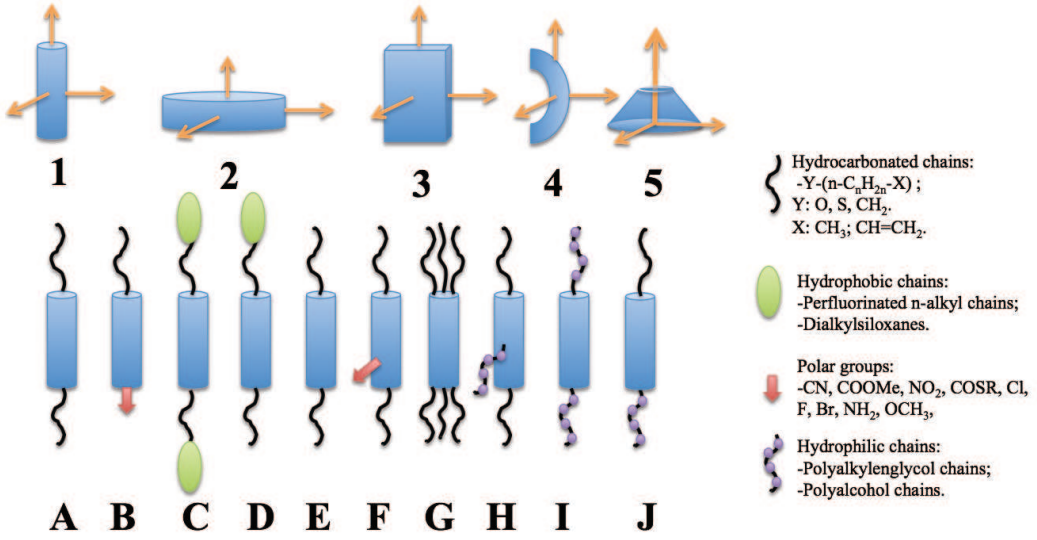

Figure 1.1. Top: Different core anisotropies (rod, disc, sanidic, bow and bowl) Bottom: different functionalizations of rigid cores. (Rodlike model is used as example).

The next paragraph describes the different phases, resulting from the chemical design and the interactions between molecules.

[8] Paleos C. M. and Tsiourvas, D., *Liq. Cryst.*, **2001**, 28, 1127.
[9] Tschierske, C. *, Annu. Rep. Prog. Chem., Sect. C: Phys. Chem.*, **2001**, 97, 191.
[10] Takezoe, H., Kishikawa K., Gorecka, E., *J. Mater. Chem.*, **2006**, 16, 2412.

1.1.2. *Typical, Nonpolar Mesophases*

The structural factors determining mesophase morphology are the shape anisotropy of the constituent molecules and the nano-scale segregation of chemically distinct subunits into different regions (also called micro or nanosegregation).[5,9,11] Herein, the most commonly observed mesophases are described.

Nematic mesophase: The parallel alignment of anisometric rigid units (either rod-like or discotic) due to minimization of the excluded volume, leads to orientational long range order giving rise to the nematic phase (N), illustrated in scheme 1.1. This mesophase has the simplest structure of all mesophases and its one–dimentional orientational order of the molecules is given by virtue of correlations of the principal molecular axis, although this orientational order is not polar and molecules are free to flip.[12]

This mesophase is commonly observed in calamitic mesogens but also is exhibited by disc like molecules as randomly discs parallel in average one to the other, known as the nematic discotic (N_D) mesophase.[13] When columnar aggregates of discotic molecules are uniformly oriented along a main direction, a nematic columnar (N_{col})[5] mesophase is formed. A more unusual variant of nematic mesophase consists in nematic domains which are organized in layers parallel to the main director (laminated phases). This submesophase is called lamellar nematic (Lam_N) mesophase. When the molecules that generate the mesophase do not present a calamitic shape i.e. a sanidic or a bent molecule, biaxiality can occur and the corresponding mesophase

[11] Tschierske, C., *J. Mater. Chem.,* **2001**, 11, 2647.
[12] *Handbook of Liquid Crystals*, ed. Demus, D., Goodby, J. W., Gray, G. W., Spiess H.W., Vill, V., Wiley-VCH, Weinheim, **1998**.
[13] Kumar, S., *Chem. Soc. Rev.*, **2006**, 35, 83.

will be denomined as biaxial nematic. This last type of mesophase will be discussed in paragraph 1.1.4.

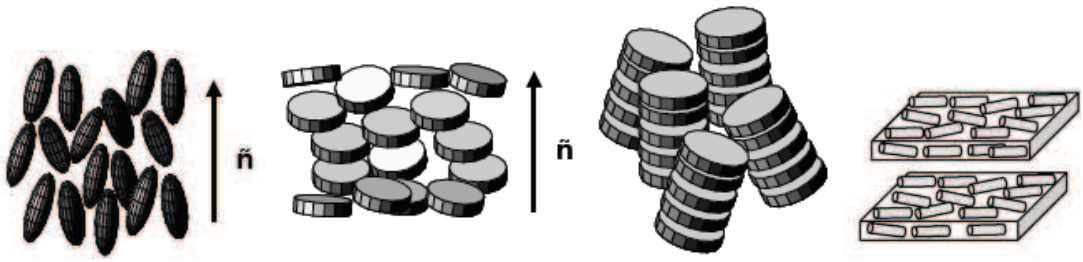

Scheme 1.1. Types of nematic phases. From left to right: calamitic nematic (N); nematic discotic (N_D); Columnar nematic (N_{Col}); lamellar nematic (Lam_N).

The segregation of incompatible parts of the molecules is a main factor leading to long range positional order in one, two or three dimensions, giving rise to three fundamental organizations in liquid crystalline systems classified as Smectic (Sm) Columnar (Col) and cubic (Cub) mesophases. The description of these three groups is given below.

Smectic mesophases:[12] Smectic phases (scheme 1.2) are generally constituted of calamitic mesogens. They consist of the superposition of equidistant molecular layers, and are characterized by orientational correlations of the principal axis, and by partial translational ordering of the molecules within layers. It is important to note that no in-plane long-range positional order is present.[14] The simplest of all the smectic phases is the smectic A (SmA) in which the long molecular axes of the rods are oriented on average in the same direction to the layer normal, but molecules are loosely associated within layers. If the molecular director is now tilted with respect to the layer normal, the SmC phase is obtained. Since tilting affects symmetry operations of

[14] Gray, G. W., Goodby, J. W., *Smectic Liquid Crystals; Textures and Structures*, Leonard Hill, Glasgow, **1984**.

the molecule, we can derive two variants of this mesophase by comparing adjacent layers, either the tilt-direction is uniform (synclinic: subscript s, SmC_s) or alternating (anticlinic: subscript a, SmC_a). Synclinic tilt is usually preferred due to the LC phase dynamics, which includes out-of-plane fluctuations. In the case of anticlinic tilt, these fluctuations are more difficult, which leads to an entropic penalty for this type of organization. However, anticlinic arrangement can be favoured enthalpically by steric and polar interactions at the layer interfaces,[15,16] or in some cases, at reduced temperature below SmC_s (SmC in rod-like LC systems).

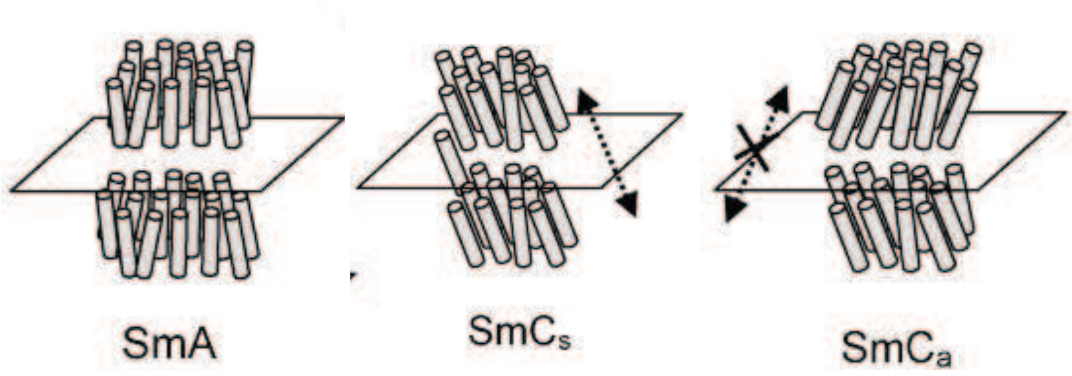

Scheme 1.2. True smectic phases. Double pointed arrows indicate flucuation between layers.

By increasing the in-plane (short range) and long range bond orientational orders, hexatic smectic phases arise. In the hexatic smectic B (SmB^h) mesophase, the molecules are located at the nodes of a bidimensional hexagonal lattice and untilted with respect to the layer normal. There are two tilting possibilities in the 2D hexagonal lattice: when the molecules are tilted towards the vertex (SmF) or towards the edge (SmI) (Scheme 1.3). In all the hexatic cases, molecular long axis rotation and diffusion between layers is concerted. The soft crystalline phases are derived from the

[15] Fukuda, A., Takanishi, Y., Ishikawa, T., Ishikawa, K., Takezoe, H., *J. Mater. Chem.*, **1994**, 4, 997.
[16] Thisayukta, J., Samulski, E. T., *J. Mater. Chem.,* **2004**, 14, 1554.

true smectics and characterized by the appearance of inter-layer correlations and, in some cases by the loss of rotation and diffusion. Thus SmB^t, SmG and SmJ phases are derived from interlayer correlated SmB^h, SmF and SmI mesophases respectively. Also, SmE, SmH and SmK phases are SmB^t, SmG and SmJ phases without rotational freedom. Containing a high disorder, these phases are considered as intermediate states between the crystalline state and the true smectic mesophases. Smectic mesophases are essentially induced in calamitic mesogens but also sanidic mesogens present such mesophases[9] and are inherent to the bent-core systems, discussed later. Variants of lamellar (Lam_{sm})[11] have also been reported.

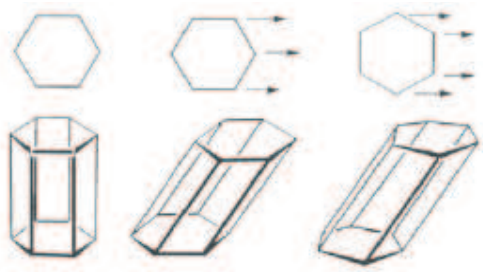

Scheme 1.3. Hexagonal lattice of hexatic and soft crystalline mesophases. From left to right: SmB, SmI, SmF. The edges of the prisms represent the calamitic molecules.

Columnar mesophases: Columnar mesophases result from the stacking of discotic molecules, disk-like aggregates of polycatenar mesogens[19] and bent-core molecules[22,23] into columns, further organized into 2D ordered lattices.[12,13,17,18,19] They are characterized by the symmetry of the planar arrangement: hexagonal (Col_h), rectangular (Col_r), oblique (Col_o) or squared (Col_s) (Scheme 1.4).

---

[17] Levelut, A. M., *J. Chim. Phys. Phys.-Chim. Biol.*, **1983**, 80, 149.
[18] Gorecka, E., Pociecha, D., Mieczkowski, J., Matraszek, J., Guillon, D. Donnio, B., *J. Am. Chem. Soc.*, **2004**, 126, 15946.
[19] Nguyen, H.-T., Destrade, C., Malthête, J., *Adv. Mater.*, **1997**, 9, 375.

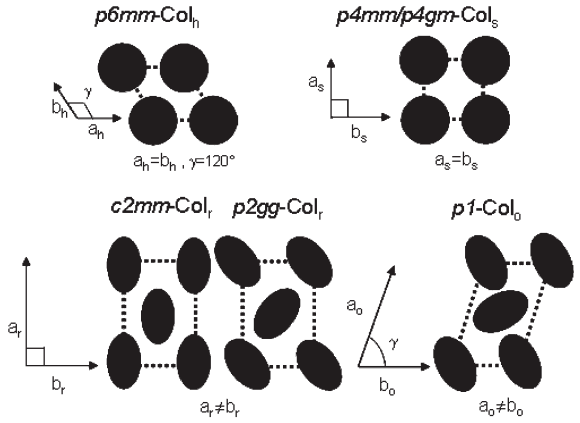

Scheme 1.4. Cross sections of the different columnar mesophases. Ovals represent non cylindrical, unpolar columns.

Diffusion between and within the columns occurs readily and the phases are fluid. In the case of non discotic units, polycatenar, polyphylic[15,19] dendrimers[20,21] and bent-core molecules,[19,22,23] self-organization by stacking/microsegregation may lead to columnar mesophases. Besides the previously commented N_D and N_{col} phases, lamellar-columnar phases (L_{Col} or Col_L) are described as the result of supramolecular columns confinement within smectic layers with or without interlayer correlations, observed with sanidic and polyphilic molecules[15] or by mixed rod-like-disc dimers.[9]

Cubic mesophases (Cub)*:* this family represent another kind of LC phases characterized by a more complicated 3D arrangement. Some examples of such organizations are micellar cubic phases (Cub_I) consisting of ordered tridimensional arrays of micelles,[5,11] found with amphipiles; bicontinuous cubic phases (Cub_v) are

[20] Cheng, X. H., Prehm, M., Das, M. K., Kain, J., Baumeister, U., Diele, S., Leine, D. Blume, A., Tschierske, C., *J. Am. Chem. Soc.,* **2003**, 125, 10977; Chen, B., Zeng, X. B., Baumeister, U., Diele, S., Ungar, G., Tschierske, C., *Angew. Chem., Int. Ed.*,**2004**, 43, 4621; Chen, B., Zeng, X. B., Baumeister, U., Ungarand, G., Tschierske, C., *Science*, **2005**, 307, 96; Marcos, M., Giménez, R., Serrano, J. L., Donnio, B., Heinrich B., Guillon, D., *Chem. Eur. J.*, **2001**, 7, 1006.
[21] Donnio, B. Barberá, J., Giménez, J.R., Guillon, D., Marcos, M., Serrano, J. L., *Macromolecules*, **2002**, 35, 370.
[22] Peltz, G., Diele, S., Weissflog, W., *Adv. Mater.*, **1999**, 11, 707.
[23] Reddy, R. A., Tschierske, C., *J. Mater. Chem.,* **2006**, 16, 907.

made of infinite, periodic 3D molecular networks[24,25] found for some classical rod-like mesogens and polycatenars. Note that a more complex M_{Tet} phase, which consists in a micellar organization with a tetragonal 3D symmetry is found in rod-coil block molecules.[26]

Additionally, if chirality is added as another order variable of the system, it can give rise to interesting effects on the macroscopic behavior. The chiral phases and their inherent properties are briefly discussed in the next paragraph.

1.1.3. *Chiral Phases, Ferroelectricity and Antiferroelectricity*

When a chiral center is introduced in the molecular structure, infinite rotation symmetry along the longest axis (C_∞) is lost. Hence, rotation along the long axis of the mesogens is biased giving rise to a helical arrangement presenting left or right handed torsion. When the order is just orientational, the phase is denominated twisted nematic or cholesteric (N*). In the case where mesogens arrange in smectic mesophases the exponent * is added, thus, chiral SmA phase is noted as SmA* and chiral SmC mesophase becomes SmC*. Not being exclusive of chiral compounds, this helical arrangement can be induced in non-chiral compounds by doping them with a small amount of a chiral additive.[27,28]

A particular behavior is observed in SmC* when successive smectic C layers show a gradual change in the direction of the molecular tilt, such that the director precesses about the z axis from layer to layer, always lying on the surface of a hypothetical cone

---

[24] Kutsumizu, S., *Curr. Opin. Colloid Interface Sci.*, **2002**, 7, 537.
[25] Imperor-Clerc, M., *Curr. Opin. Chem. Biol.,* **2005**, 9, 370.
[26] Lee M., Yoo, Y.-S., *J. Mater. Chem.*, **2002**, 12, 2161.
[27] Goodby, J. W., *J. Mater. Chem.*, **1991**, 1, 307.
[28] Goodby, J. W., Slaney, A. J., Booth, C. J., Nishiyama, I., Vuijik, J. D., Styring, P., Toyne, K. J., *Mol. Cryst. Liq. Cryst.*, **1994**, 243, 231.

of angle 2θ. The angle around the circle of precession is known as the azimuthal angle. This creates a helical structure in the chiral smectic C (SmC*) mesophase with the pitch corresponding to the distance needed to reach the same molecular orientation along the z axis.

In addition to the induction of the helical structure, spontaneous molecular polarization occurs within each layer, as shown in scheme 1.5. This polarization vector is perpendicular to the molecule and is contained in the layer plane. Therefore, all possible directions for the vector are tangential to the circle of intersection of the cone with the plane. A bulk SmC* sample, free to develop its helical structure, will not show ferroelectric behavior since the spontaneous polarization will average to zero over one pitch length (polarization vectors go around an entire circle and cancel each other out). This is often referred to as the helielectric phase. Typically, the pitch includes many layers.

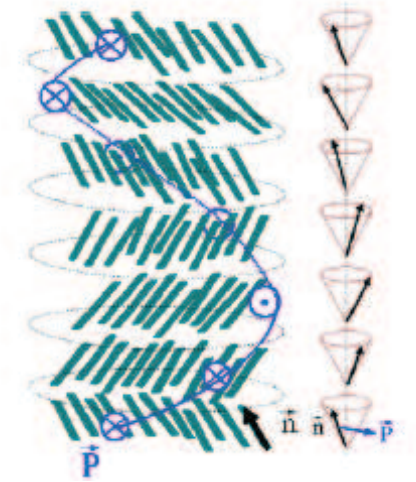

Scheme 1.5. Representation of a SmC* ferroelectric phase. Top (left) and side (right) views of polar vector precession.

Antiferroelectricity results when the polarization vector suddenly turns 180º from one

layer to the next one, hence the previously described ferroelectric effect is not present and molecules are not orientable.

Chiral molecules can arrange themselves into chiral frustrated phases. One of the most observed mesophases is the twisted grain boundary (TGB)[29] and the so called blue phases (BP).[30] TGB present a helical superstructure consisted of local smectic-like blocks separated by screw dislocations. The layer normals of the former ones rotate regularly in a helical fashion. On the other hand, blue phases consist of tridimensional arrangement of double-twisted columns.

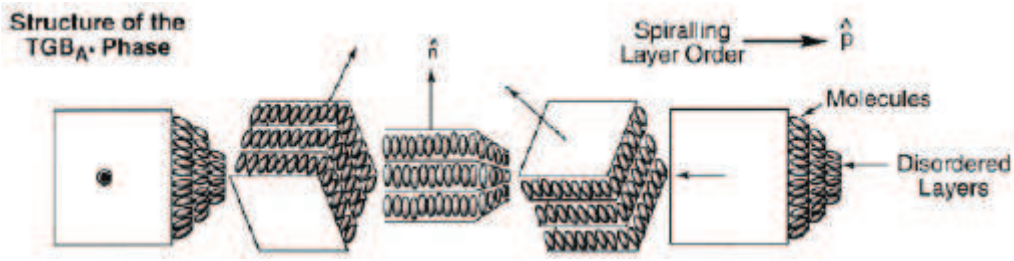

Scheme 1.6. Example of TGB phases. The illustrated mesophase is TGB_{A*}[32]

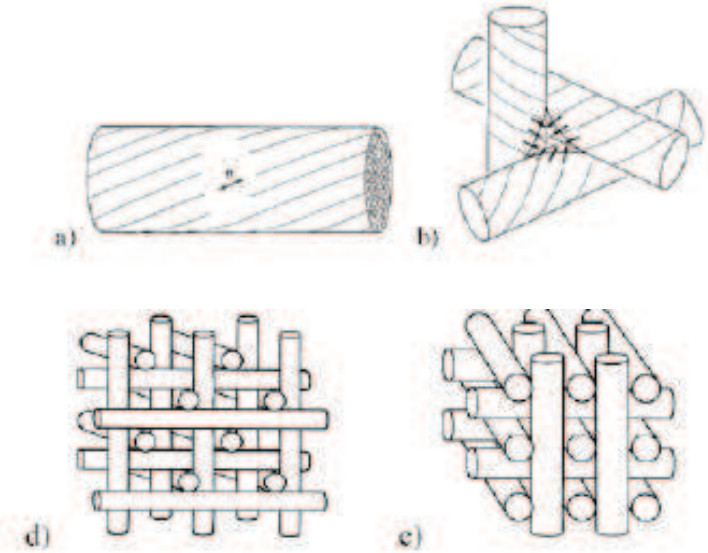

Scheme 1.7. Blue phases representation.

[29] Goodby, J. W., *Struct. Bonding*, **1999**, 95, 83.
[30] Crooker, P. P., *Liq. Cryst.*, **1989**, 5, 751.

1.1.4. *Biaxiallity Polarity and Bx phases*.

Sanidic and bent-core molecules, which present restricted rotation, are through to be able to generate biaxial nematic mesophases. Despite an intensive research for more than 20 years,[31] biaxial nematic phase (N_b) has been difficult to establish mainly due to the difficulties in characterizing biaxiality in such systems.[32] However, proofs of biaxial structure have been given recently via NMR experiments in oxadiazole derivatives.[33,34]

Biaxiality can also be observed in smectic A systems, giving the corresponding SmA_b (also called MacMillan phase) as reported by Pratibha *et. al*.[35] in binary mixtures of rod-like and banana dopant, in mettalomesogens;[35d] as well as in smectic C systems (SmC_D, SmC_T).[9]

Biaxial phases can also be polar, when they are obtained with bent-core molecules. This particular family of compounds and their corresponding mesophases are described in the next paragraphs.

Vörlander synthesized the first compound of this type in 1929.[36] He reported that the thermal stability of the observed mesophases was low compared to that of the straight core analogues. The subject was not revived until Matsunaga's group restarted the

---

[31] Bruce, D. W., *Chem. Rec.,* **2004**, 4, 10; Berardi, R., Zannoni, C*., Mol. Cryst. Liq. Cryst*., **2003**, 396, 177; Chandrasekhar, S., Geetha Nair, G., Shankar Rao, D. S., Krishna Prasad, S., Praefcke K., Blunk, D., *Curr. Sci*, **1998**, 75, 1042.
[32] Galerne, Y., *Mol. Crys. Liq. Cryst.* **1998**, 323, 211.
[33] Merkel, K.,Kocot, A., Vij, J. K., Korlacki, R., Mehl, G. H., Meyer, T., *Phys. Rev. Lett.*, **2004**, 93, 237801.
[34] Luckhurst, G. R., *Nature*, **2004**, 430, 413.
[35] Pratibha, R., Madhusudana, N. V., Sadashiva, B. K., *Science*, **2000**, 288, 2184; (b) Pratibha, R., Madhusudana, N. V., Sadashiva, B. K., *Mol. Cryst. Liq. Cryst.,* **2001**, 365, 755; (c) Pratibha, R., Madhusudana, N. V., Sadashiva, B. K., *Phys. Rev. E,* **2005**, 71, 011701. (d) Hegmann, T., Kain, J., Diele, S., Pelzl, G., Tschierske, C. *Angew. Chem. Intl. Ed.* **2001**, 40, 887.
[36] Vörlander, D. *Ver. Dtsch. Chem. Ges.* **1929**, 62 2831; Vörlander, D., Apel, A. *Ver. Dtsch. Chem. Ges.* **1932**, 65 1101.

synthesis of new bent core molecules in 1991[37] and discussed the special properties that these molecules could present. The most remarkable result came in 1996 when Niori *et. al*.[38] reached the switching of such molecules, obtaining polar phases. This has been the experimental proof that molecules incorporating bent-shaped rigid core instead of a linear one could show polar order and chiral superstructures[39] in their LC mesophases, despite the absence of chirality in the molecules and confirming models proposing that molecular chirality is not necessary for ferroelectricity.[40] This breakthrough concerning macroscopic polar order[41] and chirality provoked inmediatly a great interest and became a major topic in liquid crystal research.

The nomenclature of such phases was discussed in a workshop held in 1997 at Berlin: the letter B indicates that this phase is made of banana shaped molecules, followed by a number indicating the type of mesophase.[42] Bent-core molecules can be classified as well into the previously described mesophase families (Sm, Col).

B1: In some mesophases of bent-core compounds, partial layer collapse leads to ribbon like segments of smectic layers and rearrangement of the molecules in adjacent ribbons is antiparallel, avoiding the system to present spontaneous polar order. This effect generates undulated polar smectics (SmÃP, SmC̃P: P letter indicates polar), which can be alternatively seen as a columnar phase into a 2D lattice with an orientational correlation between the ribbons. If this orientation is nontilted and the

---

[37] Kuboshita, M., Matsunaga, Y., Matsuzaki, H. *Mol. Cryst. Liq. Cryst.* **1991**, 199, 319.
Matzusaki, H. And Matsunaga, Y., *Liq. Cryst.* **1993**, 14, 105.
Akutagawa,, T., Matsunaga, Y., Yasuhara, K. *Liq. Cryst.* **1994**, 17, 659.
[38] Niori, T., Sekine, T., Watanabe, J., Furukawa, T., Takezoe, H., *J. Mater. Chem.* **1996**, 6, 1231.
[39] Sekine, T., Niori, T., Watanabe, J., Furukawa, T., Choi, S. W., Takezoe, H., *J. Mater. Chem.*, **1997**, 8, 1307.
[40] Petschek, R. G., Wiefling, K. M., *Phys. Rev. Lett.*, **1987**, 59, 343; R. H. Tredgold, *J. Phys. D*, **1990**, 23, 119; Photinos, D. J., Samulski, E. T., *Science*, **1995**, 270, 783.
[41] Blinov, L. M., *Liq. Cryst.*, **1998**, 24, 143
[42] ''Banana-shaped Liquid Crystals: Chirality by Achiral Molecules'' held in Berlin in December **1997**, B8 was added later.

polar vectors are parallel to the lattice, the columnar rectangular phase is classified as B1 (presented for the molecule 1 in figure 1.2). In the case that nontilted molecules polar vector is perpendicular to the lattice, the $B1_{rev}$ [43] is generated. Finally, $B1_{revtilt}$[44] phase is the $B1_{rev}$ with tilted molecules. In both cases, polarization switching process remains irreversible for $B1_{rev}$ and very difficult for $B1_{revtilt}$.[44]

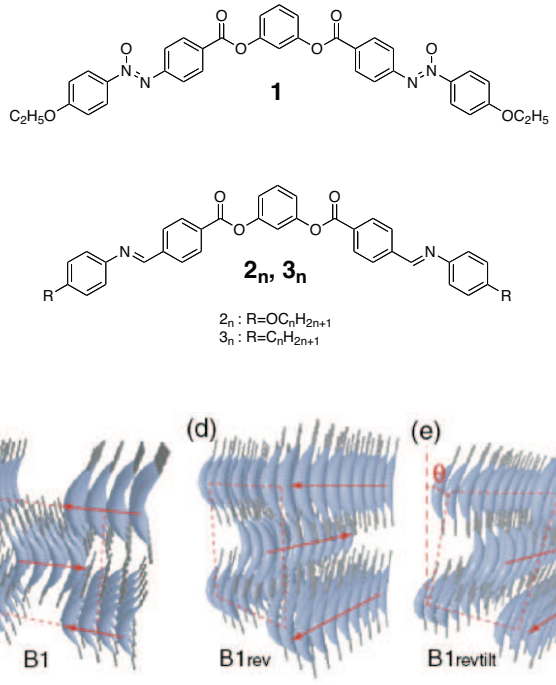

Figure 1.2. Top: Compounds exhibiting B1 mesophase. The compound **1** was synthesized by Vörlander; **2** and **3** are the first synthesized compound series by Matsunaga's group. Bottom: Types of the different B1 mesophases.[45] The arrows indicate the polar vector direction.

B2: This mesophase is undoubtedly, the most studied (and most observed) of all the Bx family. It was first observed by Niori,[46] the ferroelectric-like switching current being due to the spontaneous polarization connected to the molecules in a smectic

[43] Shen, D., Pegenau, A., Diele, S., Wirth, I., Tschierske, C. *J. Am. Chem. Soc.* **2000**, 122, 1593.
[44] Szydlowska, J., Mieczkowski, J., Matraszek, J., Bruce, D. W., Gorecka, E., Pociecha, D., Guillon, D.: *Phys. Rev. E* **2003**, 67, 031702.
[45] Takezoe, H., Takanishi, Y. *Jpn. J. Appl. Phys.*, **2006**, Vol. 45, No. 2A.
[46] Niori, T., Sekine, T., Watanabe, J., Furukawa T., Takezoe, H. Abstract 16th Int. Liquid Crystal Conf., **1996**, Kent, p. 126.

layer with a unique bending direction along a C_{2v} symmetry axis. Lately, Weissflog *et al.*[47] and Hepke and coworkers,[48] have found the antiferroelectric-like switching in similar systems. Link *et al.*[49] confirmed the molecular tilting of the molecules with respect to the layer normal by careful electrooptical investigations. More clearly, layers undulation does not happen, giving rise to different smectic layers with particular reduced symmetry. Since the molecules are tilted and polar, the previously evoked synclinal or anticlinal subscript is added. Hence, the mesophase presents two options: SmC_aP and SmC_sP. As already mentioned, polar phases are not stable and this mesophase strategy to escape from polarity is the alternating of the layer polar vectors, which generates, considering the layer clinicity, four different variants of this mesophase: the alternated layers, in which the polar vectors from adjacent layers are antiparallel (antiferoelectric), or parallel aligned polar vectors in neighboring layers (ferroelectric) as illustrated in figure 1.3. As another interesting factor, two of the conformational possibilities present an additional mirror plane that allows chirality, which can be explained in terms of coil helicity as exhibited in Folcia's molecules.[53]

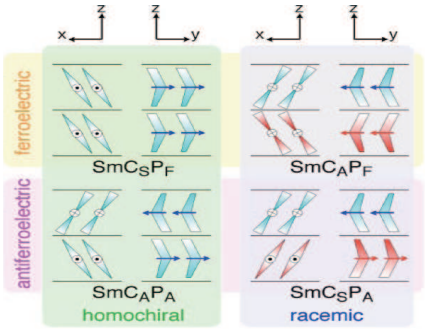

Figure 1.3. Switching possibilities of B2 phase.[45]

[47] Weissflog, W., Lischka, C., Benne, I., Scharf, T., Pelzl, G., Diele, S., Kruth, H., *Proc. SPIE 3319,* ***1998***. 14.
[48] Heppke, G., Krüerke, D., Löhning, C., Lötzsch, D., Rauch, S., Sharma, N. K., presented at Feributuger Arbeitstagung Flüssige Kristalle, **1997**, Freiburg.
[49] Link, D. R., Natale, G., Shao, R., Maclennan, J. E., Clark, N. A., Körblova E., Walba, D. M., *Science* , **1997**, 278, 1924.

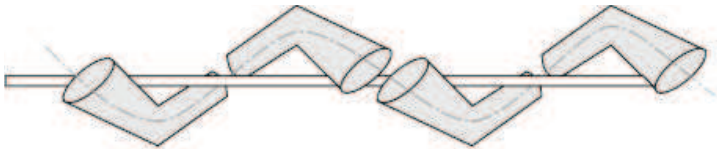

Figure 1.4. Explanation of the origin of chirality in homochiral B2 (SmC_AP_A) phase of achiral bent-core molecules, proposed by Ortega et al.[50]

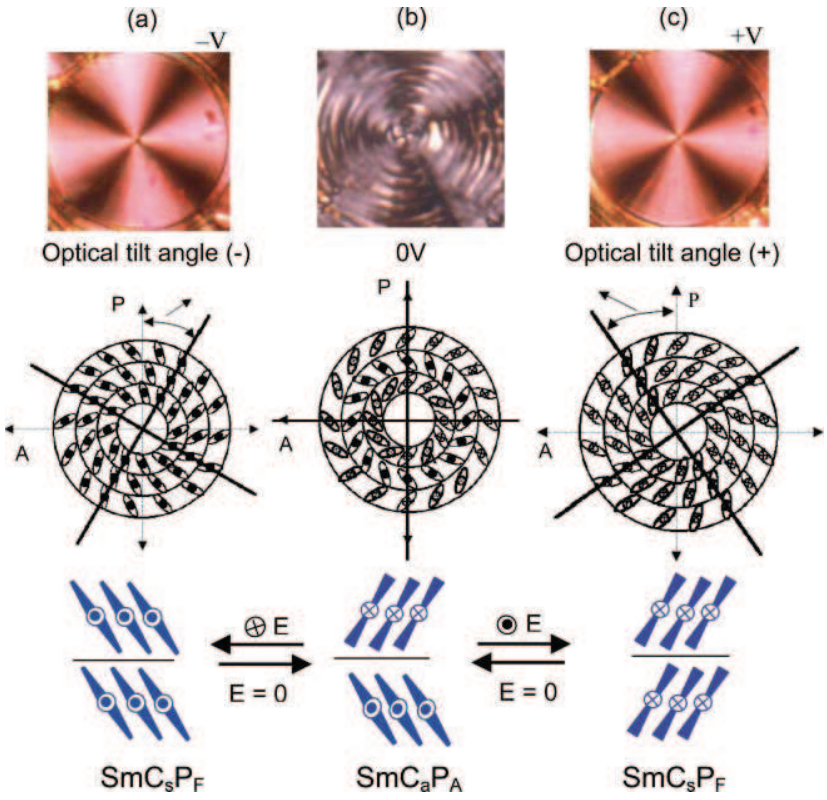

Scheme 1.8. Explanation of the molecular switching observed by polarizing microscopy.[11]

B3: is considered as a higher order (soft crystalline) smectic phase. It appears when the sample is rapidly cooled from the B2 mesophase. It frequently appears between B2 and B4. It also presents a fan-like texture as the B2 phase, but with broken

[50] Ortega, J., Folcia, C. L., Etxebarria, J., Gimeno N., and Ros., M. B. *Phys. Rev. E* **2003**, 68, 011707.

domains. Ferroelectric-like switching current indicating large spontaneous polarization was observed in spite of no electrooptic response.[51] However it remains stills doubtful due to a lack of confirmation[52] of initially observed second harmonic generation (SHG). [53] X-ray studies performed on this mesophase indicate layer spacing shorter than B2,[48] which remains close to that in the crystal state.

B4: Presenting similar properties than the previously mentioned blue phases, this phase is observed under a polarizing microscope as transparent dark-blue-colored domains, explained in terms of selective reflection due to a helical structure similar to a TGB mesophase. X-ray studies showed nontilting of the molecules and indicating high layer correlation (several orders of the layering reflections).[54] 2D patterns performed on such samples[55] also showed small angle reflections corresponding to deformed layers that reinforce the TGB model, opposite to B2 mesophase.

The model for this mesophase, is still in discussion. It consists basically in smectic slabs organized along a helical structure (Scheme 1.9), allowing the system to cancel the polarization on a macroscopic scale. As an additional fact, the macroscopically observed helix handedness, allows to add a term of supramolecular chirality due to spontaneous desymmetrization[56] ([*]) towards the mesophase *i.e*. B4[*].[57]

---

51 Sekine, T., Takanishi, Y., Niori, T., Watanabe, J., Takezoe, H., *Jpn. J. Appl. Phys.* **1997,** 36, L1201.
52 Kentischer, F., Macdonald, R., Warnick, P., Heppke, G. *Liq. Cryst.* **1998**, 25, 341.
53 Choi, S. W., Watanabe, J., Takezoe, H., *Jpn. J. Appl. Phys.* **1998**, 37, 3408.
54 Sekine, T., Niori, T., Sone, M., Watanabe, J., Choi, S. W., Takanishi, Y., Takezoe, H., *Jpn. J. Appl. Phys.* **1997**, 36, 6455.
55 Thisayukta, J., Takezoe, H., Watanabe, J., *Jpn. J. Appl. Phys.* **2001**, 40, 3277; Saletnikova, J., Schalfuss, H., Nadasi, H., Weissflog, W., Kresse, H., *Liq. Cryst.* **2000**, 27, 1663.
56 Walba, D. M., in Topics in Stereochemistry, ed. M. M. Green, R. J. M. Nolte, E. W. Meijer, Wiley, 2003, vol. 42, p. 475; Avalos, M. Babiano, R., Cintas, P., Jimenez, J. L., Palacios, J. C., *Tetrahedron: Asymmetry,* **2004**, 15, 3171.
57 This supramolecular chiralty have been also observed in supermolecules containing chiral moieties, discussing the supramolecular helicity in systems such as sesquioligosiloxane and fullerene derivatives.

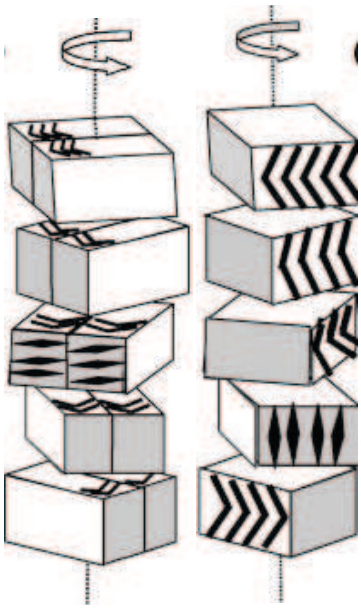

Scheme 1.9. Different models proposed for B4 mesophase.[11]

B5: There exist only few structures presenting this mesophase,[22,58] most of them observed in bent core series substituted in position 2 with a methyl group (compounds 4 and 5_n) or a fluorine atom in position 5 (compounds 6_n) or a rigid moiety central phenol and outer aromatic rings (scheme 1.10). As for B2 mesophase family, antiferroelectric and ferroelectric switching of this mesophase is also possible. In the case of the ferroelectric switching, the structure indicates synclinic layers justified by the observation of out-of-layer fluctuations of terminal chains,[58c] leading to propose the structure depicted in scheme 1.10. On the other hand, antiferroelectric switching strongly suggests anticlinicity of the layers. Further studies are necessary to solve the structure accurately.[45]

Goodby, J. W., Sáez, I. M., Cowling, S. J., Görtz, V., Drapper, M., Hall, A. W., Sia, S., Cosquer, G., Lee, S., Raynes, E.P., *Angew. Chem. Intl. Ed. Eng.*, **2008**, 47, 275.

[58] (a) Svoboda, J., Novotna, V., Kozmik, V., Glogarova, M., Weissflog, W., Diele, S., Pelzl, G., *J. Mater. Chem.,* **2003**, 13, 2104. (b) Diele, S., Grande, H., Kruth, H., Lischka, C., Pelzl, G., Weissflog, W., Wirth, I., *Ferroelectrics,* **1998**, 212, 169; (c) Nadasi, H., Weissflog, W., Eremin, A., Pelzl, G., Diele, S., Das, B., Grande, S., *J. Mater. Chem.,* **2002**, 12, 1316.

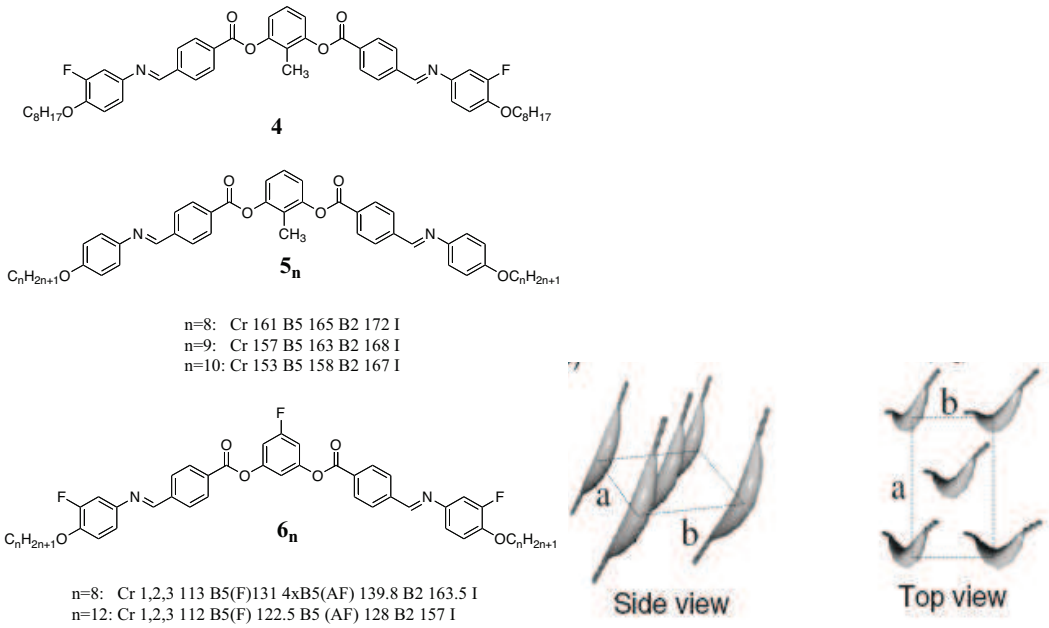

Scheme 1.10. Left: molecules presenting B5 mesophases. Right: cell model of B5 mesophase.[45]

B6: When layer ondulation occurs as previously discussed for B1 mesophase genesis and undergoes to the extreme case of layer interdigitation, B6 mesophase is generated. Observed by polarized light microscopy, the characteristic texture is similar to that corresponding to a SmA mesophase. Tilting of the molecules is still unclear[59], which settles two different subcategories: untilted molecules through interpenetrated layers, described as a SmA_c (texture of the scheme 1.11) or tilted molecules within interpenetrated networks (SmC_c).[23]

[59] There exist discrepancy about the molecular tilting according to Takezoe's Group, whereas Halle groups approve the tilted and nontilted mesophases. See references 48, p 604 and reference 63, table 1.

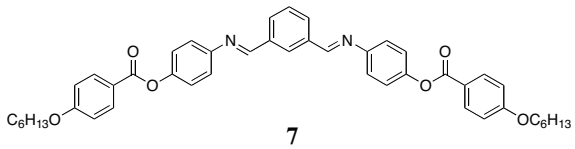

7

Cr 134 B1 142 B6 148 I

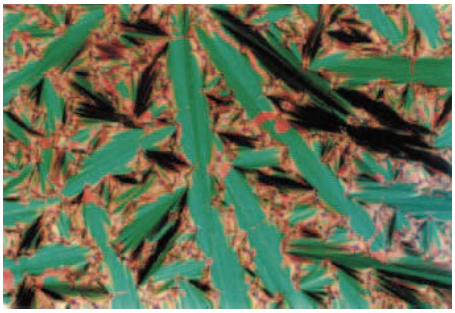

Scheme 1.11. Top: Molecule presenting B6 mesophase; Bottom left: typical texture of B6 mesophase; Bottom right: model proposed for this mesophase.[45]

B7: Perhaps the most attractive feature of this phase is the wide number of textures that it presents. It was observed first by molecules constituted by a 2-nitroresorcinol central ring, (also called the bay position),[60] as well as by 2-cyanoresorcinol derivatives.[61]

Microphotographs of this mesophase are described in which the most typical is the spiral filament when cooled from isotropic state. Jákli and coworkers reported that: 1) left and right handednesses of the helical strands exist equally and 2) the strands consist of single, double or triple coils (Figure 1.5 top right).[62] Also described in reference 66, this mesophase presents ferroelectric–like electrooptical switching at temperatures just below iso-B7 phase transition, but it suddenly changes to a tristable switching as temperature decreases. Similarly, bistable switching has been observed

[60] Weissflog, W., Nadasi, H., Dunemann, U., Pelzl, G., Diele, S., Eremin, A., Kresse, H., *J. Mater. Chem.*, **2001**, 11, 2748.
[61] Shreenivasa Murthy H. N., Sadashiva, B. K., *Liq. Cryst.*, **2003**, 30, 1051.
[62] Jákli, A., Lischka, C., Weissflog, W., Pelzl, G., Saupe, A., *Liq. Cryst.* **2000**, 27 1405.

in fluorine containing compounds.[63] Of interest, B7 phases present middle angle reflections in X-ray diffraction patterns. Undulated-modulated variants of such mesophase is called B7' when this mesophase consists of bent-core molecules bearing one[64] or two chiral aliphatic chains. Bistable ferroelectric-like behavior was observed in both optoelectronic and current profile. This behavior was directly associated to two kinds of surface-stabilized molecular orientational states, observed in the absence of the field. Sophisticated studies performed by Coleman et al. such as synchroton X-ray, microbeam, freeze fracture electron microscopy and careful optical observations lead them to propose a model for such B7' phase characterized by an undulated structure of a synclinic ferroelectric smectic phase ($U^{m}SmC_{s}P_{F}$) illustrated in figure 1.5.[65] In this case, the system escape from the macroscopic polar order, through a splay of the polarization, giving rise to a layer modulation with stripe defects (splay defects). The layers are slightly thicker along these defects and between them and this leads to an additional modulation of the layers (modulated-undulated). Recent propositions consist of local tetrahedral symmetry defects delimitating the helical zone formation.[66]

---

[63] Bedel, J. P., Rouillon, J. C., Marcerou, J. P., Laguerre, M., Nguyen, H. T., Achard, M. F., *J. Mater. Chem.* **2002**, 12, 2214.
[64] Bedel, J. P., Rouillon, J. C., Marcerou, J. P., Laguerre, M., Achard M. F., Nguyen, H. T., *Liq. Cryst.* **2000**, 27, 103.
[65] Coleman, D. A., Fernsler, J., Chattham, N., Nakata, M., Takanishi, Y., Körblova, E., Link, D. R., Shao, R.-F., Jang, W. G., Maclennan, J. E., Mondainn-Monval, O., Boyer, C., Weissflog, W., Pelzl, G., Chien, L.-C., Zasadzinski, J., Watanabe, J., Walba, D. M., Takezoe, H., Clark, N. A., *Science* **2003**, 301, 1204.
[66] Cladis, P.E. *C. R. Chimie,* **2008**, 11, 207.

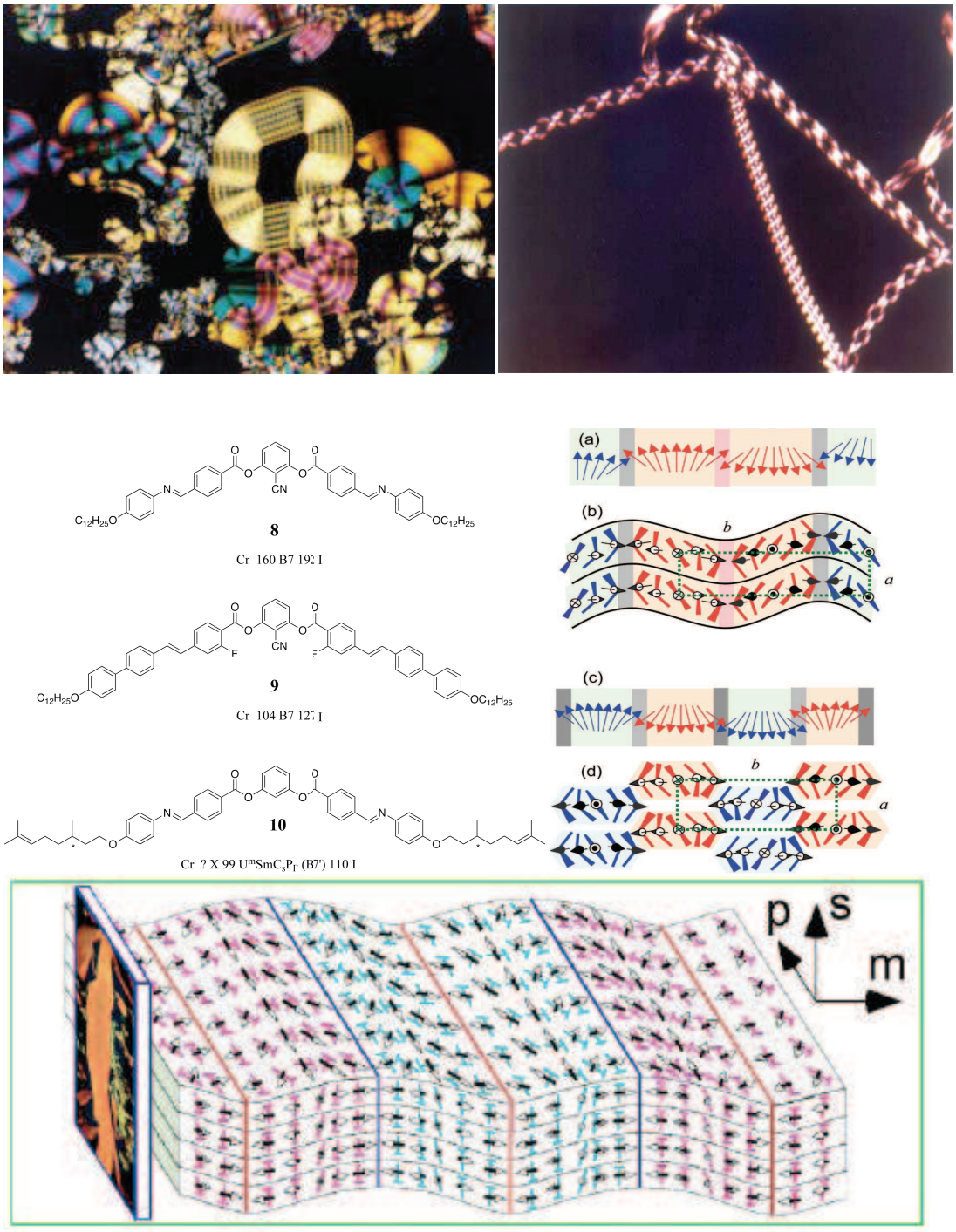

Figure 1.5. Top left: Texture of B7 mesophase; Top Right: Helical structures of B7 mesophase[23]; middle left: compounds presenting B7 and B7' mesophases; middle right: splay defects generating undulation-modulation of layers in B7' structure;[11] Bottom: Proposed model for B7' mesophase.[45]

1.2. Polymers and Elastomers.

1.2.1. *Definition:*

"An elastomer is a natural or synthetic polymeric system that possesses elasticity also known as rubber".

There are many rubber materials in nature, the oldest example being the natural rubber obtained by the olmec civilization. It has been obtained from the latex extracted from the *Castilla elastica* tree and by mixing it with the juice of *Ipomoea alba* to create an ancient rubber as early as 1600 BC.

Figure 1.6. Castilla elastica[67] (left) and Ipomea Alba (right)[68].

The first reference to rubber in Europe appears in the late 18th; it was first used as an eraser. The rubber applications were limited mainly because they were not standing up to extreme temperatures, becoming brittle in winter and liquid-like in summer. During the 1830's, many inventors tried to develop a rubber product that could last

[67] http://www.correodelmaestro.com/anteriores/2003/marzo/1anteaula82.htm
[68] http://gardenbreizh.org/photos/fer/photo-3045.html

year-round. Charles Goodyear was one of those inventors, whose research "masterpiece" was the vulcanization process[69]. In 1843, Charles Goodyear discovered that by treating the rubber with sulphur and then heating it, the material retained its elasticity becoming waterproof and winter-proof. By analyzing the process with a chemist's eye, it can be appreciated that sulphur crosslinks the polymer strands, generating an insoluble network,[70] presenting a rather lower glass transition temperature yet remaining with rubber-elastic. The concept of the glass transition temperature will be described in chapter 3.

Concerning the rubber elasticity phenomena, Kuhn studied the entropy of the process and the influence of the swelling of such a system[71] that will be discussed later.

1.2.2. *Polymerization Techniques*

There exist several polymerization methods available, some of them being briefly discussed below:

Condensation or step-growth polymerization. Step-growth polymerization is mainly used for monomers with functional groups such as -OH, -COOH etc. It is usually a succession of non-catalyzed, chemical condensation reactions associated with the elimination of low-molar-mass side-products. One of the most ancient polymers synthesized via this method was bakelite (Figure 1.6).

---

[69] inventors.about.com/od/gstartinventors/a/CharlesGoodyear.htm
[70] Green, M. M., Wittcoff, H. A., "Organic Chemistry Principles and Industrial Practice" Wiley VCH, **2003**.
[71] Kuhn, W., Hargitai, B., Katchalsky, A., Eisenberg, H., *Nature*, **1950**, 165, 514.

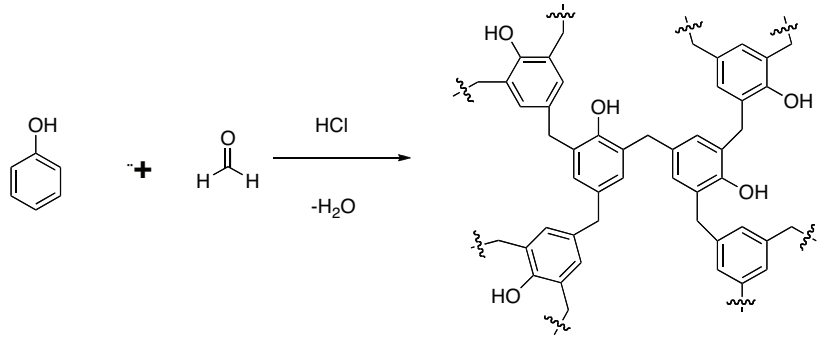

Scheme 1.12. Synthesis of Bakelite.

Addition polymerization. Usually, addition polymerizations involve the polymerization of olefinic monomers. Polymerization occurs via a chain reaction. The monomers are converted into polymers by opening of the double bond with a free radical or ionic initiator. The product, then, unlike the one obtained from step-growth polymerization, has the same chemical composition as the starting monomer. It can be catalyzed by base, or acid, depending on the growing type as living or controlled. An example is illustrated in scheme 1.13.

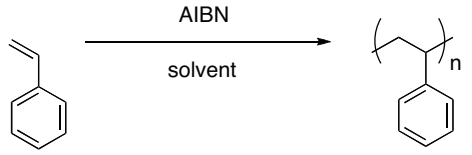

Scheme 1.13. Example of free radical addition polymerization of styrene.

Insertion polymerization. Generally, insertion polymerizations involve the polymerization of olefinic monomers. It consists of the insertion of a monomer at the end of the growing chain, mediated by a catalyst. The catalyst stays at the end of the growing chain. Polymers synthesized by insertion polymerization are typically characterized by a very high stereo regularity. An example for such a polymerization

technique is the Ziegler-Natta polymerization (Scheme 1.14). Another example is the "metathesis" polymerization.

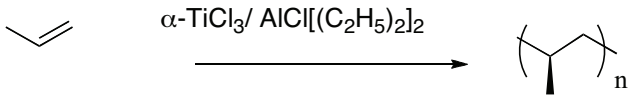

Scheme 1.14. Ziegler Natta polymerization of propylene.

When these types of macromolecules contain liquid crystalline moieties in their structure, the resulting novel species are denominated liquid crystalline polymers.

1.3. Liquid Crystalline Polymers and Elastomers.

1.3.1. *Definition and Classifications*

Liquid crystalline polymers (LCP) are a class of materials that combine the properties of polymers with those of liquid crystals. These macromolecular "hybrids" show the same mesophases characteristic of ordinary liquid crystals; yet they retain many of the useful and versatile properties of polymers. In order for normally flexible polymers to display liquid crystal characteristics, rod-like or disk-like mesogenic elements must be incorporated into the chains. The location of the mesogens plays an important role in determining the type of LCP that is formed. Main-chain liquid crystalline polymers (MC-LCPs) are formed when the mesogens are themselves part of the main chain of a polymer. Conversely, side chain liquid crystalline polymers (SC-LCPs) are formed when the mesogens are connected as side groups to the polymer by a flexible "bridge" called the spacer. Moreover, the side groups can be linked either laterally (side-on) or terminally (end-on) to the polymer backbone. The three different LCP families are schematized in figure 1.7.

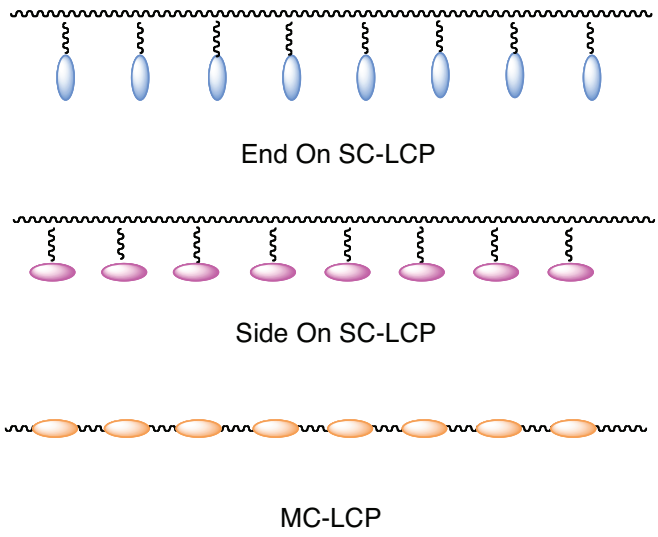

Figure 1.7. The three main families of LCP.

1.3.2. *Chronology*

The first liquid crystalline polymer reported was the poly (N-Benzyl)glutamate prepared by Elliot and co-workers.[72] This pioneering work was later followed by many other polymers such as Kevlar aramid, developed by DuPont industries in 1965.[73] This one was a lyotropic LCP in the presence of concentrated sulphuric acid during its extrusion. In 1975, P.G. de Gennes published an article about networks LCPs,[74] and proposed a deformable material without constraint, perhaps the most remarkable property of liquid crystalline elastomers. Based on both Kuhn and de Gennes concepts, H. Finkelmann's group succeeded in the synthesis of the first side-chain liquid crystalline elastomer, i.e. weakly reticulated polymer network, in 1981.[75] But the initial material was not permanently oriented until Kupfer *et al.*[76] obtained the first oriented LCE, denominated as liquid single crystal elastomer (LSCE). Despite

[72] Elliot, A.; Ambrose, E., *Discuss. Faraday Soc.,* **1950**, 9, 246.
[73] D. Tanner, J. A. Fitzgerald, B. R. Phillips., *Angew. Chem. Intl. Ed.,* **1989**, 28, 649.
[74] De Gennes, P.-G., *C. R. Scéances Acad. Sci. Ser. B,* **1975**, 281, 101.
[75] Finkelmann, H.; Kock, H.; Rehage, G., *Makromol. Rapid Commun.* **1981**, 2, 317.
[76] Kupfer, J.; Finkelmann, H., *Macromol. Chem. Rapid Commun.* **1991**, 12, 717.

the vertiginous development of this novel domain, the only type of LCE conceived was the side chain one. Once that the orientation problem was solved, they started to modulate mesomorphism and studied nematic, smectic and more recently, cholesteric[77] phases.

The limiting factors to study LCEs are the high clearing temperatures, because the actually conceived devices do not work at such high temperatures. To solve this problem, V. Percec[78] made a complete series of MC-LCP (Figure 1.7) in which chain lengths between rigid moieties (letter ***m*** in figure 1.8) varied from 4-20 carbon atoms. Polymers with ***m*** ranging from 4-10 exhibited high temperature nematic phases, whereas polymers with ***m*** from 13 to 17 presented a low temperature nematic phase. Derived from these series, the first main-chain liquid elastomer was synthesized by cross-linking these polymers.[79]

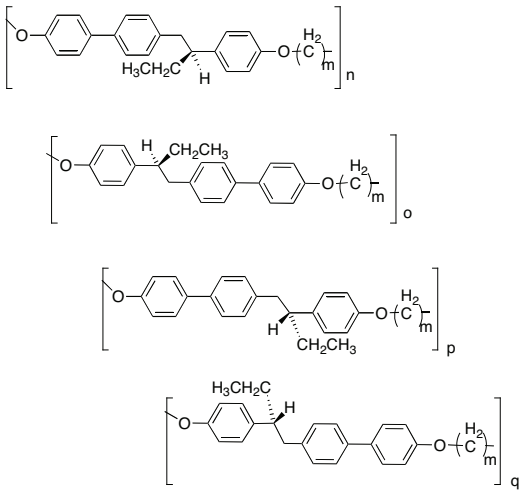

Figure 1.8. LCPs synthesized by Percec's group

[77] Kim, S.; Finkelmann, H., *Macromol. Rapid Commun.* **2001**, 22, 429.
[78] Percec, V.; Kawasumi, M., *Macromolecules* **1991**, 24, 6318.
[79] Bergmann, G.; Finkelmann, H.; Percec, V.; Zhao, M., *Macromol. Rapid Commun.* **1997**, 18 (5), 353.

A breakthrough was set by Donnio *et. al*[80] by changing the MC-LCE preparation steps for a one pot synthesis and thus to access to a large library of elastomers and this approach allowed to obtain suitable materials in a shorter time and permitted to perform systematic studies on the influence of the crosslinker concentration on system's rigidity. Nowadays, this method is actually considered as the best and the cheapest route for MC-LCE synthesis.

Another group interested in this family of liquid crystalline elastomers is undoubtedly the Terentjev and Warner group at Cambridge, who obtained a high-tech formulated MC-LCE that present the highest Young Modulus reported for a LCE. They based their MCLCEs on the polymers synthesized by Finkelmann.

Opposite to the general opinion, many developments have been done since the first one pot reaction, from photoactive MC-LCE's, composites with carbon nanotubes[81] and nanoparticles,[82] and photo crosslinked MC-LCEs[83] obtained by the traditional orientation and electrospraying.[83b.]

Parallel to this LCE characterization rush, groups from Drexel and Halle universities had worked with discrete molecular, and polymer chemistry to achieve interesting, novel dimers,[84] dendrimers[85] and polymers based on bent-core molecules.

---

80 Donnio, B.; Wermter, H.; Finkelmann, H., *Macromolecules* **2000,** 33, (21), 7724.
81 Courty, S., Mine, J., Tajbakhsh, A.R., Terentjev, E.M. *Cond. Mat.* Sep **2003**, 0309216. 1-19.
82 Chambers, M.,Zalar, B., Remskar, M., Zumer, S., Finkelmann, H. *Appl. Phys. Lett.* **2006**, 89, 243116.
83 a) Beyer, P., Terentjev, E.M., Zentel, R. *Macromol. Rapid Commun.* **2007**, 28, 1485; b) Krause, S., Dersch, R., Wendorff, J., Finkelmann, H. *Macromol. Rapid Commun.* **2007**, 28, 2062.
84 Kosata, B., Tamba, G. M., Baumeister, U., Pelz, K., Diele, S., Pelzl, G., Galli, G., Samaritani, S., Agina, E. V., Boiko, N. I., Shibaev, V. P., Weissflog, W., *Chem. Mater.,* **2006,** 18, (3), 691.
85 Keith, C., Dantlgraber, G., Reddy, R. A., Baumeister, U., Prehm, M., Hahn, H., Lang, H., Tschierske, C., *J. Mater. Chem.,* **2007,** 17, (36), 3796.

Tschierske's group had studied the switching of B2 SmCP in oligosiloxane dimers by applying triangular voltage[86] and Tenneti, synthesized and studied mesomorphism presented by end-on[87] and side-on[88] (jacketed) SC BCLCP and main-chain polymers.[89] Surprisingly however, there is no report of banana-containing MC-LCE but, by a suitable design of the molecules, an adequate polymerization technique and a good curing process it could be possible to obtain a switchable phase LCE.

Some attempts have been made by investigating different chain topography[90] and supramolecular architectures,[91,92] but most of them with low yields, low quantities,[93] lack of characterization and loss of properties.

In order to understand LCEs, we have first to describe their mechanical behavior, which is discussed next.

1.3.3. *Elastic Behavior*

The elastic behavior of classical elastomers can be explained by using statistical thermodynamics considering that polymeric chains have infinite length.

Rubber materials show an elastic behavior quite different from those of solids. Opposite to metals that resist to the stretching and bending by increasing the internal

---

86 Achten, R., Koudijs, A., Giesbers, M., Reddy, R. A., Verhulst, T., Tschierske, C., Marcelis, A. T. M., Sudholter, E. J. R., *Liq. Cryst.,* **2006,** 33, (6), 681

87 Chen, X. F., Tenneti, K. K., Li, C. Y., Bai, Y. W., Wan, X. H., Fan, X. H., Zhou, Q. F., Rong, L. X., Hsiao, B. S., *Macromolecules,* **2007,** 40, (4), 840.

88 Chen, X. F., Tenneti, K. K., Li, C. Y., Bai, Y. W., Zhou, R., Wan, X. H., Fan, X. H., Zhou, Q. F., *Macromolecules,* **2006,** 39, (2), 517.

89 Choi, E. J., Ahn, J. C., Chien, L. C., Lec, C. K., Zin, W. C., Kim, D. C., Shin, S. T., *Macromolecules,* **2004,** 37, (1), 71.

90 Jeong, K. U., Knapp, B. S., Ge, J. J., Jin, S., Graham, M. J., Xiong, H. M., Harris, F. W., Cheng, S. Z. D., *Macromolecules,* **2005,** 38, (20), 8333.

91 Tenneti, K. K., Chen, X. F., Li, C. Y., Wan, X. H., Fan, X. H., Zhou, Q. F., Rong, L. X., Hsiao, B. S., *Macromolecules,* **2007,** 40, (14), 5095.

92 Barbera, J., Gimeno, N., Pintre, I., Ros, M. B., Serrano, J. L., *Chem. Comm.,* **2006**, (11), 1212.

93 Gallastegui, J. A., Folcia, C. L., Etxebarria, J., Ortega, J., Gimeno, N., Ros, M. B., *J. Appl. Phys.,* **2005,** 98, (8), 083501.

energy, due to the positional change of their atoms face to face to the equilibrium position through the network, rubber elasticity comes together with a decrease of the entropy at the moment of stretching, due to the loss of the possible conformations of the polymer chains. It is necessary to state that the extensions reported for rubber materials are considerably higher (up to 10 times from the original length)[94] than those obtained for metals, hence, there are many possible intermediate states with equivalent energy for a partially stretched polymer chain.

To study this phenomenon, we can use the Boltzmann equation for the entropy S

$$S = k \ln \Omega \tag{1.1}$$

where k is the Boltzmann constant, and Ω the number of possible energy states. When Ω is maximized and the number of particles, the energy of the system and the volume are kept constant, we obtain the maximum entropy state, which is the equilibrium state of the system.[95] Thus it is assumed that a spontaneous shrinking of a rubber is expected after a stretching because it is statistically "preferred". In fact, the more stretched, the lower the number of possible conformations and higher the probability to keep a given conformation in this state.

This behavior is opposite to that presented by gases, but it can be explained by justifying the fact that the entropy is proportional to the volume, and in our case, by stretching the rubber, we keep the volume constant. So, the material does not present

[94] Ward, I. M., *An introduction to the mechanical properties of solid polymers*, John Wiley & Sons, **1993**.
[95] Alberty, R.; Silbey, R., *Physical chemistry (2nd edition)*, John Wiley &Sons, 1997.

dilatation and the length variation is compensated by the reduction of the cross section.[96]

$$F = U - TS \tag{1.2}$$

Based on this analogy, theoreticians started to use statistical thermodynamics to describe rubber elasticity; the state function of the Helmholtz free energy F is described as:

$$F = U - kT\ln(\Omega(r,T)) \tag{1.3}$$

where Ω is a function of the number of energetic states all along both ends of the chain r at a T temperature. The derivatization of this expression with respect to distance r gives the elastic force f.[97]

$$f = \left(\frac{\partial F}{\partial r}\right)_{T,V} = -kT\left(\frac{\partial \ln \Omega(r,T)}{\partial r}\right)_{T,V} \tag{1.4}$$

If we consider the probability to find at a given distance between the ends of the polymer chain between fixed points r and $r + dr$ as a Gaussian distribution it is assumed as:

$$f = \frac{3kTr}{\bar{r}_0^2} \tag{1.5}$$

here $\bar{r}_0^2$ represents the squared of the mean distance between both chain ends. This expression is relative to the contraction's force of a single chain. Considering the hypothesis of a slight deformation of an elastomer, $\bar{r}_0^2$ between two cross-linking points under stress is given by:

---

[96] Gordon, M., *High Polymers, Structure and Physical Properties*, Ilife Books, London, 1968.
[97] Sperling, L. H., *Introduction to Physical Polymer Science (2nd edition)*, John Wiley & Sons, **1992**.

$$\bar{r}^2 = \frac{1}{3}\left(\lambda_x^2 + \lambda_y^2 + \lambda_z^2\right)\bar{r}_0^2 \tag{1.6}$$

Where λ is the length ratio in a defined space direction, equal to *l*/*lo* (final length and initial length, respectively). Starting from the incompressibility condition:

$$\lambda_x \lambda_y \lambda_z = 1 \tag{1.7}$$

The chain stretching along the *z* axis is expressed:

$$\lambda_z = \lambda \text{ and } \lambda_x = \lambda_y = \frac{1}{\sqrt{\lambda}} \tag{1.8}$$

The integration of the relative elastic force of *n* stretched chains along the *z* axis gives another expression for the free energy variation:

$$\Delta F_{el} = \frac{nRT}{2}\left(\lambda^2 + \frac{2}{\lambda} - 3\right) \tag{1.9}$$

where *R* is the ideal gas constant and *n* can be substituted by ρ/M_c, where ρ is the density and M_c is the mean molar mass of the chains between crosslinking points.

The derivatization of the free energy function with respect to the temperature gives the stress:

$$\sigma = \left(\frac{\partial F}{\partial \lambda}\right)_{T,V} = nRT\left(\lambda - \frac{1}{\lambda^2}\right) \tag{1.10}$$

The Young Modulus *E* can be calculated from the variation of the stress with respect to the deformation:

$$E = \left(\frac{\partial \sigma}{\partial \lambda}\right)_{T,V} = nRT\left(1 + \frac{2}{\lambda^3}\right) \tag{1.11}$$

Note that for small elongations ($\lambda \sim 1$), the Young modulus is almost equal to $3nRT$.

And the shear modulus can be defined as a function of E by the following expression:

$$G = \frac{E}{2(1+\nu)} \tag{1.12}$$

where ν is the Poisson coefficient, which is ≈ 0.5 for a classic rubber without a change in volume. Thus, the relation becomes:

$$G \cong nRT \tag{1.13}$$

And the equation 1.10 can be rewritten as:

$$\sigma = G\left(\lambda - \frac{1}{\lambda^2}\right) \tag{1.14}$$

1.3.4. *Swelling Anisotropy*

An elastomer swells when immerged into a proper solvent. The solvent's molecules will fill the volume between the polymer chains, observed macroscopically as an increase of the material's volume; hence, the material becomes flexible and fragile. Network contraction is also expected when chain-chain and solvent-solvent interactions are preferred[98] over chain-solvent interactions. When the elastomer swells, the polymer chains start to stretch. This generates an elastic tension counteracting the swelling process until it reaches the equilibrium state. The free energy of the process associated to the mixture can be expressed as the sum of the mixture's free energy (ΔF_{ns}) and the nonstretched elastomer elastic free energy (ΔF_{el}).

[98] Walton, D., Lorimer, P. *Polymers*, Oxford Chemistry Primers, Oxford Science Publications, **2000**.

$$\Delta F = \Delta F_{ns} + \Delta F_{el} \tag{1.15}$$

We can define the swelling factor for each direction, α_x, α_y and α_z. This factor α can be calculated from the ratio between the dimensions in a given direction of an unswelled (L_{ns}) and a swelled material (L_s).

$$\alpha = \frac{L_s}{L_{ns}} \tag{1.16}$$

Obtaining a α value for the three dimensions allows to estimate the swelling factor q, which corresponds to the volume variation due to the absorption of a solvent.[99]

$$q = \alpha_x \alpha_y \alpha_z \tag{1.17}$$

Thus it can be expressed otherwise as:

$$q = \frac{V_s}{V_{ns}} \tag{1.18}$$

Another relation can be obtained when anisotropy is present in the elastomer. This equation will indicate the swelling anisotropy, which is defined as the rate of the swelling on the director axis (z in our case) and the swelling of another direction, expressed as:

$$q_z = \frac{\alpha_x}{\alpha_z} = \frac{\alpha_y}{\alpha_z} \tag{1.19}$$

Since:

[99]Wermter, H., Ph.D. thesis: *Flüssigkristalline Co-Elastomere: Synthese, Untersuchungen der mecanischen Eigenschaften, Direktororientierung und thermoelastisches Verhalten*, Albert-Ludwigs-Universität Freiburg i.B., **2001**.; Brandt, H., Ph.D. thesis *Statisch- und dynamisch-mecanische Untersuchungen an neuen flüssigkristallinen Hauptketten-Netzwerken*, Albert-Ludwigs-Universität Freiburg i. B., **2004**.

$$\alpha_x = \alpha_y \tag{1.20}$$

We can rewrite the swelling factor as:

$$q = \frac{V_s}{V_{ns}} = \alpha_x^2 \alpha_z \tag{1.21}$$

The crosslinking density of the elastomers can be determined by swelling experiments. In the swelling experiments, the average molar mass of the polymer chains in the network, M_c can be calculated by using the equation of the Flory's swelling theory.[100]

$$q_m^{5/3} \cong \left(\frac{V_{ns}}{\nu_e}\right)\left(\frac{0.5-\chi}{V_1}\right) = \left(\frac{M_C}{\rho}\right)\left(\frac{0.5-\chi}{V_1}\right) \tag{1.22}$$

with ν_e the effective number of network's chains in mol, r the density of the elastomer, V_1 the molar volume of the swelling liquid, q_m the swelling ratio, χ the Flory-Huggins parameter, which indicates the solvent-elastomer interactions and it varies depending of the polymer. To obtain this parameter, we are supposed to derivatize it from the second virial coefficient by using light-scattering experiments, which is specific for the solvent and the polymer. The estimation of this parameter is long and requires experiments and measurements that are beyond the scope of this thesis.

1.3.5. *Landau de Gennes theory*

The elastic behavior can also be studied by using a mechanical behavior model, like the one used for metals. By using tensorial calculations, Landau and Lifchitz[101]

[100] Flory, P. J., *J. Chem. Phys.*, **1977**, 66, 5720.
[101] Landau, L.; Lifchitz, E., *Théorie de l'élasticité*, Editions MIR, Moscou, **1967**.

proposed a model to explain phase transitions. Following this proposition, de Gennes developed some models to explain the mechanical behavior of LCEs at the nematic-isotropic transition.[102] To apply these models, an order parameter equal to zero for the isotropic phase, and greater than zero in the case of nematic phase must be defined. For this transition, we use the orientational order parameter (*S*).

In liquid crystals, the amount of order of the system is given by the average of the alignment direction of the mesogens with respect to the average director ($\vec{n}$) as illustrated in figure 1.9.

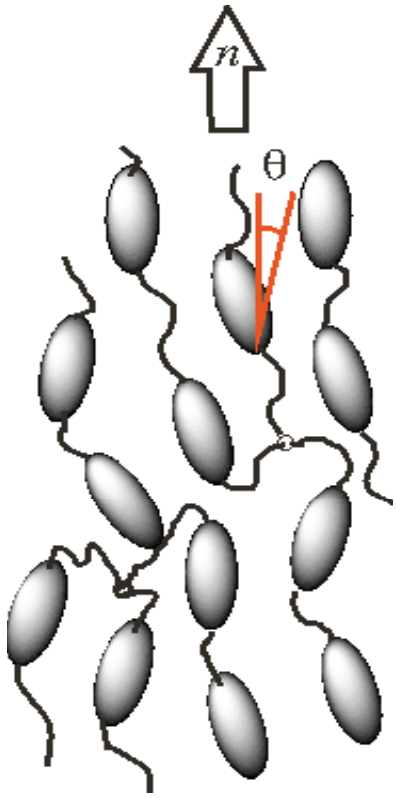

Figure 1.9. Representation of the mesogen's alignment (*n*) along a LCE.

The parameter *S* can be determined by X-ray diffraction of an aligned sample and is defined as:

[102] De Gennes, P., *Mol. Cryst. Liq. Cryst.* **1971**, 12, 193.

$$S = \frac{1}{2}\left\langle 3\cos^2\theta - 1 \right\rangle \tag{1.23}$$

If we consider a temperature range close to the clearing temperature, we can state that the S value is small, and then, describe the free energy as a function of a power series of S as:

$$F(S,T) = F_0(T) + \frac{1}{2}AS^2 + \frac{1}{2}BS^3\frac{1}{2}CS^4 + ... + \frac{1}{n}ZS^n \tag{1.24}$$

where $F_0(T)$ corresponds to the free energy in the isotropic phase. We can consider that the power terms larger than S^4 are negligible in the ordered LC phase.[102]

The A term defines the temperature at which the nematic-isotropic phase transition occurs. A can also be expressed as a linear function of temperature:

$$A(T) = A_0(T - T^*) \tag{1.25}$$

in which A_0 and T^* are constants (theoretical transition temperature between nematic and isotropic phases) slightly lower than the real T_{NI} by generally less than 1ºC.[102] Thus we can obtain the S values that minimize the free energy:

$$\frac{\partial F}{\partial S} = AS + BS^2 + CS^3 = 0 \tag{1.26}$$

By substituting the A linear function we obtain:

$$\frac{\partial F}{\partial S} = A_0(T - T^*)S + BS^2 + CS^3 = 0 \tag{1.27}$$

There are three solutions: one in which S is equal to zero and two others representing a maximum and a minimum. S = 0 corresponds to the value of S in the isotropic phase, and the corresponding energy is F_0. We derivatize once again the equation to

find the maximum, and then obtain the maximum S value for the temperature in which the free energy by volume unit between nematic and isotropic phases is the same:

$$\frac{\partial^2 F}{\partial S^2} = A_0(T - T^*) + 2BS + 3CS^2 = 0 \tag{1.28}$$

Hence we obtain:

$$S(T_c) = -\frac{2B}{3C} \tag{1.29}$$

$$A_0(T - T^*) = -\frac{2B^2}{9C} \tag{1.30}$$

So we can settle the next relation:

$$T_{NI} = T^* + \frac{2B^2}{9CA_0} \tag{1.31}$$

The isotropic-nematic transition is first order and is explained as a discontinuous variation of S with respect to temperature. Close to the transition, it exists however a critical behavior, typical from a second order transition at T^*, which can be interpreted as the temperature in which the isotropic phase becomes thermodynamically unstable and mathematically, we can consider it as the lower limit temperature at which the isotropic phase can be cooled. At the same time we can settle the limit temperature at which a nematic phase can be heated (equation 1.32)

$$T_{NI} = T^* + \frac{B^2}{4CA_0} \tag{1.32}$$

The parallel existence of these two temperatures justifies also the experimentally observed hysteresis.

To apply general thermodynamics to analyze materials deformation, specifically in the case of an elastomer, we need the object's free energy as a function of the deformation tensor. Landau proposed the development of the free energy as a power series for small deformations, by limiting to the second order considering constant volume:

$$F = F_0 + \mu e^2 \tag{1.33}$$

in which μ is the Lame's second coefficient and e is the deformation tensor. De Gennes contribution consisted in the addition of a coupling term U between mesogenic groups, the network and the elastic modulus E, rewriting the free energy equation as:

$$F(S,p,T) = F_0(p,T) + \frac{1}{2}AS^2 + \frac{1}{3}BS^3 + \frac{1}{4}CS^4 - USe + \frac{1}{2}\mu e^2 - \sigma e \tag{1.34}$$

If we consider μ as the elastic modulus E, and substitute A from equation 1.25, we obtain:

$$F(S,p,T) = F_0(p,T) + \frac{1}{2}A_0(T - T^*)S^2 + \frac{1}{3}BS^3 + \frac{1}{4}CS^4 - USe + \frac{1}{2}Ee^2 - \sigma e \tag{1.35}$$

Even without the application of a mechanic field (σ=0) a spontaneous deformation of the elastomeric network is produced in the nematic phase, since the minimization of F with respect to e leads to:

$$e_{\min} = \frac{US}{E} \tag{1.36}$$

In the case that a mechanic field is applied, ($\sigma \neq 0$), a supplementary deformation is produced additionally to the spontaneous deformation; the minimization of F, in this case, is the equilibrium value:

$$e_{\min} = \frac{\sigma + US}{E} \tag{1.37}$$

By neglecting the σ^2 terms for the small values of σ, we obtain:

$$F(S,p,T) = F_0(p,T) + \frac{1}{2}AS^2 + \frac{1}{3}BS^3 + \frac{1}{4}CS^4 - \frac{U}{2E}S^2 - \frac{\sigma U}{E}S \tag{1.38}$$

where the additional term S^2 induces a variation of T_{NI}. With this equation, we can calculate the order parameter as a function of temperature and an applied strain field. Moreover, it can be shown that a critical mechanical point (*cp*) exists:

$$S_{cp} = \frac{B}{3C} \text{ and } (T_{cp} - T_{NI}) = \frac{B^2}{9CA_0} \tag{1.39}$$

This formalism is very similar to that of the influence of a magnetic or electric field on the order parameter. However, for either the magnetic or the electric fields, the experimental verification of the theory is limited due to the weak coupling between external field and order parameter. In the case of a magnetic field, we can estimate that T_{NI} is shifted only by a few millikelvins. Experimental results on the elastomers have shown that the mechanical field has in contrast a strong influence on the order and the nematic-isotropic transition can be significantly shifted as predicted by theory.[103]

---

[103] Finkelmann, H., in *Liquid Crystallinity in Polymers,* ED A. Ciferri, **1991**, VCH Publishers, pp. 315-340.

1.3.6. *Uniaxial and Thermal Deformation*

When a liquid crystalline polymer is formed, its growing behavior is interpreted as a sphere. Thus, a polymer network can be conceived as a sphere with no anisotropy with homogeneous ratio (λ_{ISO}=1). If we perturb the system by stretching it along a given direction (or by cooling), the sphere suffers a deformation and we obtain, depending on the mean order director of the LC moieties a prolate conformation if the polymer chains are parallel to the director (λ_{ISO}>1), or an oblate conformation (λ_{ISO}<1) if the chains are in a perpendicular direction (Scheme 1.15). λ_{ISO} can be estimated by random flight statistics.

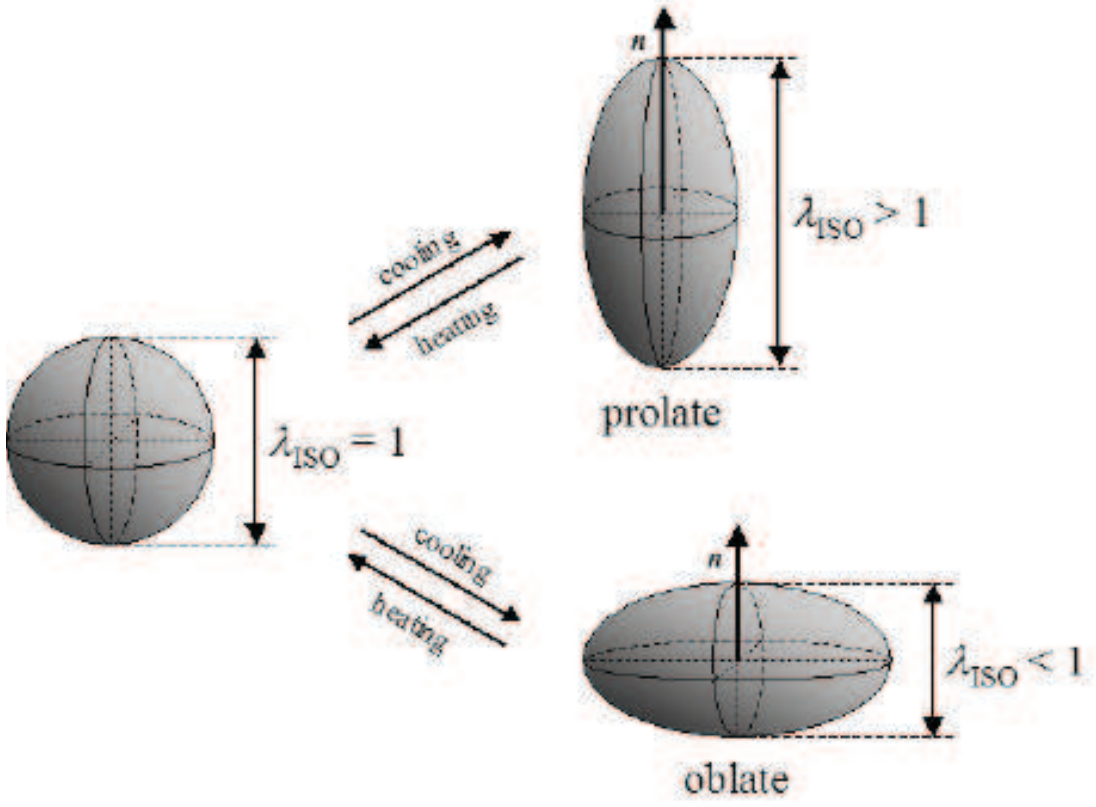

Scheme 1.15. Representation of the different conformation of a stretched LCE network.

The experimental model has been proved for side chain LCEs that, if we link an even number of carbons as a chain extender, the expected conformation will be oblate (scheme 1.16). Then, we can find that a monodomain liquid crystalline elastomer elongates when cooled from the isotropic to the nematic state, and contracts when heated back to the isotropic state. On the other hand, when mesogen is linked to the network backbone with an odd number of carbon spacers, the polymer backbone will be extended perpendicular to the director. In the case of main chain LCEs, the fact that the mesogens are intercalated along the director only allow them to adopt a prolate conformation.

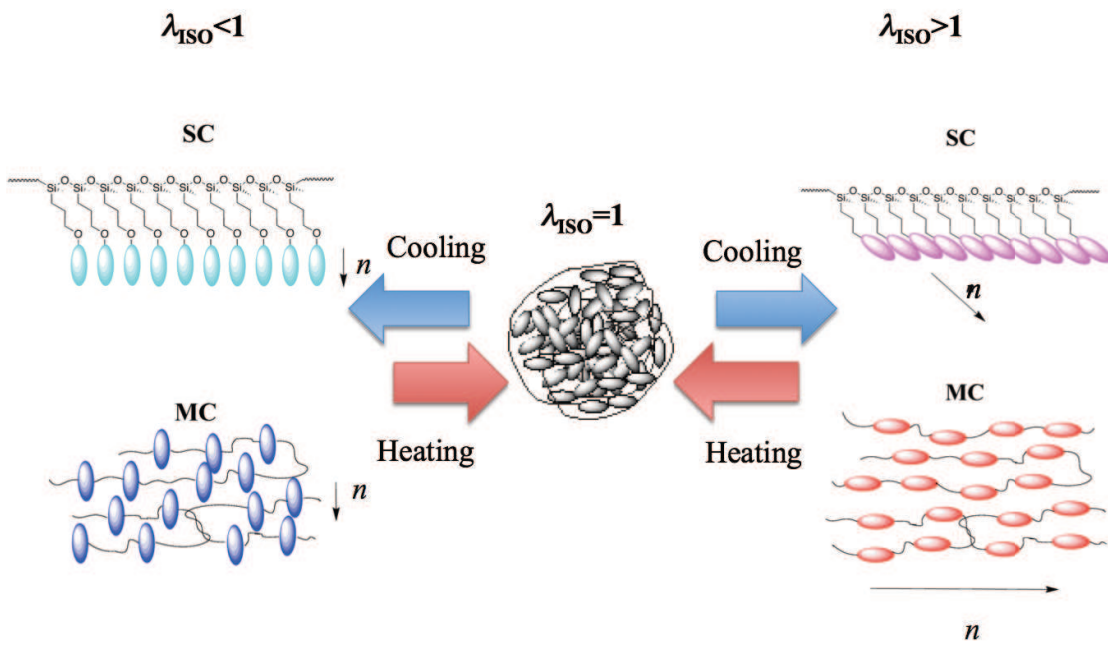

Scheme 1.16. Representation of the different conformations of the mesogens with respect to the polymer backbone in stretched LCEs.

To evaluate the spontaneous uniaxial length variation as a function of temperature we simply need to plot the length variation as a function of temperature. In the case of a smectic LCE, we observe an abrupt change in length close to the isotropic liquid transition temperature as shown in the next plot:

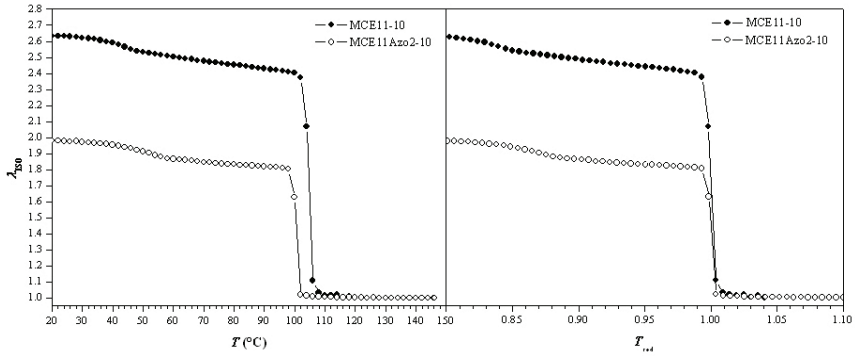

Plot 1.I. Uniaxial thermal expansion of two different smectic C MCLCE.[104]

In the case of nematic elastomers (Plot 1.2), this length variation is rather gradual than abrupt.

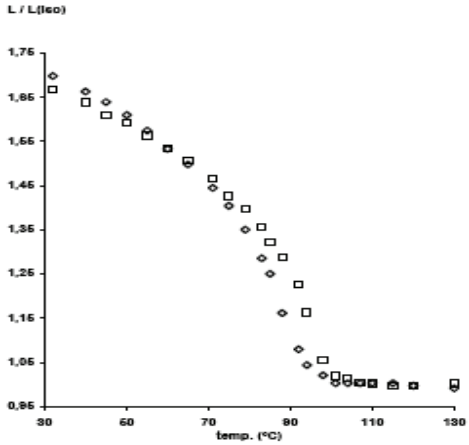

Plot 1.II. Uniaxial thermal contraction (◊) and expansion (□) of a nematic MC-LCE.[105]

The rate between the length in nematic (L_0) and isotropic state (L_{iso}) allows to obtain the λ value for a spontaneous elongation:

$$\lambda = \frac{L_0}{L_{iso}} \tag{1.40}$$

104 Sánchez-Ferrer Antoni. Ph. D. Thesis "Photoactive Liquid Crystalline Elastomers". Universidad de Barcelona, Barcelona, **2006**.
105 Bispo M. Thesis "Synthèse et caracterisation des élastomères cristaux liquides à chaîne principales. Propriétés mésomorphes et thérmo-élastiques." **2006**. Univérsité Louis Pasteur, Strasbourg.

By obtaining the plot, we can determine the clearing temperature experimentally by using the following expression:[104]

$$\lambda_{ISO} = (a_1 + a_2 T)\left((a_3 + a_4 T + a_5 T^2)\left(\frac{1}{1 + e^{\frac{T - T_0}{T_1}}} \right) + 1 \right) \tag{1.41}$$

where a_1, a_2 a_3 a_4, a_5, are fitting parameters and T_0, T_1 and T the temperatures (ºC).

By considering the constant volume condition, we can estimate the components of the cross section (x and y components) by measuring the thermal expansion coefficient:

$$\Lambda^T = \frac{l^T}{l^{T_0}} \quad \text{then} \quad x^T = \frac{x^{T_0}}{\sqrt{\Lambda^T}} \quad \text{and} \quad y^T = \frac{y^{T_0}}{\sqrt{\Lambda^T}}$$

Where l is the length in the z axis component.

1.3.7. *Rheology: Young Modulus and Shear Modulus*

Since we are creating novel materials, it is necessary to evaluate their resistance to traction and deformation and hence, to allow us to find their potential applications.

Stress is defined as a force per surface unit:

$$\sigma = \frac{F}{A} \tag{1.42}$$

In the case of a uniaxial deformation, the force is applied perpendicularly to the cross section area A=$x*y$. Its unit in SI system are $N/m^2 = Pa$.

The traction deformation can be expressed as:

$$\varepsilon = \frac{l - l_0}{l_0} \text{ for } \varepsilon << 1 \tag{1.43}$$

which is the uniaxial strain. When we perform the experiment, we obtain the type of curve shown in plot 1.3:

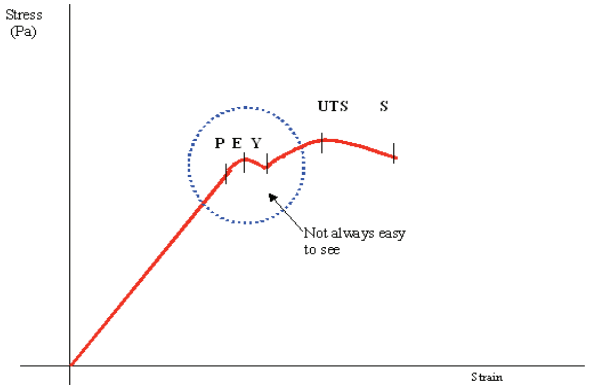

Plot 1.III. Plot of stress vs. strain[106]

Several characteristic points can then be distinguished:

P is the limit of proportionality, where the linear relationship between stress and strain finishes. **E** is the elastic limit. Below the elastic limit, the wire will return to its original shape. **Y** is the yield point, where plastic deformation begins. A large increase in strain is seen for a small increase in stress. **UTS** is the ultimate tensile stress, the maximum stress that is applied to a wire without snapping. It is sometimes called the breaking stress. Notice that beyond the **UTS**, the force required to snap the wire is less. **S** is the point where the wire snaps.

---

[106] http://www.antonine -education.co.uk/Physics_AS/Module_3/Topic_6/ topic _6 _ elastic_properties_of_so.htm

If we state the condition of linear dependence between stress and strain, which means that the material is not under an overstress situation, we can estimate the Young modulus E as:

$$E = \frac{\sigma}{\varepsilon} \tag{1.44}$$

E in the elastic region is constant and therefore can be interpreted as the necessary force amount to produce a deformation.

1.4. Objectives.

Having described the subject disciplines, which allows us to present this research as a complete and pluridisciplinary work, the thesis scope focuses on the monomer, polymer and elastomer synthetic design to obtain both temperature and mesophase control, the evaluation of their thermo and viscoelastic properties as a function of components.

In order to obtain tunable materials presenting low clearing temperatures and a wide temperature range nematic phase, the use of a mesogenic blend maybe an interesting approach to prepare nematic systems with low temperatures. Hence, It was decided to synthesize and study monomer mixtures, copolymers and coelastomers composed of two different monomers (**N1** and **N2**) in order to evaluate their mesomorphic properties. As other variation, two different chain spacers were used: the 1,1,3,3,5,5-hexamethyltrisiloxane (**HMTS**) and the 1,1,3,3-tetramethyldisiloxane (**TMDS**). To maximize the elastic properties of the final materials, the degree of elastomer crosslinking using a 5-functional unit crosslinking unit was fixed to 4%mol in all the cases.

Motivated by the creation of systems that respond to other external stimuli like in the case of previously synthesized LCEs containing azobenzene derivatives, we introduced monomers namely bent-core supposed to present ferroelectric properties in order to prepare LCEs capable to deform when a electric field is applied.

Finally, by applying all the previous knowledge we wanted to obtain new hybrid materials based on the functionalization of systems such as single molecule magnets

(SMMs) and magnetic nanoparticles in order to obtain novel systems as like magnetoactuators or superparamagnetic liquid crystalline elastomers.

Chapter 2

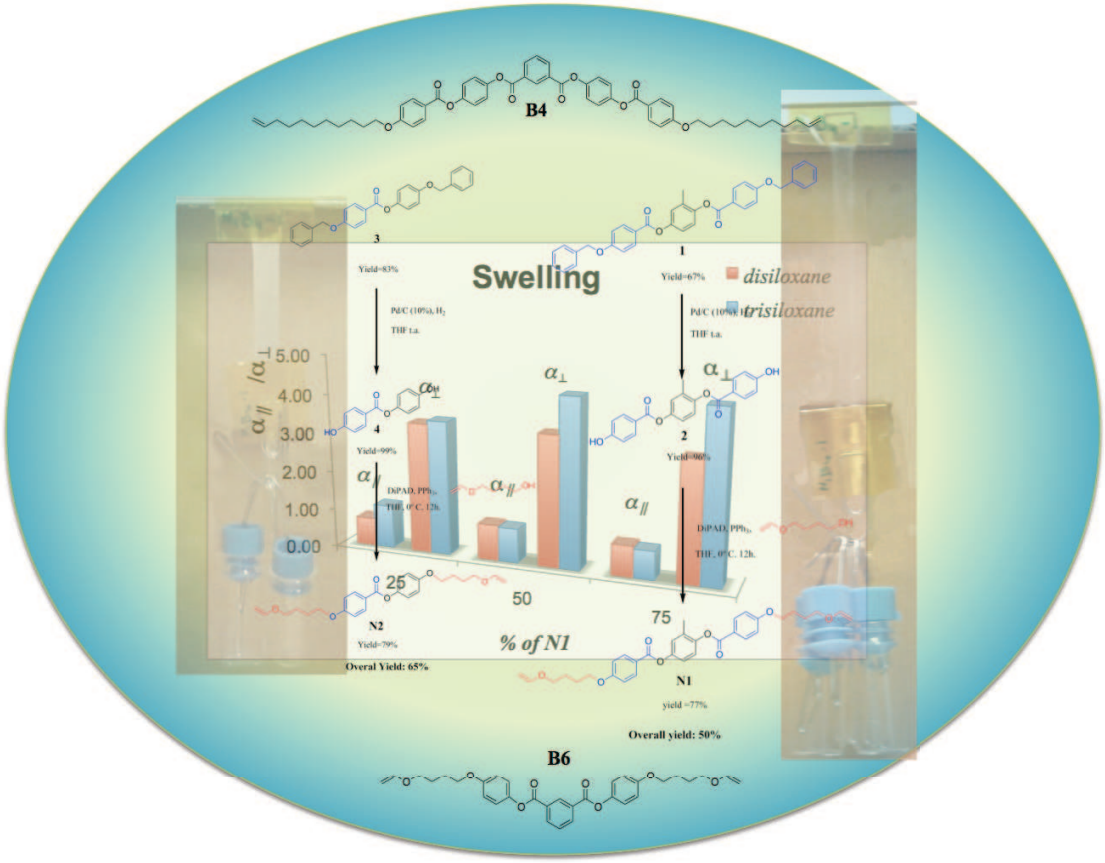

Synthesis

2. Synthesis.

2.1. Historical Background.

The initial strategy employed for the synthesis of MC-LCEs involves either the direct hydrosilylation of the terminal olefinic groups of a divinylic monomer via a one pot reaction[80] (**A**) in which both polymerization and crossliking processes take place simultaneously, or the crosslinking of a previously synthesized polymer[79] (**B**), as shown in the scheme 2.1.

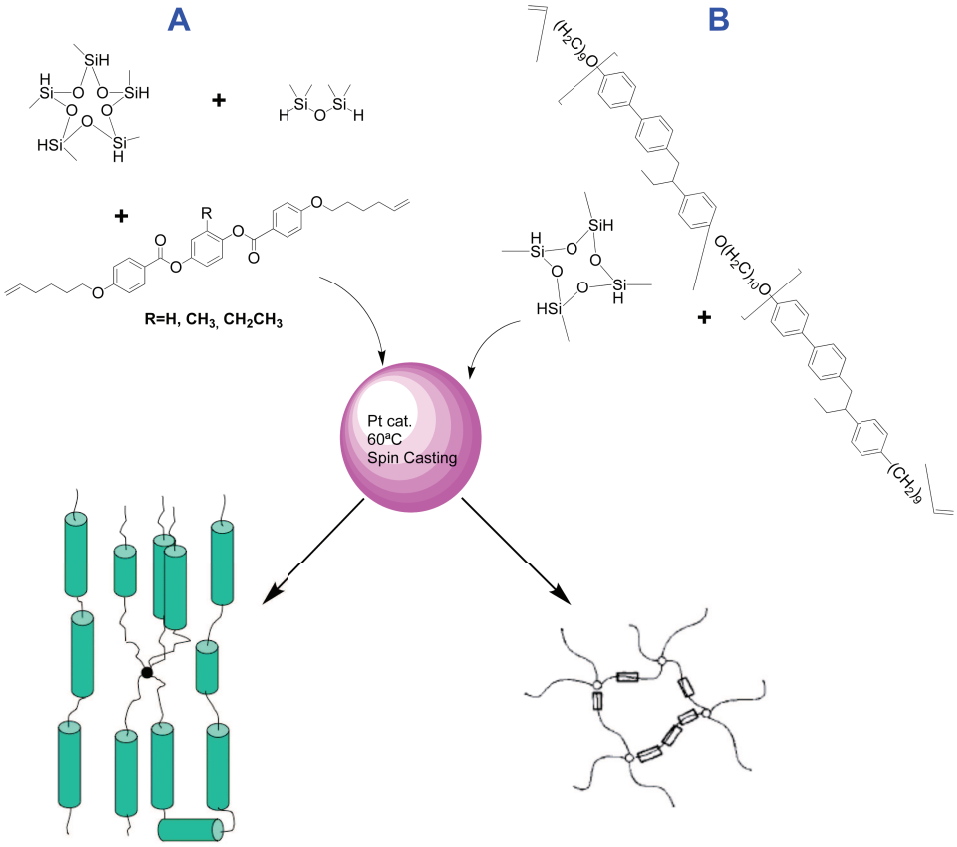

Scheme 2.1. Preparation of MC LCEs.

When synthesizing MC-LCEs via such an hydrosilylation process, two side-reactions usually occur in parallel: the α addition of the Si-H molecule and the isomerization of the terminal double bond, which leads to final products networks with high soluble

content (uncrosslinked parts). This was experimentally shown by both the swelling behavior of the elastomers and the ^{1}H-NMR experiments performed on the analogous polymer.[105] A deeper discussion of these reactions and their consequences will be brought thereafter.

As a solution to these side reactions, it was proposed by both the Freiburg and Strasbourg groups, to change the polymerizable chain from an ω-alkene chain to a vinylic ether chain to avoid double bond isomerization.[104,105] Consequently to this modification, polymers and elastomers did not undergo isomerization and additionally, no α addition was observed.[104] Despite the many advantages presented by this novel functional group, there are other side-reactions to control. Another side reaction has been reported by Marcinec[107] which results in the formation of a siloxane bond (16 %), with respect to the vinyl ether β hydrosilylation (76% yield), in the corresponding 1:5 ratio (Scheme 2.2).

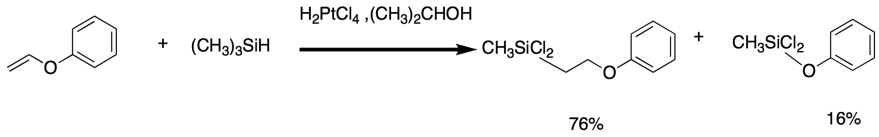

Scheme 2.2. Hydrosilylation and secondary reactions.

As it is well known, the vinylic moiety lability can also favor the formation of the corresponding hemi-ketal derivative in the presence of water, and decomposes into the resulting aliphatic alcohol and acetaldehyde, which can be easily detected by ^{1}H-NMR (scheme 3.3).

[107] Marciniec, B., Comprehensive Handbook of Hydrosilylation. **1992**, 127-128.

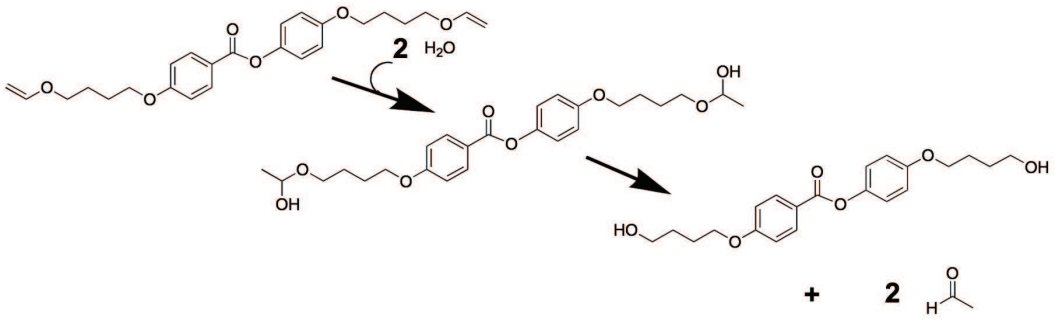

Scheme 2.3. Hydrolysis of the vinyl ether group.

In order to avoid these disagreements and ensure the survival of the vinyl ether functionality, it was decided to introduce this functionality in the last step of the monomer synthesis.

2.2. Monomer Synthesis.

2.2.1. *Calamitic monomers **N1** and **N2**.*

For this study on coelastomers, a mixture of 2 calamitic monomers was considered, differing in their anisotropic ratio (two or three aromatic rings respectively), liquid crystalline temperature range and isotropization temperature, in order to force the formation of low temperature (accessible) nematic mesophases in the final LCEs, as this is often observed in mixtures used in LCD devices.[108]

To prepare these calamitic monomers, a divergent reaction path was preferred as thought more advantageous. For instance, it allowed to leave the terminal groups free for homologation of the molecule and it avoided vinyloxy functional groups degradation along the synthesis. As just evoked, the central aromatic core structure of monomers **N1** and **N2** were synthesized first, and the vinyloxy chains were thus coupled in the next step as shown in schemes 2.4 and 2.5.

[108] Kirsh, P., Bremer, A., *Angew. Chem. Intl. Ed.*, **2000**, 39, 4216.

Protected core structures **1** and **3** were synthesized from the commercially available 4-benzyloxybenzoic acid and the corresponding hydroquinones via the Steglich estherification[109] using *N,N'*-dicyclohexylcarbodiimide as reagent in moderate yields (due to the difficult separation of the formed *N,N'*-dicyclohexylurea from the product). Since the elastomers synthesis will require high monomer quantities, we have focused our efforts to increase the efficiency of this reaction step, in order to increase the yields of **1** and **3**.

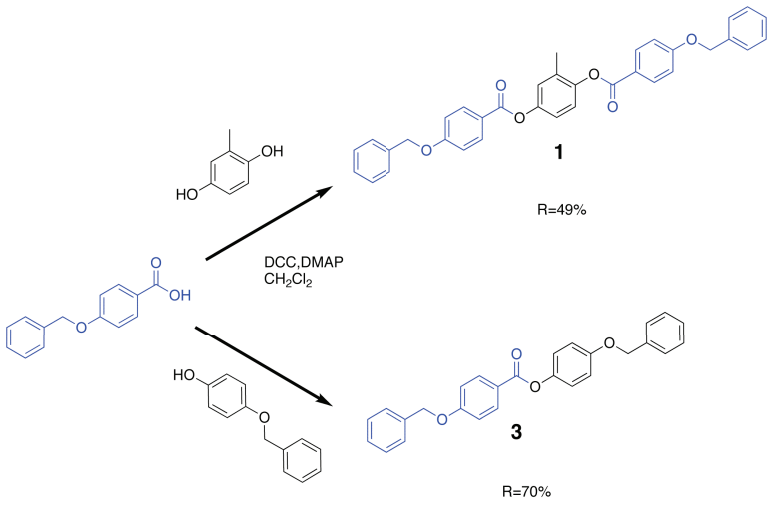

Scheme 2.4. Synthesis of protected calamitic core structures **1** and **3** via Steglich reaction.

As the addition of HOBt as catalyst did not improve the yields significantly, *N,N'*-dicyclohexylcarbodiimide (DCC) was replaced by 1-ethyl-3-(3-dimehtylaminopropyl)carbodiimide (EDCI). In this case, the urea formed was easily separated and the yields increased to 67 % for **1** and 83 % for **3**.

The activation of hydroxyl functionalities of compounds **1** and **3** was achieved by hydrogenation with palladium over charcoal (scheme 2.5). The catalyst was easily removed by filtration over Celite® and the reaction was quantitative in both cases.

[109] Neises, B., Steglich, W., *Angew. Chem. Int. Ed.* **1978,** 17, 522.

The phenols **2** and **4** were then reacted with commercially available 4-vinyloxybutanol via the Mitsunobu's reaction[110] to yield monomers **N1** and **N2** with overall yields of 50% and 65%, respectively.

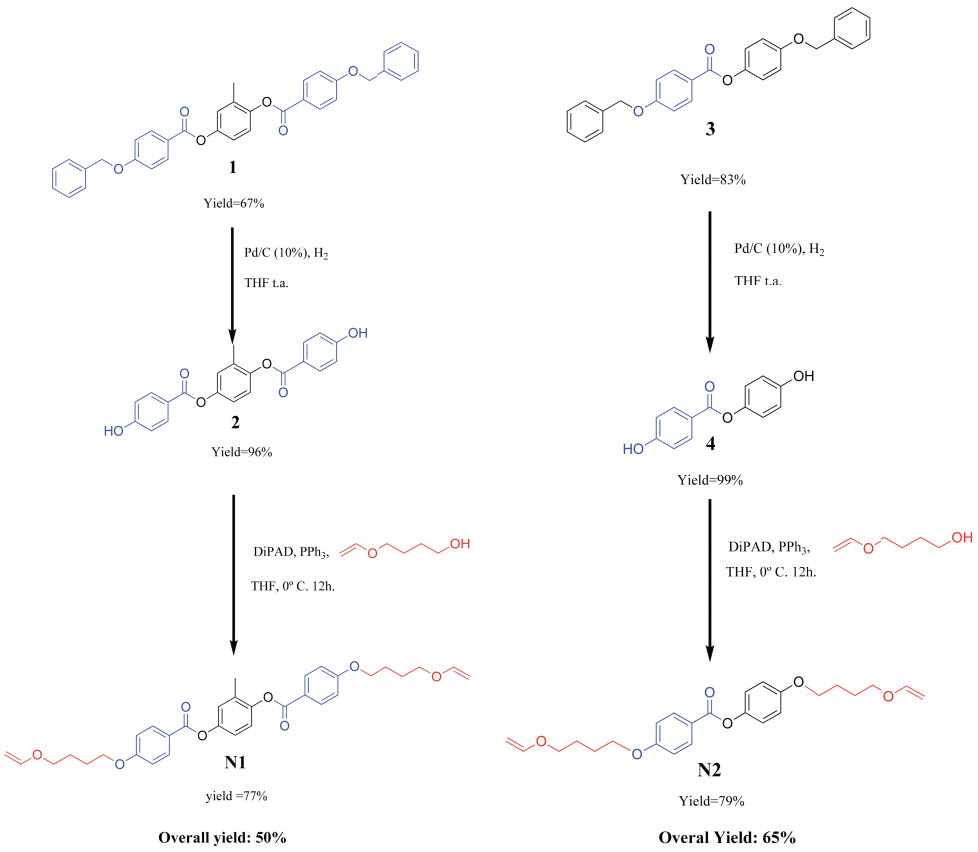

Scheme 2.5. Synthetic pathways of monomers **N1** and **N2**.

2.2.2. *Bent Core Monomers.*

Six bent-core monomers were prepared, four based on a five-ring core structure (**B1**-**B4**) and two based on a three-ring core (**B5** and **B6**). In all cases, the dihydroxy primary core structures were prepared first.

For the synthesis of the five-aromatic-ring bent-core mesogens **B1**, **B2**, **B3** and **B4**, a similar strategy as that used for monomers **N1** and **N2** was employed, that is, the

[110] Lepore, S. D., He, Y., *J. Org. Chem.* **2003,** 68, 8261.

appropriate central 3-ring rigid cores **6**, **8**, and **10** were first prepared and then the benzoic acid bearing the olefinic function linked to the core, to yield the phenyl ester molecules.[84,85,111,112] For **B5** and **B6**, exactly the same strategy employed in the case of the calamitic systems was applied. i.e. the grafting of 4-vinyloxybutanol onto the core by Mitsunobu etherification.

The olefinic acids **Hx2** and **Ud2** were obtained by a two-step synthetic pathway starting from the commercially available methyl 4-hydroxybenzoate via Mitsunobu reaction with 1-hexenol and 1-undecenol, respectively, to give the corresponding esters **Hx1** and **Ud1,** which were then readily converted into the acids **Hx2** and **Ud2**.

The preparation of the rigid counterpart was achieved in a three-step reaction similar to the strategy used for the calamitic monomers described above in paragraph 2.2.1.

The intermediates of bent-core monomers **B1**, **B2** and **B3** were obtained by a Steglich esterification of 4-benzyloxybenzoic acid and the suitable hydroquinone to give the benzyl protected phenolic esters **5** and **7**. The next step consisted in the catalytic hydrogenation of the corresponding benzyloxy moieties to yield the corresponding diphenol derivatives **6** and **8** (scheme 2.6).

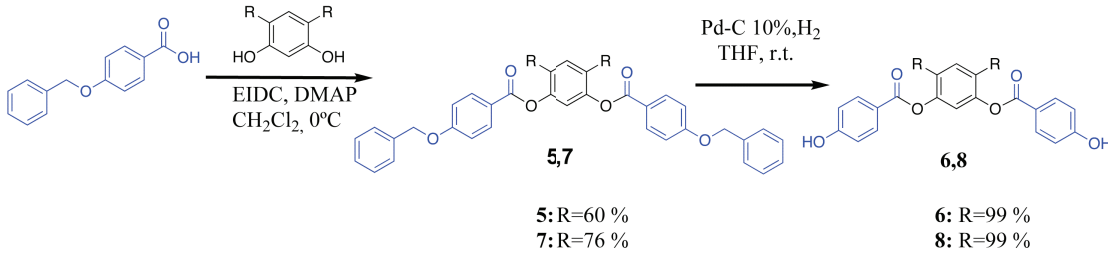

Scheme 2.6. Synthetic route of intermediates **6** and **8** (**5,6**: R=H; **7,8** R=Cl).

111 Galli, G.; Demel, S.; Slugovc, C.; Stelzer, F.; Weissflog, W.; Diele, S.; Fodor-Csorba, K., *Mol. Cryst. Liq. Cryst.* **2005,** 439, 1909.
112 Terazzi, E.; Guenee, L.; Morgantini, P. Y.; Bernardinelli, G.; Donnio, B.; Guillon, D.; Piguet, C., *Chem. Eur. J.* **2007,** 13, (6), 1674.

Compound **6**, was used to synthesize 3 different monomers, one containing 3 aromatic rings: **B5**, and the two 5-ring monomers **B1** and **B3** (scheme 2.7).

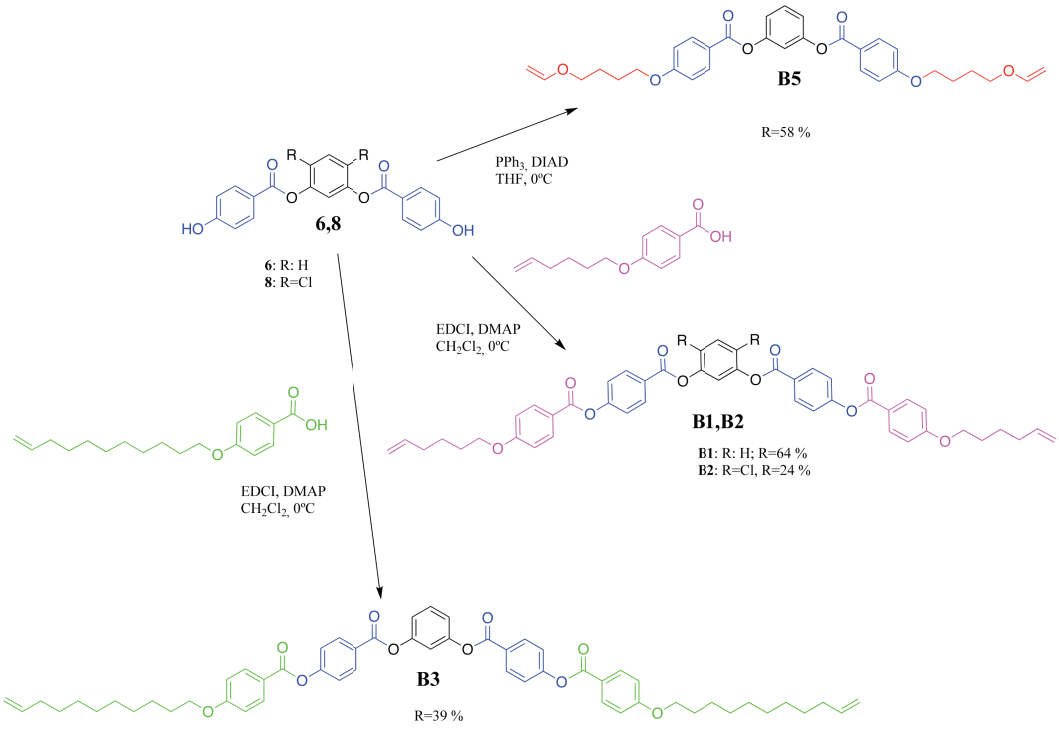

Scheme 2.7. Synthetic pathway for the monomers **B1**, **B3** and **B5**

The vinyl ether monomer **B5** was synthesized under the Mitsunobu reaction conditions and purified by crystallization from cyclohexane. Monomers **B1** and **B3** were synthesized from **6** and the acids **Hx2** and **Ud2** respectively, by the Steglich reaction; monomer **B2** was prepared by the same protocol as **B1** and **B3** from the bent-core diphenol **8** and the acid **Hx2**.

The two remaining monomers **B4** and **B6** and their intermediates were prepared by esterification between the isophtalic acid and 4-benzyloxyphenol to give the ester **9**, followed by benzyl deprotection to yield the bent-core diphenol **10** (Scheme 2.8).

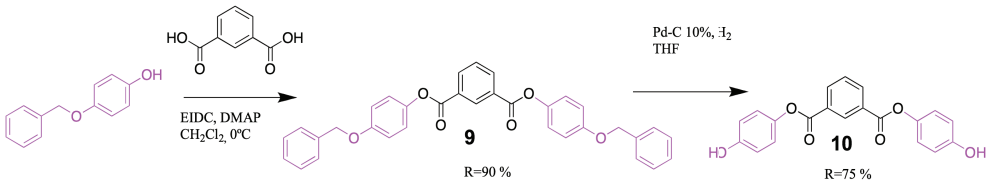

Scheme 2.8. Synthetic pathway for **B4** and **B6** rigid cores.

Compound **B4** was synthesized by mixing **10** and **Ud 2** with EDCI under the Steglich conditions and purified by column chromatography. **B6** was obtained by reacting **10** and 4-vinyloxybutanol via the Mitsunobu reaction as **B5**, purified by chromatographic column and crystallized from cyclohexane (Scheme 2.9).

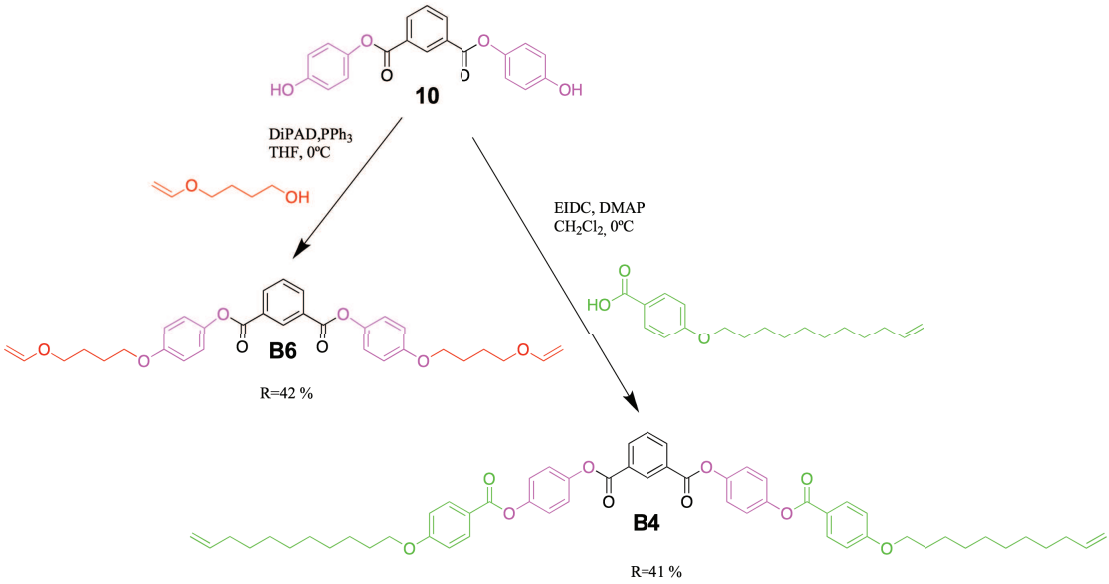

Scheme 2.9. Synthesis of **B4** and **B6**.

The obtained monomers were characterized with ^{1}H and ^{13}C-NMR elemental analysis. Their mesomorphic properties were evaluated by means of DSC and POM. Their thermal behavior is discussed in the next chapter.

2.3. Polymer Synthesis.

2.3.1. *General Concepts.*

All our polymers were synthesized by catalytic hydrosilylation polyaddition. The reaction's mechanism, proposed by Chalk and Harrod,[113] is illustrated in scheme 2.10.

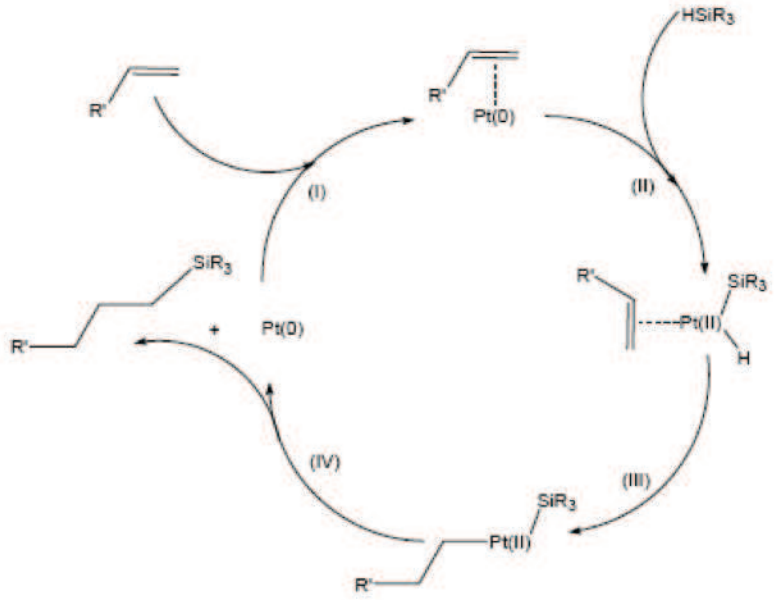

Scheme 2.10. Chalk-Harrod catalytic cycle.

The first step is the coordination of platinum (0) to the double bond followed by the oxidative addition of the silane $HSiR_3$ (II) which produces a Pt(II) complex. The hydride ion migrates to the coordinated alkene, step known as a migrating insertion. The last step of the catalytic cycle (IV) is the reductive elimination of the silylated hydrocarbon and the regeneration of the active species Pt(0).

An alternative cycle was also proposed[114] which suggests that the oxidative addition of the silane occurs before the complexation of the olefin.

---

[113] Chalk, A. J. Harrold, J. F., *J. Am. Chem. Soc.* **1965,** 87, 16.

As observed by Stein,[115] the Chalk-Harrod mechanism does not explain some experimental observations like the variability of inductive periods, the colored appearance at reaction termination and the activating effect of the oxygen, which had been already stated by Chalk and Harrod. Stein also stated that the oxygen activation inhibits the formation of platinum colloidal aggregates.[114]

As it was mentioned in paragraph 2.1, there exist two main side-reactions, namely the double bond isomerization and the α addition to the double bond.

Isomerization of the double bond is very common.[116] It has been observed by Sargent and Weber in their polymerization studies with the Karstedt catalyst,[117] which caused the formation of low molecular weight polymers due to inertness of the non terminal olefins[118] also considered as termination agents.

Isomerization was also observed in hydrosilylations catalysed by Rh(I) and Pt(IV) at 70ºC by Bianchi's group.[119] The importance of this side reaction becomes quite an effective method for olefin isomerizations, when the catalyst employed is Pd(II)[120] as reported by Crivello.[121] The reaction consisted in heating the allyl ether substrates in the presence of transition metals to yield the total isomerization of the double bond (i.e. formation of propenylethers).

---

[114] Rappoport, Z., Apeloig, Y., *The Chemistry of Organic Silicon Compounds vol 2* **1998,** John Wiley & Sons.
[115] Stein, J. L., Gao, Y., Scott, R., *Technical Information Services 98CRD115* **1998,** General Electric Research & Developed Center.
[116] Marko, I., Stérin, S., Buisine, O., Mignani, G., Branlard, P., Tinant, B., Declercq, J. P., *Science* **2002,** 298, 204.
[117] Sargent, J., Weber, W., *Macromolecules* **1999,** 32, 2826.
[118] Marciniec, B., Silicon Chemistry **2002,** 1, 155-175.
[119] Bianchi, F. P., Ugozzoli, F., Spera, S., Careri, M.; Dalcanale, E., *New J. Chem.* **2003,** 27, 502.
[120] Mirza-Aghayan, M. B., R., Bolourtchian, M., Hoseini, M., Tabar-Hydar, K., J., *J. Organomet. Chem.* **2003,** 678, 1.
[121] Crivello, J. J., K., *J. Polym. Sci. A.* **1993,** 31, 1473.

The other important side-reaction widely studied by Puyenbroek and collaborators is the siloxane's α addition to the olefin,[122] generating a positional isomer. Classified as a Markownikov addition, Puyenbriek stated that the proportion between the β and the α addition can be controlled by the catalyst employed, the temperature and the solvent.

There exist some other side reactions such as hydrogenation and dehydrogenation but they are not significant when a platinum catalyst is employed.[117]

In conclusion, controlling the side reactions enables to control the degree of polymerization (DP). The judicious choice of the catalyst, the good monomer's purity and the control of the reaction conditions (solvent, temperature, time) are essential to synthesize polymers with high molecular weights and good yields.

The relationship between the polymerization degree, monomer purity and stoichiometry was proposed by Carrothers.

In the case of a polycondensation, the average polymerization degree $\overline{DP}_n$ is defined as:

$$\overline{DP}_n = \frac{N_0}{N_t} \tag{2.1}$$

where $\boldsymbol{N_0}$ is the initial functional group number and $\boldsymbol{N_t}$ the available functional groups at a time equal to $\boldsymbol{t}$. Similarly, the reaction yield $\boldsymbol{p}$ can be defined as the ratio of the reacted functional group and the initial number of functional groups.

[122] Puyenbroek, R. J., J.; van de Grampel, J.; Rousseeuw, B.; van der Drift, E., *Polymer* **1996,** 37 (5), 847.

$$p = \frac{N_0 - N_t}{N_0} \tag{2.2}$$

Substituting equation 2.2 in 2.1 gives a new relationship of $\overline{DP}_n$ as a function of the reaction yield ***p*** (Carrothers equation).

$$\overline{DP}_n = \frac{1}{1-p} \tag{2.3}$$

The corresponding plot of the function (plot 2.1) shows the exponential decreasing of $\overline{DP}_n$ as a function of decreasing yield. The curve describes that the average polymerization degree is high when the reaction yield goes above 99 % purity, but it decreases asymptotically until reaching a $\overline{DP}_n$ equal to 10 when a 90 % yield is obtained.

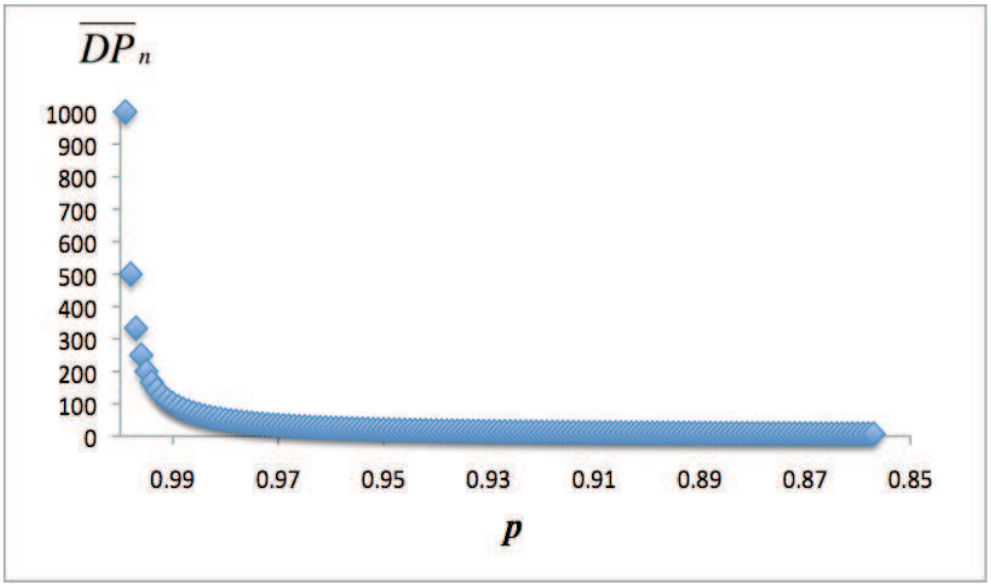

Plot 2.I. Carrothers equation's curve.

The chain extender's volatility is another problem directly involved into the polymerization efficiency, as it has previously been seen by us. This problem was partially solved by changing the former employed 1,1,3,3-tetramethyldisiloxane

(**TMDS**) by its extended homologous 1,1,3,3,5,5-hexamethyltrisiloxane (**HMTS**) due to its lower volatility and its higher purity (99 % against 97 % for **TMDS**) to reach better polymerization degrees according to the Carrothers principle discussed above.

2.3.2. *Trisiloxane Polymers and Copolymers.*

A series of two homopolymers (MC-LCP) as well as three copolymers (MC-LCCoP) differing in the percentage of diolefinic monomers **N1** and **N2**, were synthesized via catalytic hydrosilylation. The catalyst chosen was the dichloro-1,5-cyclooctadiene Platinum (II) (COD catalyst) for its better activity-efficiency ratio with respect to the Karstedt catalyst (scheme 2.11).

Each of the three monomer blends in different monomers ratios (**N1**:**N2** = 25:75, 50:50 and 75:25) were dissolved in toluene with an equimolar amount of hexamethyl trisiloxane (**HMTS**) and heated at 60º C. The catalyst was then readily added and reaction completion was fixed to 24 h. Polymers and copolymers were purified by repeated co-precipitation of a polymer solution in THF with methanol,[123] which allowed to eliminate small oligomers and unreacted monomers.

The nomenclature that will be used thereafter is as follows:

The letter **P** states that our product is a polymer and letter **T** indicates that the chain extender employed was 1,1,3,3,5,5-hexamethyltrisiloxane (**D** will be used for **TMDS**). Hence, the polymers synthesized only with a single monomer **N1** (or **N2)** and **HMTS** chain extender will be named **PN1T** and **PN2T,** respectively. In the case of copolymers, the prefix **Co** is added to **P** and the number will indicate the **N1**

[123] Brandrup, J., Imergut, E. H., Grulke, E. A., Solvents and Non Solvents. *Polymer Handbook* **1999,** 2, (VII), 497.

proportion employed for their synthesis. For example, a copolymer containing a monomer mixture **N1**/**N2** 25:75 and the chain extender **TMDS**, will be named **CoP25D**.

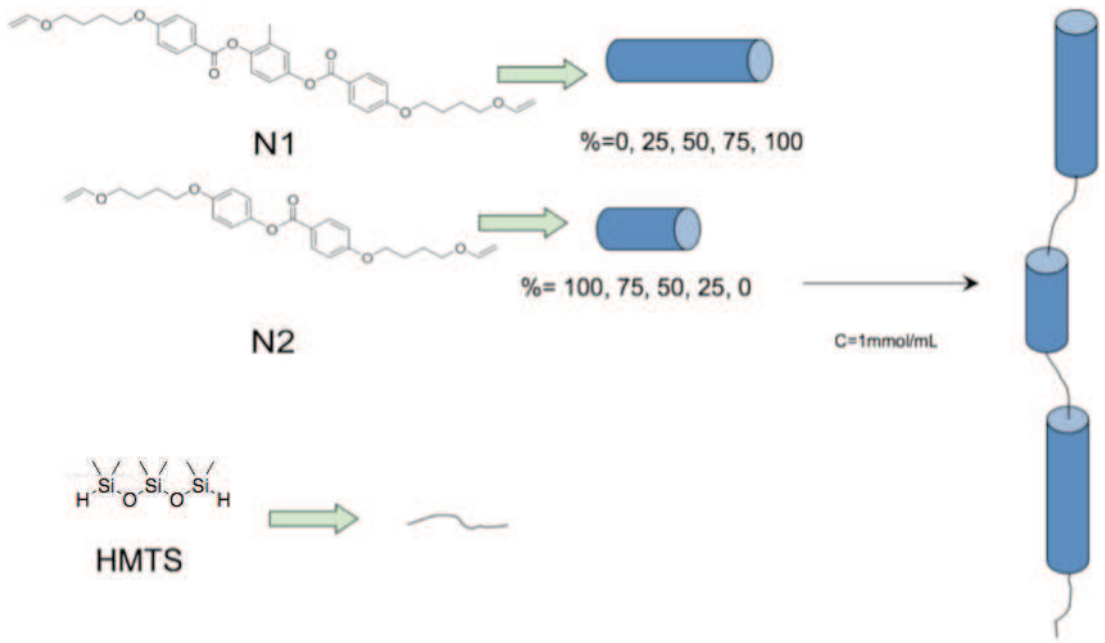

Scheme 2.11. Synthesis of main-chain liquid crystalline homo and copolymers.

The purified polymers were analyzed by gel permeation chromatography (GPC) using multi angle laser light scattering. The results are collected in table 2.1.

Table 2.1. Polymerization results of trisiloxane polymers and copolymers.

Polymer	Mn	Mw	P	DPn	DPw
PN1T	30800	186000	6	40	242
CoP25T	164000	549000	3.3	246	821
CoP50T	28500	106000	3.7	41	150
CoP75T	30900	131000	4.2	42	177
PN2T	39100	112000	2.9	62	176

The GPC analyses's conditions are reported in appendix. Mn: molecular mass in number; Mw: molecular mass in weight; P: polydispersity index; DPn: degree of polymerization in number; DPw: degree of polymerization in weight.

Since the prepared copolymers are made of three different components via polycondensation, our polymerization degrees (DPn and DPw) were calculated by taking the average molecular weight of the two vinylic monomers (**N1** and **N2**) and one trisiloxane molecule as the repeating unit. DPn and DPw are thus expressed as:

$$DPx = \frac{Mx}{(FW_{HTMS} + \overline{FW}_N)} \tag{2.4}$$

where *x* represents n or *w*; FW_{HMTS} is the molecular weight of **HMTS** and $\overline{FW}_N$ is the average of **N1** and **N2** fitted molecular weight depending of the proportion (equation 2.5).

$$\overline{FW}_N = \{(y \bullet FW_{N1}) + [(1-y) \bullet FW_{N2}]\} \tag{2.5}$$

y takes the values 0, 0.25, 0.5, 0.75 and 1 for the polymers **PN2T**, **CoP25T**, **CoP50T**, **CoP75T** and **PN1T**, respectively.

The degrees of polymerization were much higher than those obtained previously in our group[105,124] in agreement with the improvements of the reactional parameters. The polydispersities were rather high, possibly due to concentration and temperature, but nevertheless expected for this type of polycondensation.

To confirm that the monomer ratio within the polymers was preserved after polymerization, ^{1}H-NMR was employed (Scheme 2.12). Indeed, the comparison of the integrations of the Si-CH_2 bond signal and the methyl singlet from **N1** moiety allowed us to give a fairly good approximation to the blends monomer ratio (table 2.2). To estimate the molar proportion of the monomer **N1**, we used the equation:

[124] Bispo, M.; Guillon, D.; Donnio, B.; Finkelmann, H., *Macromolecules* **2008,** 41, (9), 3098.

$$\frac{I^{CoP}_{O(CH_3)_2SiO} + I^{CoP}_{O(CH_3)_2SiCH_2}}{I^{CoP}_{CH_3Ar}} = x_{N1}\left(\frac{I^{PN1T}_{O(CH_3)_2SiO} + I^{PN1T}_{O(CH_3)_2SiCH_2}}{I^{PN1T}_{CH_3Ar}}\right) \quad (2.6)$$

In which the rate between **HMTS** moiety ($I^{CoP}_{O(CH_3)_2SiO} + I^{CoP}_{O(CH_3)_2SiCH_2}$) and the aromatic ring methyl ($I^{CoP}_{CH_3Ar}$) integrations of a given copolymer is equal to the product of monomer proportion (x_{N1}) and rate in the homopolymer **PN1T** (right parenthesis of the equation)**.** Assuming this rule, rearrangement of equation 2.6 gives equation 2.7.

$$x_{N1} = \left(\frac{I^{CoP}_{O(CH_3)_2SiO} + I^{CoP}_{O(CH_3)_2SiCH_2}}{I^{CoP}_{CH_3Ar}}\right) \div \left(\frac{I^{PN1T}_{O(CH_3)_2SiO} + I^{PN1T}_{O(CH_3)_2SiCH_2}}{I^{PN1T}_{CH_3Ar}}\right) \quad (2.7)$$

Note that this approach has already been successfully used in the determination of the average ratio between 2 monomeric mesogens in functionalized codendritic systems.[125]

[125] Rueff, J. M.; Barbera, J.; Donnio, B.; Guillon, D.; Marcos, M.; Serrano, J. L., *Macromolecules* **2003,** 36, (22), 8368-8375.

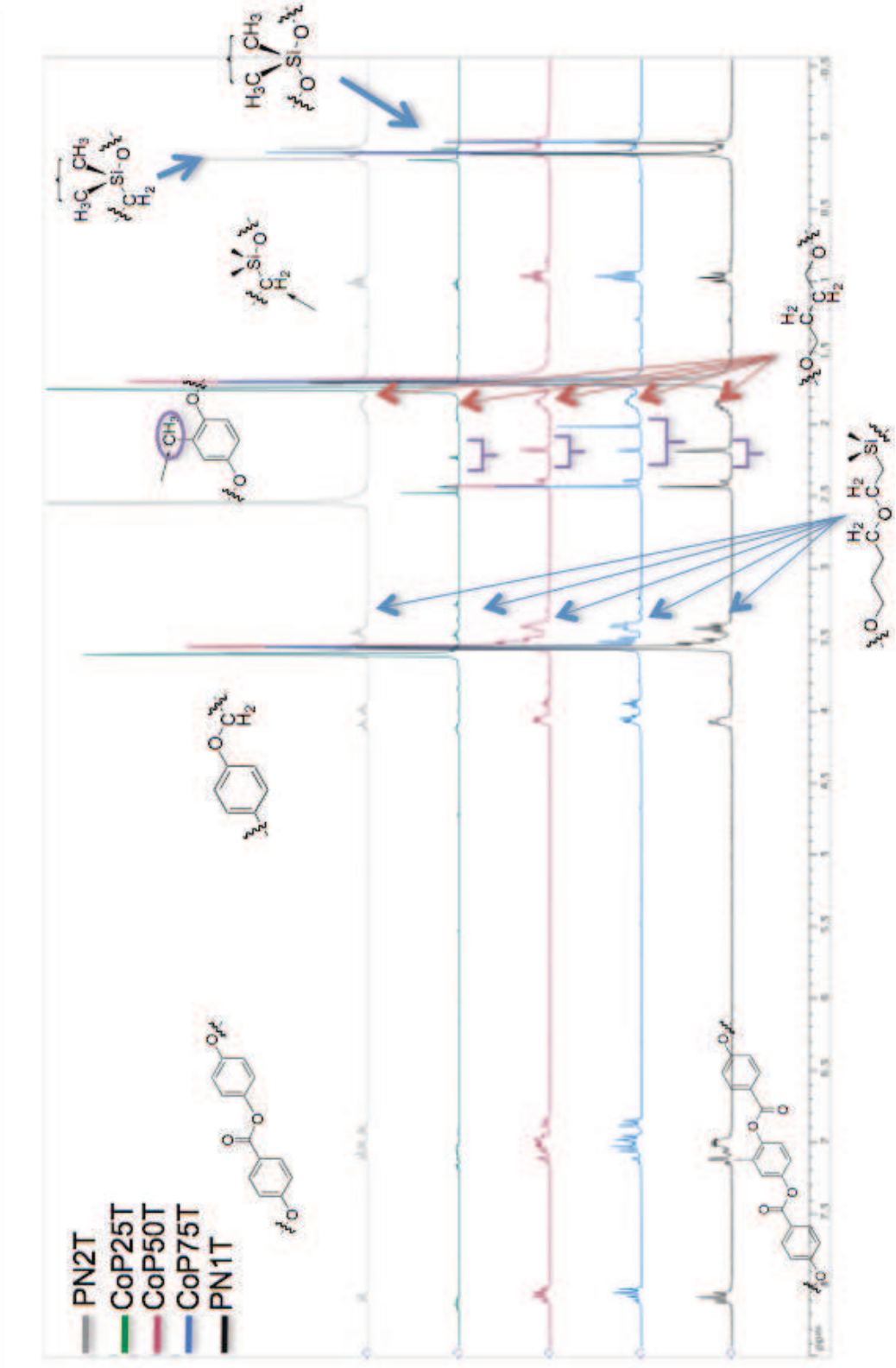

Scheme 2.12. [1]H-NMR of **HMTS** polymers; concentration: 3 mg/mL.

The rate ensures that, even if we do not have the exact molar concentration in each NMR sample, the integral proportions will be kept constant without considering polymer chains interaction.

Table 2.2. Molar percent for the **HMTS** polymers estimated by ^{1}H-NMR.

Polymer	molar % ratio (N1/N2)	%molar found (N1)
CoPN2T	0 /100	0.0
CoP25T	25/75	25.3
CoP50T	50/50	52.4
CoP75T	75/25	83.3
PN1T	100/0	100.0

The ^{1}H-NMR results presented above confirmed that the monomer proportion was maintained along polymerization as predicted, at least statistically.

2.3.3. *Disiloxane Copolymers*

In order to perform a systematic study of the influence of the chain extender on the polymer physical and mesomorphic properties, a series of 3 main-chain copolymers using **TMDS** as the chain extender was synthesized for comparison. These polymers were prepared as their trisiloxane homologues. The results obtained are shown in table 2.3.

Table 2.3. Polymerization results of disiloxane polymers.

Polymer	Mn	Mw	P	DPn	DPw
CoP25D	25800	183000	7	43.5	310
CoP50D	80400	280000	3.5	128	446
CoP75D	7400	160000	21	11	241

The GPC analyses's conditions are reported in appendix. Mn: molecular mass in number; Mw: molecular mass in weight; P: polydispersity index; DPn: degree of polymerization in number; DPw: degree of polymerization in weight.

A remarkable result is the high polydispersity index, except that of copolymer **CoP50D**. A special attention has to be given to the copolymer **CoP75D**, which exhibits two different aggregates, one with a small molecular mass in number, and another with very high molecular mass in weight. As discussed previously, we have attributed this polydispersity to the chain extender volatility that produces loss of stoichiometry control. Despite these inconveniencies, polymerization degrees are large enough to perform an efficient MC-LCCoE synthesis.

By comparing both series, we can observe that polydispersities are similar, whereas the average mass in number changes significantly from one series to the other. Polydispersity differences can be related to the siloxane chain extender. Its volatility causes loss of stoichiometric quantities, which enlarges polydispersity of the polymers and lowers reaction yields for this series. As a general observation, **HMTS** polymers are the most suitable candidates to synthesize LCEs, due to their large molecular weights, whereas those synthesized with **TMDS** chain spacer generally lead to high polydispersity, low average weight in number polymers.

2.3.4. *Bent-core polymers*.

Polymers containing bent-core units intercalated with oligosiloxane chain extenders 1,1,3,3,5,5,7,7,9,9,11,11,13,13,15,15-hexadecamethyloctasiloxane (**HDMOS**) for polymers **PB1** and **PB2** and **HMTS** for **PB3** and **PB4** and were obtained via the same conditions used for the preparation of LC polymers and copolymers containing calamitic mesogens. In this case, the resulting polymers presented a lower solubility in THF than the calamitic analogues; hence they were more difficult to purify by precipitation methods. Instead, we performed preparative GPC using Biobead S-X1 sieves, which allowed to separate molecules with a size lower than 14000 Dalton

from larger ones. Thus the monomers and small oligomers could be removed, increasing the MW of the pure polymers. Only the five-ring monomers yielded polymeric systems, whereas **B5** and **B6** polymerization attempts did not gave any result.

Table 2.4. Bent core polymerization results.

Polymer	Mn	Mw	P	DPn	DPw
PB1	25800	183900	3.7	21	81
PB2	111000	308000	2.8	79	219
PB3	7000	18000	2.6	6	17
PB4	44100	299000	6.8	30	202

The GPC analyses's conditions are reported in appendix. Mn: molecular mass in number; Mw: molecular mass in weight; P: polydispersity index; DPn: degree of polymerization in number; DPw: degree of polymerization in weight. Letter P indicates the polymer; Bx is the monomer employed.

As for the previous results, these polymers presented reasonably good DPs in most cases, which made them chemically suitable to synthesize MC-LCEs. Although, the polydispersity indices were lower than those of the polymers containing calamitic mesogens; they possess a high glass transition temperature (T_g), a disadvantageous parameter to synthesize elastomers via centrifugation.

2.3.5. *Conclusions*

New series of polymers and copolymers were synthesized by catalyzed polycondensation in concentrated solutions. The results confirmed that the process of polymerization takes place in these conditions and therefore LCE formation is expected. Our synthesis also allowed us to synthesize copolymers in the desired proportions without showing monomeric selectivity as well as linear polymers containing bent-core mesogens. The thermotropic properties of these novel systems will be discussed thereafter. Optimisation of the polymeric conditions is out of the

scope of this thesis work, but it is still feasible to reduce even more the polydispersity and keep the degree of polymerization as high as shown herein.

2.4. Elastomer Synthesis.

2.4.1. *Trisiloxane Elastomers and Coelastomers*.

The method to obtain a MC-LCCoE with 4 mol % of crosslinker (0.10 meq/mmol of **HD5**) (schema 2.13), consisted in preparing a solution with the reactants (concentration: 1 mmol of calamitic monomer/monomer mixture for 0.8 mL of solvent) in a 3 mL vial and heating at 60ºC until total solubilization of the monomer. The catalyst was then added and the reaction mixture was poured into a customized cell. The centrifugation time was found to depend on the crosslinker concentration and type of functionalization, which varies from 45 min to 24 h.[105] After several attempts, we realized that the reaction did not proceed due to lack of adequate monomer-**HMTS** ratio, which was justified by the deposition of monomer crystals in the vial's wall. To solve this problem, the reaction mixture was left to react during a short period of time (5 to 8 minutes) before the centrifugation process. In this way, the formation of small oligomers avoided the appearing of monomer crystals on the vial walls due to desolvation process. In the following discussion, the same nomenclature as that of the polymers and copolymers will be used, the letter **P** being replaced by the letter **E** (for elastomer).

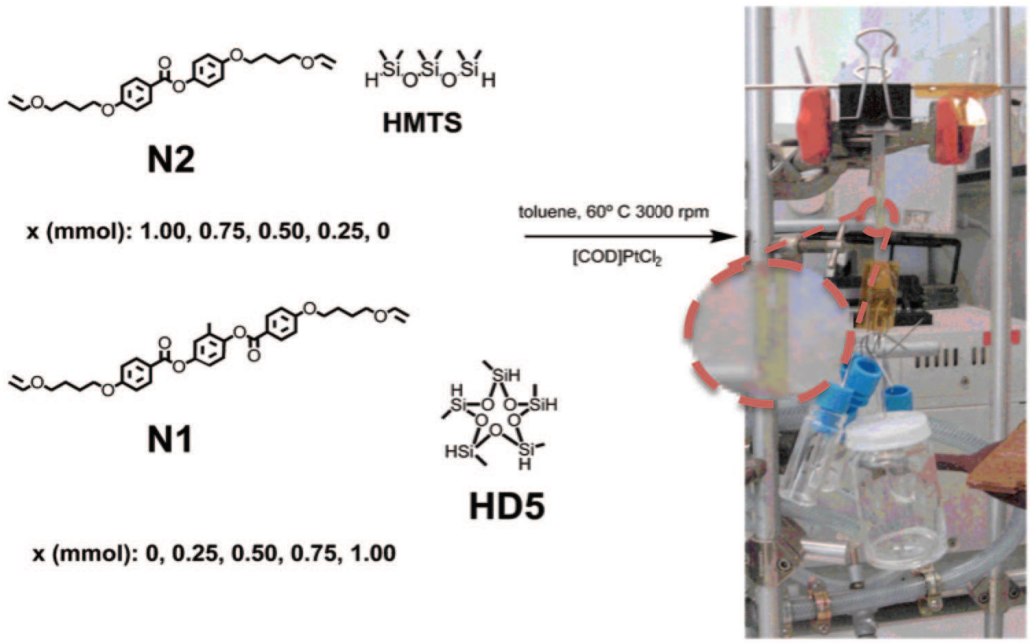

Scheme 2.13. Schematic representation of MC-LCE preparation.

The five elastomers were prepared by centrifugation at 3000 rpm for 1-3 h. The resulting fragile film gels were removed from the centrifuge cell, previously cooled to room temperature to ensure the reaction freezing. After removal from the customized cell walls, the thin film was cut in 3 pieces. Each piece was removed from the Teflon® tape and stuck in both short edges with Kryton® tape. The upper edge was designed to hang the elastomer on a metallic bar, and the other side to carry weight loads (Figure 2.1). The sample orientation was achieved by means of a mechanical force applied parallel to the long film axis. Once oriented the macroscopic configuration of the liquid crystalline gel changed and the samples became transparent, as seen in figure 2.1. These partially crosslinked gel films were reheated at 60ºC in a vacuum oven leading to the second crosslinking process, yielding the quasi-perfectly oriented material as those conceived by the Kupfer methodology.[76] The application of a mechanical force induces macroscopic orientation of the liquid crystalline order (mesogen and linear polymer chains on average alignment parallel to

the applied force), the partially formed network undergoing a stretched conformation by increasing the oriented domains sizes thus forming the so-called Liquid Single Crystal Elastomer (LSCE).

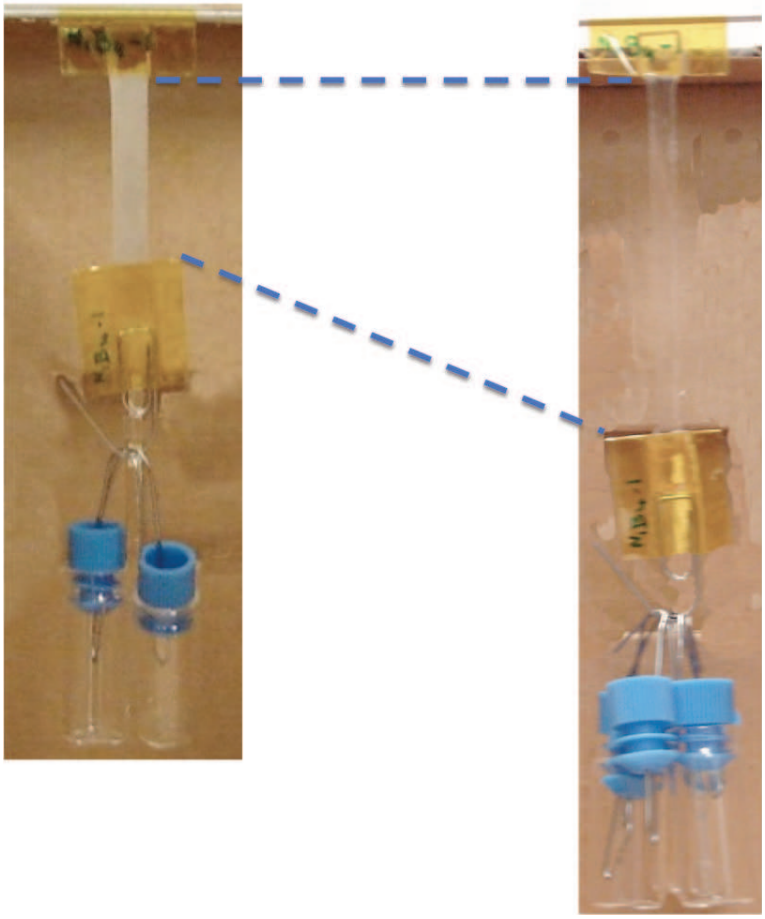

Figure 2.1. Orientation process by weight loading. Starting as an opaque film (left) the elastomer becomes transparent upon orientation (right).

After this treatment, the elastomers were washed in a suitable solvent by several succesive extractions using a Soxlet apparatus. This process allowed the removal of the unreacted monomers as well as small unbonded oligomers. These soluble products represent the soluble content also known as percentage of soluble matter (sol %). A high soluble content yields poor crosslinked, mechanically weak networks. Hence, the lower the soluble content, the better the quality of the material. The amount of soluble

content was evaluated for all the **HMTS** Coelastomers and the values are shown in plot *2. II*.

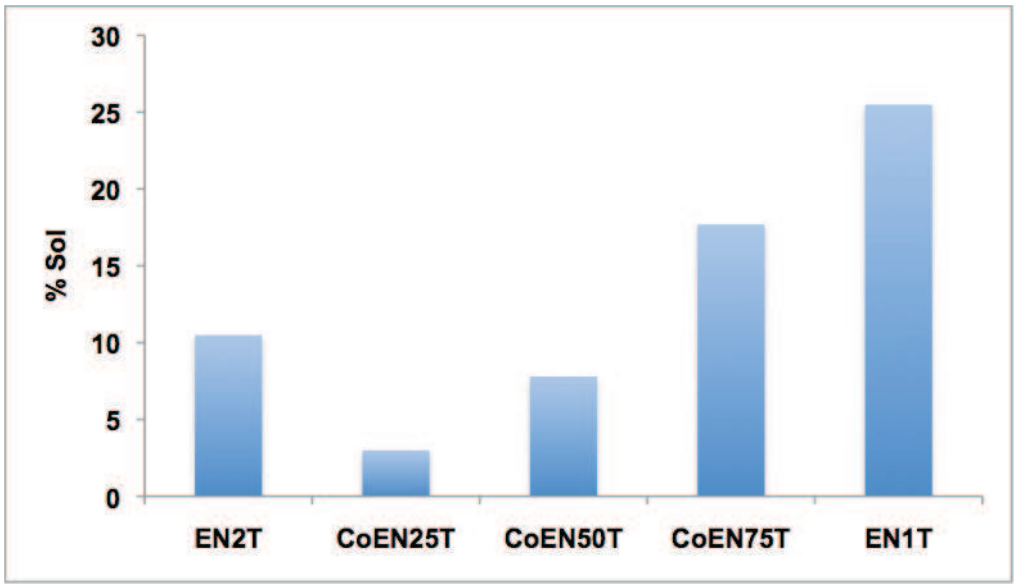

Plot 2.II. Soluble content of **HMTS** MC-LCEs and CoEs (in cyclohexane).

As it can be seen, the sol % are rather low (below 20 %) in most of the cases with 3 % as the best result. Since this sol % demonstrates that this kind of systems is never in the ideal case (perfect networks), we should consider that the side reactions representing the soluble content is due to hairpin defects which has already been studied by Muresan *et. al.*[126] As a consequence, such entanglements do not allow to estimate the exact monomer distance of MC-LCP by X-ray diffraction studies. These defects inherent to the polymer's behavior cannot be either controlled nor eliminated by stretching the sample. This interesting observation will be discussed in the next chapter.

[126] Muresan, A. S., Ostovskii, B. I., Sanchez-Ferrer, A., Finkelmann, H., de Jeu, W. H., *Eur. Phys. J. E.* **2006,** 19, (4), 385.

The next experiment to carry out is the swelling test, whose fundamental aspects have already been discussed in chapter 1. To obtain the swelling anistotropy of our materials, we have performed a series of swelling experiments using toluene as solvent. These tests allowed to calculate the percentage of expansion of elastomers swollen in a solvent. The experiment consists in measuring the film edges variations, considering the longest one as being parallel to the main director and the shortest one perpendicular to the main director. A detail of the process step is depicted in Figure 2.2.

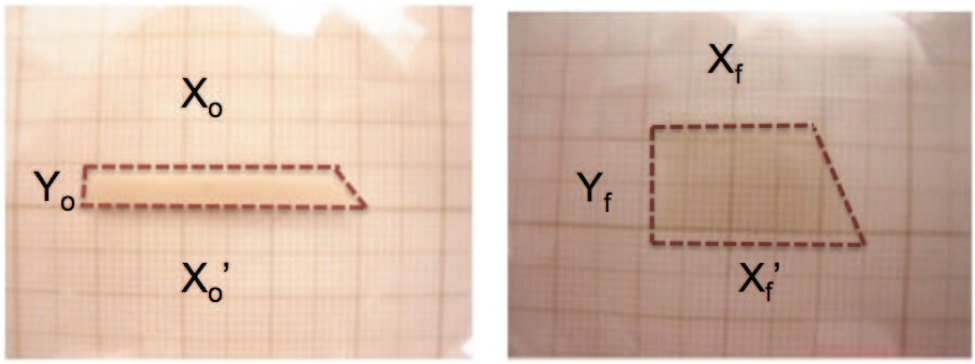

Figure 2.2. Images of the swelling experiment: unswollen sample (left) and swollen sample (right).

The estimation of these parameters leads also to the determination of the crosslinking degree of our samples, by comparison with the ideal Flory Huggins formula.[104] So the parallel and perpendicular swelling, denoted as $\alpha_{\parallel}$ and $\alpha_{\perp}$ respectively, represent the quotient between the unswollen and swollen elastomer. The swelling coefficient $\boldsymbol{q}$ represents the ratio of increased volume with respect to the unswollen elastomer and the swelling anisotropy ($\boldsymbol{q_z}$) describes the difference of the swelling with respect to the parallel and perpendicular edges: the higher $\boldsymbol{q_z}$, the larger anisotropy of the system.

Table 2.5. Swelling anisotropy results of **HMTS** elastomers and coelastomers at 25ºC using toluene as solvent.

Elastomer	q_z	$\alpha_{\perp}$	$\alpha_{\parallel}$	q
EN1T	1.1	3.0	2.8	24.9
CoE75T	5.9	4.3	0.7	13.3
CoE50T	4.9	4.3	0.9	16.1
CoE25T	3.1	3.4	1.1	12.9
EN2T	1.4	3.0	2.2	20.0

q_z: swelling anisotropy; $\alpha_{\perp}$: perpendicular to the director swelling; $\alpha_{\parallel}$:parallel to the director swelling
q: Swelling factor. ($q=\alpha_{\perp}^{2}\alpha_{\parallel}$)

As it can be observed, all the q values stay within a common range in the coelastomer series, which indicates that the crosslinking density is almost the same in all cases. Otherwise, swelling anisotropies were quite different with respect to **N1** monomer proportion, which can be interpreted as a function of the monomer length, expected to be maximal in the case of **EN1T** elastomer. Opposite to the three coelastomeric films, elastomers constituted of pure monomers **EN1T** and **EN2T** presented swelling factors (q) higher than expected for this degree of crosslinking, indicating that their crosslinking density is considerably lower than the coelastomer analogues. They present also weak swelling anisotropy due to a lack of reaction completion (high soluble content). Previously reported MC LCEs with similar crosslinking density[102] show similar values, which allow to estimate our average number of monomers between chains, being 13 in the cases of **CoE75T** and **CoE25T** and 15 in the case of **CoE50T**.

2.4.2. *Disiloxane Coelastomers.*

Three disiloxane coelastomers were also obtained by the same method as for the previously described analogues, the only difference being the chain extender length varying from **HMTS** to 1,1,3,3-tetramethyldisiloxane (**TMDS**). The MC-LCEs

containing only **N1**[124] or **N2**[104] have been synthesized previously as well as another **TMDS**-phenylbenzoate type systems.[127]

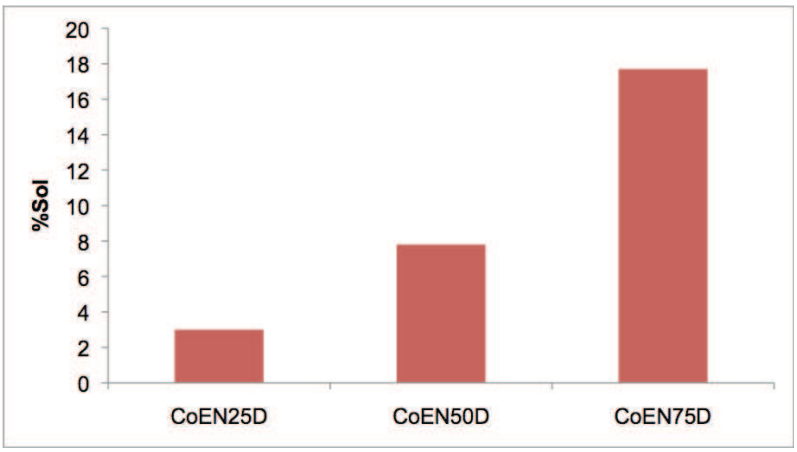

Plot 2.III. Soluble content of **TMDS** coelastomers.

The variation of the soluble content of **TMDS** coelastomers as a function of the monomer ratio is shown above. The values are rather high with respect to soluble contents reported for elastomer with **N2**, and is likely a consequence of the loss of stoichiometry due to the **TMDS** volatility. Even if these results have not been optimized, they are still acceptable and we could use these novel elastomers to perform further thermoelastic and viscoelastic experiments tests and to study their swelling behavior, whose results are collected in the next table:

Table 2.6. Swelling anisotropy of **TMDS** coelastomers.

Coelastomer	q_z	$\alpha_\perp$	$\alpha_\parallel$	q
CoE75D	3.87	3.05	0.79	7.31
CoE50D	3.67	3.33	0.91	10.10
CoE25D	4.67	3.33	0.71	7.94

q_z: swelling anisotropy; $\alpha_\perp$: perpendicular to the director swelling; $\alpha_\parallel$:parallel to the director swelling
q: Swelling factor.

[127] Rogez, D.; Brandt, H.; Finkelmann, H.; Martinoty, P., *Macromol. Chem. Phys.* **2006,** 207, (8), 735.

The three synthesized coelastomers show good swelling anisotropy due to the contribution of the liquid crystalline segments inserted along their polymeric backbones, which will be discussed in the next chapters since it is associated to their mesomorphism.

2.4.3. *Comparative Study.*

In this part, we would like to focus on the difference between the two series of coelastomers as a function of the chain extender. We first compared the swelling factor "***q***" between the two series, obtaining plot 2.IV.

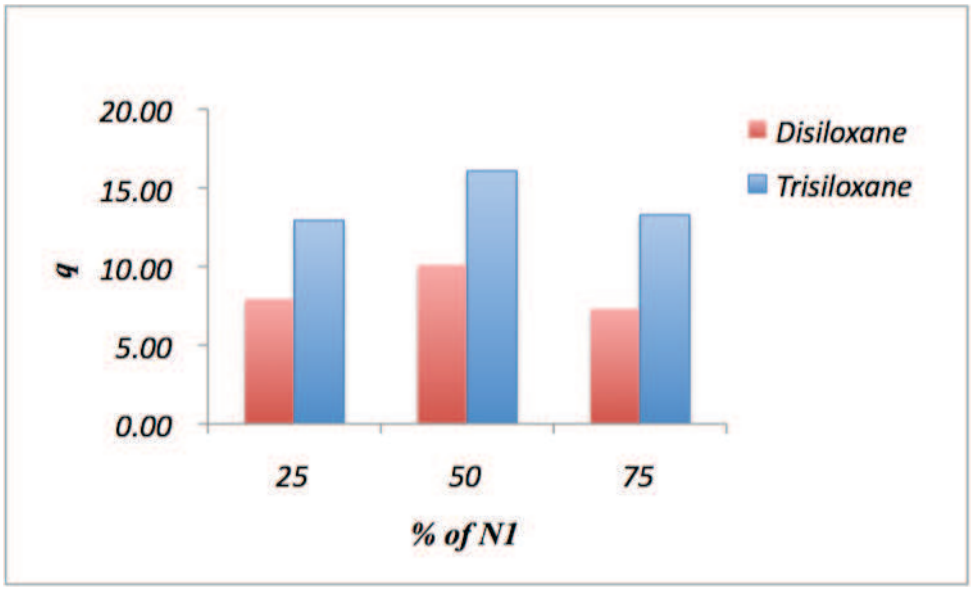

Plot 2.IV. Swelling parameters (*q*) of MC-LCCoEs synthesized.

In all cases, the swelling parameters are higher for the trisiloxane systems which show a higher capability of swelling, which is expected due to longer chain length in the former and thus an increase of the average distances between crosslinking points (wider mesh),[104,128] since the density of the network decreases. As for the network's

[128] Sanchez-Ferrer, A.; Finkelmann, H., *Macromolecules* **2008,** 41, (3), 970.

anisotropy, comparing both parallel-to-the-director ($\alpha_{//}$) and perpendicular-to-the-director ($\alpha_{\perp}$) swelling parameters, brings additional specific information.

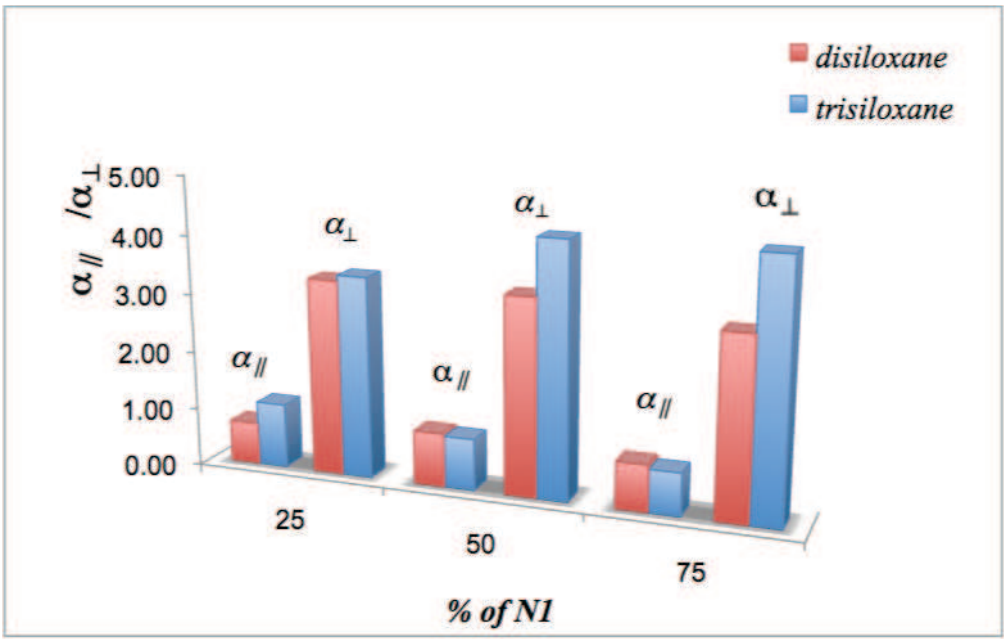

Plot 2.V. Swelling ratios (α) of MC-LCEs.

As illustrated, parallel swelling values factors remain comparable in almost all cases, in agreement with theory. On the other hand, we observed that the perpendicular swelling values were found to increase with the bulkiness of the siloxane segment and within the same series. The values reach a maximum at 50:50 monomeric ratio. Hence, increasing the amount of the **N1** monomer (longer), resulting in a higher capability of swelling, particularly in the case of the trisiloxane elastomers. The opposite is true in the disiloxane analogues for which the value remains almost constant along the series. Thus, it appears that in the disiloxane analogues, the perpendicular swelling is independent of the **N1** monomer's content. In this case, we obtained lower values for the disiloxane elastomers, and the trisiloxane elastomers's values were similar to those of disiloxane systems.[104]

2.4.4. *Bent-Core/Calamitic-Mesogen Liquid Crystalline Coelastomers.*

In this study, we have also investigated the effect of the monomer's shape, by inserting bent-core molecules into the main-chain polymer backbone. Indeed, most of the side and main-chain LCEs are constituted of linear calamitic fragments (a few only with disc-like moieties). In this work, we decided to study the influence of a bent core molecule on the mechanical and mesomorphic properties of the corresponding liquid crystalline network, expecting to give larger anisotropy changes but also ferroelectric polar smectic (or biaxial nematic) mesophases. We first attempted to synthesize elastomers containing bent-core mesogens using the procedure described for calamitic mesogen containing LCEs. However, the film preparation did not proceed when either a single or a mixture of bent-core monomers was used essentially due to the high *Tg* (discussed in section 3.5.2), and insolubility of the monomers in toluene. We then moved to the preparation of coelastomers containing mixtures of bent-core monomers and calamitic mesogens. Since available quantity of starting monomer was limited due to synthetic problems, we decided to employ just two types of bent-core monomers (out from the six synthesized) blended with a calamitic monomer in two different proportions: a weak fraction (5%) and a more significant one (25%) of the bent-core monomer. For higher content of bent-core monomer (>25%) the reaction did not proceed for the same reasons as those evoked for bent-core-containing LCEs. Due to the potential new mesophases that they could eventually present, we have chosen the monomers **B4** and **B6**. None of them presented liquid crystalline properties: **B4** presents several crystalline forms whereas **B6** is a low melting point compound (paragraph 3.5.1).

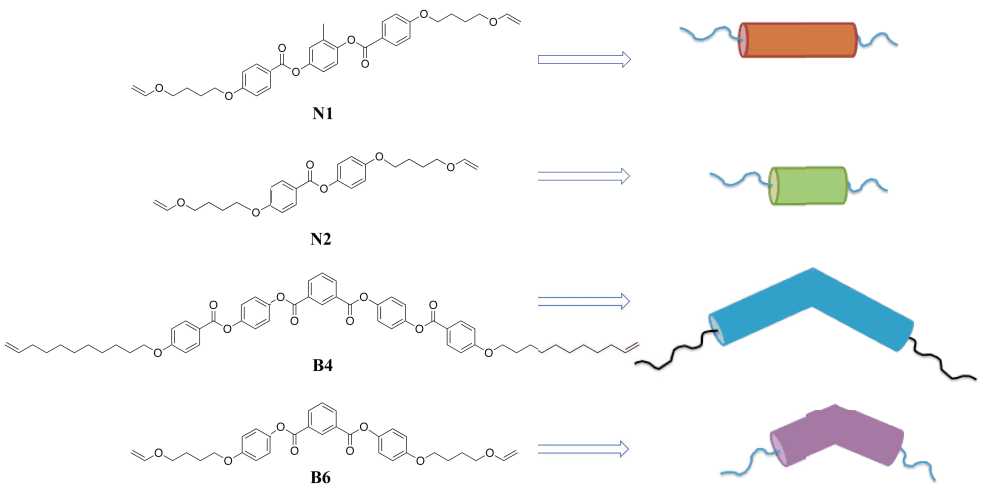

Scheme 2.14. Schematic representation of the chosen monomers for the MC BC/CM LCE.

We have elaborated a library six different LCCoEs (Table 2.7), through this combinatory approach changing monomers type and proportion in the mixture. All the coelastomers were synthesized following the same protocol as for the previous ones. As previously, the soluble content was very low (plot 2.VI).

Table 2.7. Combinatory table of bent-core/calamitic-mesogen reactions.

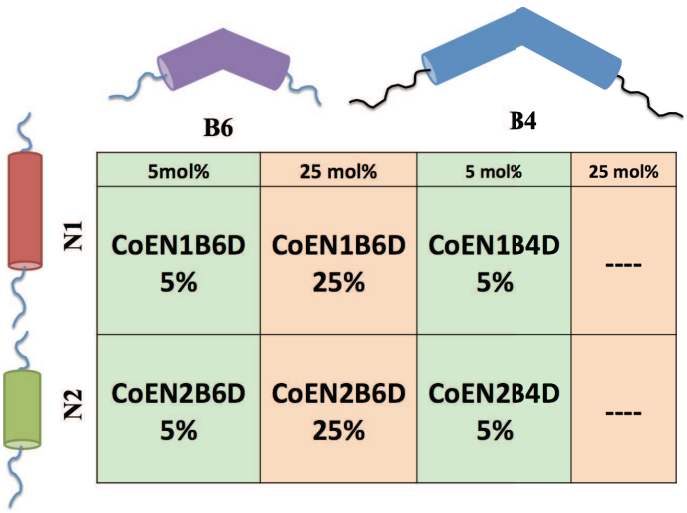

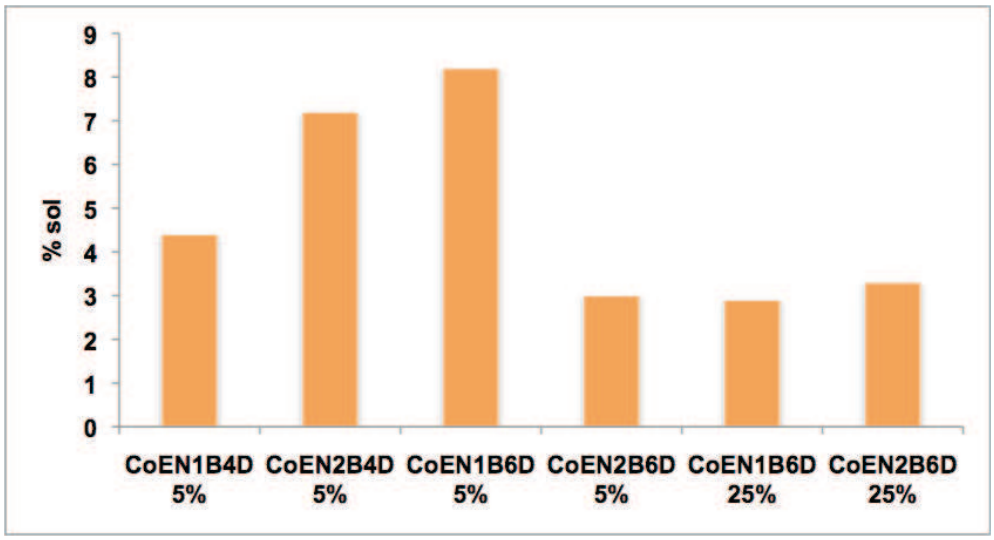

Plot 2.VI. Soluble content of MC-BC/CM LCEs.

After completing this series of coelastomers, we first evaluated the soluble content of our coelastomers which was found as low as 3 percent in some cases. In addition, interesting results were obtained for the swelling experiments as reported in table 2.8.

Table 2.8. Swelling of MC-BC/CM LCEs

Coelastomer	q_z	$\alpha_\perp$	$\alpha_\parallel$	q
CoEN1B4D 5%	3.80	2.62	0.69	4.7
CoEN2B4D 5%	4.13	3.71	0.90	12.4
CoEN1B6D 5%	2.63	2.89	1.10	9.2
CoEN2B6D 5%	1.50	2.78	1.85	14.2
CoEN1B6D 25%	2.54	2.97	1.17	10.3
CoEN2B6D 25%	1.05	2.05	1.96	8.3

q_z: swelling anisotropy; $\alpha_\perp$: perpendicular to the director swelling; $\alpha_\parallel$:parallel to the director swelling
q: Swelling factor.

The swelling parameter relationships are shown in plot 2.VII.

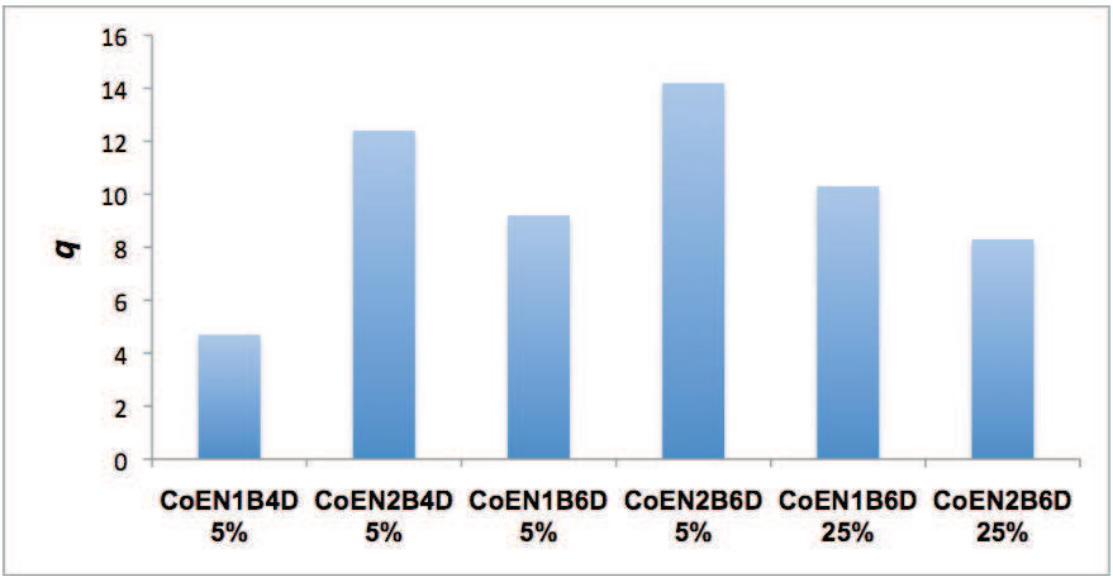

Plot 2.VII. Swelling parameter (q) of MC-BC/CM LCE.

From these characterizations, the following statements can be proposed:

- As the size of the bent core molecule increases (**B4→B6**), the swelling parameter of the samples decreases, this effect being even more remarkable when **N1** is the network's co-monomer.
- The swelling parameter increases as the monomer's length decreases (**N1→N2** or **B4→B6**), in the low content (5%) of bent-core molecule's quantity in LCEs (this turnover will be discussed later).
- Increasing the percentage of bent-core changes radically the sample's swelling anisotropy. It increases in **CoEN1B6D** elastomers, whereas it decreases along **CoEN2B6D** series.

To get a deeper understanding of the overall behavior, we plotted all the swelling results and compared them as a function of the bent-core monomer content (plot 2.VIII) and as a function of the percentage of bent-core present in the network (plot 2.IX).

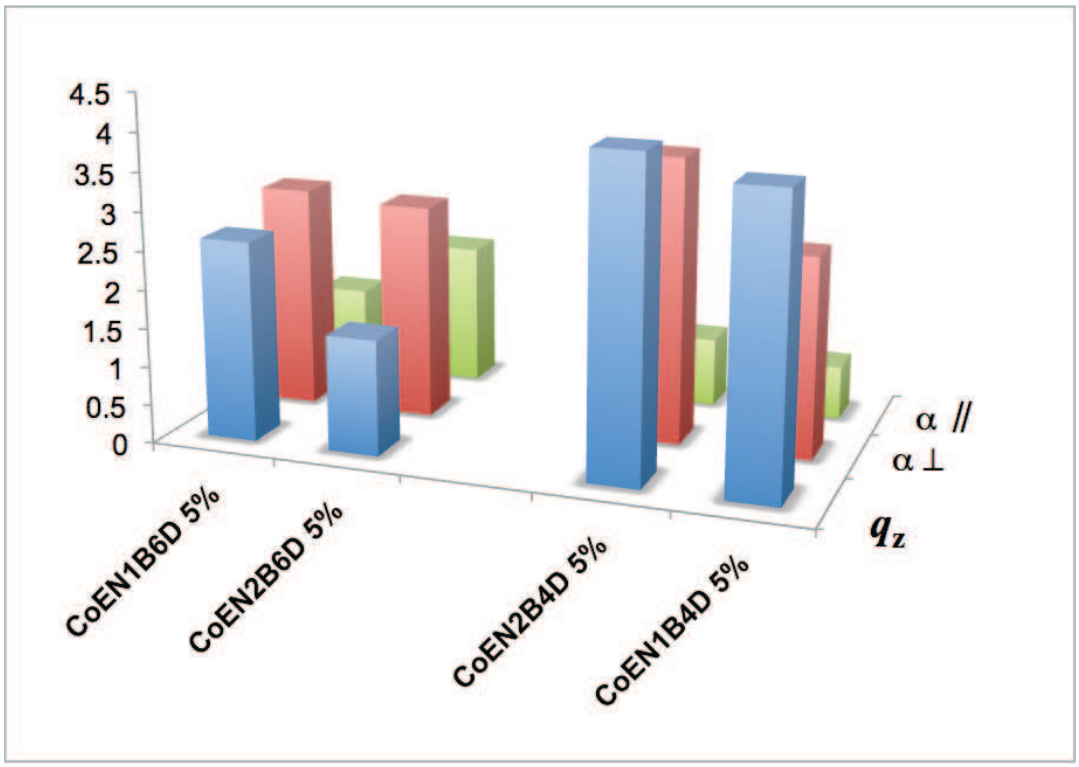

Plot 2.VIII. Swelling anisotropy as a function of the monomers.

The samples synthesized with monomer **B4** presented the largest swelling anisotropies with respect to the **B6** LCCoEs. This shows that the longest monomer enhances anisotropy values due to its molecular length. Interestingly, elastomer **CoEN2B6D 5%** presented the lowest swelling anisotropy of the 5% MC BC/CM LCCoEs synthesized, which makes it less anisotropic than the others. This was associated with the possible conformation of the bent-core molecule and the mesogens along the network, which undergoes at macroscopic scale loss of anisotropy. To confirm this hypotesis, we compared this sample with its 25 % analogue in table 2.IX.

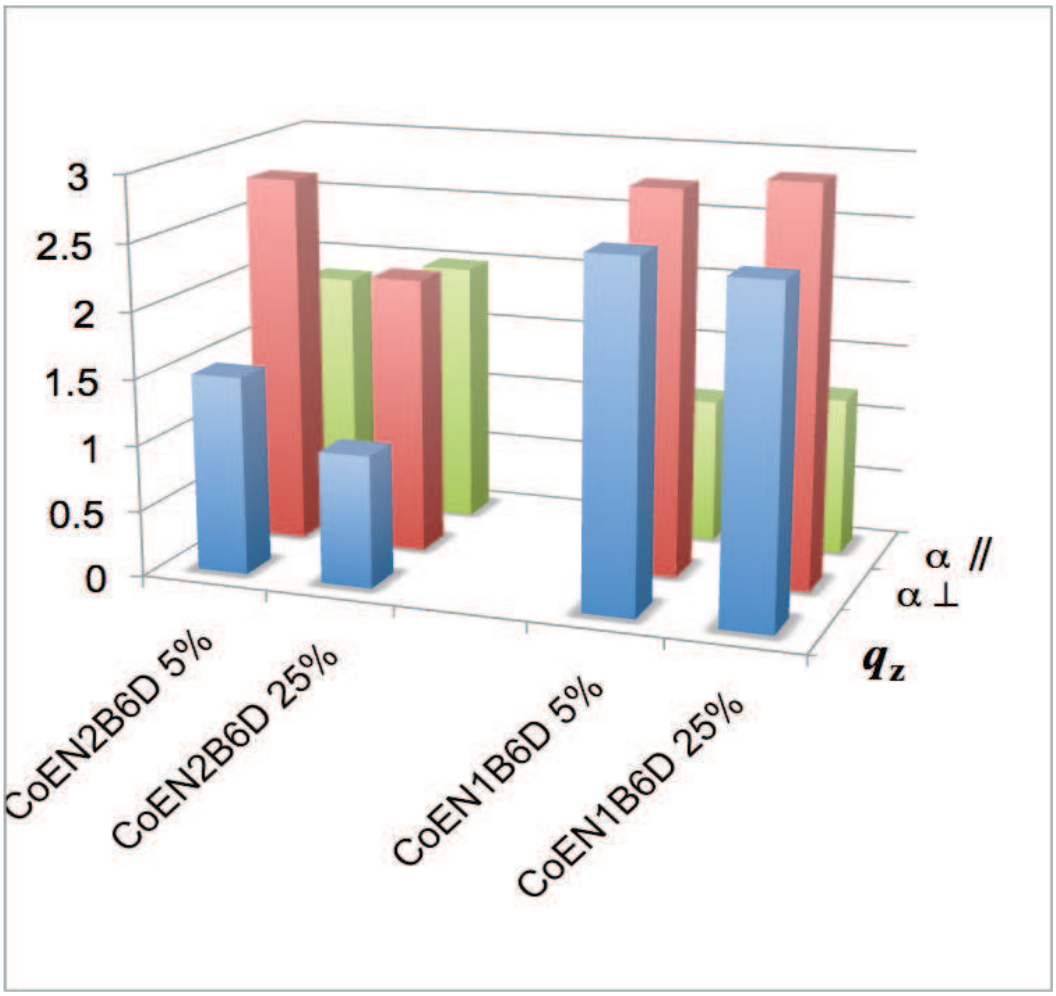

Plot 2.IX. Swelling anisotropies of the series **CoEN2B6** and **CoEN1B6** as a function of **B6** percentage.

The elastomer **CoEN2B6D** synthesized with 25% of bent-core monomer does not present network anisotropy; even if it is an isotropically swollen sample, the film presented a LC phase below room temperature (paragraph 3.5.3).

In the case of the elastomers series **CoEN1B6D**, no significant change was observed in their anisotropy, maybe because the limit of the mesophase stability was not reached. Another fact in agreement with this behavior of the **CoEN2B6D** samples is that the length of **B6** in its more stable form (estimated with Ballview software) is nearly the same as the calamitic mesogen **N2**, but with an elbow that likely deforms the overall polymer linear structure (Figure 2.3 and scheme 2.15).

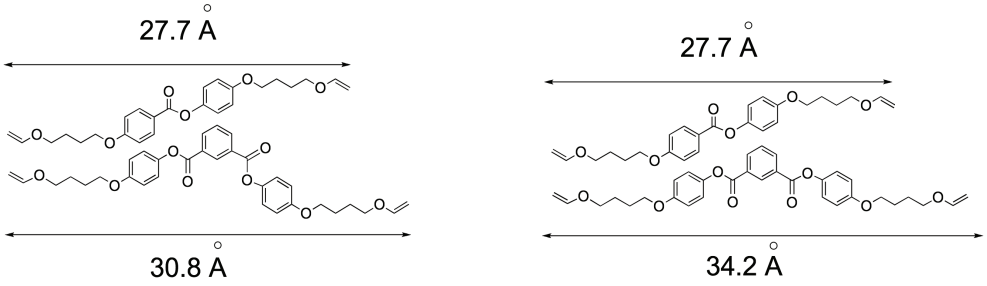

Figure 2.3. Molecular length of the monomers **N2** and **B6**. More stable conformation (left) and stretched conformation right.

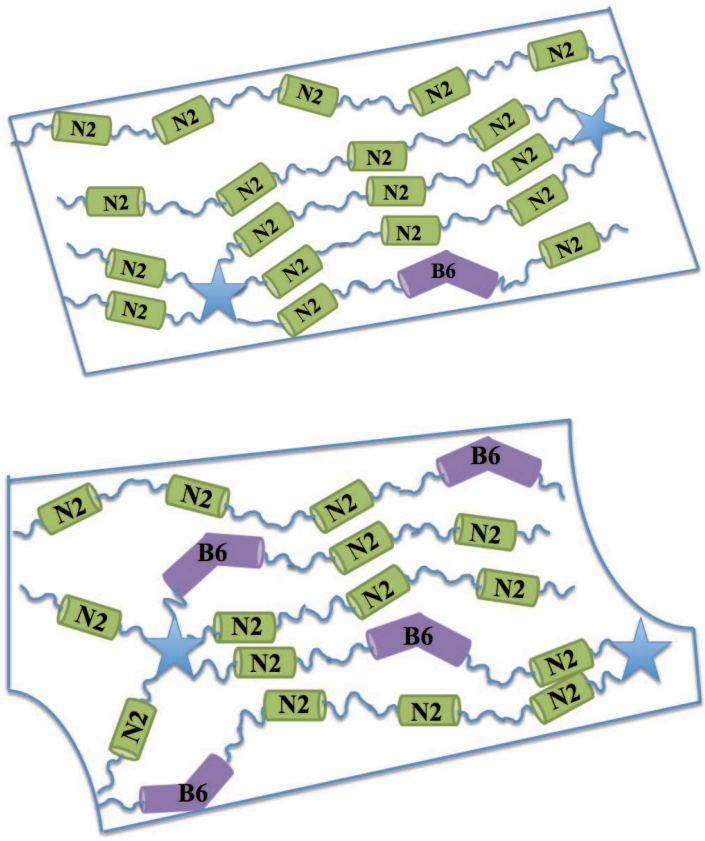

Scheme 2.15. Schematic representations of the coelastomers **CoEN2B6D 5%** (up) and **CoEN2B6D 25%** (down).

Further dilatometry experiments are in the way to be performed in order to have more evidences about these results. The dilatometry will allow obtaining **B6** molecular volume. With this value we can estimate if the anisotropy is lost along the elastomeric network.

2.5. Conclusions.

Liquid crystalline monomers, polymers and elastomers were synthesized and characterized by traditional synthetic and polymer methods. Improvement in some reaction steps allowed to reach fairly good to very good yields without risking final monomers purity.

By using longer, less volatile chain extender such as **HTMS**, polymers with high polymerization degrees and acceptable polydispersities were obtained, whereas synthesized **TMDS** analogues exhibited lower yield and degrees of polymerizations due to chain extender volatility.

Once again the one-pot synthesis and two-step curing processes indicated their high efficiency and versatility for network formation, which permitted to obtain elastomer films of the various monomer combinations proposed.

Soluble content and swelling experiments performed on our elastomers revealed the network density, crosslinking degree and anisotropy of our material. They are suitable-to-good quality, essential to perform further measurements.

Addition of a dopant with a particular shape or geometry, such as a bent-core molecule, suggest that the final material anisotropy can be controlled. The Bent-Core/Calamitic Mesogen Liquid Crystalline Coelastomers synthesized led to prove that geometry of the components play a crucial role in the network formation.

Chapter 3

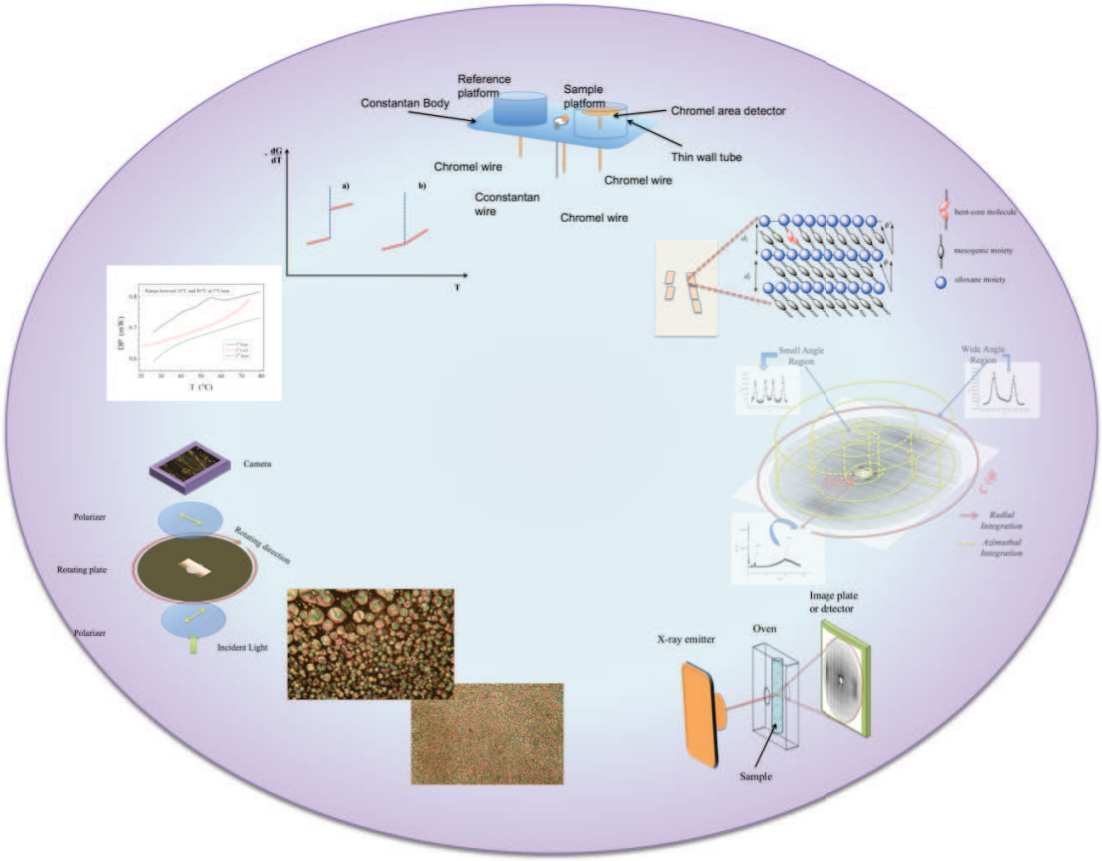

Mesomorphic Properties

3. Mesomorphic Behavior.

In this chapter, we discuss the systematic study of the liquid crystalline properties of our products, analyzed by thermodynamical, optical and spectroscopic methods. The three techniques employed to characterize the thermotropic behavior of the MC LCEs and CoEs were polarized optical microscopy, differential scanning calorimetry and X-ray diffraction, whose fundamental aspects are briefly introduced.

3.1. Background and fundamental concepts.

3.1.1. *Polarized Light Microscopy*

Liquid crystals, due to their anisotropy, present a property called birefringence, which means that they possess two refraction indices: one parallel and the other perpendicular to the director.

When light passes through a birefringent material, the phenomenon that occurs can be explained in terms of the light being splitted into two components: the ordinary and extraordinary beams. As the component's velocity also changes, the wave components get out of phase and when the beam recombines by going out of the sample the polarization state is changed.

For fluid, uniaxial liquid crystalline phase formed by calamitic molecules, free to rotate about the long axis n_z. the polarizabilities along orthogonal axes, n_y and n_x become equivalent and therefore, the two associated refractive indices become the ordinary index n_0. The refractive index along it is the already mentioned extraordinary beam, thus birefringence can be expressed as:

$$\Delta n = n_e - n_o \tag{3.1}$$

The ensemble of defects associated to the deviations of the extraordinary beam director give rise to the characteristic textures known for liquid crystalline mesophases.

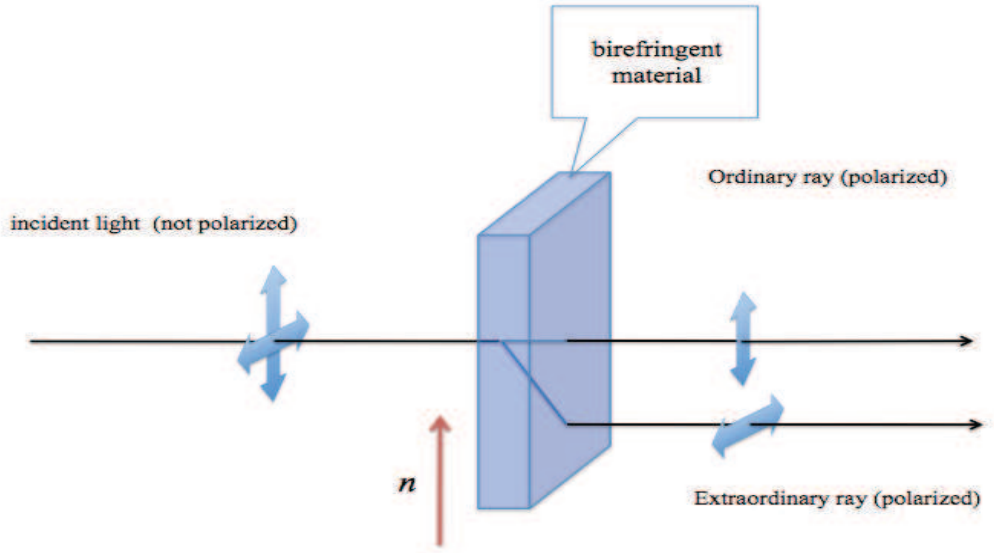

Scheme 3.1. Polarization of light due to a material's birefringence.

Let us consider a birefringent material, like a liquid crystal, between two crossed polarizers, the incident light passes through the first polarizer, whose electric vector axis is aligned at some angle between both directions of the material refraction indices; the linear polarized light becomes elliptically polarized due to the birefringence of the material. When this light reaches the second polarizer the elliptically polarized light can pass through twice a cycle and a bright region will be observed. In the case of an amorphous material (isotropic state), the light polarization will not change (no anisotropy) and the corresponding sample will generate a dark region.

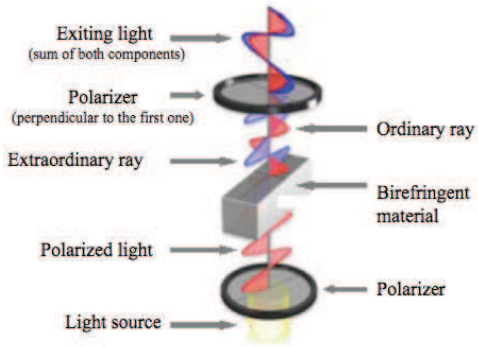

Scheme 3.2. Cross-polarizer's experiment.[102]

3.1.2. *Phase Transitions, Mesophases and Differential Scanning Calorimetry*

When heated, a crystalline solid **K** melts at a given temperature $T_{K\text{-}I}$ (known as the melting point or fusion temperature), to give the liquid state **I**. Beyond this temperature, the stable species is **I**.

$$\mathrm{K} \underset{T_{I\text{-}K}}{\overset{T_{K\text{-}I}}{\rightleftharpoons}} \mathrm{I} \qquad \text{where } T_{I\text{-}K} \leq T_{K\text{-}I} \tag{3.2}$$

This transition is described as a first order because of the enormous reorganization of the state. On the other hand, during the melting process, the entropy of the system increases due to the loss of material's positional and orientational order. The crystallization occurs at $T \leq T_{K\text{-}I}$ although the crystal is a thermodynamically stable phase between $T_{I\text{-}K}$ and $T_{K\text{-}I}$ with $T_{I\text{-}K} < T_{K\text{-}I}$. The existence of a liquid at $T < T_{K\text{-}I}$ is a product of kinetic stabilization. This is denominated as a ***supercooled*** liquid.

Some materials, such as liquid crystals, exhibit a mesophase **M**. The initial solid material melts at a given temperature $T_{K\text{-}M}$ involving a certain transition enthalpy

ΔH_{KM} to give rise to a mesophase. This intermediate state, when heated, will reach a temperature in which it will become an isotropic liquid **I**. In this case, the associated enthalpy ΔH_{MI} is generally lower than ΔH_{KM}. Since, the loss of order in liquid crystals is often gradual, the transitions in this case are weakly first order or even second order. The entire process is illustrated in the next equation.

$$K \underset{T_{M\text{-}K}}{\overset{T_{K\text{-}M}}{\rightleftharpoons}} M \underset{T_{I\text{-}M}}{\overset{T_{M\text{-}I}}{\rightleftharpoons}} I \qquad (3.3)$$

If the mesophase is observed on both heating and cooling (reversible), it is thermodynamically stable and is described as ***enantiotropic*** (3.3). Although, it is possible for a mesophase to be disfavored with respect to the crystal phase and is in this case only kinetically stable. Such mesophase appears only when cooling process is performed and is known as ***monotropic***.

A given compound can present many different mesophases. Such a behavior is known as polymorphism (3.4). Each transition state has an associated transition temperature, involving an increase of the system's entropy all along the phase behavior.

$$K \underset{T_{M\text{-}K}}{\overset{T_{K\text{-}M}}{\rightleftharpoons}} M1 \underset{T_{M2\text{-}M1}}{\overset{T_{M1\text{-}M2}}{\rightleftharpoons}} M2 \cdots \underset{T_{MN\text{-}Mx}}{\overset{T_{Mx\text{-}MN}}{\rightleftharpoons}} MN \underset{T_{I\text{-}MN}}{\overset{T_{MN\text{-}I}}{\rightleftharpoons}} I \qquad (3.4)$$

We have previously referred first or second order transitions, without describing the corresponding thermodynamics implied in the process. Let us take a look into this process's parameters in order to better understand phase transitions.

First order transitions have a discontinuity in the slope of free energy G, at the phase change ($\Delta S = -\Delta\left(\frac{dG}{dT}\right)$), whereas for a second order transition, the G function lies continuous but the slope changes at the transition (plot 3.1).

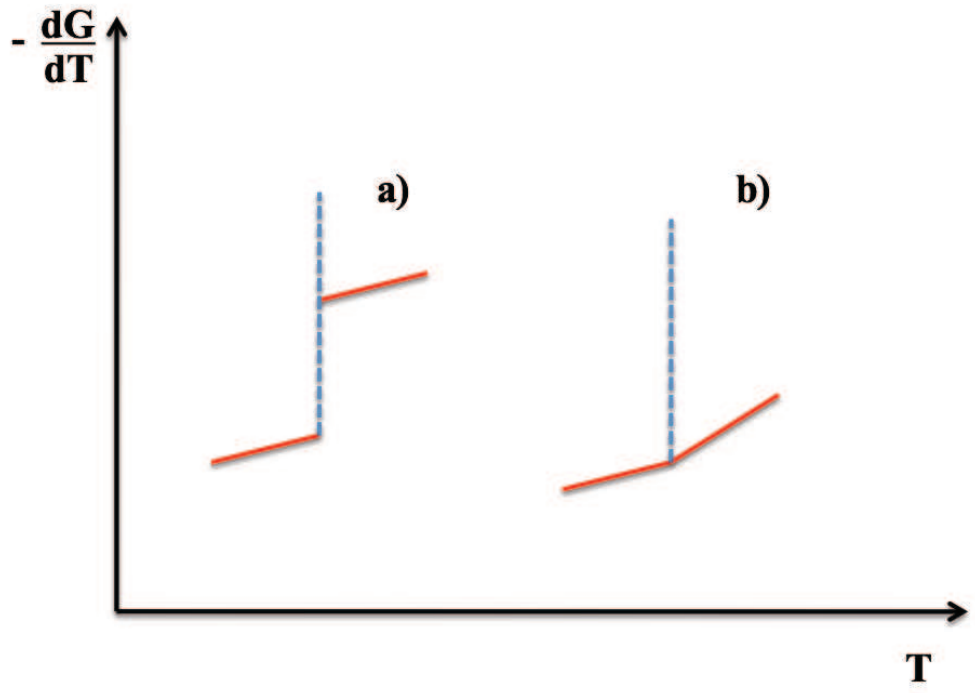

Plot 3.I. First (a) and second (b) order transition representations. G: Gibbs free energy; T temperature.

Large enthalpies correspond to marked changes of molecular organization in the structure; such transitions are first order i.e. melting transition (solid to mesophase), transition between two mesophases and clearing transition (**M-I**). In the case of the smectic C to nematic transition, the layer ordering is lost as well as the molecular tilt angle. This change implies an abrupt change into the system order and it is supposed to be first order. On the other hand, when we pass from a smectic C to a smectic A mesophase, where the only change is the vanishing of the mesogen's axis tilt angle with respect to the layer normal, the transition is generally second order in which the

change of the tilt angle is continuous. The transition is said to be second order and the only change is in its heat capacity *Cp*.

In order to determine the transition temperatures and enthalpies as well as the glass transition of our materials, we carried out a very precise experiment called differential scanning calorimetry (DSC). The employed apparatus works with a heat flux: it consists in an oven containing a single Constantan alloy plate with the reference (empty pan) and the other, with the sample, connected by a thermocouple (scheme 3.3). The oven temperature is changed according to a predetermined program, generally at constant heating rate. The temperature conduction through the platforms i.e. the heat flows, is calculated from the conduction difference between the thermocouple in the middle of the plate, the reference and the sample. A typical DSC trace is illustrated in plot 3.1 showing a glass transition and a first order phase transition.

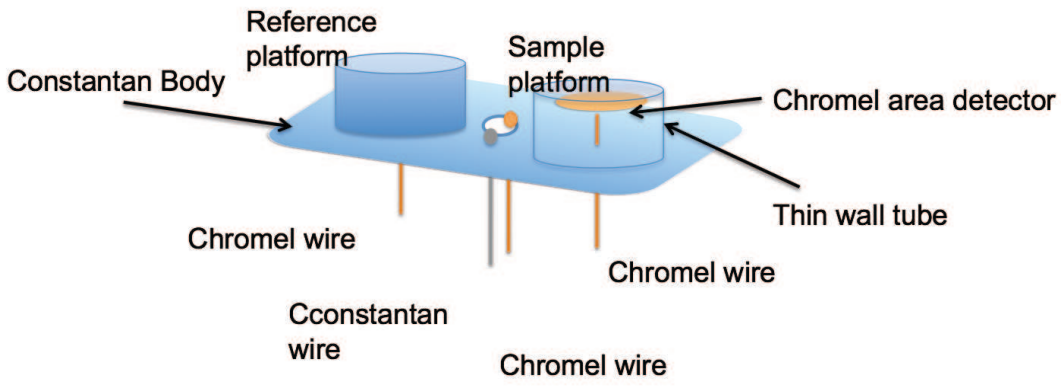

Scheme 3.3. Illustration of a DSC device.

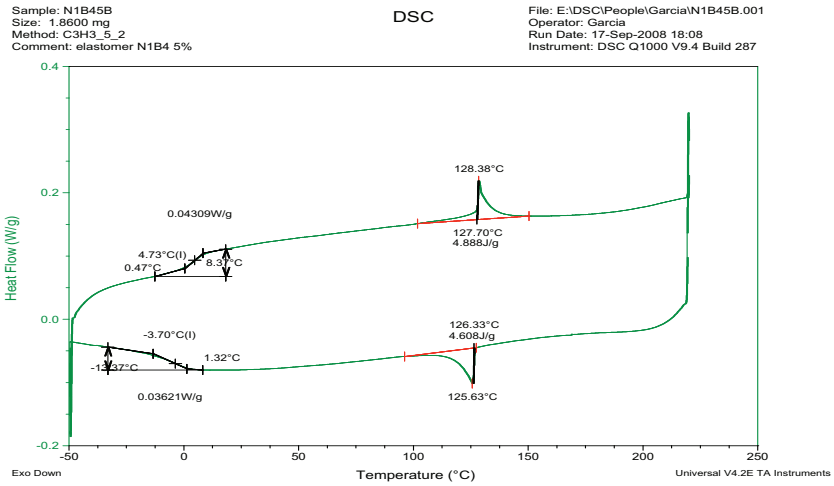

Plot 3.II. DSC plot showing glass transitions, transition phase temperatures and enthalpies of a heating cooling cycle.

The glass transition temperature is defined as the temperature in which the frozen backbone of the polymer softens, *i.e.* when the polymer in the glassy state becomes more fluid.[129] In the case of the first order transitions the peak maximum represents the phase transition temperature and the peak area corresponds to the transition enthalpy; T_{ONSET}, temperature at which the transition starts is defined as the intersection of the onset and the baseline. When the difference of the transitions is larger enough between cooling and heating cycles, we observe the previously discussed supercooling liquid.

3.1.3. *X-ray diffraction*

We have characterized our samples by small angle (SAXS) and wide angle X-ray scattering (WAXS). This method permits to determine precisely the mesophase parameters and for instance the layer spacing, the mesogen's tilt angle with respect to

[129] The IUPAC Compendium of Chemical Terminology, **1997**, 66, 583.

the layer normal, as well as the mesophase's order parameter and the correlation distance between layers.

The Bragg´s law can be visualized by the scattering of X-rays from a set of lattice planes (scheme 3.4). For one particular set of planes, constructive interference will occur when the Bragg´s law is satisfied:

$$\lambda = 2d\sin\theta \tag{3.5}$$

Where $\boldsymbol{\lambda}$ is the wavelength of the emitted radiation, in our case Cu-$K_{\alpha 1}$ =1.5405 Å; $\boldsymbol{d}$ is the plane distance, and $\boldsymbol{\theta}$ the angle of diffraction.

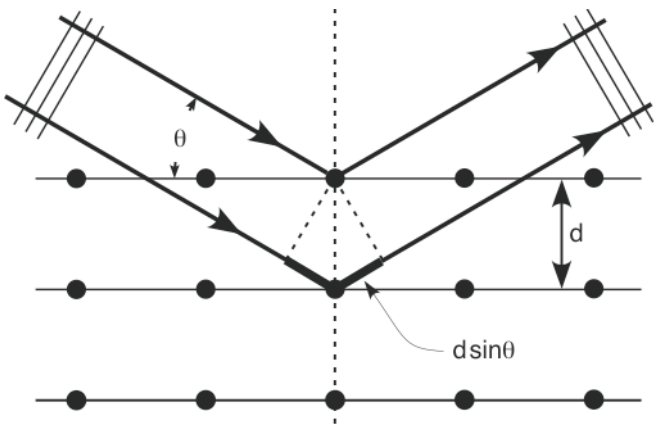

Scheme 3.4. Diffraction of the incident ray when reflected by a single lattice.

In 1913 Peter Ewald published details of a geometrical construction, which has been used ever since for interpreting diffraction patterns. When an X-ray beam hits a crystal, the Ewald's sphere shows which sets of planes are at (or close to) their Bragg angle for diffraction to occur.

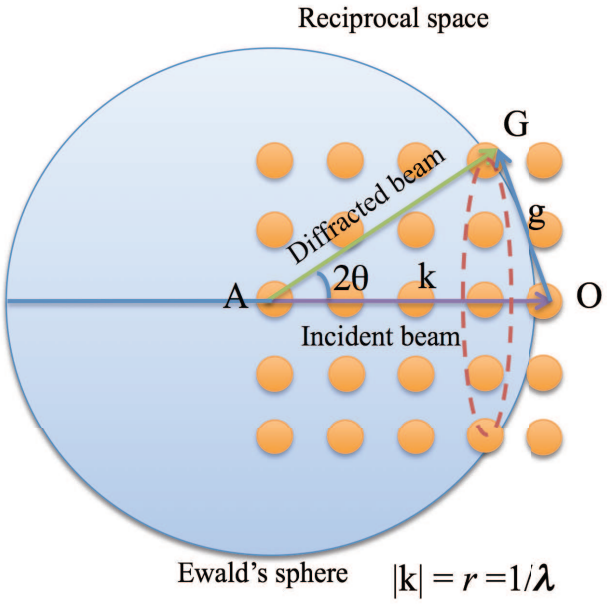

Scheme 3.5. Ewald's sphere.

The incident wave is represented by a reciprocal wave vector **AO**, with a matrix **k** which goes to **O**. The diffracted beam is another wave vector with the same matrix **k**, which is considered within the circle. Wherever a reciprocal lattice point touches the circle, Bragg's Law is obeyed and a diffracted beam will occur. **AO** represents the incident beam and **AG** is a diffracted beam. The angle between both beams must be 2θ. **OG** is the g_{120} vector and thus has magnitude $1/d_{120}$, and since $|k| = 1/\lambda$:

$$|OG| = \frac{2}{\lambda}\sin\theta = \frac{1}{d} \tag{3.6}$$

The general interpretation of the **g** vector is the change in the wave vector of the diffracted beam. Our X-ray scattering is represented as a 2 D image (Scheme 3.5), whose reflections are represented as concentric rings. In the case of our MCLCE films, we obtained fine and well defined spots in small angle region (SAXS) corresponding to layer ordering and diffuse signals assigned to mesogenic units lateral distance (figure 3.1).

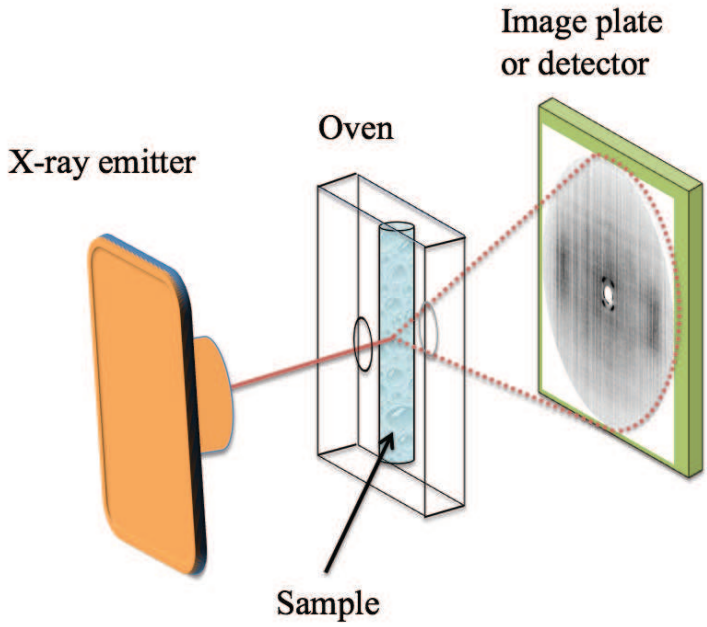

Scheme 3.6. X-ray diffraction device and x-ray scattering pattern obtained.

The obtained pattern can be seen as a 3 D image showing the reflections as conical structures as depicted in figure 3.1.

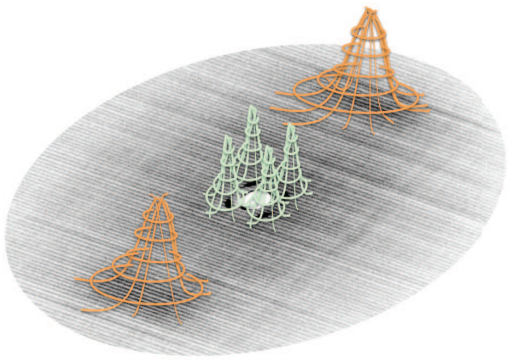

Figure 3.1. Representation of a 3 D pattern of SAXS and WAXS.

To analyze these signals, we obtained two types of integration plots. The radial integration, which consists in an integration of the radius between 0 and 360º of the azimuthal angle and allows to see the intensity of the signals as a function of the angle

2θ. As for the azimuthal integration plot, it describes the signals between two circles limiting a $2\boldsymbol{\theta}$ range as a function of the azimuthal angle $\boldsymbol{\phi}$. Two integrations are necessary, one for the small angle region and another for the wide angle. A clear scheme of the process is shown next (scheme 3.7).

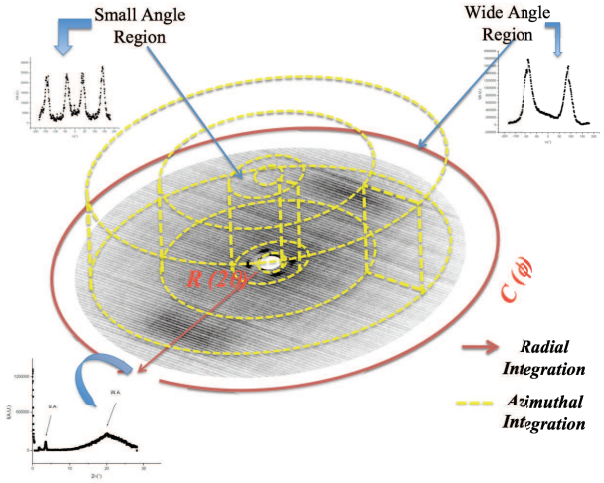

Scheme 3.7. Integration processes for pattern analysis.

To determine the correlation distance $\boldsymbol{\xi}$, we used the Scherrer's equation (3.7), which was developed to estimate the correlation length of the layers in small crystals (crystallites) without defect.

$$\xi = \frac{0.888\lambda}{w_{1/2}\cos\theta} \tag{3.7}$$

$\boldsymbol{\lambda}$ is the wavelength (1.542 Å); $w_{1/2}$ is the *full width at half maximum* of the peak (*FWHM*) and $\boldsymbol{\theta}$ the angle at this point. We can also deduce the number of correlated layers $\boldsymbol{n}$ by dividing the correlation distance by the layer distance $\boldsymbol{d_l}$.

$$n = \frac{\xi}{d_l} \tag{3.8}$$

In our case, the order parameter was not derived from the Maier-Saupe method (equation 3.9), as in most cases. Instead we made iterations by plotting the normalized wide angle signal (WAXS) until it resembles to an ideal statistical function. The analyses are rougher but give acceptable values for the smectic-C phases.

$$S = \frac{\int_0^{\frac{\pi}{2}} I(\phi)\left(3\cos^2\phi - 1\right)\sin(\phi)d\phi}{\int_0^{\frac{\pi}{2}} I(\phi)\sin(\phi)d\phi} \qquad (3.9)$$

3.2. Characterization of the liquid crystalline behavior of the monomers and their mixtures.

In order to obtain suitable LCCoEs, we first examined the monomer's liquid crystalline behavior. Aiming at forming LCEs presenting only nematic phases, we first decided to evaluate the optimum mixture of **N1** and **N2** monomers yielding the largest nematic phase temperature range and at accessible temperatures. It is known from literature that mixtures of 2 mesogens of different length or shapes[106,130] often form nematic mesophases which are commonly used in the technology of LCD devices.[131] We needed also to consider two major constraints, the first one was related to the glass transition and the second is related to the clearing temperatures. A high

[130] Hennrich, G.; Ortiz, P. D.; Cavero, E.; Hanes, R. E.; Serrano, J. L., *Eur. J. Org. Chem.,* **2008**, 27, 4575.
[131] Collings, P. J., *Liquid Crystals: Nature's Delicate Phase of Matter*, Princeton University Press, Princeton, **1990**; Goodby, J. W., Saez, I. M., Cowling, S. J., Görtz, V., Draper, M., Hall, A.W., Sia, S., Cosquer, G., Lee, S.-E., Raynes, E. P., *Angew. Chem.Int. Ed.,* **2008**, 47, 2754.

glass transition temperature is detrimental for our elastomers as this would lead to hard, non orientable materials. Secondly, usually mixtures of mesogens result in a decrease of the clearing temperature, and in their corresponding polymers, a low T*g* is also expected. Since our elastomers are weakly reticulated they will mostly behave (thermally) as their precursory polymers thus facilitating the study of their mechanical and thermotropic properties.

3.2.1 *Thermal Behavior of Pure Monomers*

The first study performed was the evaluation of the thermal behavior of the mixtures of the monomers **N1** and **N2** as a function of their proportion. As pure compounds, both **N1** and **N2** exhibit a liquid crystalline phase, as observed by both DSC studies and POM.

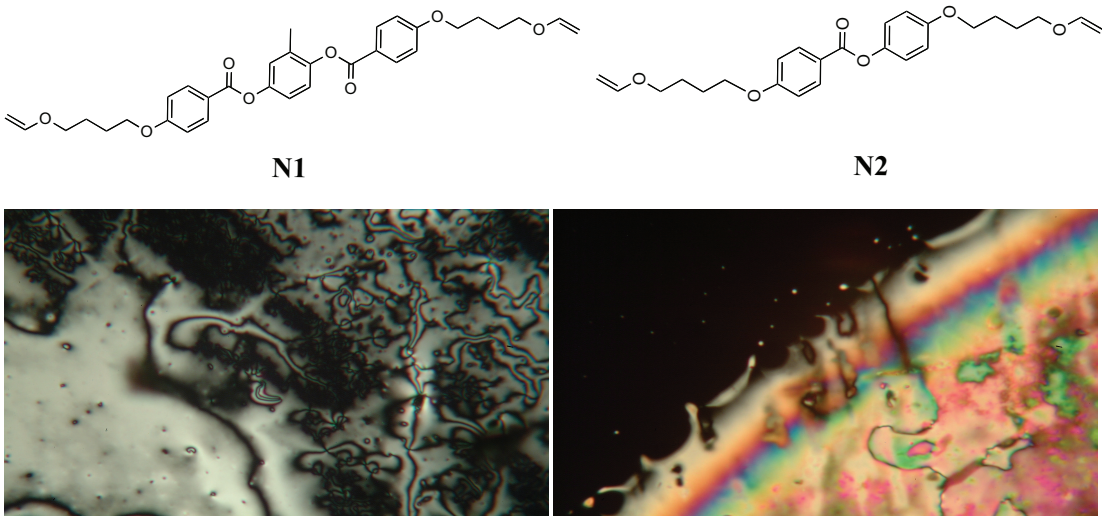

N1 **N2**

Figure 3.2. Optical textures of the monomers **N1** (left) and **N2** (right) cooling down from the isotropic state. **N1** 160ºC, nematic phase; **N2** 85ºC, smectic C mesophase.

N1 presents a nematic phase and **N2** presents a smectic C mesophase (table 3.1), in agreement with literature data.[104,105]

Table 3.1. Mesomorphic Properties of the Monomers

Compound	Thermal Behavior[a]	ΔT (LC)
N1	Cr 82 [25.5] N 168 [2.2] I	86
N2	Cr 82 [38.2] SmC 87 [1.3] I	5

[a]Transition temperatures (ºC) and enthalpies [kJ·mol^{-1}] of the monomers **N1** and **N2** obtained by DSC at a 2ºC/min heating rate during the third heating.

3.2.2. *Mixture Behavior*

Three different mixtures of both monomers were prepared by dissolving specific quantities of each monomer in dry dichloromethane. The solvent was slowly evaporated and the final mixture was analyzed by temperature scan-POM.

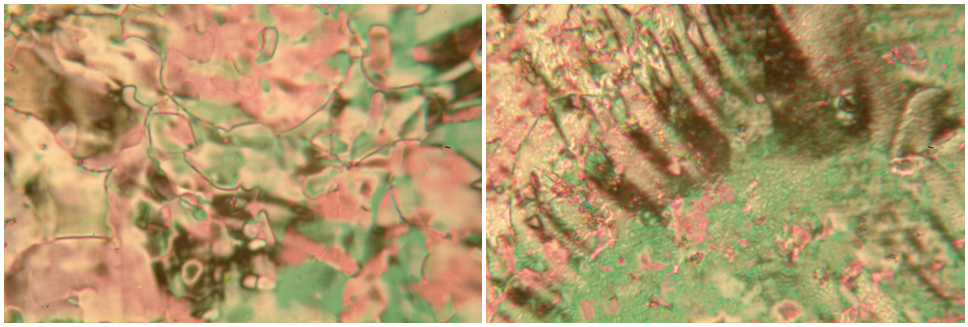

Figure 3.3. POM textures from the mixures **N1-N2** 25:75 at 70ºC, predominantly nematic mesophase (left) and **N1-N2** at 75:25 at 120ºC, predominantly nematic mesophase (right).

By mixing the monomers, we succeeded in decreasing both the melting and clearing temperatures of the mixture with respect to the pure monomers. Although, in most of the cases, DSC showed several peaks, which indicate that the monomers are not fully miscible with each other below the glass transition. Beyond the glass transition, the entire system was observed as a mixture of molten monomers where the predominant one dissolves the other giving a homogeneous blend. This can be seen by the comparison of DSC traces (plot 3.3), which shows a homogeneous and reproductible thermal behavior (absence of the single component behavior). Although it was not

possible to identify unequivocally the nature of the mesophase on the basis of POM observations, it nevertheless could be concluded to be nematic.

DSC experiments have shown that the mixture was homogeneous, as evidenced by the reversibility if the heating-cooling cycles, and the absence of any signal corresponding to the individual pure samples (plot 3.III).

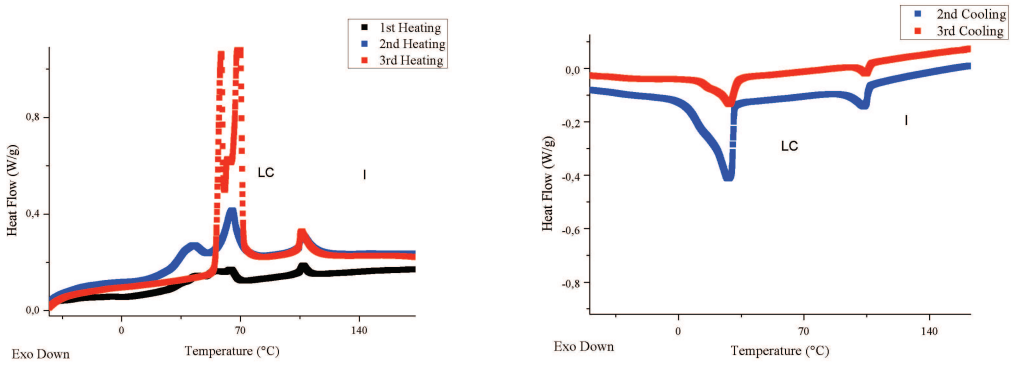

Plot 3.III. Left: Heating cycles of the mixture N1-N2 25:75. Right: Cooling cycles of the same mixture.

The next step was to determine whether these trends could be preserved along the polymerization and crosslinking processes of the corresponding polymers and elastomers.

Table 3.2. Mesomorphic Properties of Monomer Mixtures from POM.

Mixture (**N1**:**N2**)	**Thermal Behavior**[b]	***ΔT*** **(LC)**[c]
25:75	Cr_1 37 [6.6] Cr_2 65 [14.0] LC 107 [4.8] I	34/42
50:50	Cr_1-34 [7.1] Cr_2 42 [13.0] LC 129 [4.2] I	50/87
75:25	Cr 69 [35.2] LC 148 [6.0] I	40/79

[a]Transition temperatures (ºC) measurements performed in the POM hot plate with a heating rate of 10ºC/min. [b]Transition temperatures (ºC) and enthalpies [$kJ \cdot mol^{-1}$] of the monomers **N1** and **N2** obtained by DSC at a 2ºC/min heating rate during the third heating. In the case of monomer mixtures, the enthalpies are reported in $J \cdot g^{-1}$ between brackets. SmC, smectic C phase, N nematic phase, LC non identified liquid crystalline phase. [c]***ΔT*** (LC) is the temperature range expressed in ºC. The values are expressed: range obtained by POM/values obtained by DSC.

3.3. Polymer Mesomorphism.

Since two series of LCPs were prepared, it was possible to compare the variations in the phase transition temperatures and type of phases presented. This comparison is based on the effect of the chain extender (**HMTS** vs. **TMDS**) and as a function of the monomers mixtures compositions.

3.3.1. *Trisiloxane (HTMS) Polymers and Copolymers*

All the polymers and copolymers presented mesomorphic properties, and their thermal behavior was characterized by DSC. All the polymeric systems presented rather low clearing temperatures, mainly due to the high flexibility of the trisiloxane joint moiety between monomers.

Table 3.3. Mesomorphic properties of LCP.

Polymer	N1:N2 molar ratio	Thermal Behavior[a]
(**PN2T**)	0:100	g (n.d.) SmX 22.5 [8.8] SmY 42.2 [14.3] I
(CoP25T)	25:75	g (n.d.) SmX -3.3 [2.9] SmY 47.2 [12.1] I
(CoP50T)	50:50	g [0.2] SmY 53.8 [9.9] I
(CoP75T)	75:25	g -13 [0.2] SmY 71.1 [9.41] I
(PN1T)	100:0	g (n.d) SmX 14.5 [2.0] SmY 87 [9.2] I

The glass transitions T_g are expressed in ºC with their heat capacities in brackets [J/gºC]. Transition temperatures are expressed in ºC with the corresponding latent heats ΔH in brackets in [J g^{-1}]. Temperatures were estimated as the average of heating and cooling maxima of the 2 cycles with a rate of 2ºC/min. g: glassy state, SmX and SmY, non identified smectic phases. I isotropic state.

DSC experiments revealed liquid crystalline phase with a latent heat (ΔH_{LC-I}) ranging between 9 and 14 $J{\cdot}g^{-1}$. The glass transitions of polymers **PN2T, CoP25T** and **PN1T** were not detected but another phase transition was observed at 22.5, 0 and 15 ºC respectively, supposed to be likely higher order smectic phases as already observed in previous systems.[104,124]

POM experiments were mostly not very informative but we can appreciate the generation of a mesophase that undergoes a fully colored ill-defined texture likely indicating a smectic phase (figure 3.4).

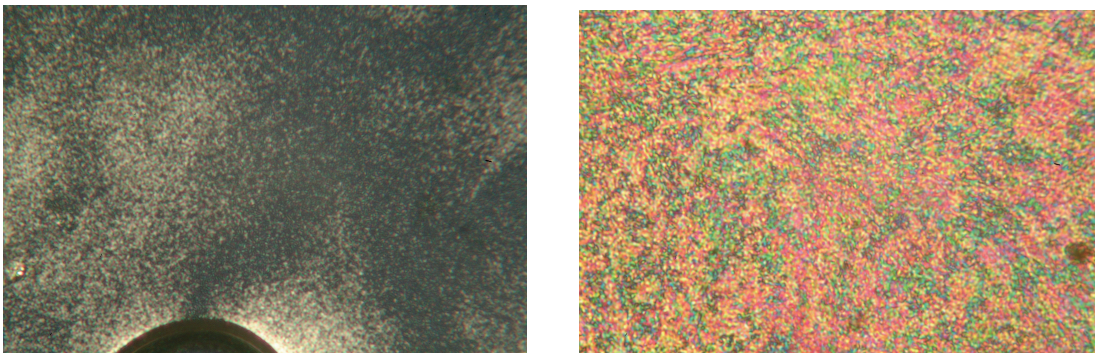

Figure 3.4. POM pictures of the sample **CoP25T** cooling from isotropic at 80ºC (left) and at room temperature smectic mesophase (right).

In order to prepare our samples for X-ray analyses, fibers of bulk polymer were obtained by shearing them between two glassplates, then filled into XRD capillaries (figure 3.5).

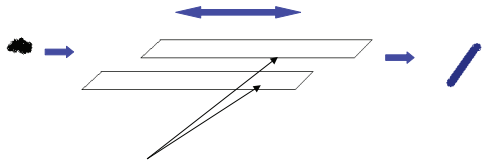

Figure 3.5. Preparation of the sample for XRD.

However, since with this method our samples are not oriented, we cannot determine the type of smectic phase. The X-ray patterns consisted of fine, intense rings in the small angle region corresponding to the smectic layer spacing and of two diffuse broad halos in the wide angle zone assigned to the mesogen distance and to the oligodimehtylsiloxane moiety, respectively. The discrepancy between the layer periodicity and the length of the **N1** mesogen (and the siloxane spacer) indicates that

the phase is likely a smectic C one, in agreement with the POM pictures. All the data are represented in table 3.4.

Table 3.4. Layer spacing and tilt angle of polymers made with **HMTS**.

Polymer	Layer spacing (d_l)*	Siloxane lateral spacing (d_s)*	Mesogens lateral spacing (d_m)*
PN2T	28.3	6.5	4.6
CoP25T	28.6	6.3	4.6
CoP50T	28.5	6.8	4.7
CoP75T	29.0	6.6	4.7
PN1T	29.7	6.6	4.8

*Distances are reported in angstrom (Å).

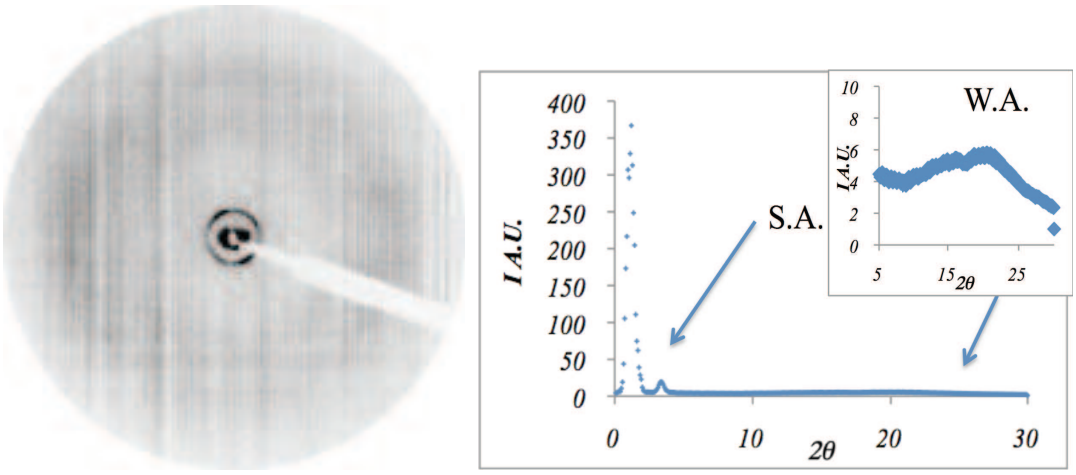

Figure 3.6. XRD pattern (left) and radial distribution plot (right) of polymer **CoP75T**.

As it can be seen, there is a slight increasing relationship between the layer spacing and the proportion of **N1** monomer. This can be explained by the growing proportion of the **N1** monomer with respect to **N2** whose maximum distance is reached in the case of **PN1T**.

To confirm this assumption we estimated the volume of some polymeric subunits using available dilatometric data. The volume of the monomeric unit (V_{MU}) can be

estimated by employing the additive law of the specific partial volumes. V_{MU} can be reduced as a sum of elementary volumes, namely:

$$V_{MU} = Vr + 12V_{CH_2} + V_{Si} \tag{3.10}$$

in which V*r* is the volume of the rigid part, V_{CH_2} is the methylene volume and V_{si} the siloxane volume. In the following paragraph, only the case of **PN2T** will be treated.

Without considering the two different orientations of the mesogen having obviously no influence on the volume segment the elemental repeating *MU* unit can be defined as:

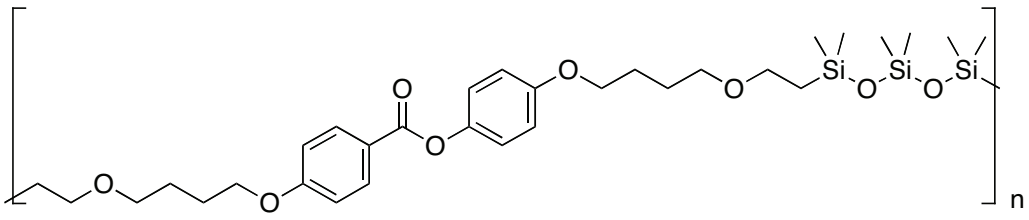

To facilitate the volume calculation of the *MU*, the various moieties were rearranged as follows:

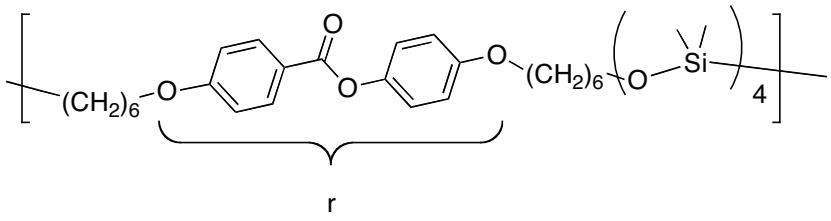

The volume of the polymer's repeating unit can be therefore written as:

$$V_{MU} = Vr + 12V_{CH_2} + 4V_{(CH_3)_2SiO} - V_{(CH_3)_2Si} \tag{3.11}$$

in which V_r is the rigid moiety's volume; V_{CH_2} is the volume of the methyl group in a hydrocarbonated chain, $V_{(CH_3)_2SiO}$ is the volume of dimethylsiloxane unit in a

polydimethylsiloxane chain and $V_{(CH_3)_2Si}$ is the volume of dimethylsilane unit in a polydimethylsilane chain.

Since the exact data from the monomer *MU* rigid moiety's volume is not available, we will extrapolate our results with those corresponding to the next molecule **N2'**, studied by dilatometry by Heinrich.[132]

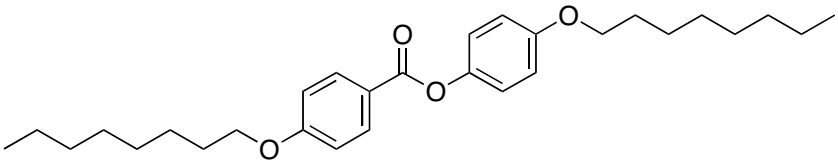

The rigid part of **N2** is the same than the one from this **N2**' molecule. Hence, its volume is expressed at 80ºC as:

$$V_{N2'} @ 80^{o}C = 778 \text{ Å}^3$$

Having the data of the molecular volume at 80ºC (in the liquid crystalline phase)[133] the volume can be calculated by knowing the aliphatic chains volume at the desired temperature by equation 3.7, which allows to extrapolate the volume to 25ºC.

$$V_{CH_2} = f(T) = 0.0202T + 26.6 \qquad \text{T in ºC} \qquad (3.12)$$

which gives:

$$V_{CH_2} @ 80^{o}C = 28.2\,\overset{o}{A}^3 \; ; \; V_{CH_2} @ 25^{o}C = 27.1\,\overset{o}{A}^3 \qquad (3.13)$$

Since the molecule presents a typical expansion coefficient of 7×10^{-4} ºC^{-1}, the molecular volume of **N2'** at 25ºC is:

---

[132] Heinrich, B., Ph.D. Thesis: *Etude de la structure et des propriétés mésomorphes de series homologues et de mélanges de composés smectogènes*, Univérsité Louis Pasteur, Strasbourg. **1993**.
[133] Doolitle, A.K., *J. Appl. Phys.* **1951,** 22, 1471.

$$V_{N2'}@25^{o}C = 747\ \text{Å}^3$$

The term that corresponds to methyl groups appears, so it has to be calculated from the next equation:

$$V_{CH_3} = f(T) = 53.8 + 0.0349T + 0.42T^2 = 55\ \text{Å}^3 \qquad (3.14)$$

to obtain our V_r for the monomer **N2** we use the next equation:

$$V_r = V_{N2'} - 14V_{CH_2} - 2V_{CH_3} = 258\,\text{Å}^3$$

By knowing V_r we can calculate the **N2** molecular volume by extracting the next data:[134]

$V_{(CH_3)_2SiO} = 126\ \text{Å}^3$ and $V_{(CH_3)_2Si} = 91\ \text{Å}^3$

which gives the corresponding molar volume:

$V_{MU} = 995\text{Å}^3$

Now the molecular cross section area ***Sx*** can be obtained by dividing the volume of the monomeric unit by the layer spacing from **PN2T** X-ray data.

$$Sx = \frac{V_{MU}}{d(l)} = 37\ \text{Å}^2 \qquad (3.15)$$

and the rigid part surface with σ_r

$$\sigma_r = \frac{V_r}{l_r} = 22\ \text{Å}^2 \qquad (3.16)$$

[134] a) Morimoto, S.; *J. Polym. Sci.* **1968**, 6A, 1547-1558. b) Kataoka, T. Ueda, S. *Polym. Lett.* **1966**, 4, 317.

where l_r = 11.8 Å is the distance of the longest edge of the rigid part of the molecule, (*estimated by molecular mechanics using Ballview software[135]). This allows to calculate the angle of tilt of the rigid moiety **Φ′**.

$$\Phi' = \arccos\frac{\sigma_r}{S} = 54^{\circ} \tag{3.13}$$

the half of this angle's meaning is the rigid part tilt respecting to the layer normal i.e. Φ/2 = 27º.

This tilt is the result of the discrepancy between the cross sections of the chains and the hard core (σ_r), the latter being forced to tilt to compensate the molecular area. On the other hand, the cross section of the dimethylsiloxane in a PDMS chain[134] is:

$$\sigma_{(CH_3)_2SiO} = \frac{V_{(CH_3)_2SiO}}{l_{(CH_3)_2SiOSi(CH_3)_2}} = \frac{126}{3.1} = 40\,\overset{o}{A}^2 \tag{3.14}$$

which suggests that our polymer bulkiness resembles to that of a chain of **PDMS**.

The presence of this smectic mesophase along the whole series is due to the microphase segregation at the molecular level, which consists in the separation in space of the molecular fragments of different chemical nature, in order to form organized systems such as those observed for the present polymers. We can now propose for the mesophase structure the following model describing the formation of a zig-zag structure throughout. This model is also applicable to **HMTS** elastomers, seen later.

---

135 Moll, A., Hildebrandt, A., Lenhof, H.P., Kohlbacher, O., *J. Comput. Aided. Mol. Des.,* **2005,** Nov; 19 (11): 791.

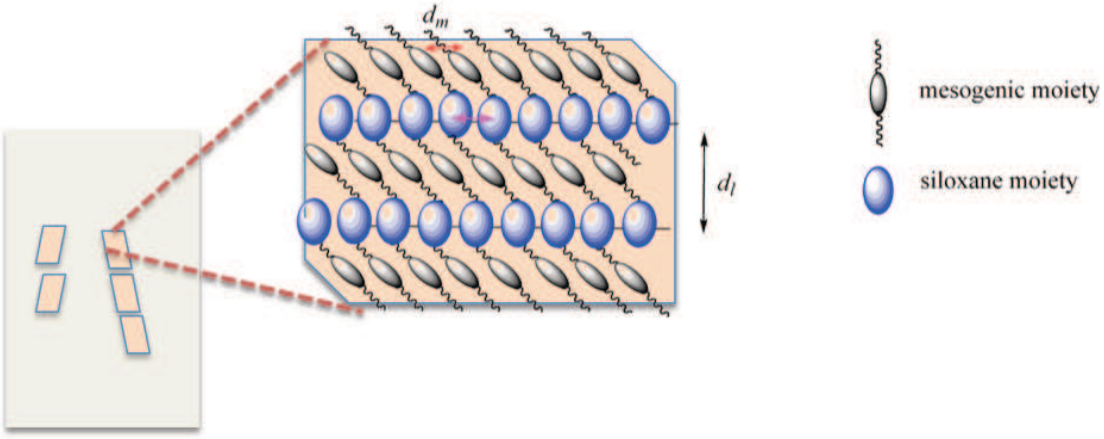

Figure 3.7. Schematic representation of the chevron structure in LCPs and LCEs.

In the study of the thermal behavior of the polymer series, we have shown that the clearing temperatures have been reduced and can be tuned (thermocontrolled systems). Since the original objective of this study was to obtain materials presenting solely a nematic mesophase, we proceeded in the synthesis of the analogous copolymers with a tetramethyldisiloxane chain spacer. The shorter length of the siloxane moiety was thought to reduce the tendency for long range microsegregation.

3.3.2. *Disiloxane Polymers.*

Changing the chain extender favors the induction of a nematic mesophase in our polymeric systems, due to a decrease in the microsegregation tendency discussed previously. After their purification, DSC as well as POM studies were performed for the three copolymers synthesized. They still presented smectic phases, as well as a nematic mesophase over small temperature domains (Table 3.5). In POM studies, cooling below the nematic-to-smectic transitions, the transformation of the ill-formed texture was clearly observed. The present texture (Figure 3.8, left), undergoes formation of small domain mosaic-like texture by decreasing temperature (Figure 3.8, right).

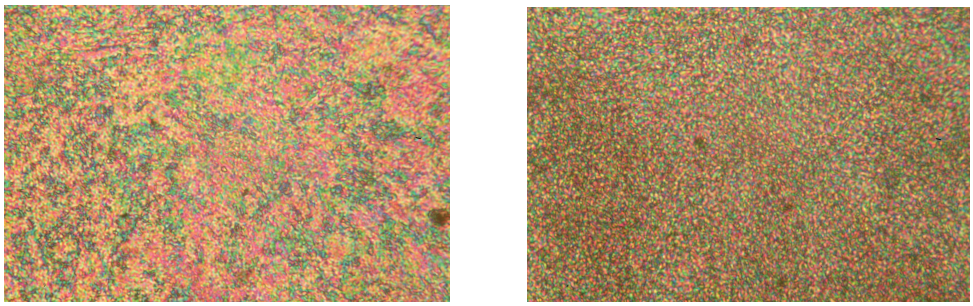

Figure 3.8. POM images from polymer **CoP75D** at 80ºC nematic phase (left) and 40ºC smectic phase (right).

Table 3.5. Mesomorphic properties of polymers synthesized with **TMDS** chain extender.

Polymer	Thermal Behavior[a]	ΔT_N (ºC)
PN2D*	g (n.d) Sm H 18 [11.0] SmC 41 [9.0] I	0
CoP25D	g -17 [0.2] Sm X 35.4 [1.2] N 52.6 [1.1] I	17
CoP50D	g -23 [0.3]Sm X 57.7 [3.9] N 71.8 [0.9] I	14
CoP75D	g -17 [0.3] Sm X 53.3 [2.4] N 79.5 [1.5] I	26
PN1D	g -8.7 [0.3] Sm X 54.5 [2.3] N 101.5 [1.6] I	47

Temperatures were estimated as the mean of heating and cooling maxima of the 2 cycles with a rate of 2ºC/min. The glass transitions T_g are expressed in ºC with their heat capacities in brackets [J/gºC]. Transition temperatures are expressed in ºC with their corresponding latent heats ΔH in brackets in [J g^{-1}]. g: glassy state, SmH: high order smectic mesophase; SmX and SmY, non identified smectic mesophases; SmC Smectic C mesophase; N: nematic mesophase; I: isotropic state. *taken from reference 102.

We can see that the stabilization of the nematic mesophase increases with the increasing amount of the monomer **N1**, which is maximum in the case of polymer **PN1D**. Thus, despite variable proportion of calamitic mesogens, distributed statistically in the polymer backbone, mesomorphism is stabilized.

The samples for XRD studies were prepared in the same way as the **HMTS** analogues. The X-ray patterns of the smectic mesophases of all the materials is described by the presence of very intense rings in the small angle region assigned to the layer spacing and a diffuse halo in the wide angle region corresponding to the lateral distance between molecular segments. The absence of signals corresponding to the siloxane moieties indicate a less efficient microsegregation between the

constitutive parts. The small angle intense rings become weaker and more diffuse when the sample was heated to the nematic mesophase temperature. The wide angle halo remained almost unchanged. The data of the two mesophases presented by the **TMDS** copolymers is presented on the following two tables.

Table 3.6. XRD data of **TMDS** copolymers smectic phase.

Polymer	T (°C)	Layer Spacing (d_1)*	Lateral distance (d_m)*
CoP25D	25	27.6	4.5
CoP50D	25	27.6	4.3
CoP75D	25	28.5	4.7

*Distances are reported in angstrom (Å).

Table 3.7. XRD of **TMDS** polymers nematic phase.

Polymer	T (°C)	d_1 (Å)	d_m (Å)
CoP25D	60	33.8	4.5
CoP50D	64	31.2	4.5
CoP75D	68	30.7	4.6

All the parameters concerning to the layer spacing (d_l) as well as the lateral spacing of the monomers (d_m) are reported in angstroms (Å)

Thus, the change on the siloxane spacer resulted in the induction of a nematic mesophase in all the copolymers, also in addition with a low temperature smectic mesophase. Moreover, a substantial increase of the isotropization temperature is observed when compared to the trisiloxane copolymers, and in the case of homopolymers we can tune the transition temperature of our samples and make it lower than that of the homopolymers **PN1T** and **PN1D**.

Now that we have synthesized and proven that both the mixtures and the chain extender can induce and stabilize the mesophases, we proceeded to the elastomer characterization to see if this behavior remains when an analogous insoluble, base oriented network is created.

3.4. Calamitic Elastomers.

For the study of the thermal behavior of these materials only DSC and XRD techniques were utilized to determine MC LCE parameters, POM being totally inappropriate.

3.4.1. *Trisiloxane Elastomers*

The corresponding elastomers and coelastomers were synthesized with 4%mol of crosslinking. The data of the thermal behavior of trisiloxane elastomers are gathered in table 3.8.

Table 3.8. Thermal behavior of **HMTS** elastomers.

Elastomer	Thermal Behavior[a]
EN2T	g (n.d.) SmX 16.4 [4.6] SmC 41.8 [10.3] I
CoE25T	g -19.1 [0.3] SmC 45.6 [8.5] I
CoE50T	g (n.d.) SmC 55.9 [8.5] I
CoE75T	g -11.5 [0.2] SmC 69.9 [3.5] I
EN1T	g -6 [0.2] SmC 84.7 [3.1] I

Temperatures were estimated as the mean of heating and cooling maxima of the 2 cycles with a rate of 2ºC/min. The glass transitions T_g are expressed in ºC with their heat capacities in brackets [J/gºC]. Transition temperatures are expressed in ºC with respect to latent heats ΔH in brackets in [J g^{-1}]. g: glassy state, SmX , non identified smectic mesophase; SmC Smectic C mesophase I isotropic state.

For the X-ray analyses, the samples were prepared by cutting a small fragment (≈ 1 mm large) from the center of the film and introduced in a capillary with a 1.5 mm diameter. The sample was set in a way that the elastomer film long axis was perpendicular to the X-ray source.

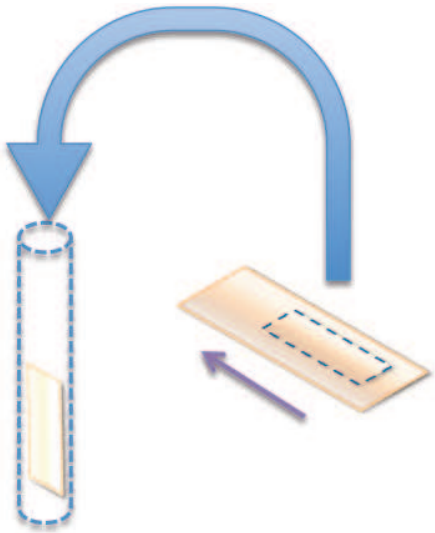

Scheme 3.8. Preparation of the XRD samples.

All the elastomers and coelastomers presented a smectic C mesophase as confirmed by XRD and the data obtained is described in table 3.9.

Table 3.9. X-ray data of **HMTS** elastomers.

Elastomer	d_l(Å)	ϕ(º)	ξ (nm)	n	d_m(Å)	Order Parameter (S)
EN2T	26.9	30	30.2	11	4.4	0.83
CoE25T	28.1	32.3	24.3	9	4.4	0.89
CoE50T	28.5	26	34.1	12	4.4	0.75
CoE75T	28.0	37.5	28.6	10	4.4	0.80
EN1T	28.6	38.8	29.0	11	4.4	N.D.

d_l: layer spacing; d_m: lateral spacing of the monomers ϕ: tilt angle, ξ: the correlation length; n: number of correlated layers; **S**: order parameter . Wide angle could not be detected in the case of the elastomer **EN1T** due to sample's spacing, hence the order parameter is not determined.

Generally, the diffraction patterns of the networks in the smectic phases presented: i) one single and sharp reflection in the small angle region which corresponds to the layer periodicities in the range between 28.0 and 28.5 Å. Tilt angles were estimated to lie in the range between 26 and 39º with respect to the film overall director. ii) a broad wide angle reflection at 4.4 Å corresponding to the lateral distance between molecular segments, remaining almost constant throughout the series.

Experimental evidence showed that the methyl substituent in **N1** mesogen, does not have a significant change in the bulkiness of the monomer, observed in X-ray as an increase of the lateral distance between the mesogens. Plane disruption has been observed in Krause's systems,[136] whose mesogenic monomer presents an ethyl group avoiding plane forming and giving rise to nematic-containing cybotactic systems (figure 3.9).

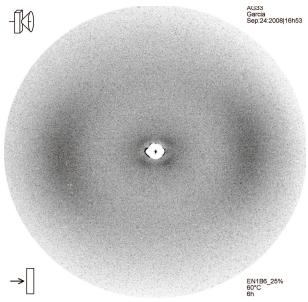

Figure 3.9. XRD pattern of a cybotactic nematic phase.

The layer spacing increases concomitantly with the increasing proportion of monomer **N1**, having an expected maximum at 100 % of **N1**. We observed a discontinuity for the case of **CoE50T**, whose layer distance is slightly lower than that of **EN1T**. The data suggest that the longest monomer **N1** leads the plane forming. In all the cases, our calculated distances for the monomers are consistent with those obtained. All of our samples have the same mesogen lateral distance, which indicates that the overall structure of the smectic C mesophase is not affected by the change of the monomers proportion. Our samples presented rather long range order (between 13 and 17 layers), which is considered in LC field as infinitely ordered according to the maximum measurable correlation length of our X-ray diffractometer (37.1 nm). As it

136 Krause, S., Zander, F., Bergmann, G., Brandt, H., Wertmer, H., Finkelmann, H., Nematic Main-Chain Elastomers: Coupling and Orientational Behavior, *C.R. Chimie* **2008,** In press.

is shown in table 3.7, the order parameter lies between 0.75 and 0.89, which indicates that a good alignment of the samples have been obtained in all the cases.

The slight inconvenience of these smectic C LCEs is a phenomenon called "shape memory", which has been extensively discussed by Lendlein and Kelch[137] and observed for the first time in MC-LCE systems by Rousseau.[138] Shape memory effect consists in the reversible recovery of the original shape of the object after passing through a large deformation process and then heated upon the transition temperature.

In the case of smectic C MC LCEs, the materials original shape is given during the casting process even for a monodomain obtained by two-step crosslinking process. Once they are heated to T_{SmC-I} they will recover the initial shape presented before the curing step.

In order to evaluate the change of the mesomorphic properties upon polymerization and crosslinking, we have plotted the transition temperatures of the pure monomer systems and mixture of monomers, the copolymers and the coelastomers. (Plot 3.IV).

The smectic C phase for **N2** monomer is preserved upon polymerization, although transition temperatures are lowered and mesophase ranges have considerably increased. This was expected since polymerization is known to stabilize the mesophase. This induction of crystallinity is also observed for polymer **PN1T** and copolymers **CoP75T** and **CoP25T**, which indicates that unequal comonomer proportions lead to higher order structures. On the other hand, equimolar amounts of monomers avoid higher ordering upon polymerization and coelastomer formation.

---

137 Leindlein, A.,Kelch, S., *Angew. Chem. Int. Ed.* **2002**, 41, 2034.
138 Rousseau, I. A.; Mather, P. T., *J. Am. Chem. Soc.,* **2003,** 125, (50), 15300.

As the **N1** proportion was increased, polymers and elastomers presented a more fluid behavior, which is systematically connected to the reduction of the glass transition temperature. However, the nematic mesophase presented by monomer mixtures and **N1**, is completely lost upon polymerization. This behavior is clearly associated to the **HTMS** segment that forces microsegregation between mesogens and chain extenders, resulting in the overall layering. Moreover, as it was expected, the clearing temperatures and to some extent, the transition temperatures to the smectic C, for the **HMTS** polymers and copolymers are close to those of elastomers with 4% mol of crosslinker, confirming in this case that for weakly crosslinked networks, it is possible to predict the thermal behavior.

Since our aim is to obtain nematic LCEs, we prepared the disiloxane analogues with the hope to preserve the already observed tendency in the previously synthesized copolymers.

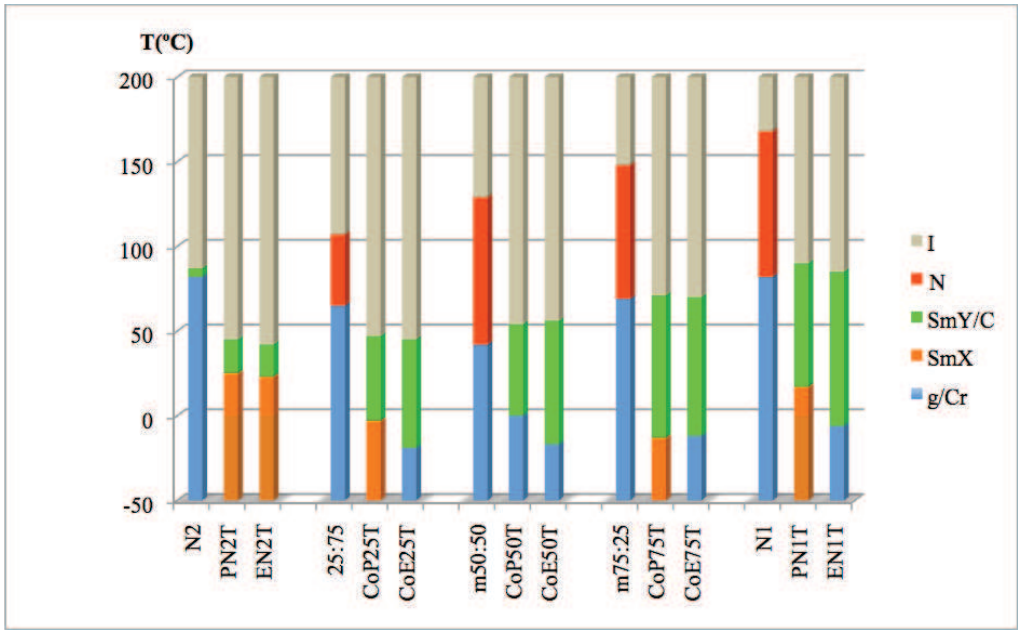

Plot 3.IV. Phase behavior of monomer mixture of **N1** and **N2**, **HMTS** polymers and **HTMS** elastomers

3.4.2. *Disiloxane Elastomers.*

First investigations by POM suggested the formation of a nematic mesophase, but at it was previously mentioned, the technique is not very useful here.

Color variation can be observed with variation of temperature (Figure 3.10) which can be associated to a phase transformation. The transition phase to the isotropic could be however observed as the birrefringent texture becomes dark.

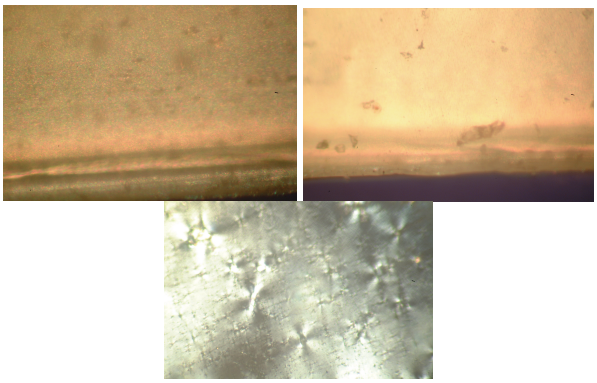

Figure 3.10. POM Images of elastomer **CoE25D** at room temperature (upside left) nematic phase at 76 ºC (upside right) and isotropic state (center). 4 fan shaped defects are associated to the surface imperfections of the coelastomer film.

Since **EN1D** and **EN2D** elastomers had already been synthesized,[104,105] we only prepared the three co-elastomers, whose thermotropic behavior obtained by DSC is depicted in the next table.

Table 3.10. Thermotropic behavior of the samples synthesized with **TMDS**.

Polymer	Thermal Behavior[a]
CoE25D	g -4.3 [0.2] SmC 61.4 [2.61] N 93.5 [1.43] I
CoE50D	g -7.7 [0.1] SmC 56.1 [3.94] N 76.3 [1.05] I
CoE75D	g -1.39 [0.2] SmC 71.5 [2.12] N 106.7 [1.31] I

Temperatures were estimated as the mean of heating and cooling maxima of the 2 cycles with a rate of 2ºC/min. The glass transitions T_g are expressed in ºC with their heat capacities in brackets [J/gºC]. Transition temperatures are expressed in ºC with the corresponding latent heats ΔH in brackets in [J g^{-1}]. g: glassy state, SmX , non identified smectic mesophase; SmC Smectic C mesophase; N Nematic mesophase; I isotropic state.

DSC showed a glass transition and two endo/exo transitions corresponding to the presence of two different mesophases later confirmed by X-ray diffraction. Beyond the glass transition, a first mesophase appears as a SmC one. On further heating a nematic mesophase is formed before clearing into the isotropic state.

The X-ray diffraction patterns of the low temperature phase presented a sharp reflection of layer periodicities of 25.5, 24.6 and 26.5 Å for **CoE25D**, **CoE50D** and **CoE75D** respectively. Layer correlation lengths confirmed the smectic layered structure with values as large as 60 nm. Azimuthal plots of the same region confirmed the existence of a smectic C mesophase in all the samples. Tilt angles varied from 40 to 43º with respect to the layer normal. In the wide angle, one reflection at 4.5 Å for the **CoE75D** and **CoE25D** and at 4.4 Å for **CoE50D** corresponding to the lateral distance between mesogens were observed. Order parameters obtained from azimuthal integrations yielded 0.9, which allowed classifying the coelastomers as monodomains. (Table 3.11).

Table 3.11. XRD results of **TMDS** elastomers at smectic C phase.

Elastomer	**T(ºC)**	d_1 **(Å)**	ϕ**(º)**	ξ ***(nm)***	***n***	d_m **(Å)**	**S**
CoE25D	25	25.5	41.5	30	12	4.5	0.90
CoE50D	25	24.6	40	>60	25	4.4	0.91
CoE75D	25	26.5	43	26	10	4.5	0.91

d_1: layer spacing; d_m: lateral spacing of the monomers ϕ: tilt angle, ξ**:** the correlation length; ***n***: number of correlated layers; **S**: order parameter.

As the sample is heated upon the transition temperature, the sharp signals of the smectic C mesophase broadened forcing the elastomer to rearrange into cybotactic groups to form a nematic phase. This is shown by a broad reflection in the small angle region corresponding to layer periodicities between 27 and 28 Å, higher than those

from the smectic C mesophase's small angle reflections. Correlation length was found to decrease significantly, with ξ values small as 12 nm, three times lower than SmC ξs averaging 30 nm. Tilt angles also increased in the range of 5º with respect to former smectic C mesophases, giving the corresponding tilting angle of about 45º. In the wide angle region larger values for lateral distance, as large as 4.6 Å, for the **CoE50D** sample have been determined. Order parameter obtained from wide angle graph exhibited a slight decrease obtaining values of 0.89, 0.80 and 0.90 for **CoE25D**, **CoE50D** and **CoE75D**, respectively. Thus, a formation of cybotactic groups in the mesophase was clearly appreciated, but the values of correlation length and order parameter were unexpectedly rather high. Since our samples presented both phases, we infer that the size of these cybotactic groups are relatively large due to monomers interactions from the remaining microsegregation observed in the vestigial smectic C phase exhibited at lower temperature. An XRD pattern example of these series is illustrated in figure 3.11.

Table 3.12. XRD results of **TMDS** elastomers at nematic phase

Elastomer	T(ºC)	d_1 (Å)	$\phi(^o)$	ξ (nm)	n	d_m (Å)	S
CoE25D	65	27.3	49	11.3	4	4.5	0.89
CoE50D	68	28.2	44	12.4	4	4.6	0.80
CoE75D	85	27.2	45	12.2	4	4.5	0.90

d_l: layer spacing; d_m: lateral spacing of the monomers ϕ: tilt angle, ξ**:** the correlation length; n: number of correlated layers; **S**: order parameter .

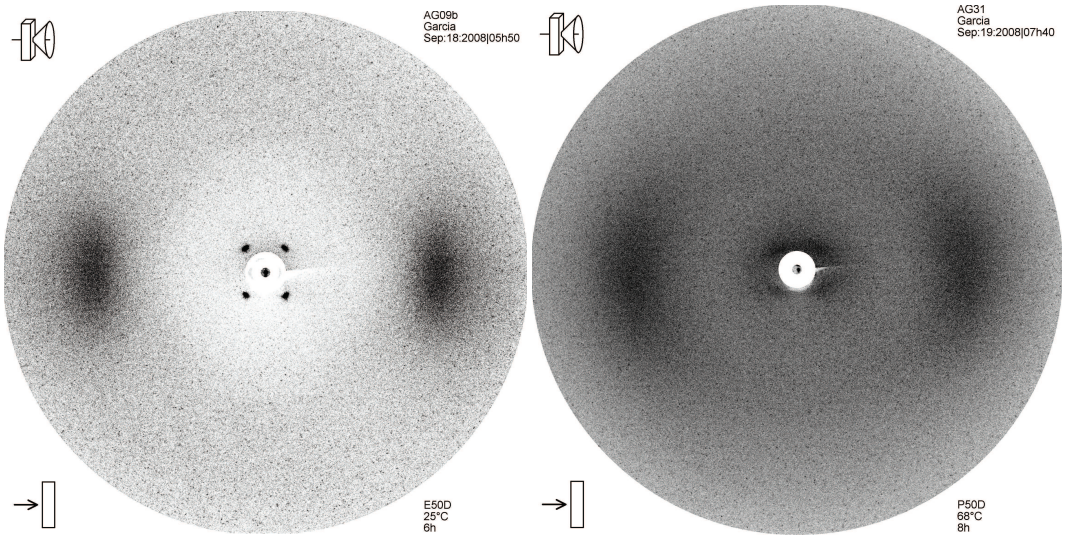

Figure 3.11. XRD patterns of **CoE50D**. Left: at 25ºC (SmC phase); right: at 68ºC (N phase).

As another representative example, both the order parameter S variation, deduced by Gaussian correlation, as well as the loss of correlation distance between layers ξ from **CoE75D** are shown in plot 3.V.

Both S and ξ remained unchanged within the SmC mesophase temperature domain. Above the SmC-N mesophase transition temperature, S first decreases slightly, then close to to the isotropization temperature falls town to 0. On the other hand, ξ decreases first dramatically, in early cybotactic nematic temperature range, and then slightly, when temperature gets close to isotropization temperature.

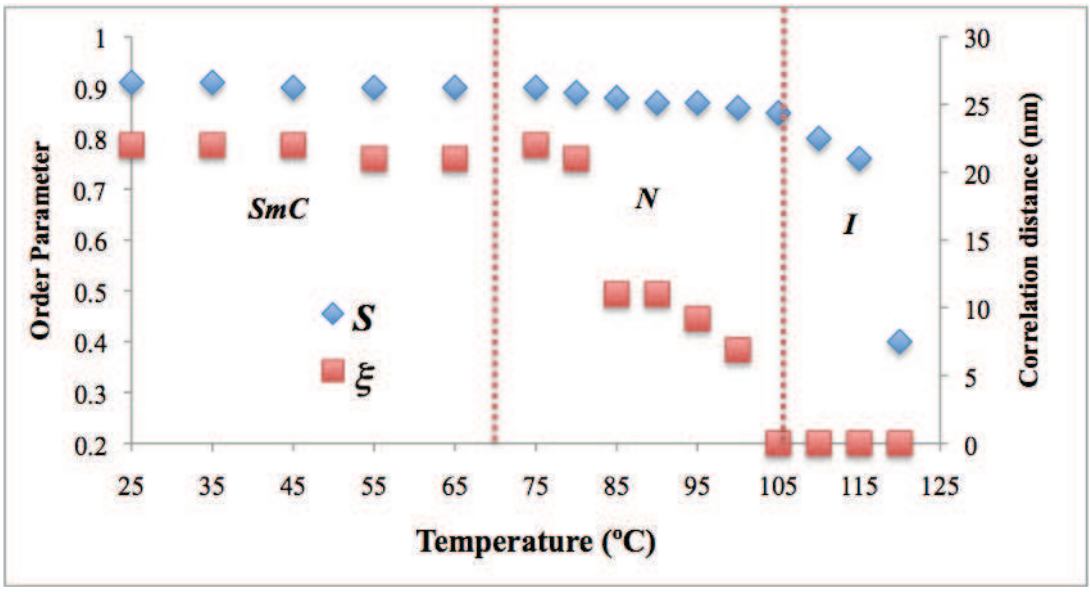

Plot 3.V. Variation of the order parameter and layer's correlation distance with temperature of elastomer **CoE75D**. ξ: correlation distance; *S*: order parameter; SmC: smectic C mesophase; N: nematic mesophase; I isotropic state.

The thermal behavior of the monomers, monomeric mixtures, copolymers and coelastomers, is plotted in the same phase diagram for comparison. As previously, a substantial drop of the transition temperatures, particularly for the isotropic transitions is observed for the samples after polymerization and reticulation. It is found that the liquid crystalline behavior of the polymers is enhanced, reaching a maximum at 50:50 monomer ratios whilst the LC behavior is enhanced with increasing % of **N1**. Opposite to the previous results with **HMTS**, a nematic mesophase is observed between SmC and I phases. The nematic phase range reaches a minimum at equimolar monomer proportion, whilst it increases by increasing the difference in the monomer proportion, reaching the maximum range in the **EN1D** elastomer. Concerning to the clearing temperatures, they are lower for copolymers than for corresponding coelastomer temperatures, with lower temperatures for the former. Another interesting trend observed is that the nematic phase range is higher in the

case of elastomers excepted for **CoE50D** whose transition diagram is almost superimposable with the analogous copolymer.

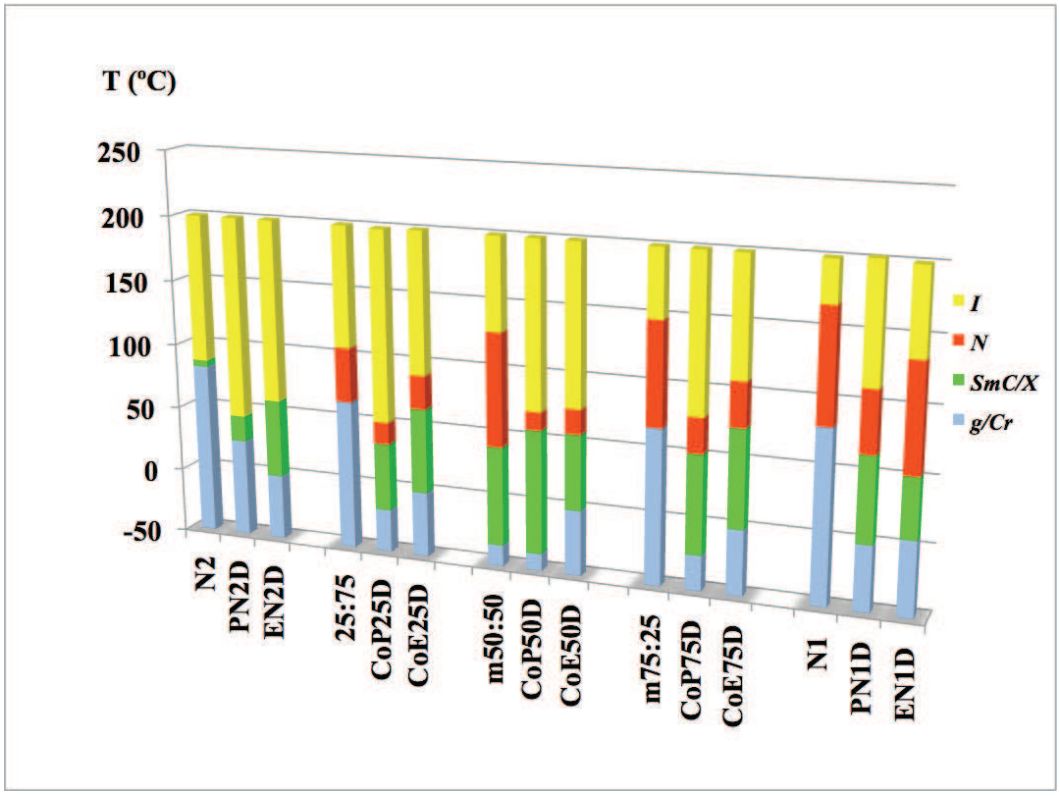

Plot 3. VI. Phase behavior of **N1** and **N2** mixtures (red), **TMDS** polymers (green) and elastomers (blue).

3.4.3. *Conclusions*

Thus, this systematic study where various monomeric mixtures and 2 different spacers were used, shows that if is possible to tune and therefore design appropriate elastomers for specific purposes. Hence, using a longer chain spacer (**HMTS** vs **TMDS**) promotes SmC mesophases over nematic. Whereas, the overall effect of the mixture of the monomers in different proportion permits a better control of the transition temperatures and an overall enlargement of mesomorphic domains, the nature of the mesophase seems independent to monomeric blend.

To try to control mesophase nature in blends. We thought of introducing in the systems a component that will disturb this fragile order further, thus, strongly structurally differing from calamitic mesogens. Bent-shape mesogens can be quite appropriate here, as the bent-core way, depending on its structure, they are able to break the layering of the systems and favor nematic phase formation. Due to their polar nature, they can be used to trigger mesophase to isotropic state transition under external electric field.

3.5. Bent-core Systems.

3.5.1. *Background and Monomer Properties*

The thermal behavior of the bent-core monomers were characterized by DSC. Unfortunately, all but **B3** monomer, which presented a monotropic antiferroelectric polar smectic C mesophase ($SmCP_A$) and non characterized M2 mesophases[139], and **B4** (figure 3.12), which presented a semiglassy structure between 129 and 139ºC classified as a molten crystal by X-ray diffraction, were devoid of mesomorphism. A possible explanation can be due to some charge alternance along the aromatic rings, which is supposed to favor liquid crystallinity as reported by Pelzl *et al*.[22] The melting point and mesomorphism of the synthesized bent-core monomers are shown in table 3.13.

---

[139] Marx, V. M.; Girgis, H.; Heiney, P. A.; Hegmann, T., *J. of Mater. Chem.* **2008,** 18, (25), 2983-2994; Reddy, A., Sadashiva, B. K., *Liq. Cryst*., **2003**, 30, 1031. Fodor-Csorba, K., Vajda, A., Galli, G., Jákli, A., Demus, D., Holly S., Gács-Baitz, E., *Macromol. Chem. Phys*., **2002**, 203, 1556; Jákli, A., Huang, Y.-M., Fodor-Csorba, K., Vajda, A., Galli, G., Diele, S., Pelzl, G., *Adv. Mater.,* **2003**, 15, 1606.

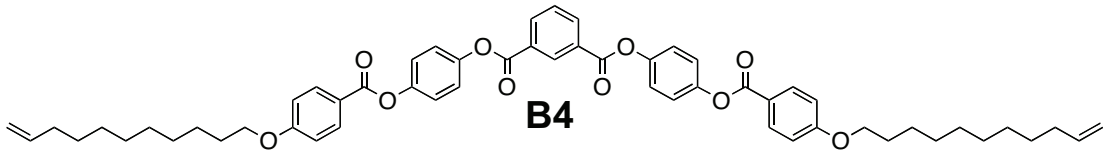

Figure 3.12. Monomer **B4** structure.

Table 3.13. Thermotropic behavior of bent-core monomers.

Polymer	Thermal Behavior[a]
B1	Cr 171.0 I
B2	Cr 159 I
B3	Cr 99.1 I 89.6* [16.7] $SmCP_A$ 79.8* [22.0] M2
B4	Cr_1 90 Cr_2 129.1 Cr_3 139.2 I
B5	Cr 64.3 I
B6	Cr 122.0 I

The [J g^{-1}] indicates the ΔH. Temperatures were estimated from peak maximum of the heating cycle with a rate of 2ºC/min. Cr, Cr_1, Cr_2 and Cr_3: crystalline states; I isotropic liquid; $SmCP_A$: anticlinal polar smectic C mesophase; M2 non identified mesophase. * Determined in the cooling cycle (monotropic mesophases).

3.5.2. *Bent-core Polymers*

The corresponding polymers of **B1** to **B4** were prepared and their thermal behavior is shown in table 3.14, considering that a possible synergic effect of both rigid bent-shape mesogen and siloxane chain could give rise to liquid crystalline polymers as in a previously reported strategy.[140] Polymers **PB5** and **PB6** could not be prepared due to small amounts of monomer available which also avoided the synthesis of copolymers of bent-core monomer blends.

[140] Choi, E. J.; Ahn, J. C.; Chien, L. C.; Lec, C. K.; Zin, W. C.; Kim, D. C.; Shin, S. T., *Macromolecules* **2004,** 37, (1), 71.

Table 3.14. Thermal behavior of bent-core polymers.

Polymer	Thermal Behavior[a]
PB1	g (n.d.) g 101.0 [11.72] I
PB2	g 23.5 Cr_1 45.6 [14.37] Cr_2 137.7[4.40]I
PB3	Cr 40.8 g 101.6 [22.0] I
PB4	g (n.d.) g_1 124.7 [6.78] g_2 170.4 [3.08] I

The [J g^{-1}] indicates the ΔH. Temperatures were estimated as the mean of heating and cooling maxima of the 2 cycles with a rate of 2ºC/min. Cr, Cr_1 and Cr_2 crystalline states; g, g_1 g_2: glassy polymer, I isotropic liquid.

None of the polymers showed mesomorphism either. Thus, the effect of the bent structure introduced in a MC polymer is detrimental to phase induction. And indeed very few examples of such polymers have been synthesized.[140,141,142] We therefore envisaged another series of copolymers made of calamitic and bent-shape mesogens with the expectations that the presence of the calamitic monomers will ensure the mesophase formation and that of the bow shape would reduce even more the tendency to produce smectic mesophases and favor nematic order instead. Interesting novel materials were obtained, and their particular properties are now discussed.

3.5.3. *Bent-Core molecules /Calamitic Mesogen Liquid Crystalline Coelastomers*.

We have synthesized a series of coelastomers by varying the proportion of the bent-core molecules. Interesting results were obtained in the case of the elastomers synthesized with **N1** in particular. The thermal behavior of the present LCEs was studied by means of DSC. They all presented mesomorphism (table 3.15).

141 Jeong, K. U.; Knapp, B. S.; Ge, J. J.; Jin, S.; Graham, M. J.; Xiong, H. M.; Harris, F. W.; Cheng, S. Z. D., *Macromolecules* **2005,** 38, (20), 8333. In this reference, the molecules are elbow-like linear mesogens and not banana-shaped mesogens.

142 Barberá, J., Gimeno, N., Monreal, L., Piñol, R., Ros, M.B., Serrano, J.L., *J. Am. Chem. Soc.* **2004**, 126, (23) 7190. UV-polymerizated bent-core monomers.

Table 3.15. DSC results from BC/CM MCLCE

Elastomer	Thermal Behavior[a]
CoEN1B4D 5%	g 2.6 [0.2] SmC/N♦ 127 [4.75] I
CoEN1B6D 5%	g -3.2 [0.2] SmC 64 [2.0] N 105 [1.2]I
CoEN2B4D 5%	g (n.d.) SmX 10 [2.9] SmC 44.8 [10.88] I
CoEN2B6D 5%	g (n.d.) SmX 5 [1.5] SmC 45.6 [8.50] I
CoEN1B6D 25%	g 0.9 [0.3] SmC 42.1 [1.60] N 71.4 [0.84]I
CoEN2B6D 25%	g -11.1 [0.2] SmC 24.3 [6.82] I

Temperatures were estimated as the mean of heating and cooling maxima of the 2 cycles with a rate of 2ºC/min. The glass transitions T_g are expressed in ºC with their heat capacities in brackets [J/gºC]. Transition temperatures are expressed in ºC with the corresponding latent heats ΔH in brackets [$J*g^{-1}$]. g: glassy state, SmX , non identified smectic mesophase; SmC Smectic C mesophase; N: nematic mesophase I isotropic state. ♦ Transition non detected.

Employing POM technique allowed to observe the main director orientation by rotating the sample between the polarizers (Schema 3.9). The images of elastomer **CoEN1B4D 5%** were taken rotating from 90 to 0º with respect to the first polarizer's starting with the long axis vertically oriented (layer normal parallel to the second polarizer) and finishing with the longest part horizontally oriented (layer order perpendicular to the second polarizer). All the pictures were taken with the same exposition time. By turning the sample plate an increase of the image luminosity, maximal at 45º position, was detected. The latter decreased again until it reaches an almost dark image at 0º. This study proved that the elastomer is macroscopically oriented suggesting a monodomain sample. (Figure 3.12). Since the maximum of transmission was obtained at 45º, indicating that the sample has a uniform director alignment along its long axis. This was also shown for other systems obtained by electrospray-oriented fibers.[81b] All the other coelastomers were birrefringent as the sample above, which indicated their liquid crystalline properties. We have then demonstrated that this orientation approach of LCE with low crosslinking degree was successful.

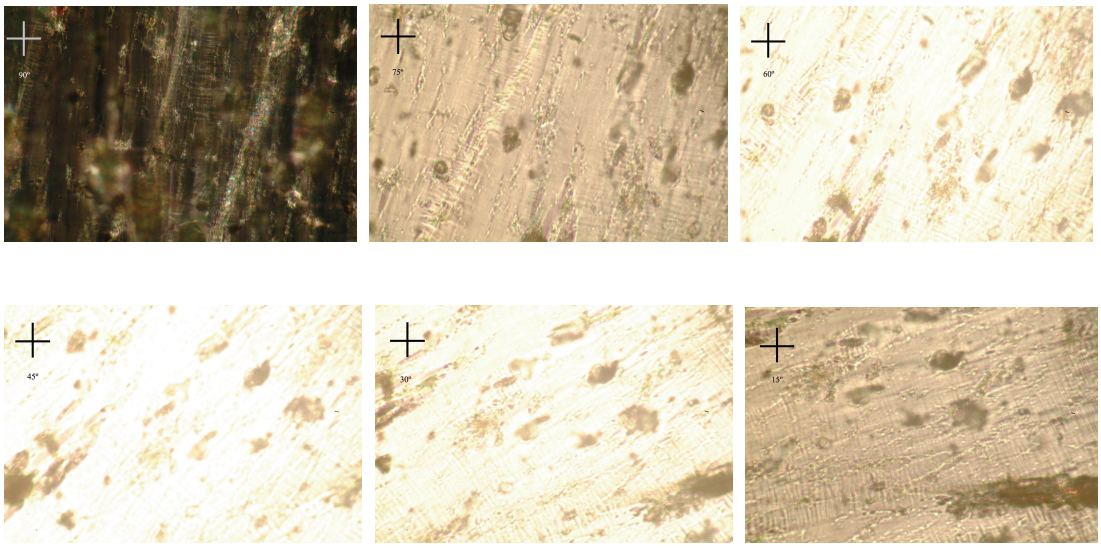

Figure 3.13. POM images of elastomer **CoEN1B4D 5%**. From left to right, top to bottom: 90º, 75º, 60º, 45º 30º, 15º from vertical. All the photos were taken with the same shooting parameters. The polarizers's position is indicated as a cross.

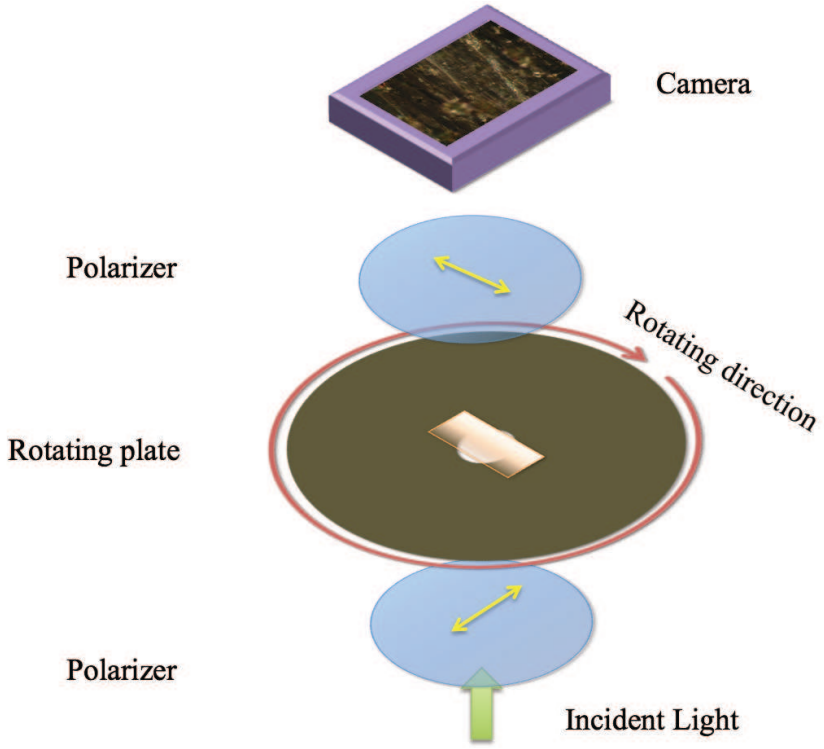

Scheme 3.9. Rotating plate POM.

All of the coelastomers presented low glass transitions, and a smectic C phase. The elastomers synthesized with **N1** monomer and **B6** bent-core monomers presented a nematic phases becoming isotropic at 105ºC, which make them suitable for

performing their thermoelastic studies.[143] The elastomer **CoEN1B4D 5%** presented a particular behavior due to an atypical smectic-to-nematic transition by DSC. All these data are discussed in paragraph 3.5.4. The effects of the intercalated bent-core monomers into the LCE network on the liquid crystalline properties were analyzed by X-ray diffraction.

Table 3.16. XRD data of BCCM MC LCE on the smectic C mesophase.

Coelastomer	T(°C)	d_1 (Å)	$\phi(^o)$	ξ (nm)	n	d_m (Å)	S
CoEN2B4D 5%	25	25.9	33.8	44	17	4.4	0.92
CoEN2B6D 5%	25	24.7	31.6/ 41.5	48	20	4.5	0.90
CoEN1B6D 5%	25	25.3	47.8	29	11	4.4	0.92
CoEN1B6D 25%	25	26.1	42	35	14	4.5	0.89
CoEN1B6D 25%	25	26.7	N.D.	62	23	4.5	0.69

d_l: layer spacing; d_m: lateral spacing of the monomers ϕ: tilt angle, ξ**:** the correlation length; n: number of correlated layers; **S**: order parameter. N.D: since the reflections are not well defined, the tilt angle was not determined.

In contradiction to our prediction, all our samples presented a low temperature smectic C mesophase, indicating that the smectic ordering tendency of the calamitic mesogens behavior is not altered upon the induction of bent-core molecules within the structure. The samples patterns exhibited in almost all the cases the typical chevron structure. It was observed for the **CoEN2B6D** series an interesting variation in the XRD patterns as a function of the bent-core monomer quantity in the network (figure 3.14). **CoEN2B6D 5%** has shown two different sets of reflections (one as a single peak and the other as a splitted one) in the azimuthal integration plot of the small angle region, which indicates the coexistence of two different layer tilt angles along

[143] The maximum temperature holded for conventional thermoelastic studies apparatus is 115º.

the network. We attributed these observations to the angle difference between the calamitic monomer and the bent-core comonomer, envisaging an increment in the layer ordering inducing the structure shown in scheme 3.10. These observations were confirmed with the **CoEN2B6D 25%** coelastomer, which did not exhibit a chevron structure, even if it had suffered an orientation process as the other elastomers. This is likely attributed to the high amount of the **B6** comonomer, which also justifies the model of network distortion proposed in paragraph 2.4.4. concerning the swelling anisotropy presented by both samples. The next scheme shows the slight distortion of a bent-core molecule into the chevron, which causes the change in the monomer's tilt angle. Only **CoN2B6D 5%** is represented.

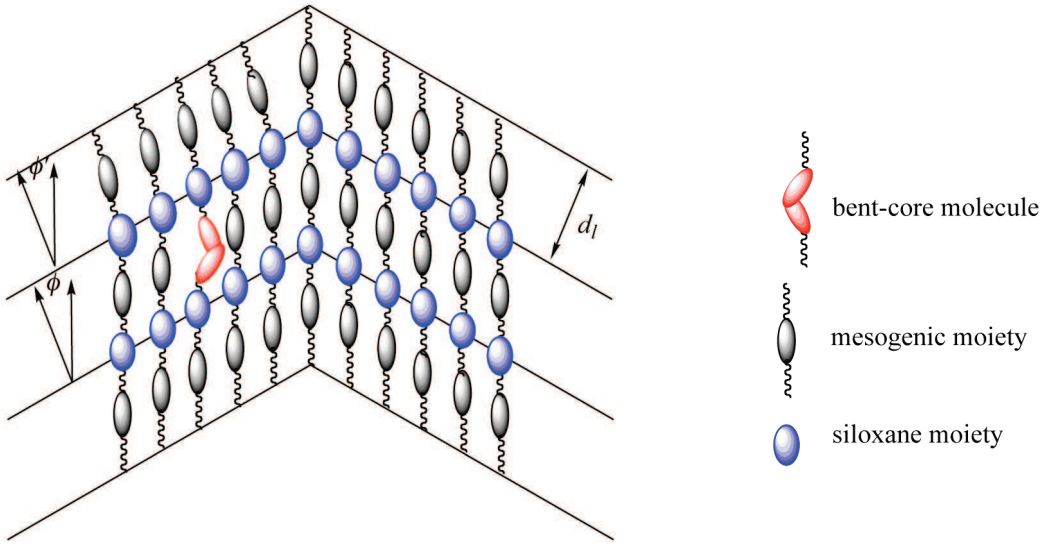

Scheme 3.10. Distorted chevron structure representing the **CoEN2B6D 5%** sample. The value of ϕ' is slightly higher than ϕ, which gives two different tilt angles. Layer distance keeps constant.

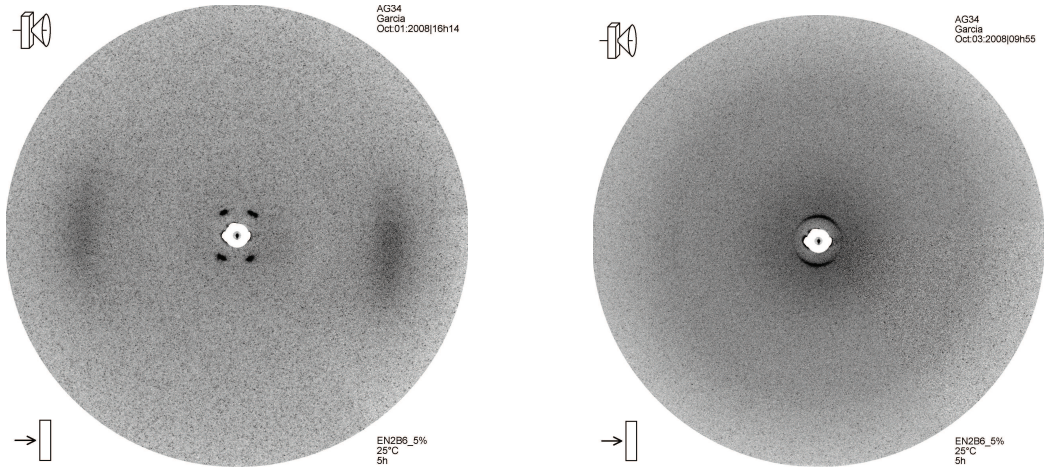

Figure 3.14. XRD patterns (oriented sample) of elastomers **CoEN2B6D 5%** (left) and **CoEN2B6D 25%** (right).

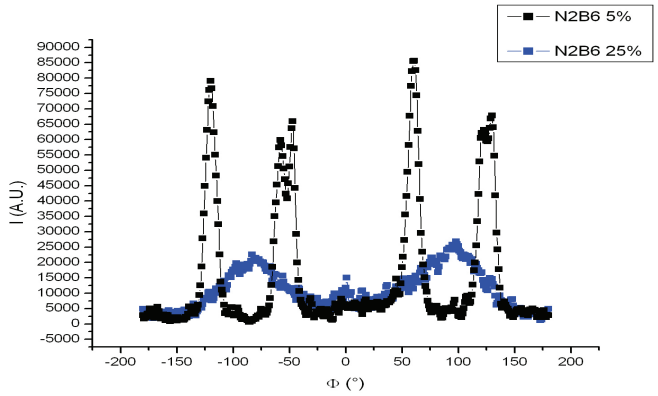

Plot 3. VII. SAXS azimuthal integrations of elastomers **CoEN2B6D 5%** (black) and **CoEN2B6D 25%** (blue). ϕ is shifted -90º.

As an illustrative scheme, all the XRD patterns are shown in scheme 3.11. They illustrate the differences between the mesogen's tilt angle and the degree of orientation by considering two different variables: the type and the proportion of the bent-core molecule present in the network.

In the case of large bent-core monomer, the signals obtained from XRD are quite large, which suggests a larger average of the layer periodicity. This suggests that **B4** moieties are suitable enough to arrange within the chevron's layers, causing a rough distortion along the elastomeric network. The clearing transition is higher than that of

EN2D elastomer, which suggests a contribution in the stabilization of the mesophase. On the other hand, we present the analogous coelastomer **CoEN2B6D 5%**. This system possesses a shorter bent-core monomer (**B6**) structure, whose stable conformation length is close to those of **N2** monomer (see paragraph 2.4.4. for length discussion). The bent angle of **B6** promotes the tilting of the aromatic moiety locally, giving rise to doubled signals (splitting) with respect to the ideal calamitic system (scheme 3.10). When the concentration of **B6** becomes important, as in the case of **CoEN2B6D 25%,** the chevron structure is totally lost as revealed by the fine reflections with semicircular patterning in the small angle region and a wide angle region diffuse halo indicating that the smectic order parameter is considerably lowered. This pattern behavior indicates that the initial **B6** concentration effect present in **CoEN2B6D 5%** leads to a point where the order is totally lost due to extreme disordered network genesis of coelastomer **CoEN2B6D 25%** from which we can only say that it presents a local ordered layered structure (ill-formed smectic C phase).

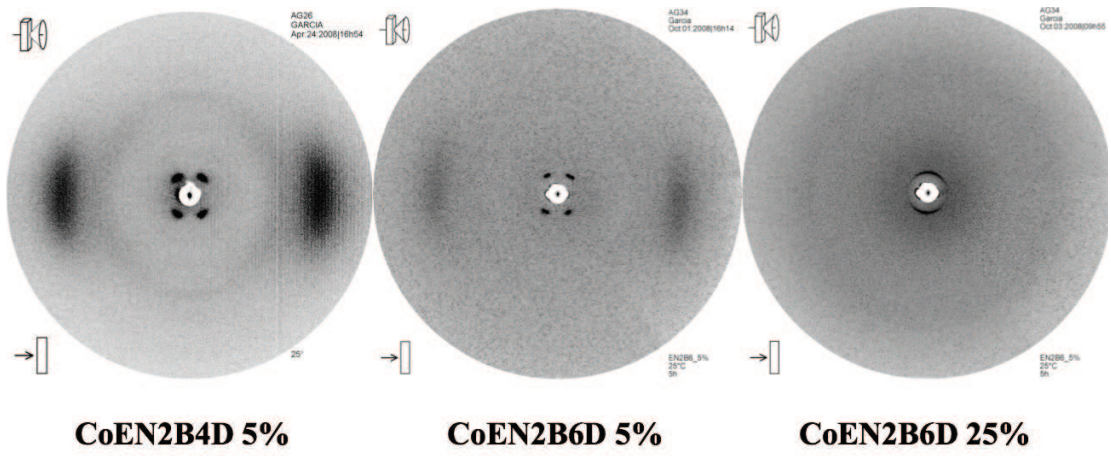

Scheme 3.11. XRD patterns of MC-BC/CM LCCoE presenting only the smectic C mesophase. With bent core mesogen **B4** at 5% mol concentration (bottom left) and **B6** at two different proportions (5%mol and 25 %mol). All possess the same calamitic mesogen **N2** within their structures.

XRD studies of the nematic phase obtained from the BC/CM LCCoEs **CoEN1B6 5%** and **CoEN1B6 25%** are presented in table 3.17.

Table 3.17. XRD data of BCCM MC LCE of the nematic mesophase.

Elastomer	T(ºC)	d_1 (Å)	$\phi(^o)$	ξ (nm)	n	d_m (Å)	S
EN1B6 5%	85	26.5	57.3	6.6	3	4.3	0.81
EN1B6 25%	60	28.0	50	10.5	4	4.5	0.79

d_l: layer spacing; d_m: lateral spacing of the monomers ϕ: tilt angle, ξ**:** the correlation length; n: number of correlated layers; **S**: order parameter.

We first made a comparative study of the small and wide angles azimuthal integrations of **CoEN1B6D 5%** in both smectic and nematic mesophases to monitor layer correlation distance loss as well as order parameter decreases as a function of temperature. Since all of the nematic mesophases presented cybotactic structures, a small correlation distance within the nematic phase has been estimated, being minimal near the clearing temperature. Wide angle reflections intensities decreased and broadened as a result of the temperature rise, demonstrating that the smectic order parameter decreased when approaching the isotropic transition.

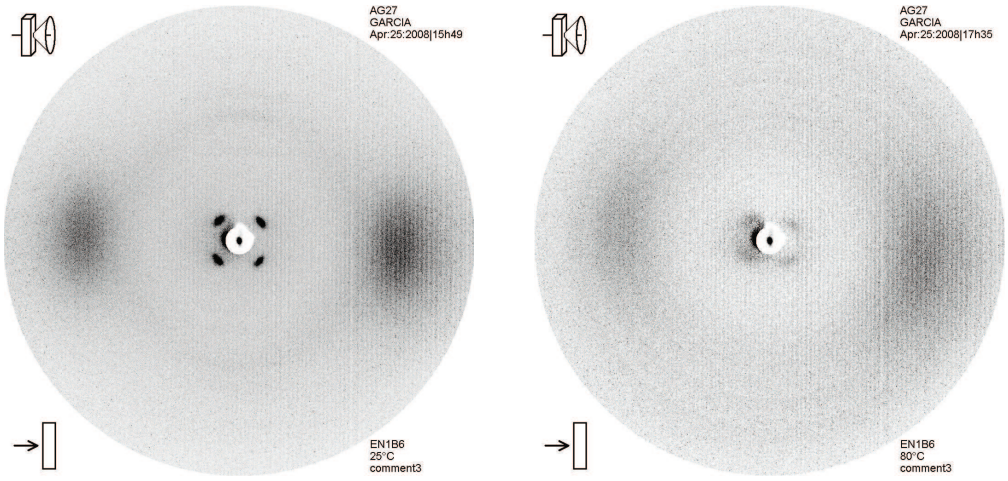

Figure 3.15. XRD patterns of elastomer **CoEN1B6 5%** at 25ºC in smectic C mesophase (left) and 80ºC in nematic mesophase (right).

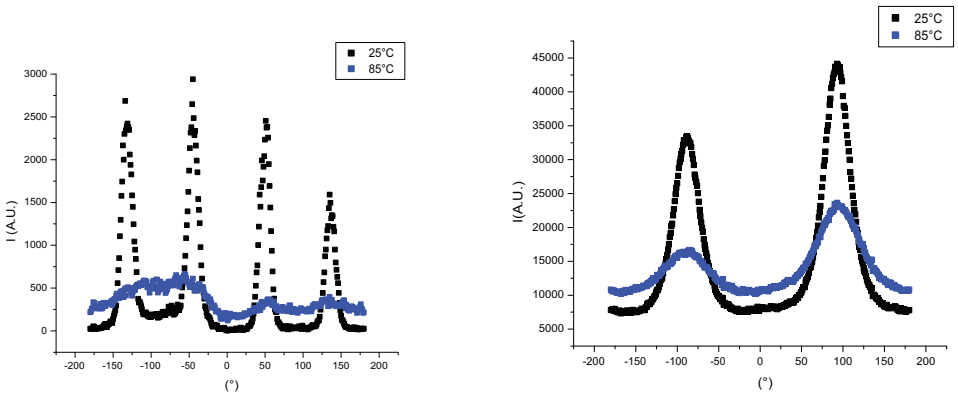

Plot 3. VIII. Azimuthal plots of SAXS (left) and WAXS (right) at smectic C (black) and nematic (blue) phases.

In order to compare these last results, an overview as a function of **B6** concentration was proposed. The evolution of the patterns corresponding to **CoEN1B6D** series is shown in scheme 3.12. When heating from the smectic to the nematic mesophase, we observed in both cases a broadening of small angle reflections, which indicates the gradual loss of the layer correlation. In the case of **CoEN1B6D 5%**, the small angle region tilt angles do not change significantly (47.8º to 50º) along the mesophase transformation. Contrasting to this small change, coelastomer **CoEN1B6D 25%** exhibits a broad tilt angle variation (from 42 to 58º) when heated into the nematic regime. This is likely associated to the eventual deformation of the chevron structure and the consequent loss of layer periodicity correlation length. Another important observation with this coelastomer is the lack of orientation in the smectic C mesophase, which showed a fine sharp halo crossing along the small angle reflection rings. This asseveration is explained as a partial orientation of the film due to some defects generated by the high concentration of the bent-core monomer **B6** through the network. (Scheme 3.12).

Coelastomers synthesized with **N1** did not show a broad difference as a function of bent-core monomer **B6** contrarily to those obtained with calamitic mesogen **N2**, whose network ordering differs considerably at high concentrations (25%mol) of **B6**.

The systems **CoEN2B6D** present a clear distortion of the overall network as a function of **B6** concentration, the *maximum concentration of mesomorphic anisotropy* (MCMA) is reached at c.a. 25mol%, and both mesomorphic and swelling anisotropies are lost. Higher concentrations will lead to isotropic elastomers.

Since **N1** still requires a special attention to determine MCMA our group will continue in the study of this value for **N1** systems.

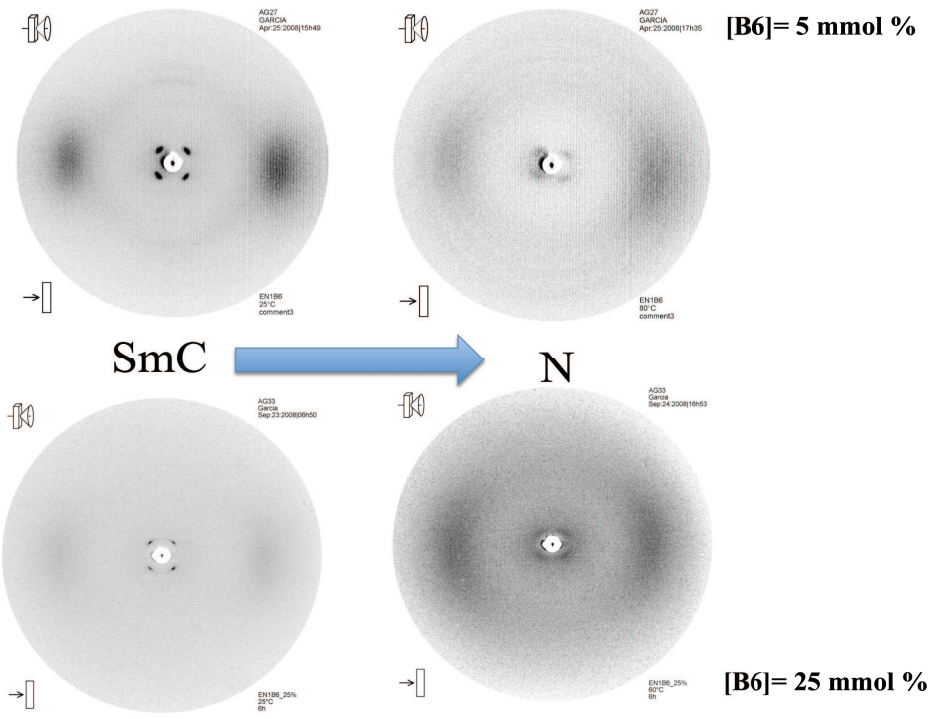

Scheme 3.12. Mesophase evolution patterns of the **CoEN1B6D** coelastomer series.

Since serendipia is part of the research, a particular coelastomer was obtained consisting of the bent-core molecule **B4** and the calamitic mesogen **N1**. Their particularities are discussed as a special paragraph, due to its lack of classification.

3.5.4. *Coelastomer **CoEN1B4D 5%.***

The DSC plot of this coelastomer exhibited a glass transition at 7.5 ºC and an isotropization temperature at 128ºC. These values were close to those given by the **EN1D** analogue, and similarly SmC and N phases were expected.

Further DSC studies revealed that whilst the **EN1D** oriented film sample exhibited reversible SmC-N transition at 53ºC, **CoEN1B4D 5%** exhibited a very broad peak between 40ºC and 70ºC at the first heating cycle run (Plot 3.IX). The first heating/cooling cycle did not show anomalies associated to the transition in the absence of a special thermal treatment.

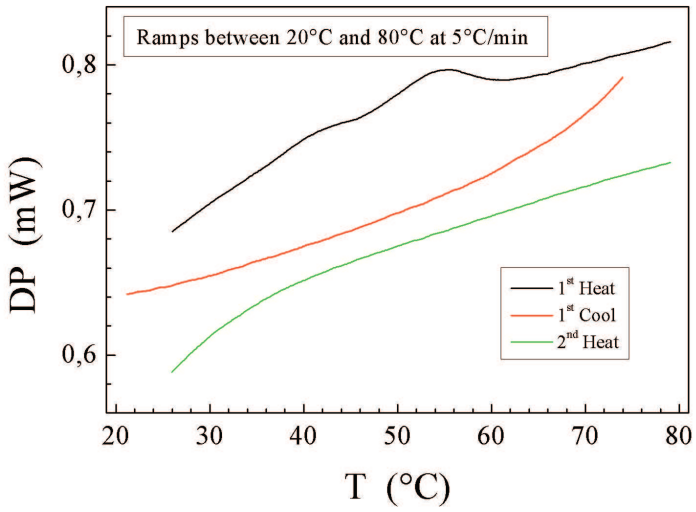

Plot 3.IX. Heating and cooling cycles of coelastomer **CoEN1B4D 5%**.

Actually, if an annealing time at room temperature of at least two hours is introduced, the peak associated to the transition temperature reappears on the following heating cycle. The maximum area was not reached after 8h of annealing time (Plot 3.X).

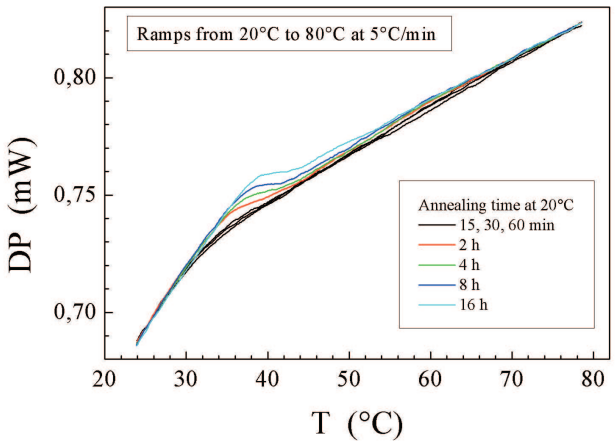

Plot 3.X. Heating cycles of coelastomer **EN1B4D 5%** with different annealing times.

XRD data of the two mesophases is presented in table 3.17. X-Ray diffraction pattern of **CoEN1B4D 5%** in the smectic C mesophase was taken at room temperature whereas a second one was recorded at 75ºC, considering that at this temperature, the mesophase presented by this coelastomer is completely nematic. After comparison of both patterns, only small subtle changes were observed, whereas the tilt angle, and the layer periodicity remained almost constant (the small angle signal was found to broaden).

More detailed small angle variation studies were performed to the coelastomer **CoEN1B4D 5%.** The tilt angle (ϕ) was measured as a function of temperature (plot 3.XI). A very weak increase was observed suggesting that the tilt angle is close to the saturation value. This can be due to the maximum disordering within layers caused by the bulkiness of the dimethylsiloxane moieties as discussed in paragraph 3.3.1.

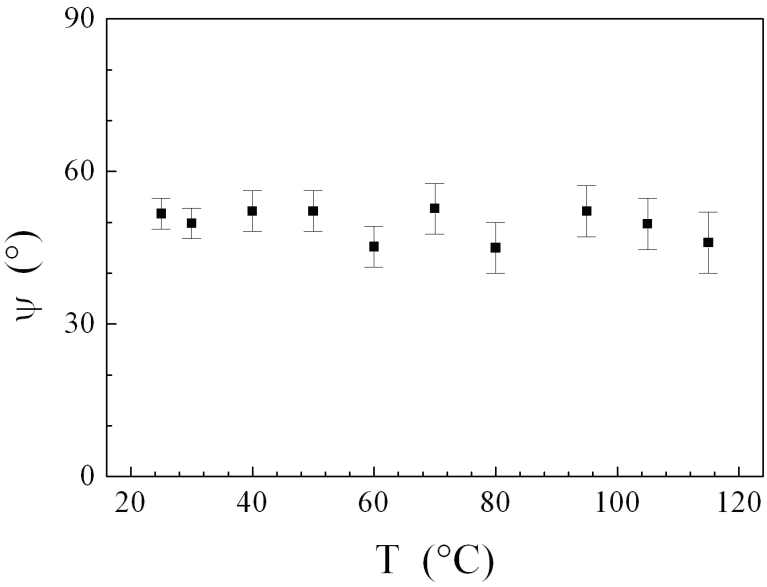

Plot 3.XI. Change of the small angle signals tilt angle ($\phi = \psi$) as a function of temperature of **CoEN1B4D 5%.**

A deeper study of the small angle profile variation as a function of temperature was then performed for the present coelastomer. It showed that the signal transformation is gradual along the temperature interval. (figure 3.XII). Layer correlation parameter constantly decreased from 150 at room temperature to about 50 Å at 70ºC. A possible explanation for this phenomenon could be the splitting of the SmC to N transition line along the entire LC domain due to some inhomogenic dispersion of the bent-core monomeric moiety within the network, considering the former one behaving as a mesomorphically inert moiety. The biphasic region would then extent below room temperature, since correlation distances associated to the layer piling in smectic phases are typically two order of magnitude larger than the value measured for **CoEN1B4D 5%** at room temperature. Unfortunately, the effective reduction of correlation distance associated to the doping cannot be quantitatively appreciated since the model **EN1D** oriented film sample just gives sharp spots, meaning that the correlation distance is larger than the limit of detection of our setup e.g. 600 Å. On the

other hand, data corresponding to the pattern at 70ºC, are typical of cybotactic nematic domains with comparable values of the **EN1D** oriented film.

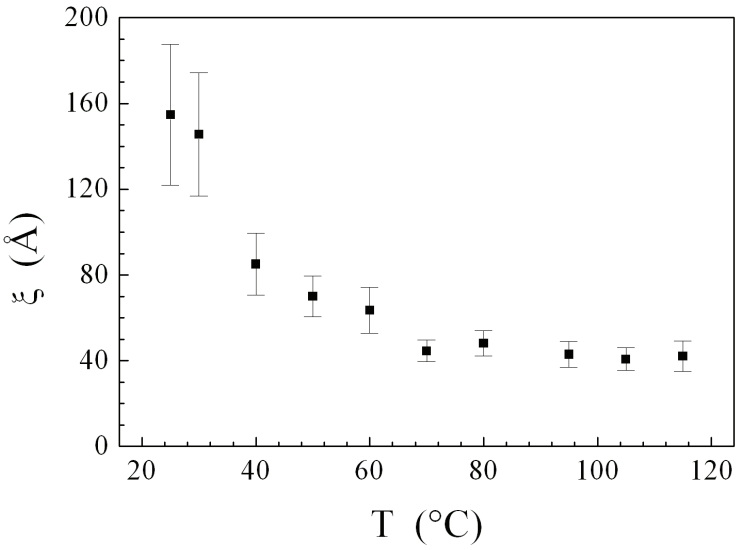

Plot 3.XII. Layer correlation distance **(ξ)** vs. temperature plot of coelastomer **CoEN1B4 5%.**

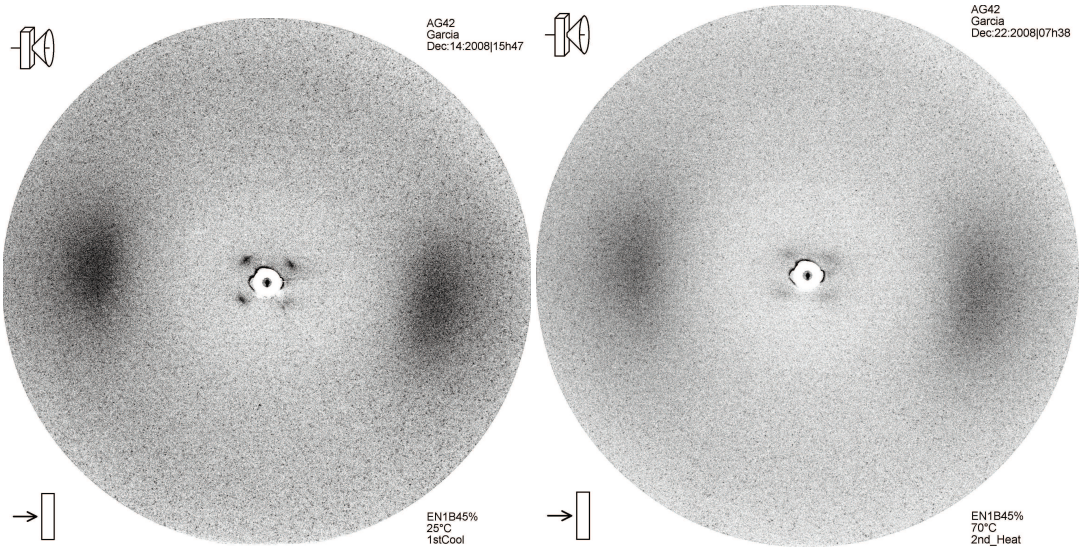

Figure 3.16. XRD patterns of **CoEN1B4D 5%** at room temperature (left) and at 70ºC (right).

Order parameter values from both smectic and nematic mesophases remained close to 0.8-0.9 along the entire mesophase range up to few degrees below the isotropization temperature. (plot 3.XIII).

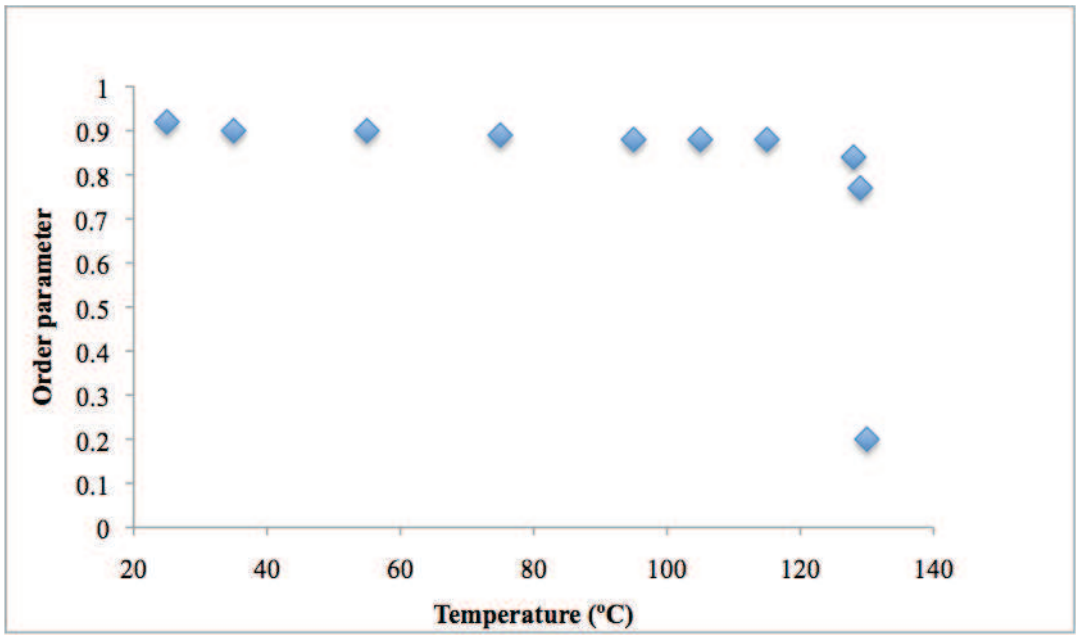

Plot 3.XIII. Order parameter calculated from **CoEN1B4D 5%.**

Inhomogeneities in the distribution of the bent-core moiety in the **EN1D** matrix would therefore explain the thermodynamics of the coelastomeric system, but allow also the understanding of the particular kinetics associated to the smectic to nematic phase transition. Thus, since the **B4** and the **N1** mesogens exhibit mutual shape incompatibility, it is very likely and consistent with previous observation for molecular compounds,[144] that the **B4** moieties are pushed out of fully developed mesogen's sublayers in the smectic phase as well as out of the cybotactic sublayer embryos in the nematic phase. Therefore, the distribution of the **B4** dopant is much more homogeneous in the nematic phase and the crossing from the smectic to the nematic mesophase does not imply any former modification of the **B4** distribution.

[144] Sebastião, P. J., Corsellis, E., Heinrich, B., Guillon, D., *Liq. Cryst.*, **2002**, 29, (3), 479.

Nevertheless, by cooling down into the thermodynamic stability domain of the smectic phase, the **B4** moieties first have to re-segregate in a less homogeneous state, before the development of the smectic layers takes place. This re-segregation process necessarily involves molecular diffusion, thus slow time rate at room temperature would then be responsible of the annealing time effect evidenced in the DSC study.

3.6. Conclusions.

We have characterized the liquid crystalline phases of each one of our monomers, polymers, copolymers, elastomers, and coelastomers obtaining characteristic data for the layer spacings, correlation length of the layers in the smectic C and Nematic mesophases.

Mixing two different liquid crystalline calamitic monomers, permits to induce a nematic mesophase, whose domain can be decreased or enlarged by the monomers proportion. The nematic character of these systems is dictated by the most liquid crystalline monomer (**N1**).

Furthermore, adding a long, bent-core monomer permits a time dependent mesophase transition, promoted by the disorder of the rearrangement of the rigid bent-core units along the mesomorphic network. Adding a bent-core comonomer that possesses a length close to that of the calamitic comonomer, promotes a slight disorder into the system, giving rise to tilt angle fluctuations within the coelastomer structure. As bent-core monomer concentration increases, we can estimate a *maximum concentration of mesomorphic anisotropy* (MCMA).

All the elastomers and coelastomers synthesized were aligned samples, with an order parameter between 0.78 and 0.91 in the smectic C phase and from 0.78 to 0.81 for the nematic ones, which indicates that mesogens are homogeneously aligned.

We have proven by XRD the induction and the order of the mesophases by changing the chain extender as well as the bent-core mesogen shape and proportion. These observations confirm once again the swelling tests concerning the swelling anisotropy.

Chapter 4

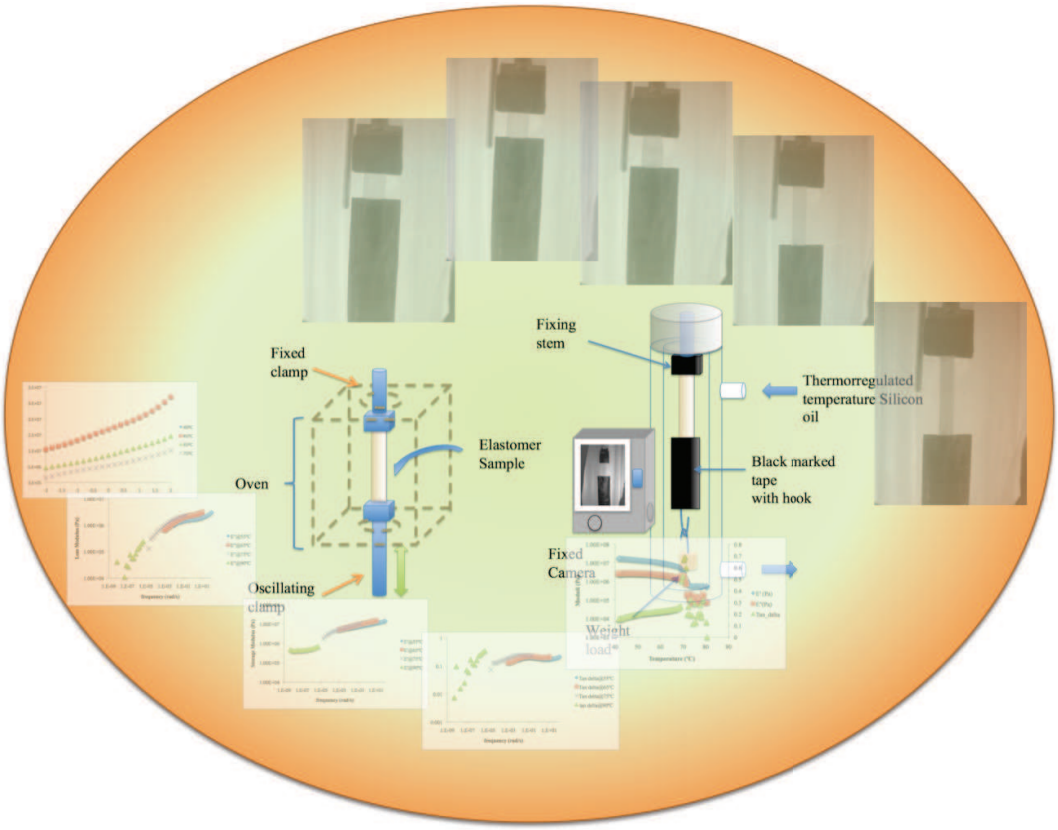

Thermoelastic and Mechanical Properties

4. Thermoelastic and Mechanical Properties.

4.1. Background and Fundamental Concepts.

As seen in the previous chapters, we were able to synthesize and characterize three series of elastomers. The implemented synthetic approach allowed us to tune the mesophases (SmC and/or N), their stability ranges and transition temperature intervals. This chapter summarizes the studies performed on the previously prepared LCEs and LCCoEs in order to characterize the influence of the molecular design on the mechanical parameters, in particular on the maximal elongation and the hardness of the elastomers. Two types of experiments have been performed: thermoelastic and dynamic traction rheometry. A brief description of both techniques is given in the next paragraphs after a more general introduction to rheology. As this is not supposed to be a thesis on rheology, we shall not engage into a detailed discussion of all results but rather focus only on some important points. The whole set of experimental data is given in the appendix C.

Rheology, the study of the mechanical behavior of materials, is an old science. This results from the importance of knowing and being able to predict the mechanical properties of all the materials involved in most human activities. Architecture, metallurgy and plasturgy probably are the most obvious ones but rheology is also important in domains such as geology, chemistry, paints, mechanics, biology or even food processing. The motto of The American Society of Rheology is taken from Heraclitus: "παντα ρει", everything flows. Most rheological experiments are conceptually simple, even if it sometimes takes decades to understand their result: some sort of stress is applied to the sample and the resulting deformation or strain is

recorded. The thermal and/or time dependant behavior of the strain/stress ratio is the raw data on which rheologists work.

Even though elastomers are not solids *stricto senso*, they usually are treated as such. A basic experiment consists therefore in applying some stress to the sample through deformation, and measuring the resulting induced strain. All applied deformations can be decomposed into some combination of compression and shear. We have limited ourselves to compression/elongation studies, static and dynamic. Such a geometry is schematically depicted in figure 4.1.

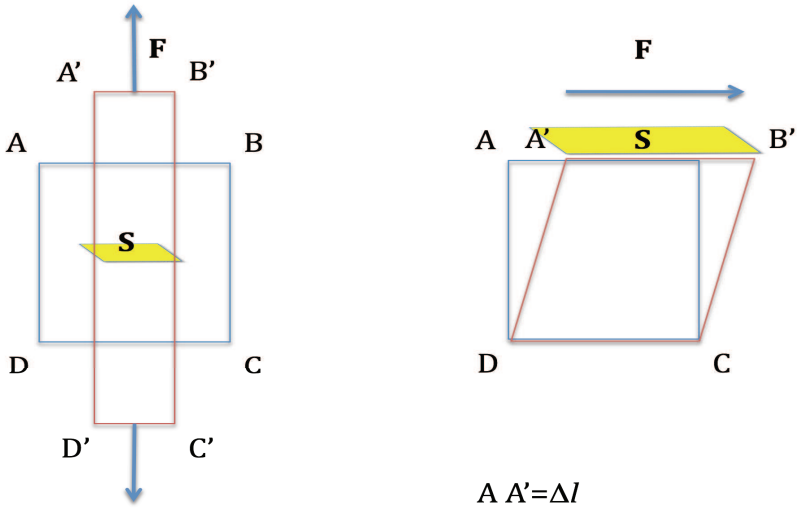

Figure 4.1. Geometry of a given material in elongation (left) and shear (right) studies. Cross sections (**S**) in yellow

A solid rod of length L = AD and cross-section S is submitted to forces F. The rod's profile ABCD becomes A'B'C'D' and its length becomes L'. The applied stress is defined as $\sigma = F/S$ and the resulting strain applied is defined as $\varepsilon = (L'-L)/L$. In the case of shear deformation, the stress ($\tau = \sigma$) is defined similarly, but the strain now depends on the tangential displacement of the surface defined as $\gamma = \Delta l/L$. The elasticity modulus or Young's modulus of the rod is then defined as $E = \sigma/\varepsilon$, measured in Pa or

$N \cdot m^{-2}$ and the shear modulus as $G=\tau/\gamma$. The cross-section obviously contracts when the length increases, the coupling parameter being known as Poisson's ratio ν. There is an equation linking E, G and ν: $E=2G(1+\nu)$. For elastomers all deformations are made at constant volume and $\nu = 0.5$ in this case.[145] The applied stress can be constant with time, or vary at a given rate, usually sinusoidally. One then either measures the static or dynamic elasticity modulus. A typical static measurement of the elasticity modulus for a smectic elastomer is given in plot 4.1.

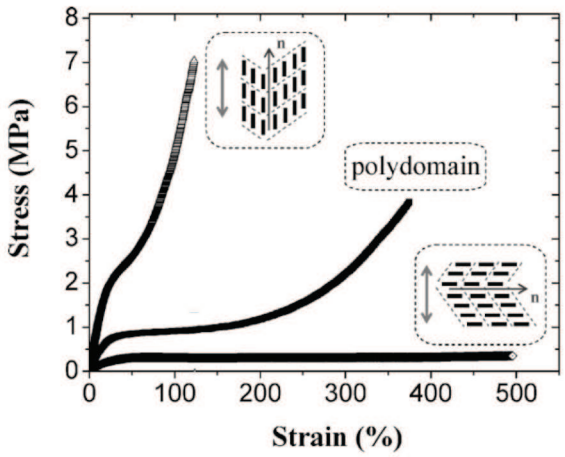

Plot 4.I. Static measurement of a smectic elastomer.[145]

Stress and strain are proportional up to a certain elongation limit where various non-linear behaviors take place until the sample finally breaks. In the case of anisotropic samples such as oriented elastomers, the rheological behavior is obvisously anisotropic, as exemplified in the plot above.

Most materials and more particularly elastomers are not purely elastic but rather visco-elastic: in a given stress-strain experiment some energy is irreversibly lost in viscous flow. One then defines a complex elasticity modulus, E=E'+iE". The real part

[145] Ren, W., McMullan, P., Griffin, A. C., *Macromol. Chem. Phys*., **2008**, 209, 1896. These authors report $\nu = 0.4$ to 0.5 for SmC monodomain elastomers.

E' (storage modulus) is responsible for the elastic properties while E" (loss modulus) is responsible for the damping or irreversible processes. The proportion of elastic to viscous behavior is usually given as the loss tangent or loss factor, tan δ=E'/E". These parameters are accessed through dynamic experiments since a viscous body shows no response to a static strain. The figure below depicts the expected (theoretical) dynamic behavior of an elastomer having a single relaxation mode. The real part E' of the modulus exhibits two plateaus at both ends of the spectrum (zero frequency and infinite frequency) while E" exhibits a maximum located at the relaxation frequency. The low-frequency plateau and the subsequent relaxation mode(s) are strongly dependent on the molecular nature of the monomers and cross-linker and on the cross-linking density. In a first order crude approximation, the high-frequency plateau is almost independent on the molecular details.

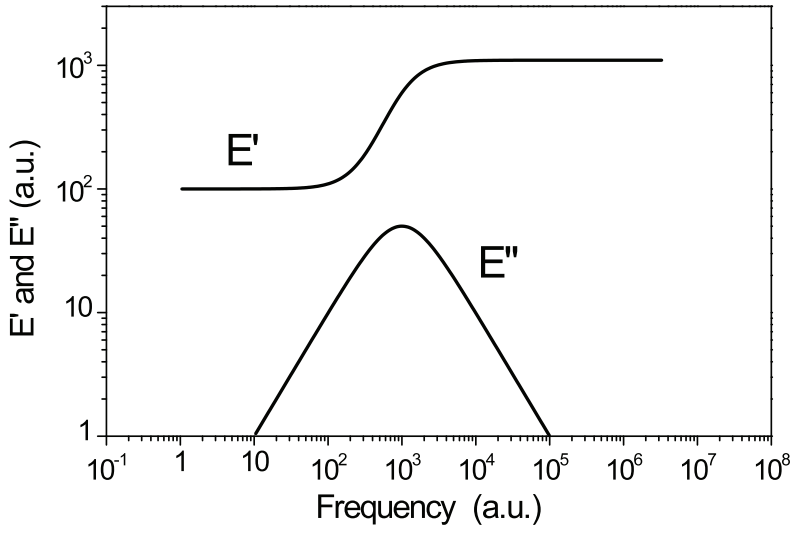

Plot 4.II. Schematic variation of E' and E" with frequency for an idealized elastomer having a single relaxation mode.

The whole frequency variation of Young's modulus easily spans 10 decades, it is therefore technically impossible to record it entirely. Fortunately, the empirical time-temperature superposition principle (TTS) enables to nevertheless access to this

information: it has been shown for most polymers and traditional elastomers that, instead of measuring *e.g.* slow relaxations at low temperature, it was equivalent to measure faster relaxations at higher temperatures. Using the so-called shift factors, it is then possible to construct a *master curve* at any given temperature. An example taken from literature is given in plot 4.III.[146] This particular curve is for the shear modulus G but the principle is the same for Young's modulus E.

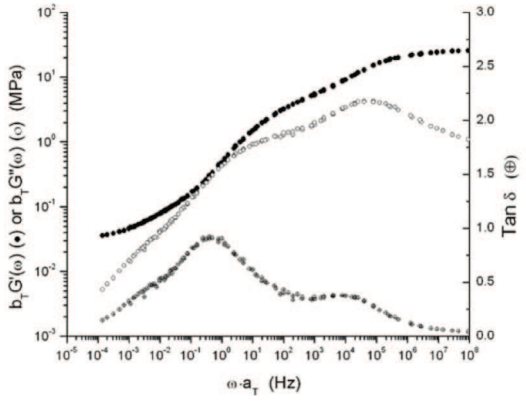

Plot 4.III. Master curve of dynamic shear modulus of an LCE.[146] a_T and b_T are called shift factors. G': storage shear modulus; G'': loss shear modulus.

This master curve of a polydomain smectic main chain elastomer has been built from data recorded with frequency sweeps from 1Hz to 100Hz with the temperature varying from 5°C to 100°C. In spite of a frequency range spanning from 10^{-4} to 10^{8} Hz the curve is still "uncomplete", the low frequency regime being just approached, with only the beginning of a plateau at 10^{-4}Hz. The arbitrary reference temperature of the master curve is T_{ref}=50°C.

Mesomorphic elastomers are not traditional since they exhibit mesophases. The time-temperature superposition principle usually holds in the nematic and isotropic phases

146 Patil, H.P., Hedden, R. C., *J. Polym. Sc. B.*, **2007**, 45, 3267. The data are presumably taken all in the Sm phase. From the published SAXS spectra and DSC curves we rather believe that the mesophase actually is a nematic one. This point is also supported by the fact that it has been possible to built a master curve.

but unfortunately breaks down at any transition involving a smectic phase. Most of the time it is therefore impossible to draw complete master curves for such elastomers, only partial ones.

We give here as an example our attempt at building a master curve in one of our samples, **CoEN1B4D 5%**. Even though it has been possible to construct a master curve for E', as can be seen in plot 4.IV, using the same shift factors on E" and tanδ led to obviously "incorrect curves" (plots 4.V and 4.VI, respectively), but still permitted a crude overview of the viscoelastic behavior.

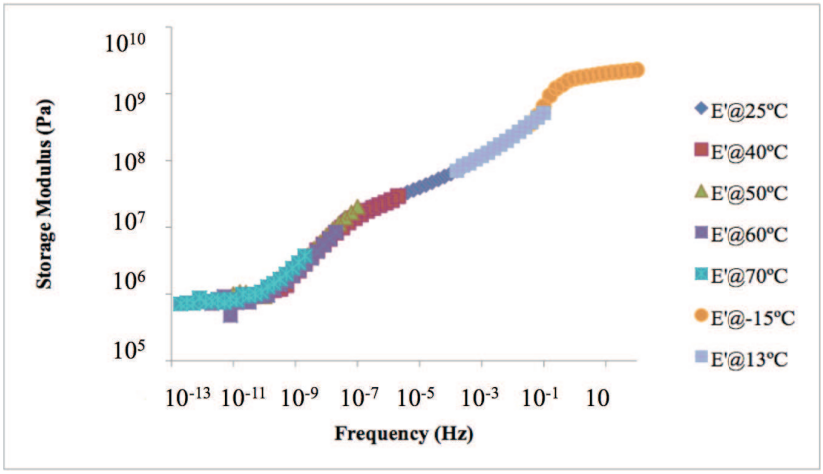

Plot 4.IV. E' vs Frequency graph by applying the TTS principle.

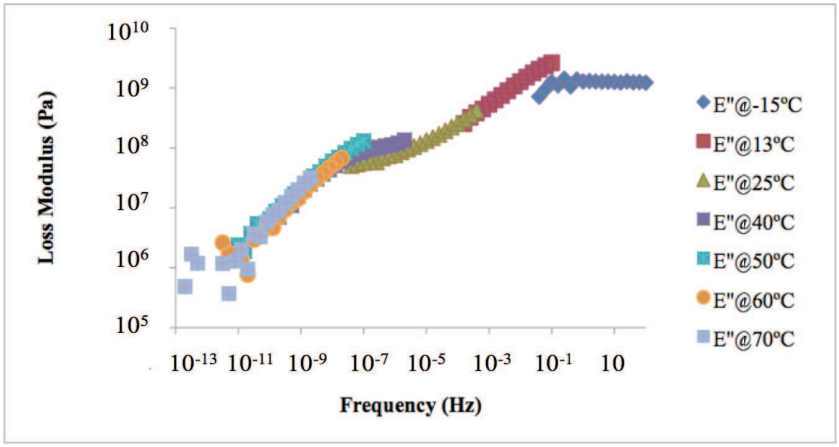

Plot 4.V. E'' vs Frequency graph by applying TTS principle. The various curves obviously do not assemble properly.

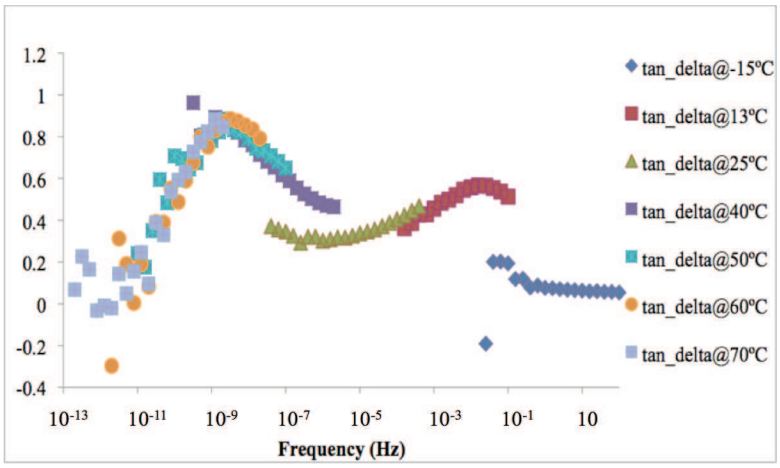

Plot 4.VI. Tanδ *vs.* Frequency graph by applying the TTS principle.

Most of the published rheological studies have been performed on side chain liquid crystalline elastomers, usually in shear-mode.[147] In some cases their particular behavior is considered "unconventional" since they can display elastic distortion without applied stress, also known as soft elasticity and semi-soft elasticity.[148] This theory is mostly advocated by M. Warner and E. Terentjev. Other groups disagree with this behavior and suggest that LCE are best described by a Rouse-like behavior.[147g,h,149] As of today, this debate is still open[150] and it is beyond the scope of this work to discuss it further. Only a few mechanical studies have so far been

---

147 a) Clarke, S. M.; Terentjev, E. M., *Phys. Rev. Lett.* **1998,** 81, (20), 4436; b) Terentjev, E. M., *J. Phys.-Cond. Matter* **1999,** 11, (24), R239; c) Edwards, S. F.; Takano, H.; Terentjev, E. M., *J. Chem. Phys.,* **2000,** 113, (13), 5531; d) Stein, P.; Assfalg, N.; Finkelmann, H.; Martinoty, P., *Eur. Phys. J. E,* **2001,** 4, (3), 255; e) Clarke, S. M.; Hotta, A.; Tajbakhsh, A. R.; Terentjev, E. M., *Phys. Rev. E,* **2001,** 6406, (6), 061702; f) Zanna, J. J.; Stein, P.; Marty, J. D.; Mauzac, M.; Martinoty, P., *Macromolecules,* **2002,** 35, (14), 5459; g) Martinoty, P.; Stein, P.; Finkelmann, H.; Pleiner, H.; Brand, H. R., *Eur.Phys. J. E,* **2004,** 14, (4), 311, h) Brand, H. R.; Pleiner, H.; Martinoty, P., *Soft Matter,* **2006,** 2, (3), 182; and many others.

148 Warner, M.; Terentjev, E. M., *Progress in Polym. Sci.,* **1996,** 21, (5), 853.

149 The model is explained in: Rouse, P.J., *J. Chem, Phys.*, **1953**, 21, (7), 1272.

150 A few representative papers, in order of appereance : a)Terentjev, E. M., Warner, M., Commentary on "Mechanical properties of domain side chain nematic elastomers" by P. Martinoty, P. Stein, H. Finkelmann, H. Pleiner and H.R. Brand. *Eur. Phys. J. E* **2004,** 14, (4), 323; c) Martinoty, P., Stein, P.; Finkelmann, H., Pleiner, H., Brand, H. R., Reply to the Commentary by E.M. Terentjev and M. Warner on "Mechanical properties of monodomain side chain nematic elastomers". *Eur. Phys. J. E,* **2004,** 14, (4), 329; Martinoty, P., Stein, P., Finkelmann, H., Pleiner, H., Brand, H. R., Reply to the Commentary by O. Stenull and T.C. Lubensky on "Mechanical properties of monodomain side chain nematic elastomers". *Eur. Phys. J. E* **2004,** 14, (4), 339.

performed on main chain LCEs.[128,151,152] This is due to the rather late appearance of the main-chain compounds on the elastomer scene: the traditional method of preparation, based on the crosslinking of mesomorphic polymers, is almost totally unadapted for main-chain compounds as recalled in the introduction. In the next paragraph we briefly discuss the techniques employed to analyze both rheological behavior and thermoelastic response of our LCE films.

4.2. Device Description.

4.2.1. *Thermoelastic Experiments*

Thermoelastic experiments allow to determine the expansion coefficient of materials. The device employed to perform these experiments, depicted in figure 4.2, consists of a specially designed glass chamber. This chamber is double-walled, its temperature is controlled by circulating thermostated silicon oil with a pump. Oil temperature is regulated by a computerized temperature controller.

A typical thermoelastic experiment is schematically described in plot 4.VII. Basically the experiment consists in heating the sample to the first temperature stabilizing for 50 minutes. At the end of this stabilization step, a picture is automatically taken by a camera. The temperature is then increased to the next programmed step and the sequence is repeated until the maximum set temperature is reached. During the second

---

[151] a) Rogez, D., Brandt, H., Finkelmann, H., Martinoty, P., *Macromol. Chem. Phys.,* **2006,** 207, (8), 735; b) Giamberini, M., Ambrogi, V., Cerruti, P., Carfagna, C., *Polymer,* **2006,** 47, (13), 4490; c)Patil, H. P., Liao, J., Hedden, R. C., *Macromolecules,* **2007,** 40, (17), 6206. d) Ren, W., McMullan, P.J., Griffin, A.C., *Macromol. Chem. Phys.* **2008**, 209, 1896.

[152] Beyer, P., Teretjev, E.M., Zentel, R., *Macromol. Rapid Commun.*, **2007**, 28, 1485.

part of the process, the sample is cooled stepwise while pictures are also taken at fixed temperature/time intervals.

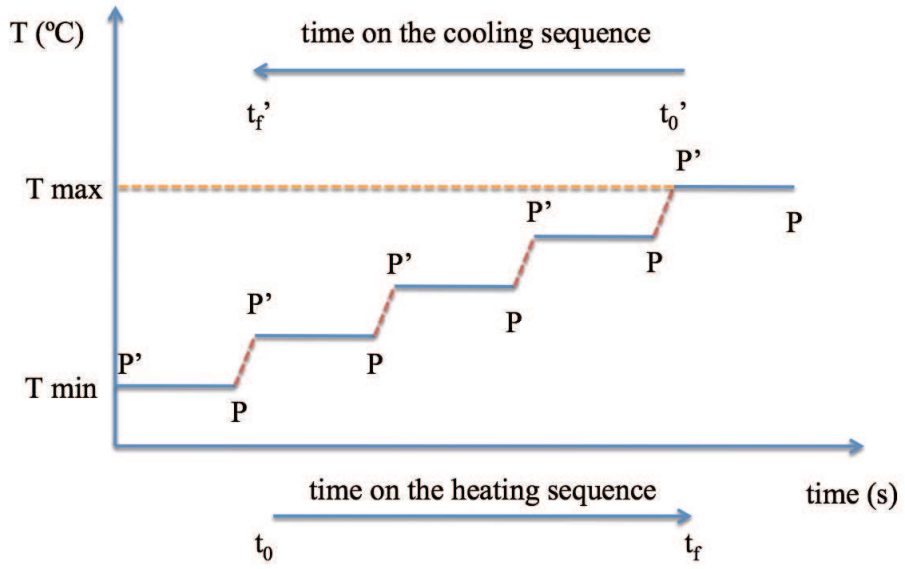

Plot 4.VII. Process performed by the thermoelastic device to obtain the corresponding plots. P indicates the time of pictures (P) taken during the heating cycle. P' indicates pictures taken during the cooling cycle.

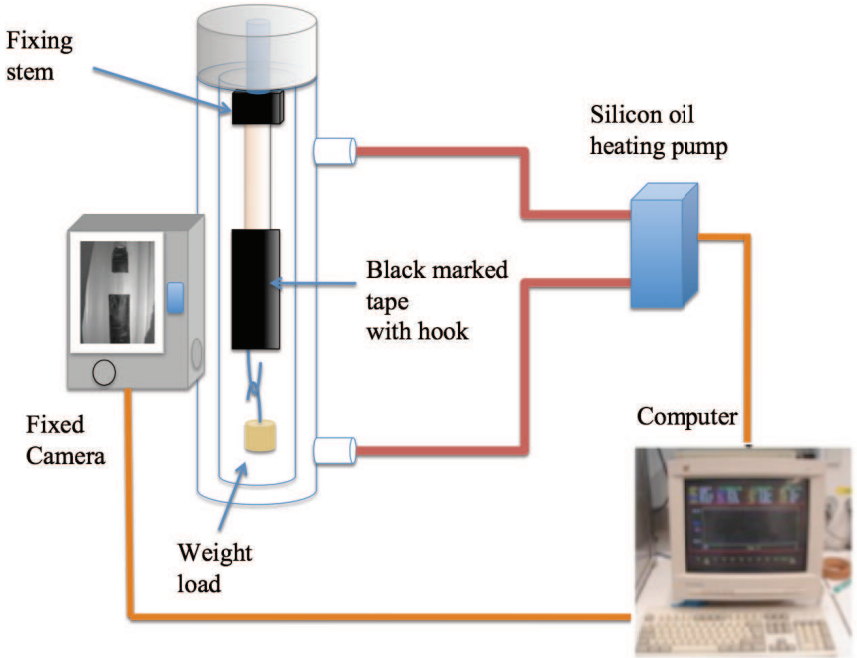

Figure 4.2. Thermoelastic device.

4.2.2. *Dynamic Traction Rheometry*

We originally determined the static Young's modulus by loading the sample with weights at constant temperature in order to obtain the strain *vs.* stress curve. The Young's modulus is the slope of the curve at a given strain value. Since this experiment ultimately destroys the sample, it was decided to perform dynamical traction experiments instead. These experiments have been performed at LIPHT in Strasbourg, in collaboration with Dr. Guy Schlatter. They aim at determining the complex dynamic Young's modulus E*=E' + iE", E' being the storage modulus and E" the loss modulus.

The rheometer consists in two clamps that hold the sample vertically. One of them is fixed and the other oscillates at a given frequency. Stress and strain are simultaneously recorded, as well as their phase shift. The sample chamber is illustrated in figure 4.3.

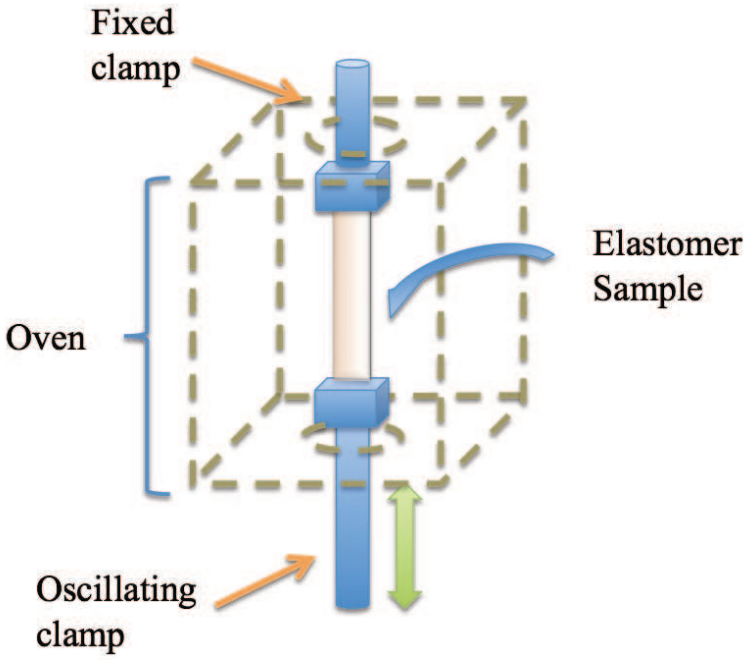

Figure 4.3. Illustration of the dynamic traction rheometer.

This machine allows to control the different variables of the test such as strain, oscillating frequency, and temperature. In order to avoid samples overstress, which could eventually lead to imprecise results, all the measurements were performed at a small, constant strain (0.1%). The variables involved into these studies were therefore temperature and strain frequency. In a first type of measurement the temperature is kept constant while the variation of the elastic and the viscous components of Young's modulus is recorded while varying the oscillating frequency. In a second type of measurement, a temperature ramp is applied while E* is measured at a fixed frequency. Several tests were performed on our elastomers in order to compare their modulus as a function of monomer proportion, chain extender and presence of bent-core moieties into the network as a hardening agent. The results and discussion are given in the next paragraph.

4.3. Results and Discussion.

4.3.1. *Dynamic Traction Rheometry*

Let us first give the results of typical experiments such as those described hereabove. The figures below represent the frequency variation of E', E" and loss factor for the **CoE25T** elastomer. The spectrum on the left has been recorded in the SmC phase while the spectrum on the right has been recorded in the isotropic phase.

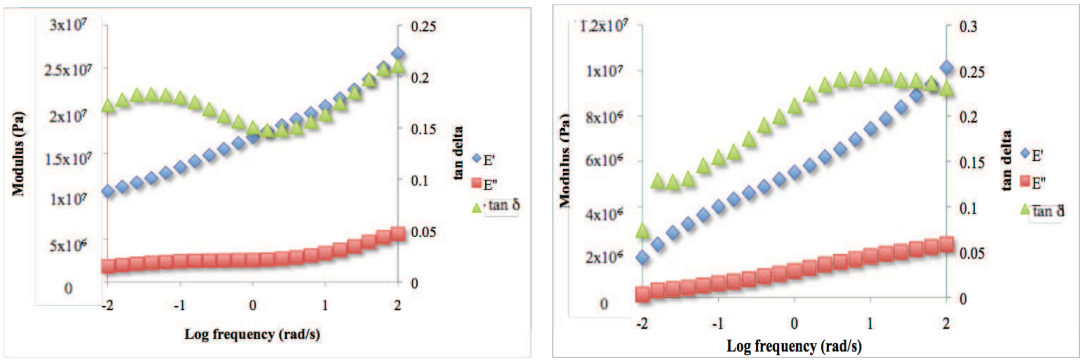

Figure 4.4. Variation of E', E" and loss factor in the smectic phase (T=40°C, left) and isotropic phase (T=75°C, right) for **CoE25T**.

Both spectra are obviously recorded at frequencies higher than the hydrodynamic regime : E' does not display any low-frequency plateau which must therefore occur at lower frequencies. This is confirmed by the presence of a maximum in the tan δ curve and the rather high value (~10MPa at 40°C and ~2MPa at 75°C) of E'. We could not estimate the value of E at zero frequency, E_0, which is unfortunate because much information is already unveiled by the low frequency regime. For a main-chain elastomer Ren *et al.*[145] have measured E_0=11.9MPa, presumably at room temperature. Their sample had a smectic phase from –25°C to 104°C (clearing point). The crosslink density was 10%, which is rather high (our sample have 4%), and probably explains the high modulus reported. Beyer *et al*[152] report E_0 =1.7MPa at 39°C (Sm phase) and E_0=0.2MPa at 72°C (isotropic). The crosslink density is undertermined and given as "light".

Let us now try making comparisons between samples. As each sample has a specific phase diagram, the question of temperature is not an easy one. The common use in such studies is to make the comparisons as a function of the reduced temperature $T_{red}=(T-T_c)/T_c$, with T_c being a phase transition temperature. This choice is somewhat arbitrary as we might also have chosen the glass transition temperature T_g, since it is

well known that all polymeric materials are strongly under the influence of this transition.

Let us compare the thermal behavior of all the elastomers for which we have data, with E' being measured at 1Hz, as shown in the plot 4.VIII. Depending on the sample, the aforementioned phase transition temperature T_c is the smectic-to-nematic or smectic-to-isotropic transition temperature. The main observation is that all co-elastomers essentially have the same behavior, regardless of their composition, when the plot is made as a function of the reduced temperature. Its seems that elastomer **EN1T** intrinsically has a larger high-temperature modulus, since either pure or when slightly doped with **B6**, its high-temperature modulus is about two times larger than that of all other samples. The length of the spacer (**D** or **T**) does not seem to play a major role in the rheological behavior, which is probably to be expected (see for example the disiloxane and the trisiloxane MC LCCoE curves). Comparative plots of trisiloxane and disiloxane are shown in appendix C.

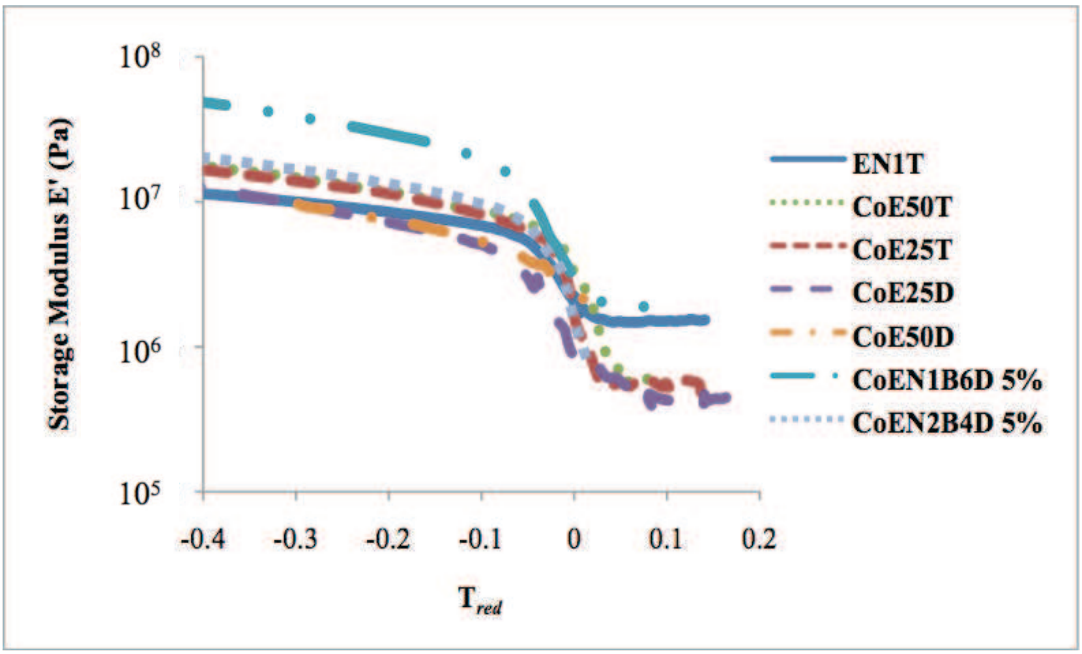

Plot 4.VIII. E' vs Reduced temperature plot of calamitic MC LCEs, critical temperatures (T_c) were: **EN1T**=89.3ºC; **CoE50T**=71.3ºC; **CoE25T**=70.9ºC; **CoE25D**=83.88ºC; **CoE50D**=57.33ºC.

The following figure compares the storage modulus E' of the elastomers for which we have relevant data as a function of the percentage of mesogen **N1** (Plot 4.IX).

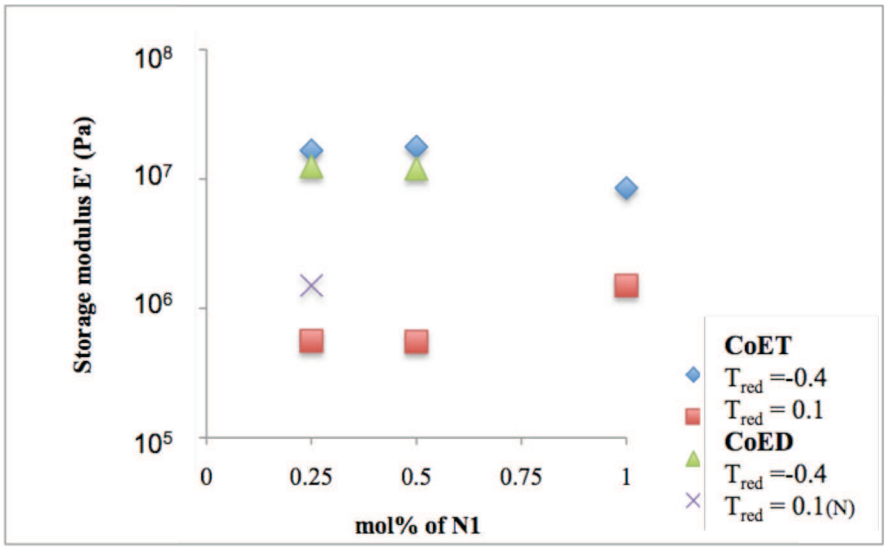

Plot 4.IX. Storage modulus E' as a function of two reduced temperatures (-0.4 in smectic C mesophase; 0.1 in isotropic liquid), the chain extender and **N1** molar proportion. **CoET**: trisiloxane elastomer; **CoED**: disiloxane elastomer; D: disiloxane coelastomer; (N): corresponding to nematic mesophase. T_{red} for **CoE50D** was not determined due to sample breaking at transition temperature.

In the smectic phase (negative T_{red}) the modulus decreases when the proportion of mesogen **N1** is increased, whereas the opposite occurs in the isotropic phase (positive T_{red}). Given the very limited number of data points we have, it would probably be adventurous to try drawing strong conclusions from these observations. E' is expected to be higher in SmC phase than in N or isotropic mesophases because of the order in the system. However, it seems too early to connect this behavior with the nature of the monomer mixture. Several of such experiments on other elastomers are being carried out and in preparation (coll. Dr. P. Martinoty at ICS and Dr. G. Schlatter at LIPHT) in order to complete this systematic study. Moreover, comparisons can not be made as there are no available uniaxial traction data for MCLCEs of this nature.

4.3.2. *Thermoelastic Studies of Disiloxane LCCoEs.*

Since we could not perform reversible experiments with the **HTMS** elastomers due to the previously evoked shape memory effect, thermoelastic experiments were performed with coelastomers **CoE25D** and **CoE75D**. These experiments have been conducted at Prof. Heino Finkelmann's laboratory, in Freiburg im Breisgau, Germany.

To avoid any "frozen effect" which can induce some reduction of the maximum length of a sample, as previously observed by Bispo,[105] the experiment was programmed as a cooling-heating sequence starting 10 degrees above the isotropization temperature (as determined by DSC studies). The first part of the experiment consists in cooling down the sample to its smectic phase, and the second one in heating it back to the original temperature. Sample cross-section was monitored in order to estimate the strain for each applied load. Two heating/cooling cycles were performed for each LCCoE, the first one with an attached load of 0.5g,

the second with 5.0g, in order to see if the maximal elongation were changed. Results obtained for the first cycle are illustrated in figure 4.5. A feature of these systems is that the length remained constant throughout the smectic mesophase range, and decreased slightly upon reaching the nematic transition. A similar behavior has been reported for an elastomer synthesized with **HD5** crosslinker at the SmH-SmC transition.[104] But, opposite to these results, a main-chain liquid crystalline elastomer synthesized by Bispo containing a disc-like crosslinker[105] showed an expansion of about 11% upon reaching the SmC/N[153] transition which is comparable with a SmA LCE previously synthesized.

Comparing our results with the previously described cases leads us to conclude that in the case of our MC LCCoE the nature of the crosslinker **HD5** fixes the maximum length variation at the SmC/N transition (Figure 4.5). The maximum length is totally recovered after the entire cycle in both cases, demonstrating the reversibility of such systems.

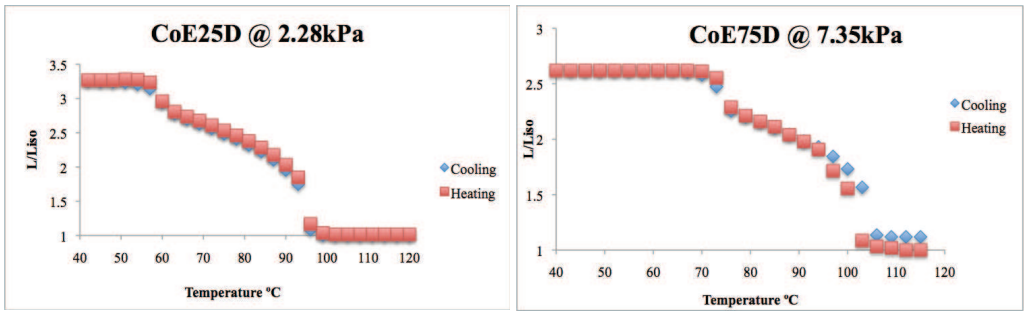

Figure 4.5. Thermoelastic curves of **CoE25D** and **CoE75D** loaded with mass=0.5g. Stress (kPa) is obtained with the equation $\sigma = m*g/s$. *m* is the loaded mass, *g* is the gravity force and ***s*** is the cross section of each sample.

Upon performing the first cycle, the transition temperatures for each mesophase can be determined by plotting the derivative $d(L/L_{iso})/dT$ versus temperature (plot 4.X). It

[153] Assfalg, N., Finkelmann, H., *Macromol. Chem. Phys.,* **2001,** 202, (6), 794.

then interesting to compare the values maxima with the values obtained by DSC studies (table 4.1). As can be seen in the table, both experiments are in good agreement.

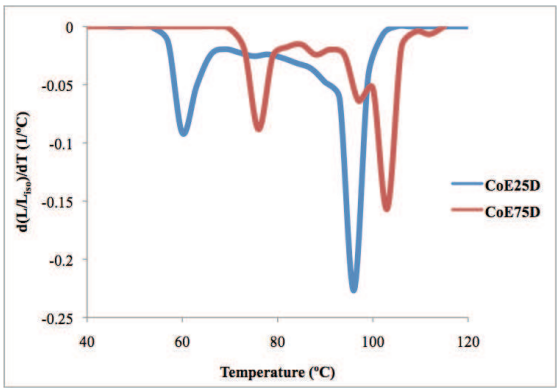

Plot 4.X. d[(L/L$_0$)/dt] vs. T for disiloxane coelastomers.

Table 4.1. Comparative values of transition temperature of disiloxane elastomers.

Coelastomer	$T_{SmC/N}$ (te)	$T_{SmC/N}$ (DSC)	$T_{N/I}$ (te)	$T_{N/I}$ (DSC)
CoE25D	60	65 [61]	96	96 [93]
CoE75D	76	75 [67]	109	109 [103]

All the temperatures are expressed in degrees Celsius (ºC) with the onset temperature [T_{ONSET}] reported between brackets. $\mathbf{T_{SmC/N}}$: smecticC/nematic transition temperature; $\mathbf{T_{N/I}}$: Nematic to isotropic transition temperature; (te): temperature determined from thermoelastic experiment data (heating cycle); (DSC): temperature determined from the heating cycle of DSC experiments.

In order to better compare the thermoelastic behaviors of these coelastomers, we also have made plots as a function of the reduced temperature (plot 4.XI). The largest elongation is obtained when the proportion of monomer **N2** is higher. The soluble content of **CoEN75D** was much higher than that of **CoEN25D**, which could also explain the larger elongation value, **CoEN25D** having maybe more pending chains and uncompletely substituted croslinking units. Except for that, the two curves are very similar. This behavior is typical to MC LCE with an elongation of the same order of magnitude as those reported.[104,105,136]

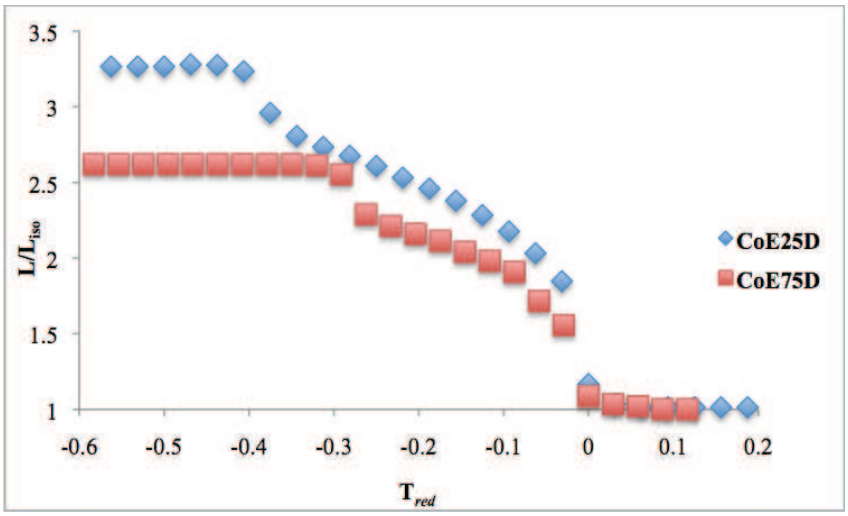

Plot 4.XI. Thermoelastic curves of **CoE25D** and **CoE75D** expressed in reduced temperature.

For these coelastomers, it was also important to determine the expansion coefficient, at every temperature in order to know the sample dimensions. This coefficient is obtained as briefly indicated in chapter 1 section 1.3.6 (page 49). initial temperature T_0 = 40ºC since it is the lowest working temperature employed in our thermoelastic experiments as well as that of many rheology devices. The Plot 4.XII shows the expansion coefficient as a function of temperature.

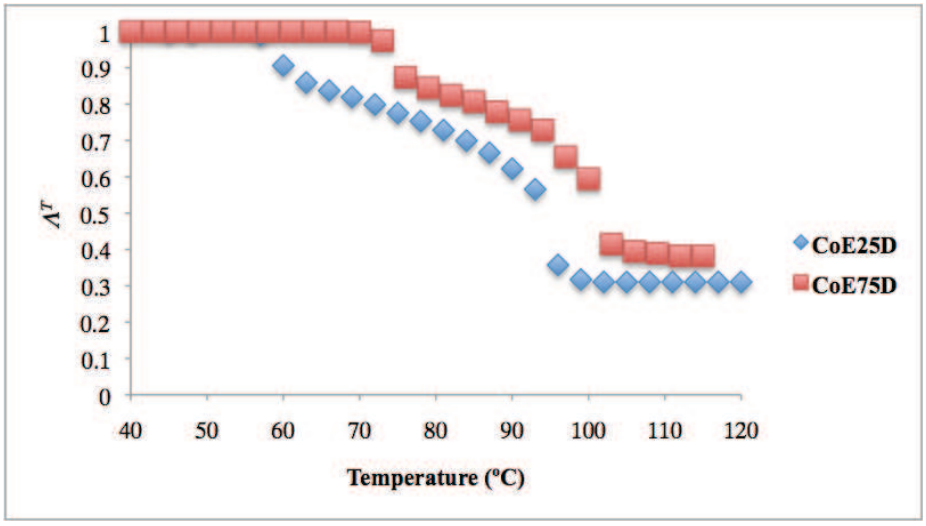

Plot 4.XII. Expansion coefficient of **CoE25D** and **CoE75D** as a function of temperature. $\Lambda = l^T / l^{40ºC}$

The results obtained for the second cycle with a stress 10 times larger were compared with the first cycle ones. Since the stress difference was larger for **CoE25D** sample (Plot 4.XIII), a significant shift in the transition temperatures was observed, indicating an induction of order through stress, also known as parasmectic and paranematic states.[154] Another interesting observation is the increase of the starting length, 280% at 40ºC, resulting also of the larger applied stress. Transition temperatures are shifted by about 5ºC, which indicates stress-induced ordering in the sample.

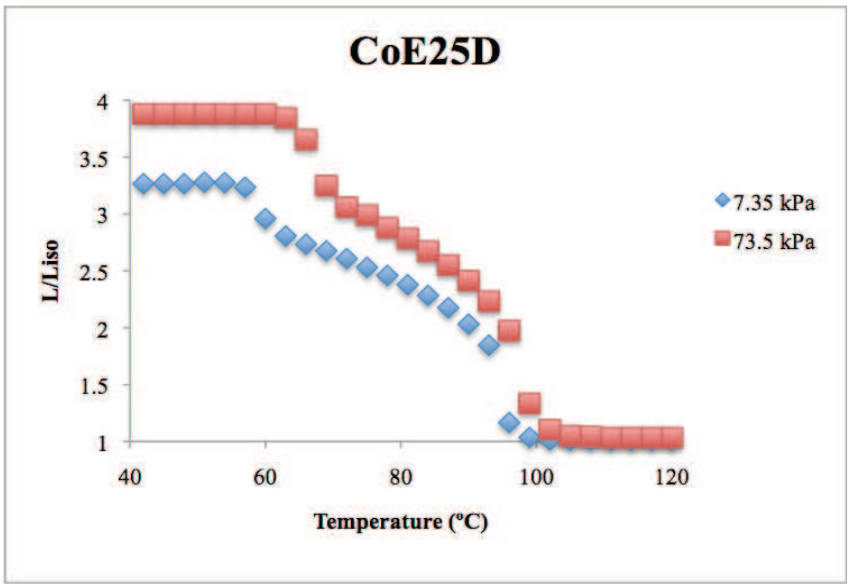

Plot 4.XIII. Thermoelastic plots of **CoE25D** as a function of temperature at different weight loads.

Otherwise, in the case of **CoE75D** film (Plot 4.XIV), no transition temperature shift could be seen. The shift observed for SmC/N transition is within experimental errors. No hysteresis of the elongation cycle was observable, demonstrating that the coelastomer remained in the linear regime of stress/strain.

---

[154] Lebar, A., Kutnjak, Z., Zumer, S., Finkelmann, H., Sanchez-Ferrer, A., Zalar, B., *Phys. Rev. Lett.,* **2005,** 94, (19), 197801.

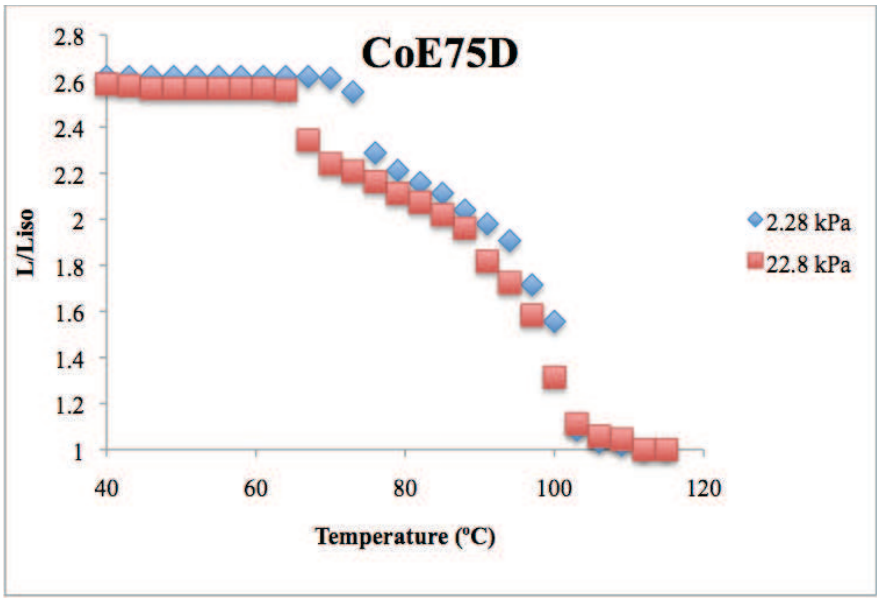

Plot 4.XIV. Thermoelastic plots of **CoE75D** as a function of temperature at different weight loads.

Thermoelastic experiments of the other BC/CMLCCoEs are on the way to be performed in order to see if this behavior is generalized for all our systems, which seems very promising for high deformation actuators's applications.

4.4. Conclusions.

Rheological experiments allowed to determine the viscoelastic properties of our samples in the different mesophases. However, more detailed investigations should be carried out in order to fully characterize their complete rheological properties. These experiments are still in progress (Dr. G.Schlatter and Dr. P.Martinoty in Strasbourg).

Thermoelastic experiments had shown that when employing **HD5** crosslinker in low concentrations, it is possible to prepare MC LCEs with very large elongation factors, which is useful for plastic actuators. These experiments allowed also to determine accurately the transition temperatures and the expansion coefficient of the samples. The former is very useful to perform rheological experiments and the latter to confirm the mesomorphic behavior obtained by DSC studies.

Although, the monomer proportion, type of mesophase and maximum elongation did not seemed to show any specific relationship with the rheological properties. LCEs containing bent-core monomers seemed to present higher resistance, however, to confirm these observations, more investigations should be performed.

The MC LCE synthesized presented good characteristics such as high elongation factors and high Young modulus and they are promising materials for actuator applications.

Chapter 5

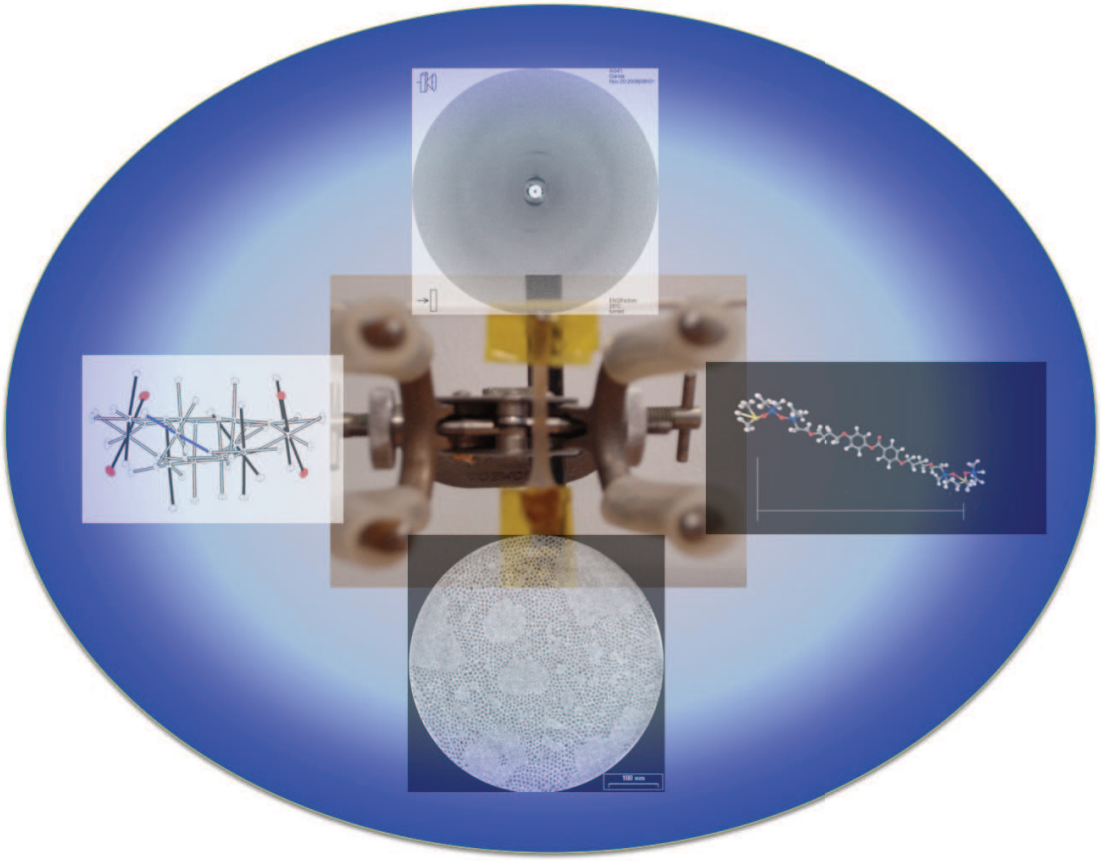

Magnetic Functional Networks

5. Magnetic Functional Networks.

5.1. Introduction and Concept.

As often evoked throughout this study, our first intention was to decrease the transition temperatures of liquid crystalline elastomeric networks in order to facilitate their use in practical applications. Their ability to reversibly change their shape and size significantly with temperature make them attractive in order to be potentially incorporated into actuating materials that could mimic muscle performances (contraction/elongation cycles).[155] Of importance are the contraction length, the stress, and the speed of the response of these materials, the three necessary parameters to optimize for successful and viable implementation into devices. Temperature induces changes, mainly governed by heat conductivity and sample size, may be under some circumstances too slow, limiting the applications of LCEs into a restricted variety of devices. It is therefore essential to trigger shape changes in LCEs with other external stimuli than temperature, and recent reports have shown promising developments in systems excited by electric[156] or magnetic[157] fields or

---

155 a) de Gennes, P.-G. *C. R. Acad. Sci. Paris, Ser. IIb* **1997**, *324*, 343. b) Finkelmann, H., Kaufhold, W., Noirez, L., Tenbosch, A., Sixou, P. *J. Phys. II* **1994**, *4*, 1363; c) Knight, D. P., Vollrath, F. *Philos. Trans. R. Soc. London, B* **2002**, *357*, 155; d) Li, M.-H., Keller, P., *Philos. Trans. R. Soc. London, A* **2006**, 1; e) Buguin, A., Li, M.-H., Silberzan, P., Ladoux, B., Keller, P., *J. Am. Chem. Soc.* **2006**, *128*, 1088; f) Spillmann, C. M., Naciri, J., Martin, B. D., Farahat, W., Herr, H., Ratna, B. R., *Sens. Act. A* **2007**, *133*, 500.

156 a) Zentel, R., *Liq. Cryst.* **1986**, *1*, 589; b) Barnes, N. R., Davis, J. F., Mitchell, G. R., *Mol. Cryst. Liq. Cryst.* **1989**, *168*, 13; c) Lehmann, W., Skupin, H., Tolksdorf, C., Gebhard, E., Zentel, R., Kruger, P., Losche, M., Kremer, F., *Nature* **2001**, *410*, 447; d) Köhler, R., Stannarius, R., Zentel, R., *Appl. Phys. A: Mater. Sci. Process.* **2005**, *80*, 381; e) Yusuf, Y.; Huh, J.-H.; Cladis, P. E.; Brand, H. R.; Finkelmann, H.; Kai, S. *Phys. Rev. E* **2005**, *71*, 061702. f) Spillmann, C. M., Ratna, B. R., Naciri, J., *Appl. Phys. Lett.* **2007**, *90*, 021911. g) Yusuf, Y., Hashimoto, S., Cho, D.-U., Brand, H. R., Finkelmann, H., Kai, S., *Mol. Cryst. Liq. Cryst.* **2007**, *477*, 127.

157 a)Song, H. M., Kim, J. C., Hong, J. H., Lee, Y. B., Choi, J., Lee, J. I., Kim, W. S., Kim, J.H., Hur, N.H., *Adv. Funct. Mater.* **2007**, 17, 2070; b)Kaiser, A.; Winkler, M.; Krause, S.; Finkelmann, H.; Schmidt, A. M. *J. Mater. Chem.* **2009**, 19, 538.

electromagnetic irradiation.[158] While important progress was achieved with electro-[156,159] or optoactive-containing[104,128,158] systems, examples of magnetoactive LCEs remain rather rare.[157] The effects of magnetic particles confined in a cross-linked polymer gels (ferrogel composites) have already been studied,[160,161,162] indicating variations on the response of the network in the presence of a magnetic field. Therefore, hybrid LCEs containing magnetic nanoparticles could be potentially good candidates for incorporation into fast actuating systems, and this interest could be two-fold: through the reversible coupling between flow and director orientations upon application of a magnetic field (field dependent shape change) or through the energy transfer into heat due to relaxation processes upon pulsed electromagnetic irradiation (local thermal phase changes in the particle environment).

In the following and final chapter of this thesis, we will present our preliminary investigations in this direction illustrated by 2 exemples and some opened perspectives, of our study on incorporation of magnetic objects within LC elastomers. A first part will deal with the incorporation within the elastomeric matrix of the single molecular magnet Mn12 acetate, MnOAc, (abbreviation of $[Mn_{12}O_{12}(MeCO_2)_{16}.4H_2O]$), and the second part with iron oxide nanoparticles, with a

---

158 a) Finkelmann, H., Nishikawa, E., Pereira, G. G., Warner, M., *Phys.Rev. Let.* **2001**, 87, 015501. b) Cviklinski, J., Tajbakhsh, A. R., Terentjev, E. M., *Eur. Phys. J. E* **2002**, 9, 427. c) Hogan, P. M., Tajbakhsh, A. R., Terentjev, E. M., *Phys Rev. E* **2002**, 65, 041720. d) Warner, M., Terentjev, E., *Macromol. Symp.* **2003**, *200*, 81; e) Li, M. H., Keller, P., Li, B., Wang, X., Brunet, M., *Adv. Mater.* **2003**, 15, 569; f) Camacho-Lopez, M., Finkelmann, H., Palfy- Muhoray, P., Shelley, M., *Nature Mater.* **2004**, 3, 307; g) Beyer, P., Zentel, R., *Macromol. Rapid Commun.* **2005**, 26, 874; h) Kondo, M., Yu, Y., Ikeda, T., *Angew. Chem. Int. Ed.* **2006**, *45*, 1378; i) Ikeda, T., Mamiya, J., Yu, Y., *Angew. Chem. Int. Ed.* **2007**, 46, 506; j)Yu, Y. L., Nakamo, M., Ikeda *Nature* **2003**, 425, 145.

159 Chambers, M., Zalar, B., Remškar, M., Žumer, Finkelmann, H., S. *Appl. Phys. Lett.* **2006**, 89, 243116.; Chambers, M., Zalar, B., Remškar, M. Kovač, J, Žumer, Finkelmann, H., *Nanotech.* **2007**, 18, 415716.

160 Auernhammer, G. K., Collin, D., Martinoty, P., *J. Chem. Phys.* **2006,** 124, (20), .

161 Collin, D., Auernhammer, G. K., Gavat, O., Martinoty, P., Brand, H. R., *Macromol. Rapid Commun.* **2003,** 24, (12), 737.

162 Schmidt, A. M. *Macromol. Rapid commun.* **2006**, *27*, 1168.

diameter of 3.3 nm. This study is done in collaboration with colleagues from the IPCMS, namely Drs E. Terazzi, J.L. Gallani and G. Rogez (Mn12), and Pr S. Bégin-Colin and Dr A. Demortière (Fe_3O_4 NPs).

5.2. Mn12 networks.

Single molecule magnets (SMM) are materials that are able to retain magnetization at the molecular level below a certain temperature, known as blocking temperature.[163] This family of compounds currently elicits sustained research activity: as quantum objects they are envisioned as qubits for quantum computers, and due to their magnetic properties, they can be considered as the ultimate storage bits of molecular memory storage. Some examples of compounds exhibiting this behavior are rare, and are some 4*f* coordination compounds (lantanide complexes),[164] polymetallic cages,[165] and oxometalloclusters.[163,166] One of the most interesting clusters of this kind is Mn12ac cluster, which was first synthesized by Lis[167] in 1980. This SMM marked the beginning of an intensive research due to i) its low-cost, ii) easily synthetic accessibility, iii) a high ground spin state (S=10) and iv) its magnetic anisotropy. Mn12 presented the highest blocking temperature reported[168] until very recently.[169]

The structure of the dodecanuclear manganese acetate cluster consists of a roughly planar disk made up of a central $Mn^{IV}{}_4O_4$ cube surrounded by a ring of eight Mn^{III}

163 "Single-Molecule Magnets and Related Phenomena": *Struct. Bonding* (Berlin) **2006**, 122.
164 a) Osa, S., Kido, T., Matsumoto, N., Re, N., Pochaba, A., Mrozinski, J., *J. Am. Chem. Soc*., **2004**, 126, 420; b) Zaleski, C. M., Depperman, E. C., Kampf, J. W., Kirk, M. L., Pecoraro, V. L., *Angew. Chem. Int. Ed.,* **2004**, 43, 3912.
165 Winpenny, R. E. P. , *J. Chem. Soc. Dalton Trans.* **2002**, 1.
166 a) Gatteschi, D., Sessoli, R., Cornia, A., *Chem. Commun.* **2000**, 725. b) Roubeau, O.; Clerac, R. *Eur. J. Inorg. Chem*. **2008**, 4325. c) E. K. Brechin, E. J. L. McInnes, *Eur. J. Inorg. Chem.*, 2006, 2725. G. Aromí, E. K. Brechin, *Struct. Bonding*, 2006, **122**, 1. E. K. Brechin, *Chem. Commun.*, 2005, 5141.
167 Lis, T., *Acta Crystallogr. Sect. B,* **1980**, 36, 2042.
168 Gatteschi, D., Sessoli, R., *Angew. Chem. Int. Ed*. **2003,** 42, 268, and references therein.
169 Milios, C. J., Piligkos, S., Brechin, E. K., *Dalton Trans.*, **2008**, 1809.

centres connected to the cube by eight μ_3-O_2^- and four κ^2-μ_2-carboxylate groups perpendicular to the plane of the disk (two on each side), as shown in Figure 5.1. Furthermore, the peripheral Mn^{III} centres are connected to each other by eight equatorial and four axial κ^2-μ_2-carboxylate groups. Two types of Mn^{III} ions can be distinguished: type I, doubly bridged to one Mn^{IV} centre; and type II, singly bridged to two Mn^{IV} centres. Four different isomers of Mn12 have been described in the literature: 1:1:1:1, 1:2:1:0, 1:1:2:0, and 2:2:0:0 (the notation indicates the number of water molecules coordinated to type II Mn^{III} ions). Mn^{III} ions show the typical elongated octahedral coordination seen in most Mn^{III} complexes. Mn^{III} and Mn^{IV} ions respectively have a spin 2 and 3/2; whereas all the Mn^{III} or Mn^{IV} ions are coupled ferromagnetically respectively, the Mn^{III} and Mn^{IV} are coupled antiferromagnetically.

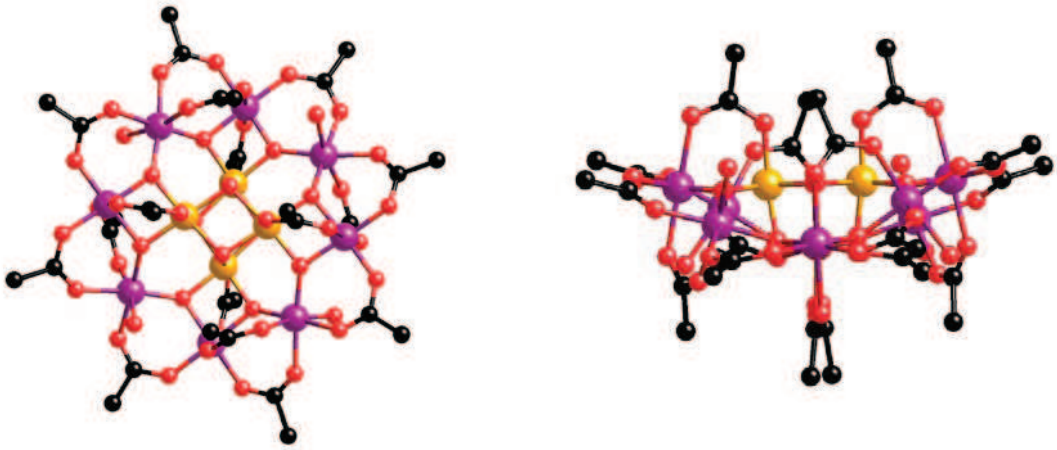

Figure 5.1. Axial and equatorial view of the Mn12ac cluster. Mn^{IV} atoms in yellow, Mn^{III} in purple, oxygen atoms in red and carbon atoms in black.

$[Mn_{12}O_{12}(OAc)_{16} \cdot 4H_2O]$ is prepared *in situ* from manganese acetate ($MnOAc_2$) and $KMnO_4$. Clusters with the general formula $[Mn_{12}O_{12}(RCO_2)_{16} \cdot 4H_2O]$, where R is an aliphatic chain or benzoate group, are prepared by direct ligand exchange reaction between the acetate cluster and the appropriate acid. The original acetic acid substituent forms an azeotrope with toluene which is easily removed by distillation.

These reaction conditions have been proved sufficiently soft to functionalize Mn12 with polymerizable groups,[170] and it is therefore conceivable to easily functionalize Mn_{12} clusters as potential cross-linkers, with an elevated connectivity, for novel types of LCE networks. The strategy we have developed consisted therefore in the ligand exchange of the acetates with an excess of the olefinic benzoic acid **Hx2** in toluene under reflux.[171] The brownish **Mn_{12}Hx2** compound was purified by GPC column and obtained in a yield of 80%. (Scheme 5.1).

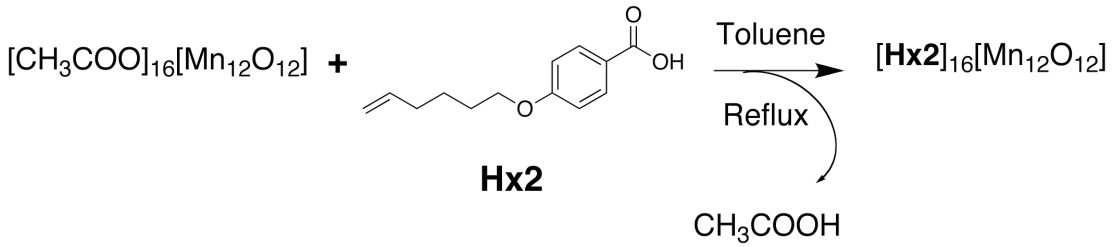

Scheme 5.1. **Mn_{12}Hx2** Crosslinker synthesis. Water molecules were omitted.

We then proceeded in the preparation of various magnetic polymeric networks as well as liquid crystalline elastomers using this molecule as the crosslinking agent. Three of such networks were envisaged: i) a network, **EMn1**, made of **Mn_{12}Hx2** as cross-linker, and polydimethylsiloxane as spacer (ratio **HDMOS-Mn_{12}Hx2** 8:1); ii) a second network, **EMn2**, containing 1,10-decadiene-polydimethylsiloxane (**DD**), **HDMOS** and **Mn_{12}Hx2**, (ratio **DD-HDMOS-Mn_{12}Hx2** 4:8:1); and iii) a third network, **EMn3**, **N2**, **HDMOS**, and Mn_{12}**Hx2**, expected to yield magnetic mesogenic networks (ratio **N2-HDMOS- Mn_{12}Hx2** 4:8:1).

---

[170] Palacio, F., Oliete, P., Schubert, U., Mijatovic, I., Husing, N., Peterlik, H., *J. Mater. Chem.,* **2004,** 14, (12), 1873.
[171] Terazzi, E.; Bourgogne, C.; Welter, R.; Gallani, J. L.; Guillon, D.; Rogez, G.; Donnio, B., *Angew. Chem. Intl. Ed.,* **2008,** 47, (3), 490.

As general considerations for the synthesis of these three networks, it is important to avoid temperatures higher than 60ºC to prevent cluster decomposition, and fast reaction times by employing an efficient catalyst to avoid **Hx2** dissociation from the cluster. In our protocol, the reaction mixture was heated at 40ºC in toluene and Karstedt catalyst (3%w) was used. First step of the synthesis consisted in dissolving all the starting products in toluene by keeping the solution at room temperature. The catalyst was then added and the mixture was heated up to 40ºC. In all cases rapid gelification was observed, yielding brownish solids after a brief period of time (15 minutes). Network gel **1**, **EMn1**, is illustrated in figure 5.2.

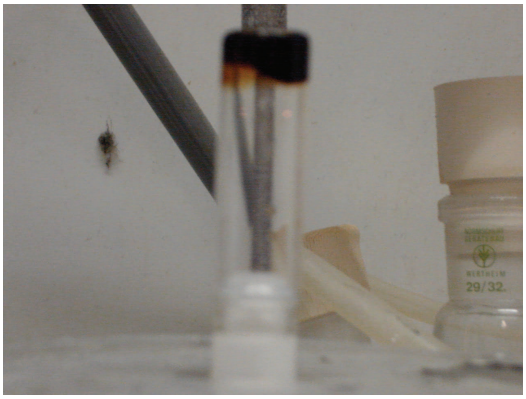

Figure 5.2. Picture of network **EMn1**.

The magnetic behaviour of **EMn1** and **EMn2** was characterized by SQUID (Plots 5.1), but the discussion will only focus on the first network **EMn1**. Plots a and b show respectively the temperature dependence of the AC susceptibility (in-phase and out-of-phase field components of the magnetic susceptibility, respectively) at different frequencies. Two peaks were observed in the in-phase component plot: a rather small peak at low temperatures, barely observed at low oscillation frequencies and an intense peak at higher temperatures detected as a shoulder or as a well defined peak depending on the sample. The frequency-dependent decrease in the χ'T versus T on

lowering the temperature (not shown here) indicates that the relaxation of the magnetization rate becomes close to the ac field frequency. The occurrence of a frequency-dependent out-of-phase ac susceptibility signal (χ'') is considered as a signature for SMM properties.[168,172] In an ac susceptibility measurement, an out-of phase signal (χ'') is expected to appear if the relaxation frequency of the magnetization of the sample becomes close to the frequency of the AC field.

The occurrence of two peaks in out-of-phase susceptibility, one in the region 4–7 K, the other in the region 2–4 K, is not an unusual feature for Mn12 derivatives. The origin of these two relaxation processes has been attributed to Jahn–Teller isomerism: for $[Mn_{12}(OAc)_{16}]$, all the Jahn–Teller elongation axes of the peripheral Mn^{III} centers are oriented perpendicularly to the plane of the molecule, whereas for systems that present the low-temperature χ'' peak, it has been shown that one of the peripheral Mn^{III} ions has an unusual orientation of its Jahn–Teller elongation axis, almost perpendicular to the elongation axis of the other Mn^{III} center. This Jahn–Teller isomerism is responsible for the lowering of the temperature at which the molecule experiences slow relaxation of the magnetization (blocking temperature), provoking an overall lowering of the magnetic anisotropy of the molecule (a key parameter for the slow relaxation process). This results in an increase of the rate of the reversal of the magnetization by quantum tunneling. The presence of two peaks suggests the

[172] a) Sessoli, R. *Mol. Cryst. Liq. Cryst*. **1995**, 274, 145; b) Caneschi, A., Gatteschi, D., Sessoli, R.,*J. Am. Chem. Soc.* **1991**, 113, 5873.

coexistence of different Jahn–Teller isomers within the sample,[173] as already observed for other Mn12 derivatives.[174]

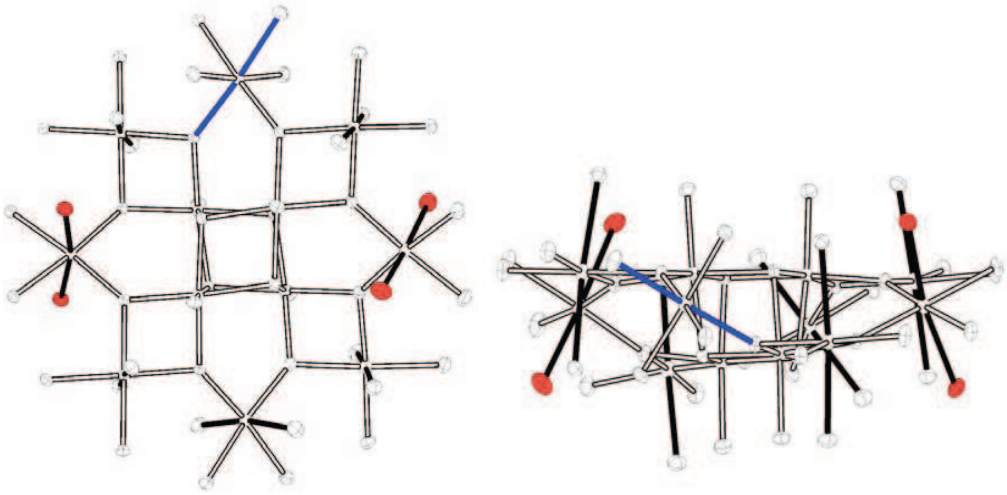

Scheme 5.2. ORTEP views of $[Mn_{12}L_{16}]$ perpendicular (left) and parallel (right) to the plane of the molecule. For clarity sake, hydrogen atoms have been omitted and only oxygen atoms of the carboxylate groups have been represented. The oxygen atoms of water molecules are indicated in red. The Jahn-Teller elongation axis of the Mn^{III} coordination sphere are indicated by bold lines. The blue bold line underlines an unusual orientation of the elongation axis.

Due to the unprecise origin of the low temperature species, only the high temperature species peak has been treated. The shift detected in the temperature peak position with respect to the frequency (ν) results from a large relaxation time (τ) leading to the freezing of the magnetization at the characteristic time of the experiment determined by $\tau = \frac{1}{\nu}$, this being the expected behavior for a superparamagnet. The relaxation time τ needed to reverse the magnetic moments is found to follow the Arrhenius law $\tau = \tau_0 \exp\left(\frac{\Delta}{k_B T}\right)$ in which τ_0 is the Arrhenius prefactor, Δ is the effective barrier energy, k_B is the Boltzman constant and T is the temperature. Plot 5.1.c) shows $ln(1/\nu)$ as a function of the inverse of the maximum temperature (1/Tmax) at which the

[173] Sun, Z.M. Ruiz, D, Dilley, N.R., Soler, M., Ribas, J., Folting, K., Maple, M. B., Christou, G., Hendrickson, D. N., *Chem. Commun.* **1999**, 1973.
[174] Evangelisti, M., Bartolome, J., Luis, F., *Solid State Commun*. **1999**, 112, 687.

maximum of the high temperature peak in χ'' occurs. A clear linear dependence indicates that the Arrhenius law is observed. The linear fit allows the linear values of Arrhenius prefactor τ_0 and the effective barrier energy Δ, 7.9×10^{-9} s and 58 K respectively, to be determined. The values obtained for this cluster are similar to those reported by Mn12ac in mesoporous silica[175,176] and free Mn12ac complex,[177] demonstrating a typical Mn12 behavior (Table 5.1).

The shape of the magnetization versus field curves at 1.8 K (plot 5.1 d) corresponds to randomly oriented polycrystalline Mn12 species.[178] The magnetization curve of the cluster network **EMn1** exhibits an open hysteresis loop characteristic of SMM behavior. A rather large coercive field was determined for the network presenting a T_B value (for the high temperature species peak) of 2.5 K (T_B is arbitrarily defined as the temperature for which t=100 s).

[175] Coradin, T., Larionova, J., Smith, A. A., Rogez, G., Clerac, R., Guerin, C., Blondin, G., Winpenny, R. E. P., *Adv. Mater*. **2002**, 14, 896.
[176] Clemente-León, M., Coronado, E., Forment-Aliaga, A., Martínez-Agudo, J.M., Amorós, P., *Polyhedron*, **2003**, 22, 2395.
[177] Novak, M. A., Sessoli, R., Caneschi, A., Gatteschi, D., *J. Magn. Magn. Mater.* **1995**, 146, 211.
[178] Awaga, K., Suzuki, Y., Hachisuka, H., Takeda, K., *J. Mater. Chem.* **2006**, 16, 2516.

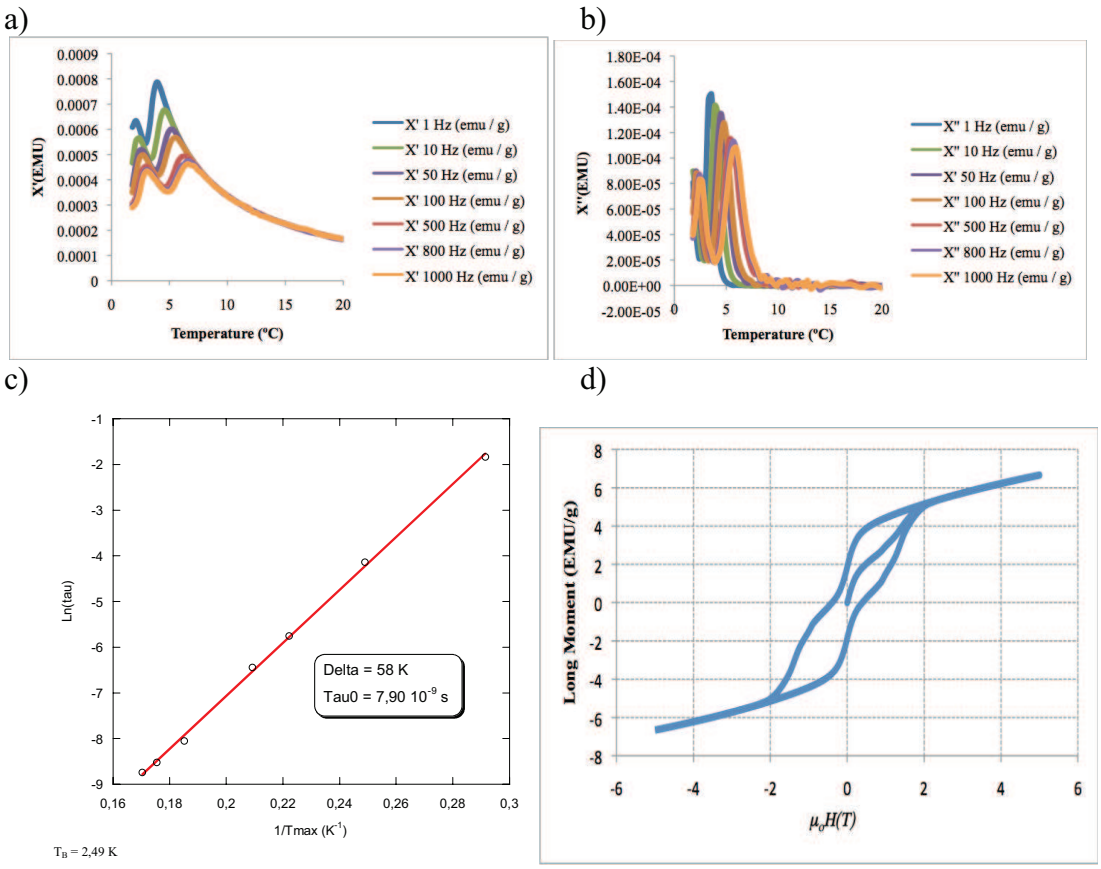

Plot 5.I. Magnetic studies performed to the compound **EMn1** (**$Mn_{12}Hx2_{16}$-PDMS**). a) In-phase component; b) out-of-the phase component; c)Arrhenius linear fit of high temperature species; d Magnetization curve recorded at 1.8 K.

Table 5.1. Magnetization values of $[(Mn_{12}\mathbf{Hx2})(PDMS)_8]_n$ (**EMn1**) compound.

Compound	**Δ(K)**	**τ_0 (s)**
$[(Mn_{12}Hx2)(PDMS)_8]_n$	58	$7.9x10^{-9}$

Δ: effective barrier energy; τ_0 Arrhenius factor; $[(\mathbf{Mn_{12}Hx2})(PDMS)_8]_n$ Polymeric network of the Mn12 cluster bearing ligands **Hx2,** using hydride terminated polydimethylsiloxane (PDMS) as polymeric chain.

Thus, the good result is that the SMM behaviour of the cluster is not damaged when inserted within an elastomeric network. However, we were not able to analyze **EMn3** in details due to its poor thermal stability and tendency to decompose; this network was also devoid of mesomorphic behavior.

In order to obtain liquid crystalline networks, the formulation was modified. It consisted of the mesogenic monomer, **N2**, the chain extender, **HMTS**, and **Mn_{12}Hx2** and **HD5** as the crosslinkers in 1.25 and 2 mol% respectively (Scheme 5.3). We have carried out two types of elastomer syntheses: the first one was performed in the bulk yielding un-oriented material and the second one by employing the spin casting technique, in order to obtain both a bulk polydomain and a mechanically oriented monodomain film, respectively.

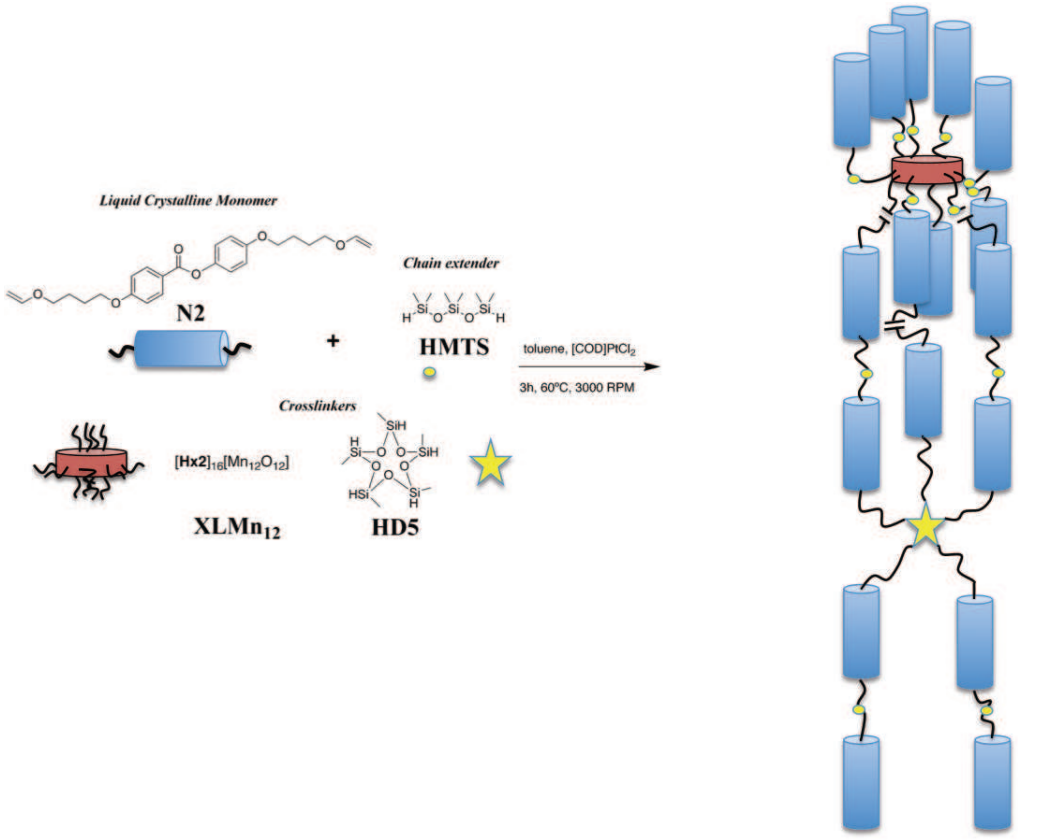

Scheme 5.3. Schematic representation of the preparation of mixed crosslinked MC LCE.

Both experiments yielded ill-formed networks. In the case of the bulk materials, a soft rubber with 30% of soluble content was obtained. Regarding the monodomain elastomer, a thin fragile film with high soluble content (50%) was obtained (Figure 5.3).

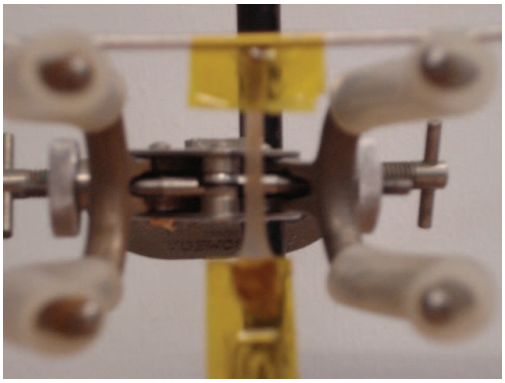

Figure 5.3. **Mn_{12}Hx2/HD5** mixed MC LCE.

DSC studies revealed thermal transitions occurring at temperatures similar to that of the analogous elastomer **EN2T** (Table 5.2).

Table 5.2. DSC data for mixed crosslinker MC LCE.

Elastomer	Thermal Behavior[a]
EN2T	g (n.d.) SmX 16.4 [4.6] SmC 41.8 [10.3] I
EN2TMn12(b)	g (n.d.) SmX 16.0 [4.6] SmC 41.8 [10.2] I
EN2TMn12(f)	g (n.d.) SmX 14.4 [2.0] SmC 35.8 [6.7] I

Temperatures were estimated as the average of heating and cooling maxima of the 2 cycles with a rate of 2ºC/min. The glass transitions T_g are expressed in ºC with their heat capacities in brackets [J/gºC]. Transition temperatures are expressed in ºC with respect to latent heats ΔH in brackets in [J g^{-1}]. g: glassy state, SmX , non identified smectic mesophase; SmC Smectic C mesophase, I isotropic state.

The soluble content was found to be rather high, ca 50%. Clearly, the synthesis of LCEs with **Mn_{12}Hx2** cross-linker is not optimal, and needs to be improved. Indeed, from previously prepared MC LCE systems having high connectivity cross-linking groups (5 and 6), we have shown that the full crosslinking process efficiency led to moderate to high soluble contents as well as a relatively low stretching capability.[103]

XRD studies were performed on the bulk elastomer (figure 5.4). The results are summarized in table 5.3. A SmC mesophase was unequivocally determined, demonstrating that the insertion of the polyoxometallic cages in the elastomeric matrix did not alter the mesomorphic properties.

Figure 5.4. XRD pattern of elastomer **EN2TMn12(b)** at 25ºC.

Table 5.3. XRD data of elastomer **EN2TMn12(b)** at 25ºC (SmC).

Elastomer	d_l (Å)	ϕ(º)	ξ (nm)	n	d_m(Å)	Order Parameter (S)
EN2TMn12(b)	27.3	N.D.	27	10	4.4	N.D.

d_l: layer spacing; d_m: lateral spacing of the monomers ϕ: tilt angle, ξ**:** the correlation length; n: number of correlated layers; **S**: order parameter. N.D.: not determined.

The characterization of the magnetic behavior revealed the complete loss of the magnetic properties. This could be attributed to the deformation of the coordination sphere of the peripheral Mn^{III} ions of the cluster due to the application of a mechanical force during the curing process. This deformation is detrimental to the magnetic behavior. In order to prove if this hypotesis is correct, further XMCD studies should be performed in order to observe the eventual deformation of the equatorial **Mn_{12}Hx2** of the crosslinker crown. The other explanation could be caused by the low concentration of **Mn_{12}Hx2** in the network, rendering the behavior undetectable by the SQUID magnetometry.

The previous hypoteses would also indicate that a careful selective design of the crosslinker should be considered in order to let equatorial crown of Mn12 intact during the curing process. Selective functionalization of Mn12 molecule may solve this problem, by letting the ligands and Mn^{III} atoms in the same configuration during the polymerization.

5.3. Polydomain Liquid Crystalline Elastomers containing ferrite nanocrystals derivatives.

Nanoparticles exhibit unique properties mainly due to their high surface to volume ratio and quantum size effects. They possess indeed physico-chemical properties (electronic, magnetic, optic …) which are neither those of the bulk material, nor of the single molecular material. Nowadays, they are considered as building blocks for future nanotechnological devices and the development of strategies for processing nanoparticles into thin films or into 3D architectures has become a challenge. In particular, magnetic nanoparticles[179] are interesting for their promising potential applications in catalysis,[180] as magnetic fluids,[179] in data storage and information transport,[179] and in biology[181] where they are already used as contrast agents in RMI or for cancer treatment by hyperthermia.

---

[179] Lu, A.-H., Salabas, E. L., Schüth, F., *Angew. Chem. Intl. Ed.,* **2007**, 46, 1222; Hyeon, T., *Chem. Commun.* **2003**, 927.
[180] a) Lu, A. H., Schmidt, W., Matoussevitch, N., Bönnemann, H., Spielhoff, B., Tesche, B., Bill, E., Kiefer, W., Schüth, F., *Angew. Chem. Intl. Ed.,* **2004**, 43, 4303; b) Tsang, S. C., Caps, V., Paraskevas, I., Chadwick, D., Thompset, D., *Angew. Chem. Intl. Ed.,* **2004**, 43, 5645.
[181] Kumar-Gupta, A., Gupta, M., *Biomaterials,* **2005**, 26, 3995; Mornet, S., Vasseur, S., Grasset, F., Veverka, P., Gioglio, G., Demourgues, A., Portier, J., Pollert, E., Duguet, E., *Prog. Solid State Chem.* **2006**, 34, 237; Li Z., Wei, L., Gao, M. Y., Lei, H., *Adv. Mater.,* **2005**, 17, 1001.

It has been recently reported by Song *et. al* that a side chain LCE containing dopamine-functionalized ferrite nanocrystals (with an average diameter of 6 nm) within its structure exhibits magnetic as well as mesomorphic properties.[157] According to the authors, the composite displays a mesophase between 1.5 and 70.6° C, and is superparamagnetic at *c.a*. room temperature, and ferromagnetic below. Moreover, the system behaved as a transparent gel matrix with suspended nanocrystals which were covalently linked within the structure. Motivated by these exciting results, but also by some interesting studies about LCEs reprocessed with carbon nanostructures,[159] we moved onto the synthesis of MC-LCEs homologous systems, with solely ferrite nanoparticles as crosslinkers. The choice of MC systems was preferred as known to suffer larger deformations at the transition to the isotropic liquid than their SC homologues.

Using and adapting the method developed by Hyeon *et al.,*[182] which consists of the thermal decomposition of iron oleate precursor in high boiling solvent, monodisperse ferrite nanoparticles with an average diameter of ca 3 nm were obtained. TEM observations of nanocrystals in suspension (dichloromethane) reveal nanocrystals with polyhedral shape, and with a rather narrow particle size distribution (σ = 23%; $\sigma/<D>$=7%) (Figure 5.5).

[182] Park, J., An, K., Hwang, Y., Park, J.-G., Noh, H.,-N., Kim, J.-Y., Park, J.-H., Hwang, N.,-M., Hyeon, T., *Nature Mater.* **2004**, 3, 891.

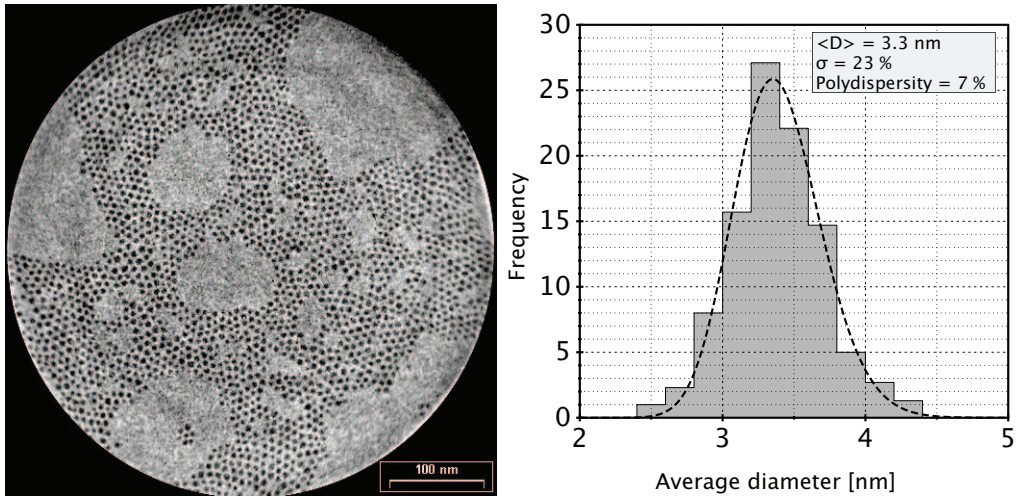

Figure 5.5. Left: micrography of ferrite nanoparticles. Right: size distribution plot.

The outer shell of such particles consisted of oleate moieties, which were readily substituted with carboxylic acid **Hx2** to give the corresponding terminal olefin functionalized nanoparticles after preparative GPC purification, presenting about 40 functional groups as estimated from the effective surface (Scheme 5.4).

The spin casting technique used for the monodomain MC LCEs cannot be employed in this case due to the large molecular weight difference between the polymer components and the nanoparticles, causing the deposition of the nanoparticles in the bottom of the cell, avoiding the crosslinking of small oligomers formed in the solution. This inconvenient limited the synthesis to bulk synthesis experiment. Thus a mixture made of **N2** (390 mg) **HMTS** (208 mg), and functionalized nanoparticles (10 mg) was stirred in 1 mL of toluene in a 3 mL vial, and heated to 40ºC (scheme 5.4). The addition reaction was activated by the Karstedt catalyst (2%), yielding a brownish gel after 24 h (figure 5.6). The gel was washed thoroughly with cyclohexane (immersed for 72h in order to remove small-size unreacted oligomers and unbound polymers), and washed with water, and dried. Since the nanoparticle is the only

crosslinker present, we can conclude that the final material is a hybrid rubber that behaves like a polydomain MC LCE.

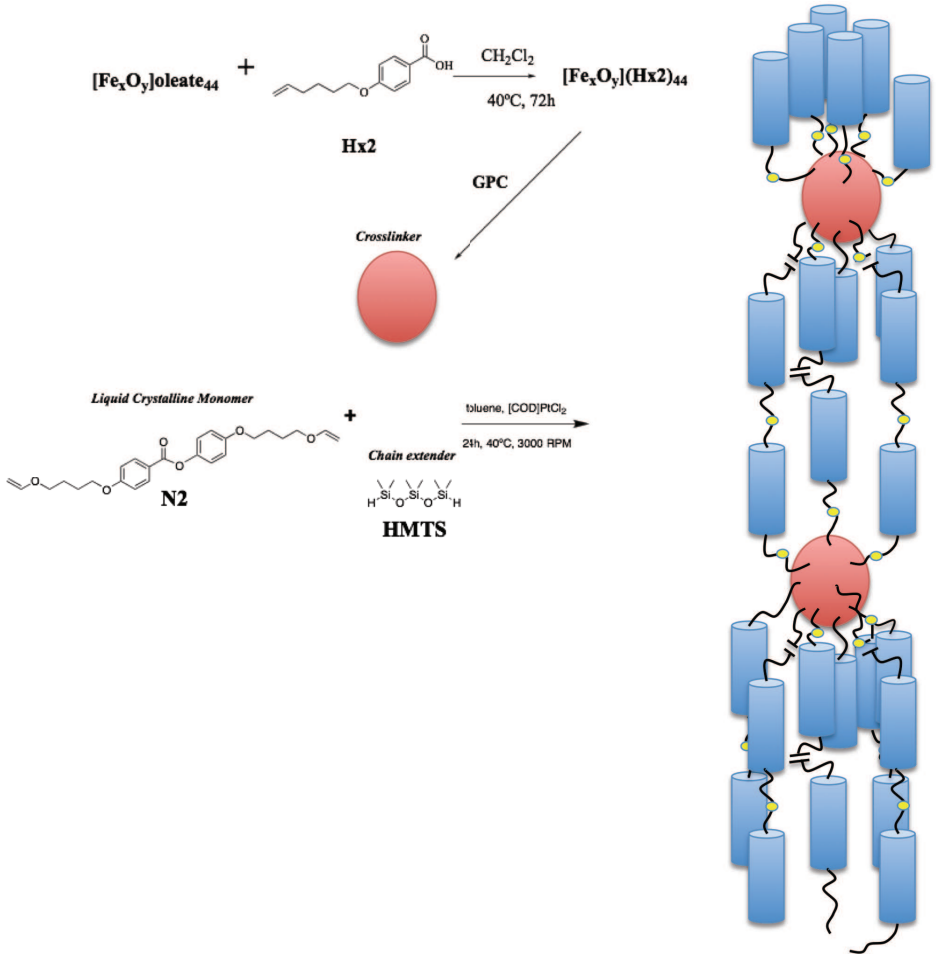

Scheme 5.4. Schematic representation of functionalized ferrite nanoparticles and hybrid elastomer synthesis

Figure 5.6. Ferrite crosslinked MC-LCE before soluble content extraction.

DSC traces show two sharp endotherms, at *c.a.* 20 and 40°C (Scheme 5.5, table 5.5). The first transition was later assigned by XRD to a higher order smectic-smectic C phase transition, whereas the second one corresponded to the transition to the isotropic rubber. The thermal behavior of the ferrite-containing LCE is similar to that of the **EN2T** elastomer, evidencing that the macroscopic nature of the gel remained unchanged by the insertion hybrid component within the network.

Table 5.4.DSC data for ferrite crosslinked liquid crystalline elastomer

Elastomer	**Thermal Behavior**[a]
EN2FeNP3	g (n.d.) SmX 16.5[8.75] SmC 34.3 [10.5] I

The glass transitions T_g are expressed in ºC with their heat capacities in brackets [J/gºC]. Transition temperatures are expressed in ºC with the corresponding latent heats ΔH in brackets in [J g^{-1}]. Temperatures were estimated as the average of heating and cooling maxima of the 2 cycles with a rate of 2ºC/min. g: glassy state, SmX unidentified smectic phase; SmC smectic C mesophase. I isotropic state.

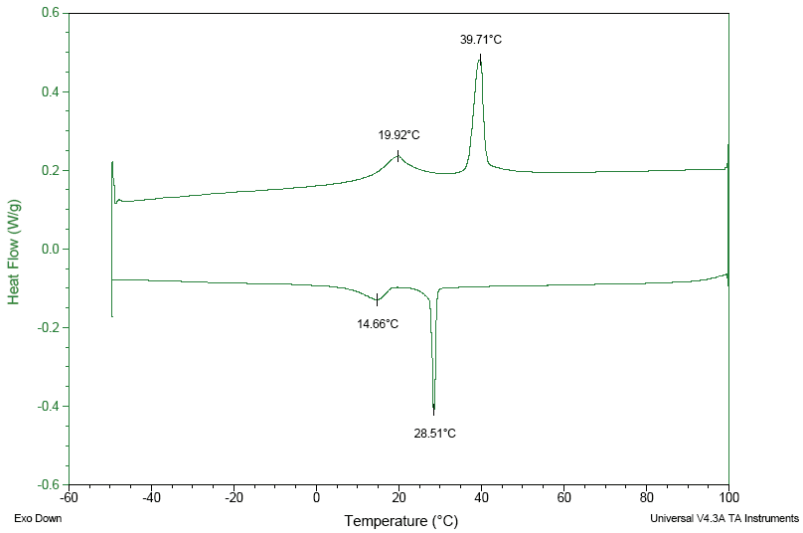

Scheme 5.5. DSC traces of the ferrite elastomer.

X-ray studies were performed on the sample to confirm the nature of the mesophase. In order to obtain reliable and reproducible results, two different XRD studies were accomplished: the first one on the bulk sample, and the second one on a sheared

sample. The shearing process employed is the same as the one previously reported for the polymers and copolymers (Section 3.3.1).

The smectic mesophase nature was deduced from XRD experiments, carried out at 25°C: the observation of a fine ring in the small angle region, corresponding to the layering of the structure, as well as a wide halo at wide angle region, assigned to the mesogen lateral distance. These data indicated the absence of ordered domains in the network confirming the previously predicted polydomain. As for the sheared sample, two fine signals parallel to the sample director present three different harmonics corresponding to a layered structure. Wide angle region exhibited four reflections shifted by 45º with respect to cardinal points (Figure 5.7). This pattern indicates that the sheared network mesogens were aligned but the aliphatic chains were tilted in average with respect to the plane normal, justifying the mesophase determination of a smectic C.[102] Layer periodicity and mesogen lateral distance are reported in table 5.5.

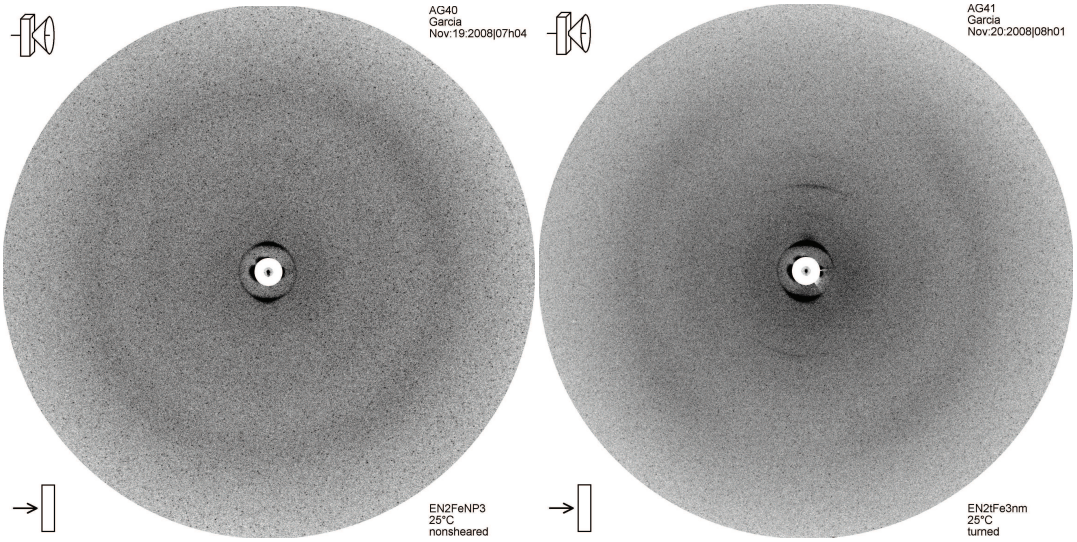

Figure 5.7. XRD patterns of polydomain (left) and sheared (right) elastomer **EN2TFeNP3**.

Table 5.5. XRD data for sheared elastomer **EN2TFeNP3**.

Elastomer	d_l(Å)	*Plane*	ϕ(º)	ξ *(nm)*	*n*	d_m(Å)	Order Parameter (S)
EN2TFeNP3	26.9 13.6 9.0	[001] [002] [003]	45*	30.2	11	4.4	N.D.

d_l: layer spacing; d_m: lateral spacing of the monomers ϕ: tilt angle, ξ**:** the correlation length; ***n***: number of correlated layers. N.D.: not determined; *determined by wide-angle.

The magnetic properties were studied by SQUID. In-phase and out-of-phase component plots (plots 5.3a and b) show a single peak that is shifted to higher temperatures as the field oscillation frequency is increased. As for the Mn12 systems, it was possible to determine energy barrier of activation and Arrhenius parameter giving values for Δ and τ_0 of 206 K and 8.8×10^{-12} s, respectively (red line of plot 5.3 c) The magnetization curve recorded at 1.5 K (plot 5.III d) did not show very small hysteresis, confirming that the material exhibits simple superparamagnetic behavior.

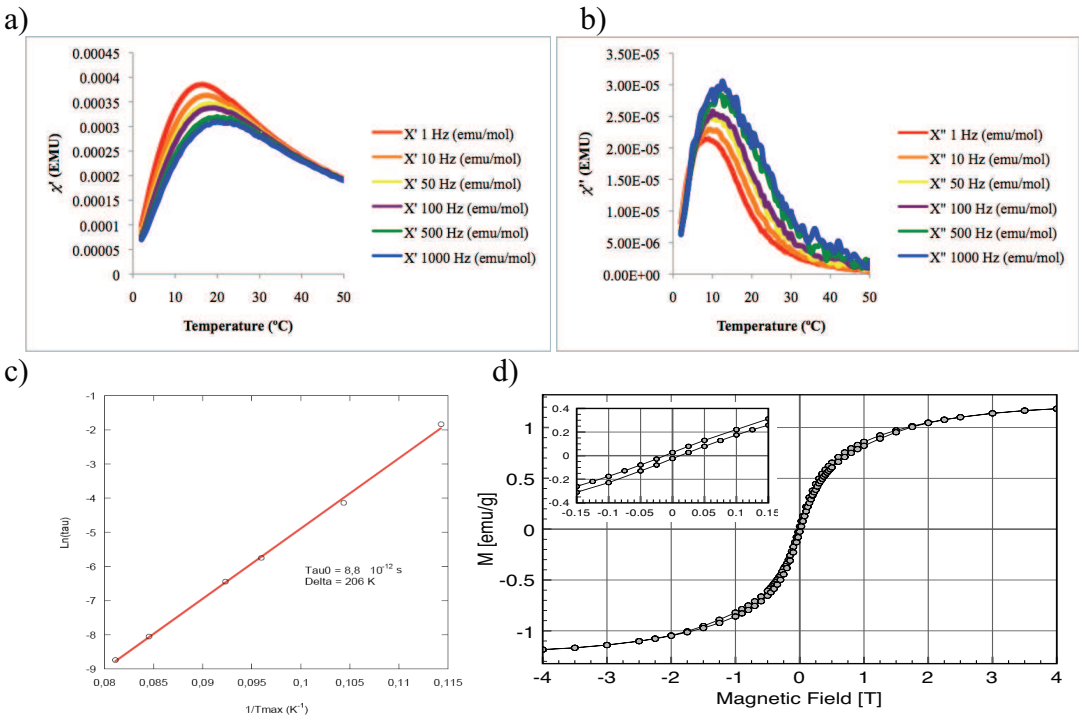

Plot 5.II. Magnetization curves for ferrite crosslinked LCE.

This behavior has already been reported for analogous polymeric systems synthesized by De Palma *et al*.[183] Nevertheless this is the first step of the preparation of a whole new series of magnetic-liquid crystalline actuators, whose development will consist in the procedure improvement to obtain a base ordered film, a degree of crosslinking, until the point of particle-particle interaction, and a polymeric network design capable to hold the system allowing a homogeneous magnetic network.

Rheology studies of such systems could maybe show, the influence of a magnetic dependence of viscoelastic properties and anisotropy of the system, as previously studied by Auernhammer in totally isotropic polymeric systems with magnetite particles. [160,161] Such experiments are still in progress.

[183] De Palma, R., Peeters, S., Van Bael, M. J., Van den Rul, H., Bonroy, K., Laureyn, W., Mullens, J., Borghs, G., Maes, G., *Chem. Mater.*, **2007**, 19, 1821.

5.4. Conclusions.

Two novel types of magnetic networks have been synthesized by hydrosilylation reactions, yielding in both cases to remarkable properties: An optically anisotropic SMM derivative randomly oriented network preserves the original properties of the single molecule mangets; and a simple superparamagnetic polydomain LCE in which the only crosslinker agent is a terminal olefin functionalized ferrite nanocrystal derivative.

The sensitivity of the Mn12 core to mechanical stress and the very low blocking and decomposition temperatures will probably prevent any application of such a material. On the other hand the magnetic elastomer based on ferrite nanoparticles could probably find an intresting use once improved.

Chapter 6

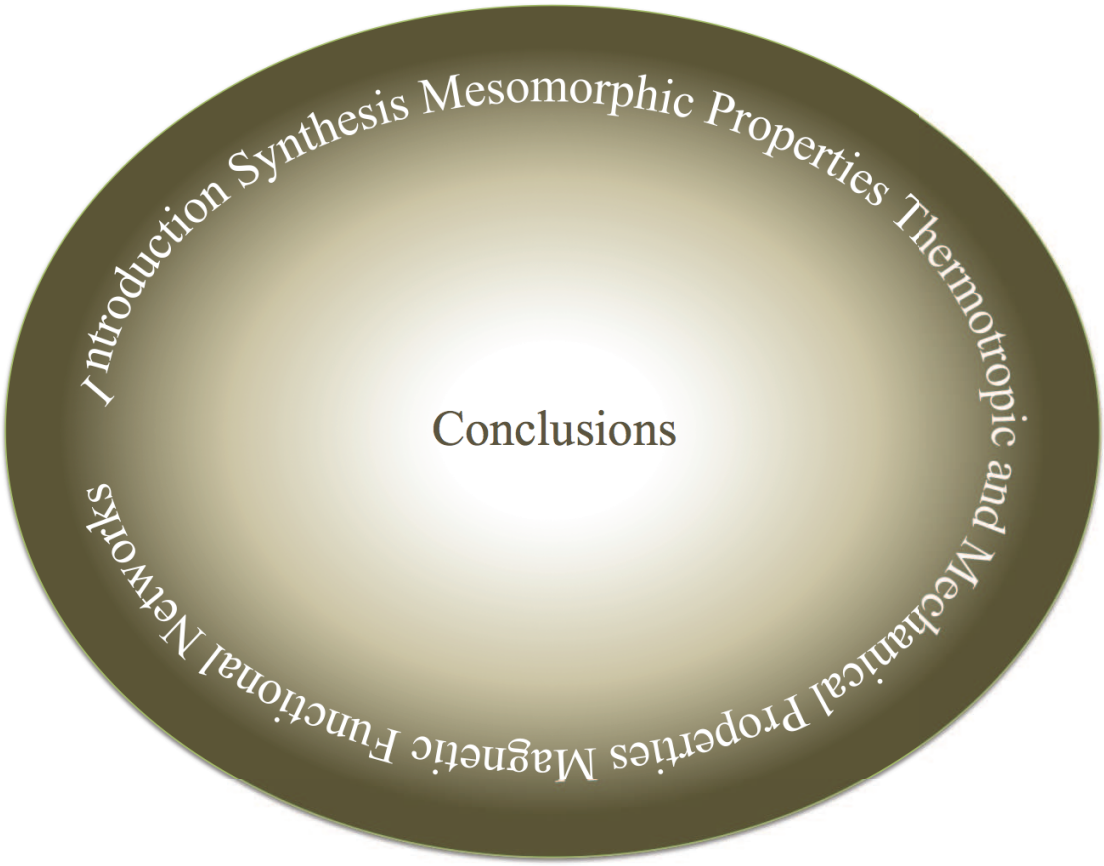

Conclusions and Perspectives

6. Conclusions and Perspectives.

The main objectives of the thesis was firstly the design of new main-chain liquid crystalline co-elastomers constituted by pairs of mesogenic monomers in various proportions, and secondly to study the mesomorphism and the mechanical behavior of the final rubbers as a function of the constitutive components. This study aimed in particular at defining basic relationships between the structure of the molecular ingredients and the physico-chemical activity in order to design systems with desired properties for various actuating applications (temperature-electric field, temperature-magnetic field activation). The versatility of the synthetic approach, based on the one-pot method,[80] has allowed us to perform an original study and to synthesize families of elastomers in which the mesomorphic monomer ratio, the structure of the mesogens, the length of the oligosiloxane spacers and the crosslinker could be easily and systematically varied. One important goal was to produce LCEs having accessible transition temperatures, i.e. isotropization temperature below 100°C, and preferably exhibiting a nematic phase.

The one-pot method, which consists in mixing in the same pot, the mesogenic monomer (here a mixture of two monomers), the siloxane spacer (trisiloxane, **HMTS**, or disiloxane, **TMDS**) and the cross-linker, has been improved (purity of the monomers, reaction conditions) and led to good polymerization indices in the case of polymers and copolymers and fair to low soluble contents in the case of elastomers and coelastomers.

Three novel series of LC coelastomers (MC LCCoEs), along their precursory mesogenic monomers and the related linear polymers and copolymers have been

synthesized and thoroughly characterized. Note that for all elastomers, the cross-linking density was kept identical throughout, and lower than 5%. In the first two series of MC LCCoEs, we varied the proportion of two calamitic mesogenic monomers, **N1** and **N2**, within the mixture, **N1** showing a sole nematic phase, though at high temperature, and **N2**, a SmC phase at room temperature. Coelastomers based on the **HMTS** spacer yielded solely a SmC phase, with low isotropization temperature. On the other hand, **TMDS**-based coelastomers yielded SmC and N phase, below 100°C. In general, it was found that the monomer proportion permitted the control of the clearing temperatures in the case of the **HMTS** series, as well as modifying the temperature range of the nematic mesophase in the **TMDS** analogues.

The last series of coelastomers was prepared with mixtures of bent-core molecules and either **N1** and **N2**. Strong network perturbations resulting from the insertion of such molecules as well as kinetically dependent mesophases could be observed in these systems. The preliminary studies of bent-core systems are very promising and tend towards the development of electrically activated systems (ferroelectric phases and/or biaxial nematic phase). The field remains opened to a huge series of studies in order to see more specifically at which point the nature network can be disturbed (collapsing effect; MCMA) by a non mesogenic bent-core monomer, or enhanced (synergic effect) by employing as co-monomer a mesogenic monomer (*i.e.* **B3**).

Some coelastomers were selected as representative case studies to carry out mechanical and thermoelastic measurements. Experiments performed on films allowed to analyze the viscoelastic behavior under uniaxial stress as well as to determine the expansion coefficient and elongation capability, being in the best case as large as 280%. It was also observed that the mechanical behavior was marginally

affected by the nature of the components (mesogens, spacer, proportion). However, since such studies are long and require a considerable amount of samples, only some available results have been presented. Consequently, at this stage it appears to ambitious to draw some conclusions and observe trends of the mechanical behavior of these MC LCCoEs.

A last exploration of the topic led us to synthesize and study hybrid liquid crystalline networks in which the cross-linker is a superparamagnetic polymetallic cluster or ferromagnetic ferrite nanoparticle, bearing at most 16 and 43 coordinating sites. This preliminary study proved that it is possible to prepare magnetic LC networks, although the presence of the mesomorphism and the magnetic properties are strongly dependent on the system composition. Nevertheless, a novel and exciting area is opened and should lead to an intense activity towards magnetically activated actuators.

Chapter 7

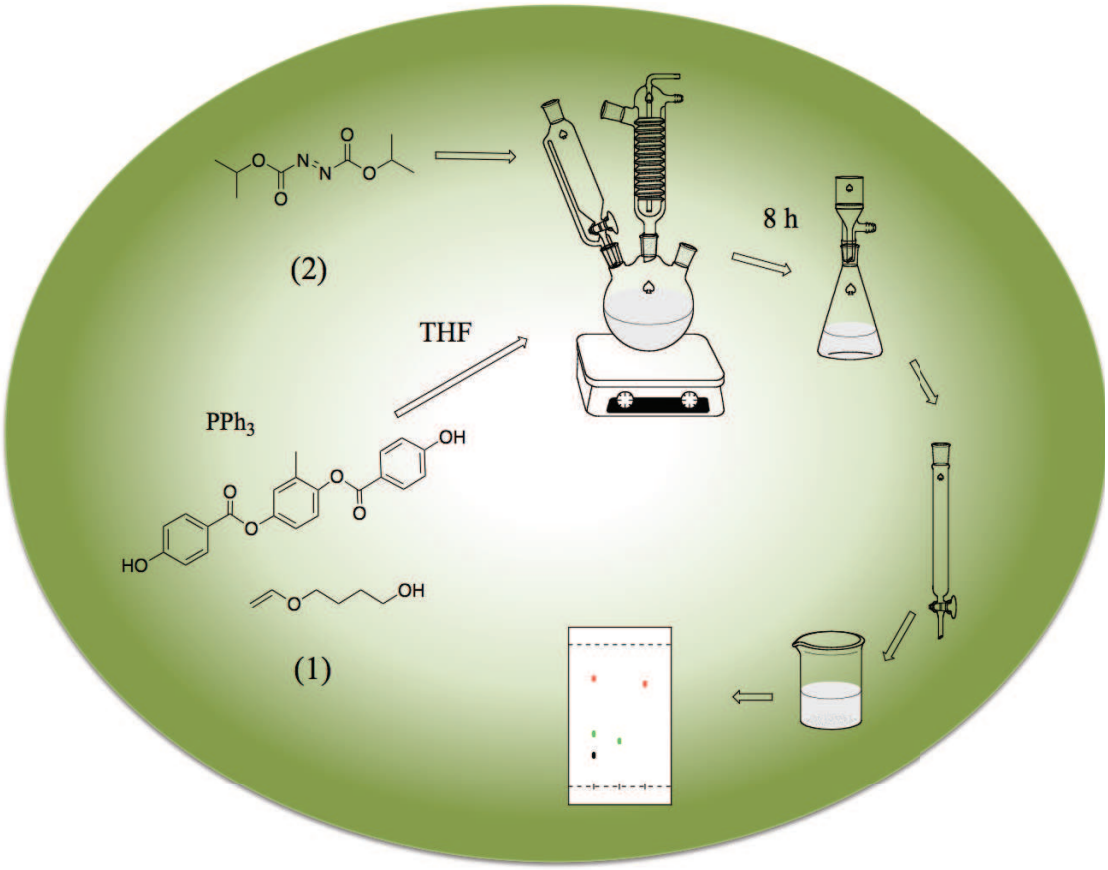

Experimental

7. Experimental.

2-Methyl-1,4-phenylene bis(4-(benzyloxy)benzoate) **(1)**

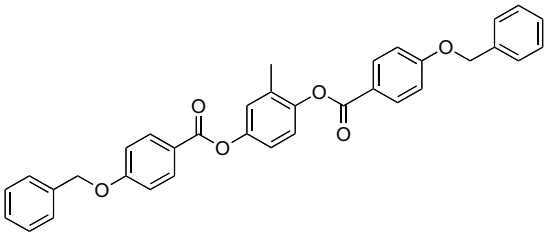

In a 500 mL three-necked, round-bottom flask, 6.00 g (26.3 mmol) of 4-benzyloxybenzoic acid, 1.65 g (13.3 mmol) of 4-hydroxy-2-methylphenol (methylhydroquinone) and 0.43 g (3.5 mmol) of 4-(*N,N*-dimethylamino)pirydine (DMAP) were added, dried in vaccuo with a heating gun and then dissolved in 100 mL of dry dichloromethane. Argon was added and the emulsion cooled to 0º C. 7.30 g (38.1 mmol) of 1-ethyl-3-(3-dimethylaminopropyl)carbodiimide hydrochloride (EDCI) were added and the reaction mixture was magnetically stirred for 5h. The resulting solution was extracted with brine (2x 500 mL) and the organic phase was then recovered and concentrated in vaccuo. The residue was purified by chromatography column (SiO_2, dichloromethane) to obtain 5.80 g of a white solid (67 %).

^{1}H-RMN (300 MHz, $CDCl_3$) δ (ppm): 2.26 (3H, s, CH_3), 5.19 (4H, s, $BnCH_2O$), 7.08 (2H, d, ^{HH}J=8.8 Hz, *m*-Ar'' [a]), 7.10 (2H, d, ^{HH}J=9.0 Hz, *m*-Ar' [a]), 7.19 (3H, m, Ar [a]), 7.47 (10H, m, Ph-H), 8.18 (2H, d, ^{HH}J=7.9 Hz, *o*-Ar''), 8.21 (2H, d,^{HH}J=8.5 Hz, *o*-Ar').

2-Methyl-1,4-phenylene bis(4-hydroxybenzoate) **(2)**

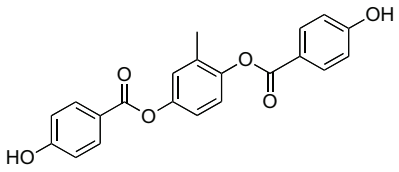

In a 500 mL two-necked, round-bottom flask, 4.50 g (8.26 mmol) of **1** were dissolved

[a] Both Ar' and Ar'' rings are unequivalent due to the methyl substituent in the central ring (Ar), which reduces the overall-symmetry of the molecule.

in 250 mL of dry tetrahydrofuran (THF) and the solution flushed with argon. 25 mg of palladium in charcoal (10%) were slightly added and placed in a specially designed hydrogenation system. The mixture was stirred at room temperature until the starting product was consummed. The black suspension was filtered on Celite ® and the solvent evaporated in vaccuo to give 2.88 g of a white solid (96 %).

^{1}H-RMN (300 MHz, $(CD_3)_2CO$) δ (ppm): 2.22 (3H, s, CH_3), 6.99 (2H, d, ^{HH}J=8.6, *m*-Ar''), 7.01 (2H, d, ^{HH}J=8.6 Hz, *m*-Ar'), 7.18 (3H, m, Ar), 8.05 (2H, d, ^{HH}J=8.5 Hz, *o*-Ar''), 8.08 (2H, d, ^{HH}J=8.5 Hz, *o*-Ar').

4-(Benzyloxy)phenyl 4-(benzyloxy)benzoate **(3)**

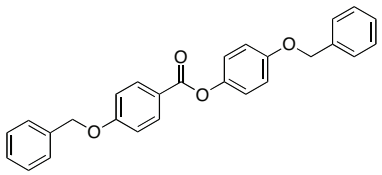

In a three-necked, round-bottom flask, 5.75 g (24.4 mmol) of 4-benzyloxybenzoic acid, 4.89 g (24.4 mmol) of 4-benzyloxyphenol and 0.36 g de DMAP were dried in vaccuo with a heating gun and then dissolved in 100 mL of dry dichloromethane. Argon was added and the emulsion cooled to 0ºC. 5.61 g (29.3 mmol) of EDCI were added and the reaction mixture was magnetically stirred for 18h. The resulting solution was extracted with brine (2x 200 mL). The organic phase was then recovered and concentrated in vaccuo. The residue was purified by chromatography column (SiO_2, dichloromethane) to give 8.28 g of a white solid (83 %).

^{1}H-NMR (300 MHz, $CDCl_3$): δ (ppm): 5.07 (2H, s, PhC$\underline{H}_2$), 5.17 (2H, s, PhC$\underline{H}_2$), 7.00 (2H, d, ^{HH}J=8.5 Hz, *m*-Ar), 7.05 (2H, d, ^{HH}J=8.9 Hz, *m*-Ar'), 7.12 (2H, d, ^{HH}J=8.9 Hz, *o*-Ar), 7.39 (10H, m, $\underline{Ar}CH_2$), 8.15 (2H, d, ^{HH}J=8.5 Hz, *o*-Ar').

4-Hydroxyphenyl 4-hydroxybenzoate **(4)**

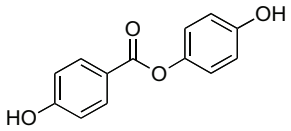

In a 500 mL two-necked, round-bottom flask, 7.50 g (18.3 mmol) of **3** were dissolved in 250 mL of dry THF and the solution flushed with argon. 100 mg of palladium in charcoal (10%) were slightly added and placed in a specially designed hydrogenation system. The mixture was stirred at room temperature until the starting product was consummed. The black suspension was filtered on Celite ® and the solvent evaporated in vaccuo to obtain 4.2 g of a white solid (99 %).

^{1}H-NMR (300 MHz, $(CD_3)_2CO$): δ (ppm): 6.93 (2H, d, ^{HH}J=8.5 Hz, *m*-Ar), 7.07 (2H, d, ^{HH}J=8.9 Hz, *m*-Ar'), 7.23 (2H, d, ^{HH}J=8.9 Hz, *o*-Ar'), 7.95 (2H, s, OH), 8.03 (2H, d, ^{HH}J=8.5 Hz, *o*-Ar).

Monomer **N1**.

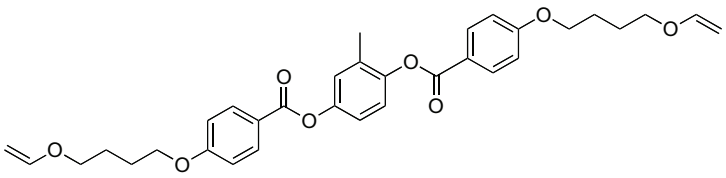

In a three-necked, round-bottom flask, 2.78 g (7.63 mmol) of 4-hydroxyphenoyl 4-hydroxybenzoate **2** and 4.80 g (18.3 mmol) of triphenylphosphine (PPh_3) were added. An argon flush was performed and the solids were dissolved in 150 mL of anhydrous THF. The mixture was stirred and cooled down to 0ºC. Then 2.27 mL (18.3 mmol) of 4-vinyloxybutanol were added followed by 3.34 mL (16.0 mmol) of diisopropylazodicarboxylate (DIAD), added dropwise. The reaction mixture was kept at 0ºC for 1 h and left to warm up to room temperature for 8 h. The resulting solution was concentrated to dryness and redissolved in a minimum quantity of a mixture of dichloromethane-cyclohexane (1:3) and purified by chromatography column (triethylamine-neutralized SiO_2, dichloromethane-cyclohexane (1:3)). The crude product was dried and crystallized from anhydrous methanol (white crystals 3.3 g, 77 %).

Elemental analysis for $C_{33}H_{36}O_8$: Calcd: C% 70.70, H% 6.47; Found: C% 71.19, H% 6.34.

^{1}H-RMN (300 MHz, $CDCl_3$) δ (ppm): 1.91 (8H, m, C$\underline{H_2}$-CH_2O), 2.25 (3H, s, CH_3), 3.78 (4H, t, ^3J=5.9 Hz, CH_2O), 4.02 (2H, dd, ^{2gem}J=2.0 Hz; ^{3cis}J=6.0 Hz, C$\underline{H_2}$=CH-O), 4.11 (4H, t, ^3J=4.6 Hz, CH_2-O), 4.21 (2H, dd, ^{2gem}J=2.0 Hz; $^{3trans}J$=12.0 Hz, C$\underline{H_2}$=CH-O), 6.50 (2H, dd, ^{3cis}J=6.8 Hz; $^{3trans}J$=7.4 Hz, CH_2=C$\underline{H}$-O), 6.98 (2H, d, ^2J=6.8 Hz, *m*-Ar''), 6.99 (2H, d, ^{HH}J=6.8 Hz, *m*-Ar'), 7.11 (3H, m, Ar), 8.14 (2H, d, ^{HH}J=7.8 Hz, *o*-Ar''), 8.17 (2H, d, ^{HH}J=7.9 Hz, *o*-Ar').

^{13}C-NMR (75 MHz, $CDCl_3$) δ (ppm): 16.4 (CH_3), 22.0 (CH_2), 25.6 (CH_2), 25.8 (CH_2), 67.4 ($\underline{C}H_2OCH=CH_2$), 67.5 ($\underline{C}H_2OCH=CH_2$), 67.7 (CH_2OAr''), 67.8

(CH_2OAr'), 86.4 ($CH=\underline{C}H_2$), 114.2 (*m*-ArH), 120.0 (*o*-Ar'H), 121.5 (Ar''$_{ipso}$COO), 121.8 (Ar'$_{ipso}$COO), 122.5 (2C, *o'*-Ar''H), 131.7 ($Ar_{ipso}CH_3$) 132.2 (*o*-ArH), 147.0 (Ar'$_{ipso}$OCO), 148.4 (Ar''$_{ipso2}$OCO), 151.8 ($\underline{C}H=CH_2$), 163.3 ($ArOCH_2$), 164.5 (Ar''$\underline{C}$OOAr), 164.9 (Ar'$\underline{C}$OOAr).

Monomer **N2**.

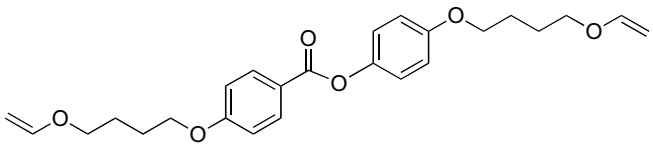

In a three-necked, round-bottom flask, 4.00 g (17.4 mmol) of di-4-hydroxyphenoyl 4-hydroxybenzoate **(4)** and 10.94 g (41.7 mmol) of PPh_3 were added. An argon flush was performed and the solids were dissolved in 150 mL of anhydrous THF. The mixture was stirred and cooled down to 0ºC. Then 5.16 mL (41.7 mmol) of 4-vinyloxybutanol were added, immediately followed by 7.61 mL (36.5 mmol) of DIAD added dropwise. The reaction mixture was kept to 0ºC for 1 h and left to warm up to room temperature for 8 h. The resulting solution was concentrated to dryness and redissolved in a minimum quantity of a mixture of dichloromethane-cyclohexane (1:3) and purified by chromatography (triethylamine-neutralized SiO_2, dichloromethane-cyclohexane (1:3)). The fractions were collected and the solid obtained was finally crystallized from anhydrous methanol to give white crystals, 5.88 g (79 %).

Elemental analysis for $C_{25}H_{30}O_6$: Calcd: C% 70.40, H% 7.09; Found: C% 70.42, H% 6.91.

^{1}H-RMN (300 MHz, $CDCl_3$), δ (ppm): 1.88 (8H, m, C$\underline{H}_2$-CH_2O), 3.77 (4H, t, ^3J=5.9 Hz, CH_2O), 4.02 (2H, dd, ^{2gem}J=2.0 Hz; ^{3cis}J=6.0 Hz, C$\underline{H}_2$=CH-O), 4.10 (4H, t, ^3J=6.1 Hz, CH_2OAr), 4.20 (2H, dd, ^{2gem}J=1.3 Hz; $^{3trans}J$=14.5 Hz, C$\underline{H}_2$=CH-O), 6.50 (2H, dd, ^{3cis}J=6.8 Hz; $^{3trans}J$=14.3 Hz, CH_2=C$\underline{H}$-O), 6.92 (2H, d, ^{HH}J=6.8 Hz, *m*-Ar), 6.99 (2H, d, ^{HH}J=6.8 Hz, *o*-Ar), 8.14 (2H, d, ^{HH}J=7.8 Hz, *m*-Ar'), 8.17 (2H, d, ^{HH}J=7.9 Hz, *o*-Ar').

^{13}C-NMR (75 MHz, $CDCl_3$) δ (ppm): 25.6 (CH_2), 25.7 (CH_2), 25.8 (CH_2), 25.9 (CH_2), 67.4 ($\underline{C}H_2$OCH=CH_2), 67.5 ($\underline{C}H_2$OCH=CH_2), 67.7 (CH_2OAr'), 67.8 (CH_2OAr), 86.4 (CH=$\underline{C}H_2$), 86.5 (CH=$\underline{C}H_2$), 114.2 (*m*-ArH), 115.0 (*m*-Ar'H), 121.8

(ArCOO), 122.5 (*o*-Ar'H), 132.2 (*o*-ArH), 144.4 (Ar'OCO), 151.8 (<u>C</u>H=CH_2), 156.6 (Ar'OCH_2), 163.2 (ArOCH_2), 165.2 (COOAr).

Methyl 4-undecenyloxybenzoate **(Ud 1)**

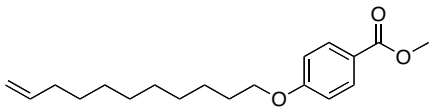

In a 500 mL round-bottom flask, 10.00 g (65.7 mmol) of methyl 4-hydroxybenzoate, 22.41 g (85.4 mmol) of PPh_3 and 13.43 g (78.9 mmol) of undecenol were dissolved in 250 mL of anhydrous THF. The mixture was magnetically stirred and cooled down to 0º C for 15 minutes and then 14.6 mL (65.7 mmol) of DIAD were added dropwise. After the addition, the mixture was left to react for 12h. The solvent was dried and the remaining solid was purified by column chromatography (SiO_2, dichloromethane-cyclohexane (60:40)) (white crystals, 15.2 g, 76 %).

^{1}H-RMN (300 MHz, $CDCl_3$) δ (ppm): 1.31 (12H, m, CH_2), 1.80 (2H, m, ^3J=6.3 Hz, CH_2), 2.04 (2H, q, ^3J=6.2 Hz, CH_2) 3.89 (3H, s, CH_3O), 4.00 (2H, t, ^3J=6.4 Hz, CH_2O) 4.96 (2H, m, $C\underline{H_2}$=CH), 5.82 (1H, m, CH_2=C$\underline{H}$), 6.90 (2H, d, ^{HH}J=8.8 Hz, *m*-Ar), 7.98 (2H, d,^{HH}J=8.8 Hz, *o*-Ar).

4-Undecenylbenzoic acid **(Ud 2)**

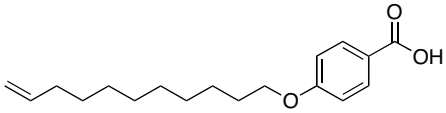

In a 500 mL round-bottom flask, 10.4 g (34.1 mmol) of **Ud 1** were dissolved in 300 mL of ethanol. After total solubilization, 2.7 g (48.1 mmol) of potassium hydroxide dissolved in 40 mL of water were added. The reaction mixture was set at reflux for 15 h. After reaction completion, the solvent was evaporated and the remaining solid redissolved in 500 mL of water. The resulting solution was acidified until reaching pH=2 to obtain a white solid which was filtered and then crystallized in methanol (7.80 g, 79%).

^{1}H-RMN (300 MHz, $CDCl_3$) δ (ppm): 1.35 (12H, m, CH_2), 1.80 (2H, m, ^3J=6.3 Hz, CH_2), 2.06 (2H, q, ^3J=6.2 Hz, CH_2), 4.02 (2H, t, ^3J=6.2 Hz, CH_2O) 5.03 (2H, m, $C\underline{H_2}$=CH), 5.83 (1H, m, CH_2=C$\underline{H}$), 6.93 (2H, d, ^{HH}J=8.8 Hz, *m*-Ar), 7.94 (2H, d, ^{HH}J=8.8 Hz, *o*-Ar).

Methyl 4-hexenyloxybenzoate **(Hx 1)**

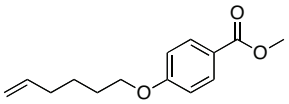

In a 500 mL round-bottom flask, 9.63 g (63.3 mmol) of methyl 4-hydroxybenzoate, 18.36 g (67.3 mmol) of PPh_3 and 6.34 g (63.3 mmol) of 1-hexenol were dissolved in 250 mL of anhydrous THF. The mixture was magnetically stirred and cooled down to a 0ºC for 15 and then 14.9 mL (67.0 mmol) of DIAD were added dropwise. After the addition, the mixture was left to react for 3h. The solvent was dried and the remaining solid was purified by column chromatography (triethylamine-neutralized SiO_2, dichloromethane) to give a white solid which was crystallized from methanol (white crystals, 13.2 g, 89 %).

^{1}H-RMN (300 MHz, $CDCl_3$) δ (ppm): 1.60 (2H, m, CH_2), 1.82 (2H, m, CH_2), 2.14 (2H, m, CH_2) 3.89 (3H, s, CH_3O), 4.02 (2H, t, ^3J=6.5 Hz, CH_2O) 5.03 (2H, m, $C\underline{H_2}$=CH), 5.83 (1H, m, CH_2=C$\underline{H}$), 6.92 (2H, d, ^{HH}J=9.0 Hz, *m*-Ar), 7.99 (2H, d, ^{HH}J=9.0 Hz, *o*-Ar)

4-Hexenylbenzoic acid **(Hx 2)**

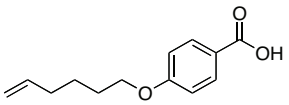

In a 500mL round-bottom flask, 10.9 g (46.5 mmol) of **Hx 1** were dissolved in 300 mL of ethanol, 2.7 g (48.1 mmol) of potassium hydroxide dissolved in 40 mL of water were then added and the reaction mixture was set at reflux for 15 h. After reaction completion, the solvent was evaporated and the remaining solid redissolved in 500 mL of water. The resulting solution was acidified until reaching pH=2 to obtain a white solid, which was filtered, dried and crystallized in ethyl acetate (9.80 g, 96%).

^{1}H-RMN (300 MHz, $CDCl_3$) δ (ppm): 1.60 (2H, m, CH_2), 1.84 (2H, m, CH_2), 2.15 (2H, m, CH_2), 4.05 (2H, t, ^3J=6.5 Hz, CH_2O) 5.03 (2H, m, $C\underline{H_2}$=CH), 5.83 (1H, m, CH_2=C$\underline{H}$), 6.92 (2H, d, ^{HH}J=9.0 Hz, *m*-Ar), 7.99 (2H, d, ^{HH}J=9.0 Hz, *o*-Ar).

1,3-Phenylene bis-(4-benzyloxybenzoate) **(5)**

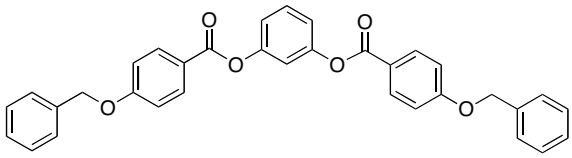

In a three-necked, round-bottom flask, 4.58 g (20.1 mmol) of 4-benzyloxybenzoic acid, 1.10 g (10 mmol) of resorcinol and 0.18 g (0.15 mmol) of DMAP were dried in vaccuo with a heating gun and then dissolved in 200 mL of dry dichloromethane. Argon was added and the emulsion cooled to 0ºC. 4.70 g (24.7 mmol) of EDCI were added and the reaction mixture was stirred for 15h. The resulting solution was extracted with brine (2x 200 mL). The organic phase was then recovered and concentrated in vaccuo. The residue was purified by chromatography column (SiO_2, dichloromethane) to obtain 3.20 g of a white solid (60 %).

^{1}H-NMR (300 MHz, $CDCl_3$): δ (ppm): 5.17 (4H, s, PhC$\underline{H}_2$), 7.06 (4H, d, ^{HH}J=9.0 Hz, *m*-Ar'), 7.14 (3H, m, *o'*-Ar + *m*-Ar), 7.39 (11H, m, $\underline{Ph}CH_2$ + *o*-Ar), 8.15 (4H, d, ^{HH}J=9.0 Hz, *o*-Ar').

1,3-Phenylene bis-(4-hydroxybenzoate) **(6)**

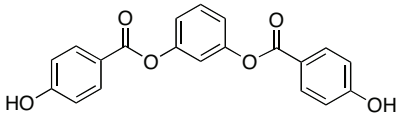

In a 500 mL two-necked, round-bottom flask, with magnetic stirring, 1.25 g (3.57 mmol) of **5** were dissolved in 250 mL of dry THF. The solution was flushed with argon. Palladium in charcoal (10%w, 25 mg) was added carefully and the flask was placed in a specially designed hydrogenation system. The mixture was stirred at room temperature until the starting product was consummed. The black suspension was filtered on Celite ® and the solvent was evaporated in vaccuo to give 0.81 g of a white solid (99 %).

^{1}H-NMR (300 MHz, $CDCl_3$) δ (ppm): 6.99 (4H, d, ^{HH}J=9.0 Hz, *m*-Ar'), 7.17 (1H, s, *o*-Ar), 7.20 (2H, s, *o'*-Ar), 7.51 (1H, t, ^{3}J=8.1 Hz, *m*-Ar), 8.04 (4H, d, ^{HH}J=9.0 Hz, *o*-Ar'), 9.31 (2H, Br, OH).

4,6-Dichloro-1,3-phenylene bis(4-(benzyloxy)benzoate) **(7)**

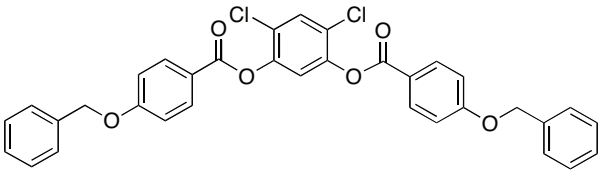

In a three-necked, round-bottom flask, 3.00 g (13.1 mmol) of 4-benzyloxybenzoic acid, 1.06 g (5.92 mmol) of 4,6-dichloro-3-hydroxyphenol, 0.16 g (1.31 mmol) of DMAP and a catalytic amount of 1-Hydroxy-1H-benzotriazole (HOBt) were dried in vaccuo with a heating gun an then dissolved in 100 mL of dry dichloromethane. The emulsion was flushed with argon and cooled to 0º C. Dicyclohexylcarbodiimide (DCC) (3.01 g; 14.5 mmol) was added and the reaction mixture was stirred for 12 h. The resulting solution was extracted with brine (2x 200 mL). The organic phase was then recovered and concentrated in vaccuo. The residue was purified by column chromatography (SiO_2, dichloromethane) to give 2.70 g of a white solid (76 %).

^{1}H-NMR (300 MHz, $CDCl_3$) δ (ppm): 5.18 (4H, s, PhC$\underline{H_2}$), 7.08 (4H, d, ^{HH}J=9.0 Hz, *m*-Ar'), 7.34 (1H, s, *o*-Ar), 7.44 (10H, m, $\underline{Ph}CH_2$), 7.61 (1H, s, *m*-Ar), 8.15 (4H, d, ^{HH}J=9.0 Hz, *o*-Ar').

4,6-Dichloro-1,3-phenylene bis(4-(hydroxy)benzoate) **(8)**

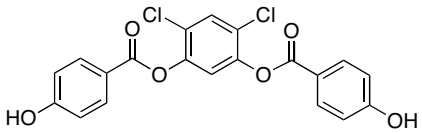

In a 500 mL two-necked, round-bottom flask, 2.50 g of **7** were dissolved in 250 mL of dry THF and the solution flushed with argon. Palladium in charcoal (10%w, 25 mg) was slowly added and the flask placed in a specially designed hydrogenation system. The mixture was stirred at room temperature until the starting product was consummed. The black suspension was filtered on Celite ® and the solvent was evaporated in vaccuo. The residue was purified by chromatography column (THF-cyclohexane 30:70) giving 1.80 g of a white solid (99 %).

^{1}H-NMR (300 MHz, $(CD_3)_2CO$): δ (ppm): 7.02 (4H, d, ^{HH}J=9.0 Hz, *m*-Ar'), 7.59 (1H, s, *o*-Ar), 7.82 (1H, s, *m*-Ar), 8.07 (4H, d, ^{HH}J=9.0 Hz, *o*-Ar').

Di(-4-benzyloxybenzoyl) isophtalate **(9)**

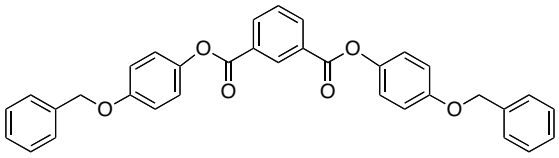

In a three-necked, round-bottom flask, 4.15 g (25.0 mmol) of isophtalic acid, 10.10 g (50.4 mmol) of 4-benzyoxyphenol, 0.61 g (5.0 mmol) of DMAP were dissolved in 200 mL of dry dichloromethane. Argon was added and the emulsion cooled to 0ºC. DCC (10.80 g; 52.3 mmol) was added and the reaction mixture was stirred for 12h. The resulting suspension was filtered and washed with an excess of dichloromethane, the collected fractions were extracted with 10 % HCl (2x 500 mL) and brine (2x 200 mL). The organic fractions were recovered and concentrated in vaccuo. The residue was purified by column chromatography (SiO_2, dichloromethane) to recover 11.90 g of a white solid (90 %).

^{1}H-RMN (300 MHz, $CDCl_3$) δ (ppm): 5.09 (4H, s, CH_2Ph), 7.03 (4H, d, ^{HH}J=9.0 Hz, Ar'), 7.17 (4H, d, ^{HH}J=9.0 Hz, Ar'), 7.44 (10H, m, PhCH$_2$), 7.68 (1H, t, ^3J=6.8 Hz, *m*-Ar), 8.46 (2H, dd, ^3J=7.8 Hz; ^4J=1.6 Hz, *o'*-Ar), 9.00 (1H, s, *o*-Ar).

Bis(4-(hydroxy)phenyl) isophtalate **(10)**

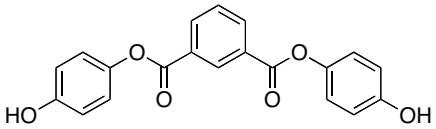

In a 500 mL two-necked, round-bottom flask, 2.01 g (3.79 mmol) **9** were dissolved in 250 mL of dry THF and the solution flushed with argon. Palladium in charcoal (10%w, 25 mg) was carefully added and placed in a specially designed hydrogenation system. The mixture was stirred at room temperature until the starting product was consummed. The black suspension was filtered on Celite ® and the solvent evaporated in vaccuo giving 1.00 g of a white solid (75 %).

^{1}H-RMN (300 MHz, $(CD_3)_2CO$) δ (ppm): 6.89 (4H, d, ^{HH}J=6.8 Hz, *m*-Ar'), 7.13 (4H, d, ^{HH}J=6.8 Hz, *o*-Ar'), 7.80 (1H, t, ^3J=6.8 Hz, *m*-Ar), 8.44 (2H, dd, ^3J=7.8 Hz; ^3J=1.7 Hz, *o'*-Ar), 8.87 (1H, t, ^4J=1.5 Hz, *o*-Ar).

Monomer **B1**

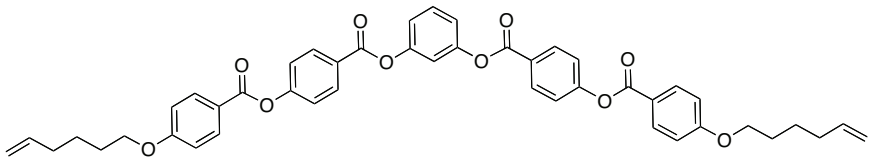

In a 250 mL three-necked, round-bottom flask, 1.05 g (4.76 mmol) of **Hx 2**, 0.72 g. (2.27 mmol) of **6** and 0.05 g (0.41 mmol) of DMAP were dried in vaccuo with a heating gun, then dissolved in 100 mL of dry dichloromethane. The emulsion was argon flushed and cooled down to 0º C. EDCI (1.36 g, 7.14 mmol) was added and the reaction mixture was magnetically stirred for 5h. The resulting solution was extracted with brine (2x 200 mL). The organic phase was then recovered and concentrated in vaccuo. The residue was purified by chromatography column (SiO_2, dichloromethane) to obtain 1.1 g of a white solid (64 %).

Elemental analysis for $C_{46}H_{42}O_{10}$: Calcd: C% 73.20, H% 5.61; Found: C% 72.97, H% 5.35.

^{1}H-RMN (300 MHz, $CDCl_3$) δ (ppm): 1.61 (4H, m, CH_2), 1.87 (4H, m, CH_2), 2.16 (4H, q, ^{3}J=7.2 Hz, -CH_2-C$\underline{H}_2$-CH=CH_2), 4.18 (4H, t, ^{3}J=6.5 Hz, Ar-O-C$\underline{H}_2$), 5.30 (4H, m, CH=C$\underline{H}_2$), 5.85 (2H, m, C$\underline{H}$=CH_2), 7.00 (4H, d, ^{HH}J=9.0 Hz, *m*-Ar''), 7.19 (1H, s, *o*-Ar), 7.22 (2H, s, *o'*-Ar), 7.39 (4H, d, ^{HH}J=8.5 Hz, *m*-Ar'), 7.39 (1H, t, ^{3}J=8.5 Hz, *m*-Ar), 8.17 (4H, d, ^{HH}J=8.9 Hz, *o*-Ar''), 8.29 (4H, d, ^{HH}J=8.9 Hz, *o*-Ar').

^{13}C-RMN (75 MHz, $CHCl_3$) δ (ppm): 25.3 (CH_2), 28,5 (CH_2), 30,3 (CH_2), 33.4 (CH_2), 68.2 (CH_2), 114.4 (Ar), 114.9 (Ar), 119.3 ($\underline{C}H_2$=CH), 121.0 (Ar), 122.2 (CH_2=$\underline{C}$H), 125.5 (Ar), 126.6 (Ar) 131.9 (Ar), 132.4 (Ar), 138.3 (Ar), 151.4 (Ar), 155.5 (ArO), 164.1 (COO), 164.3 (COO).

Monomer **B2**

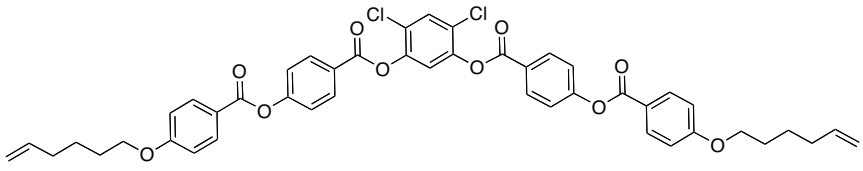

In a three-necked, round-bottom flask, 1.39 g (6.31 mmol) of **Hx 2**, 1.26 g (3.01 mmol) of **8** and 0.07 g (0.60 mmol) of DMAP were dried in vaccuo with a heating gun, then dissolved in 100 mL of dry dichloromethane and 2 mL of dimethylformamide (DMF). Argon was added and the emulsion was flushed with argon and cooled down to 0º C. DCC (1.55 g, 7.51 mmol) was readily added and the reaction mixture was magnetically stirred overnight. The resulting suspension was extracted with brine (2x 200 mL). The organic phase was then recovered and concentrated in vaccuo. The residue was purified by chromatography column (SiO_2, dichloromethane) and 0.70 g of a white solid were recovered (24 %).

Elemental analysis for $C_{46}H_{40}Cl_2O_{10}$: Calcd: C% 67.07, H% 4.89; Found: C% 66.61, H% 5.22.

^{1}H-RMN (300 MHz, $CDCl_3$) δ (ppm): 1.62 (4H, m, CH_2), 1.85 (4H, m, CH_2), 2.18 (4H, q, ^{3}J=7.2 Hz, C<u>H</u>$_2$-CH=CH$_2$), 4.08 (4H, t, ^{3}J=6.5 Hz, Ar-O-C<u>H</u>$_2$), 5.03 (4H, m, CH=C<u>H</u>$_2$), 5.85 (2H, m, C<u>H</u>=CH$_2$), 7.00 (4H, d, ^{HH}J=8.8 Hz, *m*-Ar''), 7.39 (1H, s, *o*-Ar), 7.40 (4H, d, ^{HH}J=8.8 Hz, *m*-Ar'), 7.66 (1H, s, *m*-Ar), 8.17 (4H, d, ^{HH}J=8.8 Hz, *o*-Ar''), 8.31 (4H, d, ^{HH}J=8.8 Hz, *o*-Ar').

^{13}C-RMN (75 MHz, $CHCl_3$) δ (ppm): 25.3 (CH_2), 28,5 (CH_2), 33.4 (CH_2), 68.2 (CH_2), 114.5 (Ar), 114.9 (Ar), 119.5 (<u>C</u>H$_2$=CH), 121.0 (Ar), 122.3 (Ar), 125.14 (Ar), 125.7 (Ar) 130.8 (Ar), 132.1 (Ar), 132.5 (Ar), 138,3 (CH$_2$=<u>C</u>H), 146.1 (Ar), 155.9 (ArO), 163.0 (COO), 163.8 (COO), 164.2 (COO).

Monomer **B3**

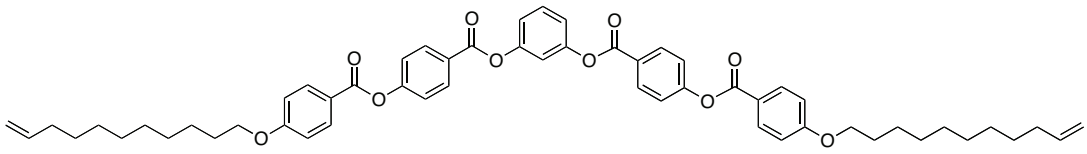

B3 was prepared in the same way as **B1**: **Ud 2**: 0.58 g (2.01 mmol); **6**: 0.35 g (1.00 mmol); DMAP: 0.03 g (0.20 mmol); dichloromethane: 100 mL; EDCI: 0.75 g (2.51 mmol); 24 h. The resulting solution was extracted with brine (2x 200 mL). The organic phase was then recovered and concentrated in vaccuo. The residue was purified by column chromatography (SiO_2, dichloromethane) giving 0.35 g of a white solid (39 %).

Elemental analysis for $C_{56}H_{62}O_{10}$: Calcd: C% 75.14, H% 6.98; Found: C% 74.91, H% 7.24.

^{1}H-RMN (300MHz, $CDCl_3$) δ (ppm): 1.33 (20H, br, CH_2), 1.49 (4H, br, CH_2), 1.84 (4H, m, CH_2), 2.06 (4H, q, ^3J=8.0 Hz, C<u>H</u>$_2$-CH=CH_2), 4.06 (4H, t, ^3J=6.6 Hz, Ar-O-CH_2), 4.93, 4.97, 5.04 (4H, m, CH=C<u>H</u>$_2$), 5.83 (2H, m, C<u>H</u>=CH_2), 7.00 (4H, d, ^3J=8.8 Hz, *m*-Ar''), 7.18 (1H, d, ^4J=1.9 Hz, *o*'-Ar), 7.21 (1H, s, *o*-Ar), 7.22 (1H, d, ^2J=1.9 Hz, *o*'-Ar), 7.39 (4H, d, ^3J=8.6 Hz, *m*-Ar'), 7.51 (1H, t, ^3J=8.5 Hz, *m*-Ar), 8.16 (4H, d, ^3J=8.6 Hz, *o*-Ar''), 8.29 (4H, d, ^3J=8.6 Hz, *o*-Ar').

^{13}C-RMN (75 MHz, $CHCl_3$) δ (ppm): 25.9 (CH_2), 28.9 (CH_2), 29.1, 29.3, 29.4, 29.5, 33.8 (CH_2), 68.4 (CH_2O), 114.2 (Ar), 114.5 (Ar), 119.3 (<u>C</u>H_2=CH), 121.04 (Ar), 122.15 (CH_2=<u>C</u>H), 125.5 (Ar), 126.6 (Ar) 131.9 (Ar), 132.4 (Ar), 138.3 (Ar), 151.4 (Ar), 155.5 (ArO), 163.8 (COO), 164.1 (COO), 164.3 (COO).

Monomer **B4**

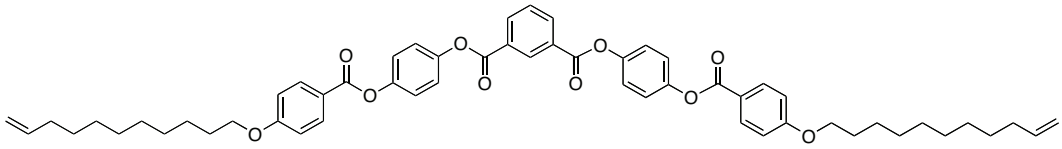

In a three-necked, round-bottom flask, 0.86 g (3.00 mmol) of 4-undecyloxybenzoic acid **Ud 2**, 0.53 g (1.50 mmol) of **10** and a catalytic amount of DMAP were dried in vaccuo with a heating gun an then dissolved in 100 mL of dry dichloromethane and 10 mL of DMF. Argon was added and the emulsion cooled to 0º C. EDCI (1.02 g; 3.50 mmol) was added and the reaction mixture was magnetically stirred for 18 h. The resulting solution was extracted with brine (2x 200 mL). The organic phase was then recovered and concentrated in vaccuo. The residue was purified by chromatography column (SiO_2, dichloromethane) to yield 0.55 g of a white solid (41 %).

Elemental analysis for $C_{56}H_{62}O_{10}$: Calcd: C% 75.14, H% 6.98; Found: C% 74.82, H% 6.93.

^{1}H-RMN (300 MHz, $CDCl_3$) δ (ppm): 1.92 (24H, m, CH_2), 1.84 (4H, m, CH_2), 2.06 (4H, q, ^{3}J=7.2 Hz, -CH_2-C<u>H</u>$_2$-CH=CH_2), 4.06 (4H, t, ^{3}J=6.7 Hz, CH_2O), 4.97 (4H, m, CH=C<u>H</u>$_2$) 5.83 (2H, m, C<u>H</u>=CH_2), 6.99 (4H, d, ^{HH}J=8.8 Hz, Ar''), 7.31 (8H, d, ^{HH}J=7.8 Hz, Ar'), 7.72 (1H, t, ^{3}J=7.8 Hz, *m*-Ar), 8.16 (4H, d, ^{HH}J=8.8 Hz, *o*-Ar''), 8.47 (2H, dd, ^{3}J=7.8 Hz; ^{4}J=1.5 Hz, *o*'-Ar), 9.04 (1H, t, ^{3}J=1.5 Hz, *o*-Ar).

^{13}C-RMN (75 MHz, $CHCl_3$) δ (ppm): 26.0 (CH_2), 28.9 (CH_2), 29.1(CH_2), 29.3 (CH_2), 29.5 (CH_2), 33.8 (CH_2), 68.4 (CH_2O), 114.1 (CH_2=CH-), 114.4 (Ar), 121.35 (Ar), 122.4 (Ar), 122.8 (Ar), 129.1 (Ar), 130.2 (Ar), 131.8 (Ar), 132.3 (Ar), 135.0 (Ar_{quat}), 139.2 (CH_2=CH-), 148.0 (Ar), 148.8 (Ar), 163.6 (ArO) 164.1 (COO), 164.8 (COO').

Monomer **B5**

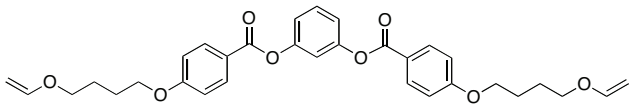

In a three-necked, round-bottom flask, 0.65 g (1.85 mmol) of **6** and 1.16 g (4.42 mmol) of PPh_3 were added. An argon flush was performed and the solids were dissolved in 150 mL of anhydrous THF. The mixture was stirred and cooled down to 0ºC. Then 0.50 mL (4.05 mmol) of 4-vinyloxybutanol were added and immediately, DIAD (0.81 mL; 3.84 mmol) was added dropwise. The reaction mixture was kept to 0ºC for 1 h and left to warm up to room temperature for 8 h. The resulting solution was concentrated to dryness and redissolved in a minimum quantity of a mixture of dichloromethane-cyclohexane (1:1) and purified by column chromatography (triethylamine-neutralized SiO_2, dichloromethane). The crude product was finally crystallized from distilled cyclohexane (white crystals, 0.58 g, 58 %).

Elemental analysis for $C_{32}H_{34}O_8$: Calcd: C% 70.31, H% 6.27; Found: C% 69.98, H% 6.52.

^{1}H-RMN (300 MHz, $CDCl_3$) δ (ppm): 1.92 (8H, m, C$\underline{H}_2$-CH_2O), 3.78 (4H, t, ^{3}J=5.7 Hz, CH_2O), 4.01 (2H, dd, ^{2gem}J=2.0 Hz, ^{3cis}J=6.8 Hz, C$\underline{H}_2$=CH_2O), 4.10 (4H, t, ^{3}J=5.9 Hz, CH_2OAr), 4.20 (2H, dd, ^{2gem}J=2.0 Hz; $^{3trans}J$=14.5 Hz, C$\underline{H}_2$=CH-O), 6.49 (2H, dd, ^{3cis}J=6.8 Hz; $^{3trans}J$=14.3 Hz, CH_2=C$\underline{H}$-O), 6.98 (4H, d, ^{HH}J=9.0 Hz, *m*-Ar'), 7.13 (1H, s, *o*-Ar), 7.16 (2H, s, *o'*-Ar), 7.46 (1H, t, ^{3}J=6.0 Hz, *m*-Ar), 8.14 (4H, d, ^{HH}J=9.0 Hz, *o*-Ar').

^{13}C-RMN (75 MHz, $CDCl_3$) δ (ppm): 25.7 (CH_2), 25.9 (CH_2), 67.4 (CH_2O), 67.8 (*C*H_2OAr), 86.5 (*C*H_2=CH-O), 114.3 (Ar), 115.9 (Ar), 119.1 (Ar), 121.5 (Ar), 129.7 (Ar), 132.3 (Ar), 151.6 (ArO), 151.8 (CH_2=C$\underline{H}$-O), 163.4 (ArO), 164.5 (COO).

Monomer **B6**

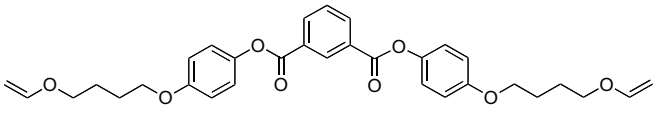

Monomer **B6** was prepared in the same way as **B5**: 1.00 g (2.86 mmol) of **10**; 1.80 g PPh_3: (6.85 mmol); THF: 150 mL; 4-vinyloxybutanol: 0.80 mL (6.28 mmol); DIAD: 1.27 mL (6.01 mmol). 0ºC for 1 h; room temperature for 5 h. Chromatography column (triethylamine-neutralized SiO_2, dichloromethane). The crude product was dried and crystallized from distilled cyclohexane (white crystals, 0.65 g, 42 %).

Elemental analysis for $C_{32}H_{34}O_8$: Calcd: C% 70.31, H% 6.27; Found: C% 69.79, H% 6.09.

^{1}H-RMN (300 MHz, $CDCl_3$) δ (ppm): 1.94 (8H, m, C<u>H</u>$_2$-CH_2O), 3.77 (4H, t, ^3J=5.7 Hz, CH_2O), 4.09 (4H+2H, t+signal, ^3J=5.7 Hz, CH_2O+C<u>H</u>$_2$=CH), 4.20 (2H, dd, ^{2gem}J=1.95 Hz; $^{3trans}J$=14.3 Hz, C<u>H</u>$_2$=CH-O), 6.49 (2H, dd, ^{3cis}J=6.8 Hz; $^{3trans}J$=14.3 Hz, CH_2=C<u>H</u>-O), 6.94 (4H, d, ^3J=9.0 Hz, *o*-Ar'), 7.16 (4H, d, ^3J=9.0 Hz, *m*-Ar'), 7.68 (1H, t, ^3J=7.9 Hz, *m*-Ar), 8.45 (2H, d, ^3J=7.9 Hz; ^4J=1.7 Hz, *o'*-Ar), 9,00 (1H, s, *o*-Ar).

^{13}C-RMN (75 MHz, $CDCl_3$) δ (ppm): 25.7 (CH_2), 25.9 (CH_2), 67.5 (<u>C</u>H_2OCH=CH_2), 67.9 (CH_2OAr), 86.5 (<u>C</u>H_2=CHO), 115.2 (Ar), 122.4 (Ar), 129.0 (Ar), 130.4 (Ar), 131.7 (Ar), 134.8 (Ar), 144.2 (Ar), 151.8 (CH_2=<u>C</u>H), 156.9 (Ar), 164.6 (COO).

Appendix A

A.1. Chemicals and Solvents.

4-Benzyloxybenzoic acid (99%), 4-Benzyloxyphenol (99%), DMAP (4-dimethyl aminopyridine, 99%) and toluene (99.5%), were purchased form Alfa Aesar. Methyl-hydroquinone (98%), $Pt(COD)Cl_2$ (98%), Karstedt catalyst (2% in hexanes), EDCI (1-Ethyl-3-[3-dimethylaminopropyl]carbodiimide Hydrochloride, >98%), 1,4-butanediol vinyl ether (99%), 10-undecenol (99%), TMDS (1,1,3,3-tetramethyldisiloxane, 97 %) HDMOS (polydimethylsiloxane hydride terminated, 99%) and pentamethylcyclopentasiloxane (HD5, 97%) were purchased from Aldrich. Pd/C (Pd 10%) catalyst and DCC (*N,N*-dicyclo-hexylcarbodiimide) were purchased from Lancaster (99%); DIAD (diisopropyl azodicarboxylate, 94 %), 5-hexenol (97%) and PPh_3 (triphenylphosphine, 99 %) were purchased from Acros. HMTS (1,1,3,3,5,5-hexamethyltrisiloxane, 99%) and Karstedt catalyst (3% in xylenes) was purchased from Röth chemicals. DMF (*N,N*-dimethylformamide), was purchased from Normapur (99.8%). MeOH (methanol, >99.9%), cyclohexane (99%) and CH_2Cl_2 (dichloromethane, stabilized with amylene, 99.8%) were purchased from Carlo Erba. THF (tetrahydrofurane), purchased from Ridel-de-Haën (> 99 %). HCl was obtained from Normapur (37 %).

A.2. Solvent purification

Toluene:

The technique applied to eliminate tiophene impurities from the solvent consisted in a series of successive extractions using concentrated sulfuric acid until the acid fractions turned colorless. Then, the organic phase was washed with water and dried

over sodium sulfate. The solvent was then poured into a round bottom flask and distilled over sodium wire. The distillation's body fraction was received on 4Å molecular sieves.

THF:

Prior to the distillation, commercially available THF (99 %) was dried over KOH pellets for at least 24 h. Then, it was distilled over sodium wire using benzophenone as indicator under argon atmosphere.

Dichloromethane:

Commercially available amylene stabilized dichloromethane was distilled over calcium hydride under argon atmosphere. It was mainly used for esterification reactions and catalyst solution.

Methanol:

Methanol was dried over magnesium rods and iodine, then distilled and received over active 4Å molecular sieves, just before use.

[COD]$PtCl_2$ Catalyst:

In a previously argon flushed amber vial, the right amount of [COD]$PtCl_2$ was weighed in order to prepare a 1 w/w and dissolved into previously distilled dichloromethane added by cannula. This solution was stored at -10ºC under argon e.g. in an amber vial previously flushed with argon. Typically, 50 mg of [COD] $PtCl_2$ were weighed then dissolved in 3.8 mL of fresh distilled dichloromethane.

A.2. Experimental Techniques

Elemental Analysis.

Elemental analyses were performed at the analytical services department at the Strasbourg's Faculty of Chemistry. Only the various monomers were analyzed.

Hydrogenation.

Hydrogenation reactions were performed in a special designed device that allowed continuous hydrogen flux. The device is illustrated in figure A2.1

Nuclear Magnetic Resonance.

^{1}H and ^{13}C NMR spectra were recorded with a Bruker Advance 300 apparatus using deuterated chloroform, THF and acetone as solvents. Frequency for ^{1}H experiments were 300 MHz and for ^{13}C 75 MHz.

Polarized-Light Optical Microscopy.

Microscopy studies were performed on a Leitz optical microscope and the samples were heated-cooled into a Mettler F82 Hot Stage plate.

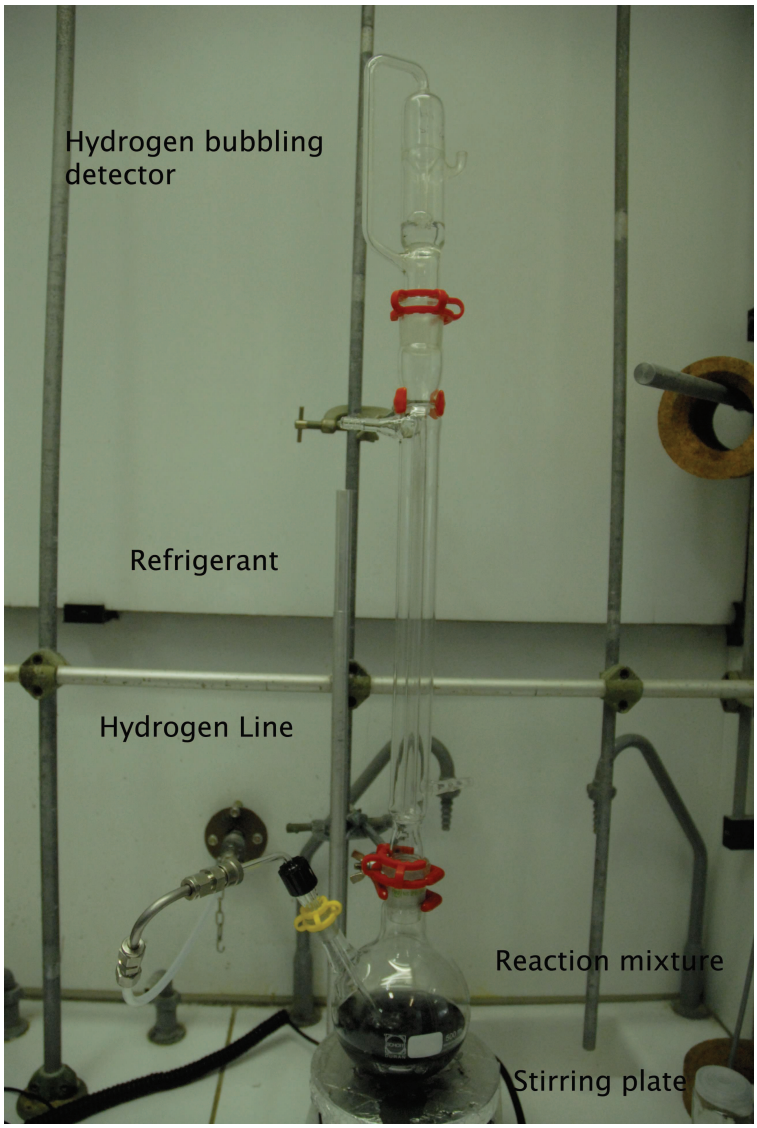

Figure A.2.1: Hydrogenation device.

Differential Scanning Calorimetry.

Calorimetric data were obtained with a DSC Q1000 Texas Analysis apparatus.

Analytical Gel Permeation Chromatography.

These analyses were performed at The Charles Sadron Institute in Strasbourg.

Molar mass determinations were done using THF as eluent into a Waters Chromatograph equipped with five, 10 μm PLGel mixed B columns. Three different

detectors were employed: a differential refractometer (Shimadzu RID-10A); A Shimadzu SPD-10A UV spectrometer using 2 different wavelengths (254 and 280 nm) and a Wyatt DAWN DSP multi angle laser light scattering (MALLS) detector with a laser wavelength of 632.8 nm and 18 angles.

Polymer Centrifugation.

The polymer centrifugation was performed into a Bioblock Scientific Sigma 3k18 centrifuge equipped with Nr 11133 rotor with 4 50 mL cells.

Oriented sample XRD patterns.

Oriented XRD patterns were recorded using a sealed-tube generator (900 W) equipped with a pinhole Cu-Kα_1 (λ = 1.542 Å) parallel beamline based on a home-mounted Kirkpatrick-Baez optics coupled with a HiStar detector (Bruker AXS) or with image plates. A piece of the elastomeric film was placed in a home-made heating apparatus. The sample temperature was controlled to within ±0.03°C. Two different detector-sample distances were used: 111.5 and 328.0 mm. The patterns were analyzed using homemade ImageJ plug-ins (ϕ and 2θ profiles).

Rheological Studies.

The experimental set-up used is a Rheometrics-RSA II strain controlled spectrometer. This RSA II spectrometer is equipped with one normal force transducer (1kFRT) that can detect normal forces within the range 0.001-10 N. The instrument is equipped with a STD motor having a strain resolution of 0.05 μm and an angular frequency range between 10-3 and 100 rad.s-1.

SQUID Experiments.

The magnetic studies were carried out with a SQUID magnetometer (Quantum Design MPMS-/XL/) covering the temperature and fields ranges 1.8-300 K, ± 5 T. ac susceptibility measurements were performed in a 0.35 mT alternative field (100 Hz). Magnetization measurements at different fields at room temperature confirm the absence of ferromagnetic impurities.

Transmission Electron Microscopy.

Transmission electron microscopy (TEM) study was carried out with a TOPCON 002B microscope, operating at 200 kV, (point resolution 0.18 nm) and equipped with a GATAN GIF 200 electron imaging filter, has been used to study the morphology and crystalline structure of nanoparticles. Samples were prepared by allowing one drop of a solution of nanoparticles in dichloromethane to evaporate under ambient conditions on a TEM copper grid coated by amorphous carbon.

A.3. Polymer preparation.

General procedure.

In a 5 mL vial, equimolar quantities of monomer(s) and chain extender were dissolved in the appropriate quantity of dry solvent to obtain a 1.1 mmol/mL of solvent solution in almost all the cases. The vial was heated at 60ºC and stirred until a colorless solution was obtained. Catalyst solution was immediately added (15 μL) and the reaction was kept at 60ºC for 24 h.

Depending on the polymer synthesized, we used two general methods to purify our polymers:

A) Precipitation

The resulting viscous solution was redissolved in 3 mL of THF, and then added into a 100 mL beaker with methanol. A viscous solid has precipitated at the bottom of the beaker. The solid and the solution were recovered and centrifuged at 15000 rpm for 20 min. The washings were discarded and the polymer, laid at the bottom of the centrifuge tubes, was recovered. This procedure was repeated three times. The remaining polymer was transferred into a hermetic vial, cooled under liquid nitrogen and lyophilized for 24h.

B) Preparative gel permeation column.

The solvent was evaporated and the polymer was purified into a GPC column containing Biorad SX1 biobeads using THF or dichloromethane as solvent.

The corresponding quantities are shown in the next tables.

Trisiloxane polymers and Copolymers.

	Monomer **N1**		Monomer **N2**		**HMTS**			
	m (mg)	**η (mmol)**	**m (mg)**	**η (mmol)**	**m (mg)**	**η (mmol)**	**Yield (%)**	**Purification method**
PN1T	184	0.325	-	-	68	0.325	80	A
CoP75T	210	0.375	53	0.175	104	0.500	99	A
CoP50T	140	0.250	106	0.250	104	0.500	90	A
CoP25T	70	0.175	159	0.375	104	0.500	98	A
PN2T	-	-	213	0.500	104	0.500	78	A

Disiloxane Copolymers.

	Monomer **N1**		Monomer **N2**		**TMDS**			
	m (mg)	**η (mmol)**	**m (mg)**	**η (mmol)**	**m (mg)**	**η (mmol)**	**Yield (%)**	**Purification method**
CoP75D	210	0.375	53	0.175	35	0.500	50	A
CoP50D	140	0.250	106	0.250	35	0.500	44	A
CoP25D	70	0.175	159	0.375	35	0.500	80	A

Bent-Core Polymers.

Polymer	**Monomer**	**η (mmol)**	**Chain extender**	**Quantity (mmol)**	**Solvent (mL)**	**Cat. (μL)**	**Yield (%)**	**Purification method**
PB1	B1	0.148	HDMOS	0.148	0.80	10	68	A
PB2	B2	0.206	HDMOS	0.206	1.20	8	74	B[a]
PB3	B3	0.177	HTMS	0.177	0.50*	10	43	B[a]
PB4	B4	0.223	HTMS	0.223	1.00	10	98	B[b]

* CH_2Cl_2 as solvent. a: CH_2Cl_2 as eluent. b: THF as eluent.

A.4. Liquid Crystalline Elastomers

General Procedure.

Liquid Crystalline Elastomer films were prepared according to the spin casting procedure developed by Finkelmann's group.

In a 5 mL vial, were introduced the corresponding quantities of the monomers, crosslinker and chain extender (always in this order) and then dissolved in toluene and heated until a homogeneous solution was obtained. 10 μL of the catalyst solution were added and the reaction mixture was let to react at 60ºC for 5 minutes coating the walls of the cell. Immediately, the reaction mixture was poured into a specially designed cell with a Teflon® film and centrifuged at 3000 rpm heating at 60ºC until the formation of a gel film, generally after 1.5 h. After this period, centrifugation was stopped, the cell was cooled down to room temperature and the fragile film deposited over the Teflon® film was carefully removed from the centrifuge wall, then removed cut in 3 pieces and removed from the Teflon® film.

Each piece was suspended and adapted to load weight to perform the orientation process. Once fully stretched the turbid samples became transparent films and were then heated at 60ºC in a vacuum oven for 72 h, to complete the crosslinking reaction.

The quantities used of the three series are illustrated in the next three tables.

Trisiloxane Liquid Crystalline Elastomers and Coelastomers.

	Monomer **N1**		Monomer **N2**		**HMTS**		**HD5**		**Toluene**
	m (mg)	**η (mmol)**	**m (mg)**	**η (mmol)**	**m (mg)**	**η (mmol)**	**m (mg)**	**η (mmol)**	**V (mL)**
EN2T	-	-	426	1.00	187	0.9	12	0.04	0.9
CoE25T	140	0.25	319	0.75	187	0.9	12	0.04	0.9
CoE50T	280	0.50	213	0.50	187	0.9	12	0.04	0.9
CoE75T	420	0.75	106	0.25	187	0.9	12	0.04	0.9
EN1T	560	1.00	-	-	187	0.9	12	0.04	0.9

Disiloxane Liquid Crystalline Coelastomers.

	Monomer **N1**		Monomer **N2**		**TMDS**		**HD5**		**Toluene**
	m (mg)	**η (mmol)**	**m (mg)**	**η (mmol)**	**m (mg)**	**η (mmol)**	**m (mg)**	**η (mmol)**	**V (mL)**
CoE25D	140	0.25	319	0.75	125	0.9	12	0.04	0.9
CoE50D	280	0.50	213	0.50	125	0.9	12	0.04	0.9
CoE75D	420	0.75	106	0.25	125	0.9	12	0.04	0.9

Bent-Core/Calamitic Mesogen Liquid Crystalline Coelastomers.

	Monomer **Nx**		Monomer **Bx**		**TMDS**		**HD5**		**Toluene**
	m (mg)	**η (mmol)**	**m (mg)**	**η (mmol)**	**m (mg)**	**η (mmol)**	**m (mg)**	**η (mmol)**	**V (mL)**
CoEN1B4D 5%	532	0.95	45	0.05	125	0.9	12	0.04	0.9
CoEN2B4D 5%	405	0.95	45	0.05	125	0.9	12	0.04	0.9
CoEN1B6D 5%	532	0.95	27	0.05	125	0.9	12	0.04	0.9
CoEN2B6D 5%	405	0.95	27	0.05	125	0.9	12	0.04	0.9
CoEN1B6D 25%	420	0.75	135	0.25	125	0.9	12	0.04	0.9*
CoEN2B6D 25%	319	0.75	135	0.25	125	0.9	12	0.04	0.9*

In this case, the monomer and the bent-core are indicated on the name. * 0.4 mL of dry dichloromethane were added to dissolve the Bent-Core monomer.

A.5. Mn12Ac and Ferrite functionalization and network synthesis.

Synthesis of Mn12Hx2.

0.50 mg (0.27 mmol) of **Mn12Ac**, and 1.89 g (8.57 mmol) of **Hx2** were dissolved in 100 mL of a mixture toluene-dichloromethane 1:1 and heated at 50ºC overnight. The crude product was filtered and redisolved in the previously evoked solvent mixture. The solvent was distilled thoroughly (azeotropic distillation) and the process still repeated two times. The final solid was dried in vaccuo for one night and then purified by GPC column (SX3 beads, dichloromethane) to yield 400 mg (34 %) of a brownish solid.

Synthesis of iron oleate complex ($Fe(oleate)_3$).

10.8 g (40 mmol) of $FeCl_3.H_2O$ (97%, Aldrich) were dissolved in 60 ml H_2O (Milli-Q) and 80 ml ethanol. 36.5 g (120 mmol) of sodium oleate (82%, Riedel-de Haën) dissolved in 140 ml hexane were mixed with the iron (III) solution. The resulting biphasic solution was refluxed at 70°C for 4 h. After cooling down the solution, the organic phase containing the iron oleate complex was separated, washed three times with 30 ml distilled water to extract salts, dried using $MgSO_4$, and finally hexane was evaporated. The resulting iron oleate complex was a reddish-brown viscous solution. The final product was stored in the refrigerator.

Synthesis of iron oxide nanocrystals.

The synthesis of iron oxide nanocrystals has been carried out by modification of synthetic parameters of the procedure elaborated by J. Park et al.[182] 2 g (2.2×10^{-3} mol) of $Fe(oleate)_3$ and 0.155 g (0.55×10^{-3} mol) of oleic acid (99%, Alfa-Aesar) were added to 20 ml octyl ether (97%, Fluka, b.p. 287°C). The mixture was kept under

vigorous stirring for 1 h to dissolve the reactants. The solution was heated to 290 °C with a heating rate of 5 °C/min, without stirring and then was refluxed for 60 min. at this temperature under air. The resultant black solution was then cooled down to room temperature and the nanocrystals were washed 3 times by addition of ethanol and centrifugation (4000 rpm, 10 min.). This step allowed us to discard the supernatant containing excess oleic acid and reaction byproducts. The nanocrystals could be easily suspended in various organic solvents (toluene, hexane, dichloromethane).

Functionalization of iron nanocrystals.

The iron oxide nanocrystals (38.7 mg) and an excess of **Hx2** (111.7 mg) were refluxed in dichloromethane at 40ºC for 72h. The solvent was evaporated and the crude product was thoroughly purified by GPC chromatography (SX1 beads in dichloromethane) to yield 30 mg (80%).

Preparation of MC-LCE with ferrite nanoparticles as crosslinkers.

In a 3 mL vial, 390 mg (0.9 mmol) of **N2**, 208.5 mg (1.00 mmol) of 1,1,3,3,5,5-hexamethyltrisiloxane and 10 mg ($3.4x10^{-3}$ mmol) of functionalized ferrite nanoparticles were dissolved in 1.00 mL of thiophene-free toluene. The mixture was put in an ultrasonic bath for 5 minutes and then heated until a homogeneous, orange-brown solution was obtained. Then, 20 mL of Karstedt catalyst (2 % wt in xylenes) were added and the reaction mixture was magnetically stirred at 300 rpm until we obtained a gel (24 h). The gel was put out of the vial and washed with a Soxhlet apparatus with hexanes for 72h. The washings were concentrated obtaining a percentage of soluble content of 12 %.

General preparation of Mn12Hx2 networks.

In a 3 mL vial the corresponding amounts of Mn12 and the corresponding starting products were dissolved in 0.2 mL of thiophene free toluene under magnetic stirring. The catalyst was readily added and the mixture was let at room temperature for 1 minute and then heated at 40ºC until gelification.

EMn1: **Mn12Hx2**: 44 mg (0.01 mmol); HDMOS: 46 mg (0.08 mmol). 2min.

EMn2: **Mn12Hx2**: 44 mg (0.01 mmol); HDMOS: 46 mg (0.08 mmol); 1,10-decadiene: 6 mg (0.04 mmol). 15 min.

EMn3: **Mn12Hx2**: 44 mg (0.01 mmol); HDMOS: 46 mg (0.08 mmol); **N2**: 17 mg (0.04 mmol). 15 min.

Appendix B

DSC plots.

All the plots presented correspond to the second heating/cooling cycle, performed at a heating rate of 2ºC/min.

Monomers.

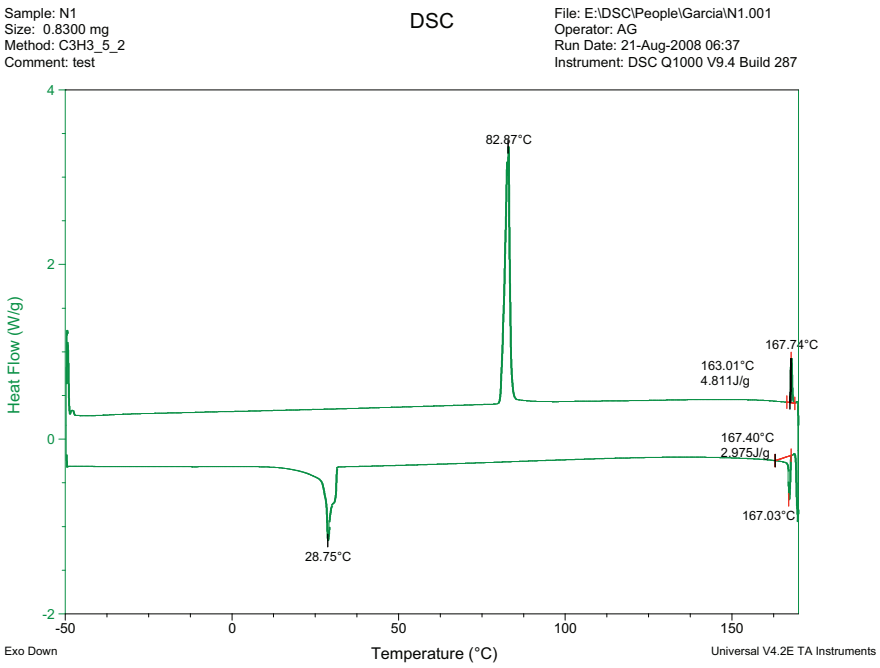

N1

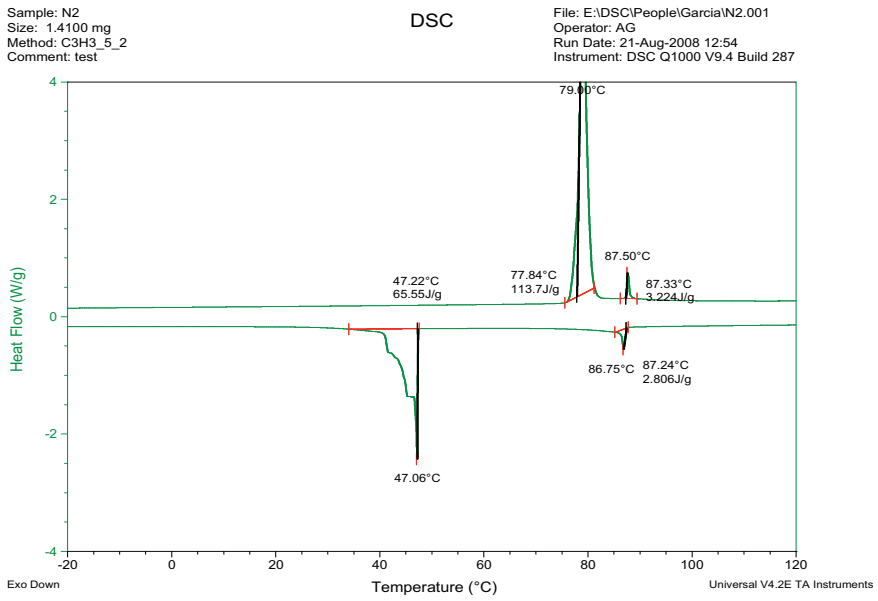

N2

Monomers Bent-Core.

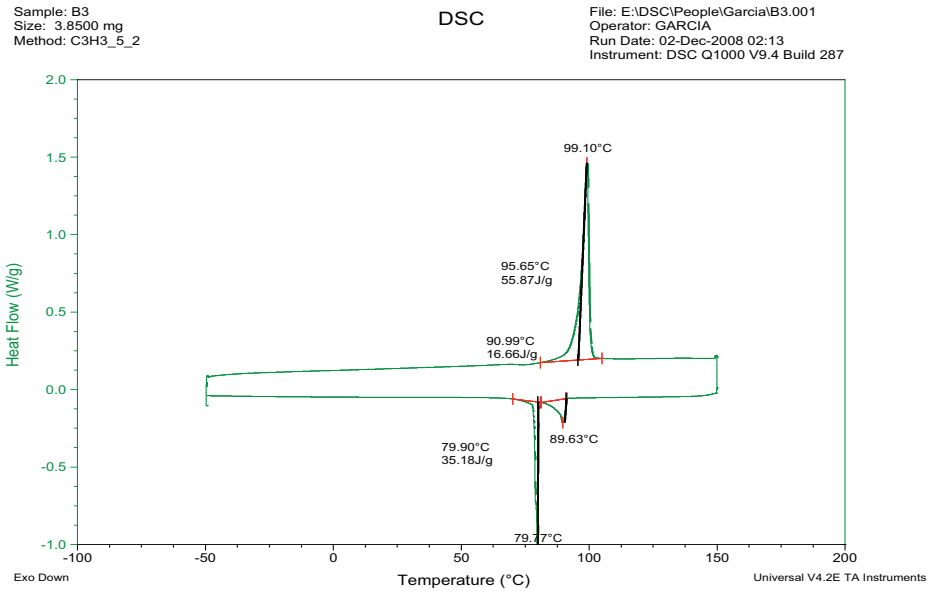

B3

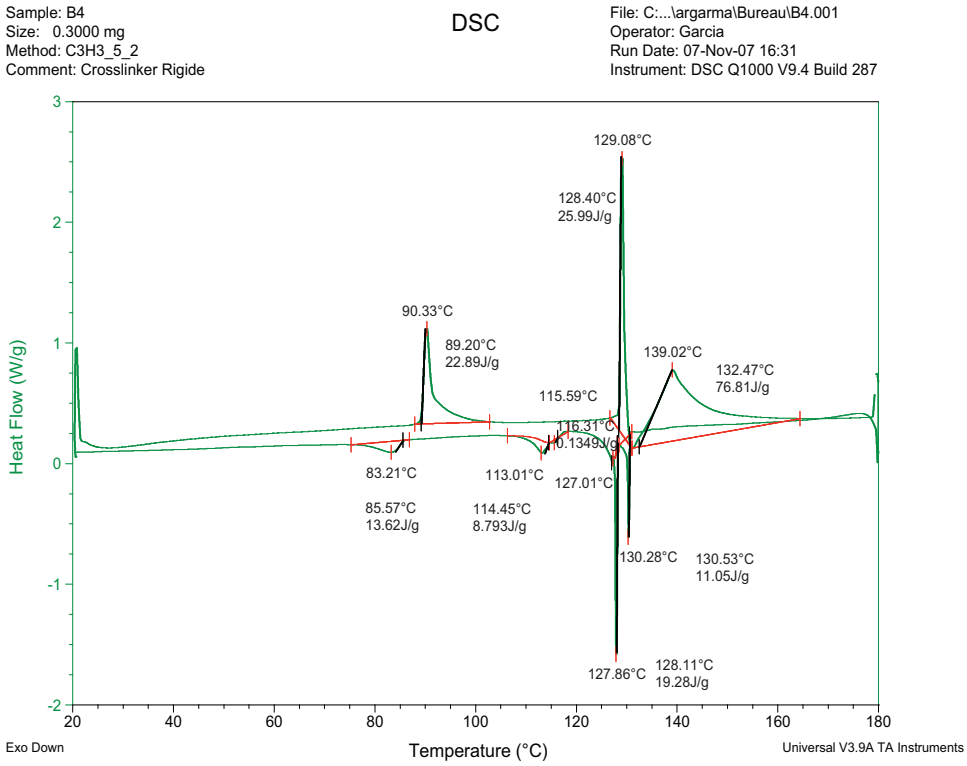

B4

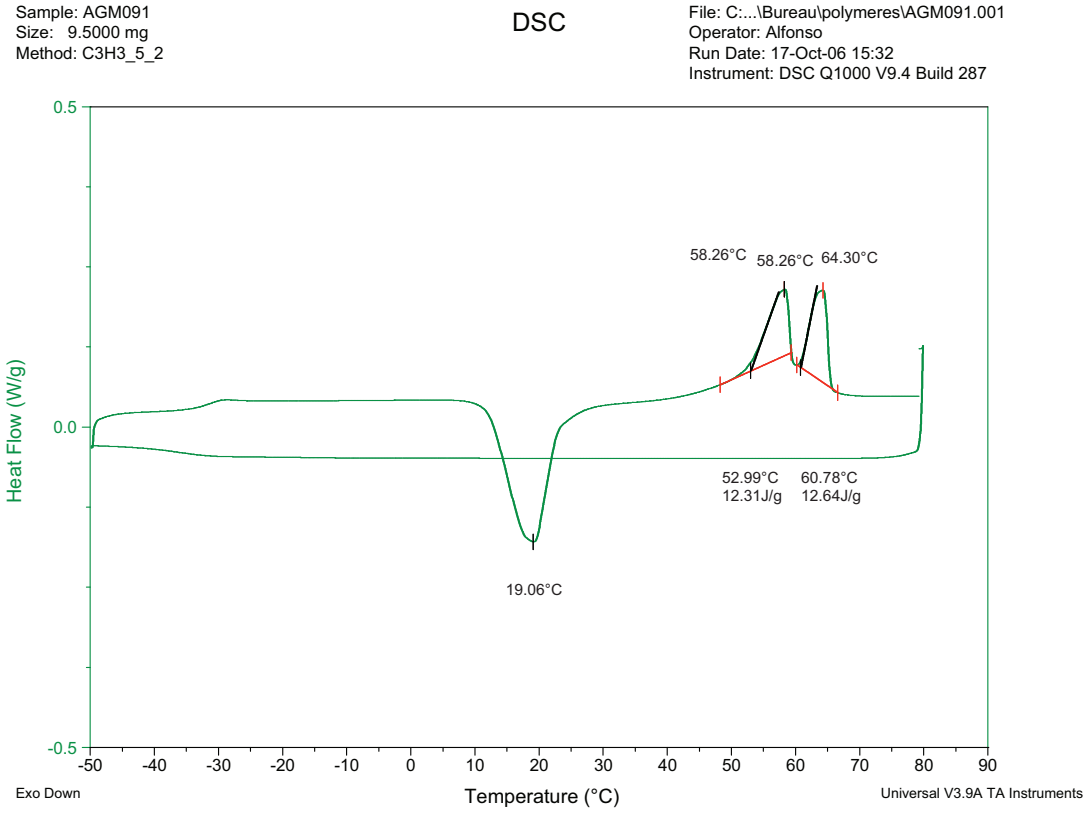
Sample: AGM091
Size: 9.5000 mg
Method: C3H3_5_2
DSC
File: C:...\Bureau\polymeres\AGM091.001
Operator: Alfonso
Run Date: 17-Oct-06 15:32
Instrument: DSC Q1000 V9.4 Build 287
58.26°C
58.26°C
64.30°C
52.99°C
12.31J/g
60.78°C
12.64J/g
19.06°C
Heat Flow (W/g)
Temperature (°C)
Exo Down
Universal V3.9A TA Instruments

B5

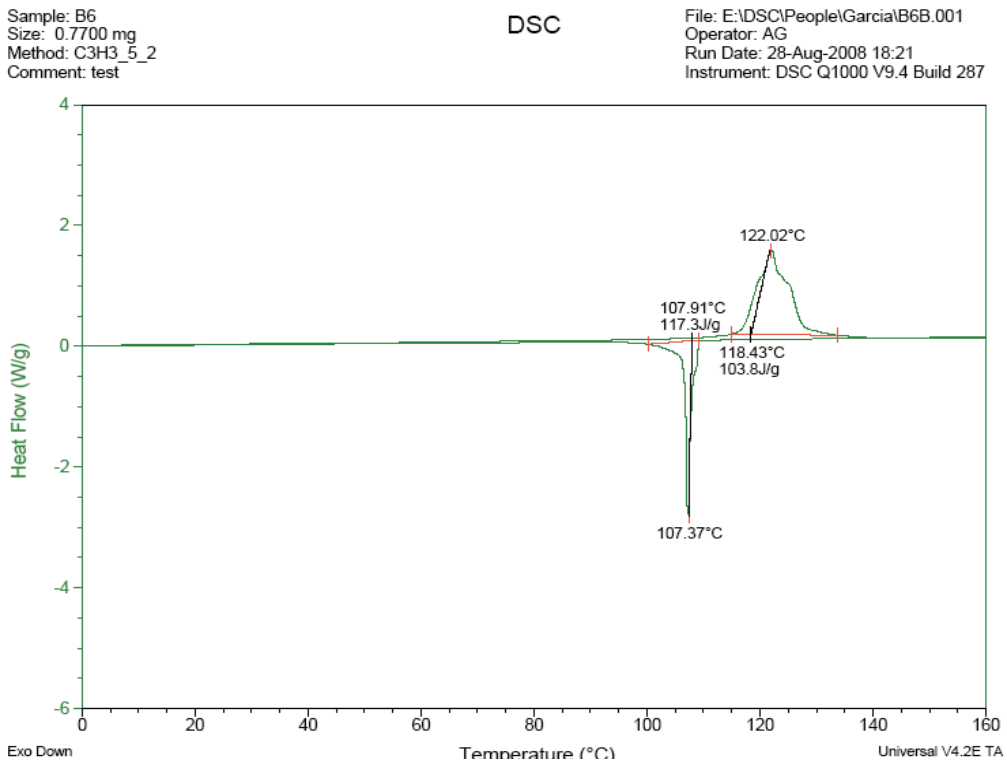
Sample: B6
Size: 0.7700 mg
Method: C3H3_5_2
Comment: test
DSC
File: E:\DSC\People\Garcia\B6B.001
Operator: AG
Run Date: 28-Aug-2008 18:21
Instrument: DSC Q1000 V9.4 Build 287
122.02°C
107.91°C
117.3J/g
118.43°C
103.8J/g
107.37°C
Heat Flow (W/g)
Temperature (°C)
Exo Down
Universal V4.2E TA

B6

Monomer Mixtures.

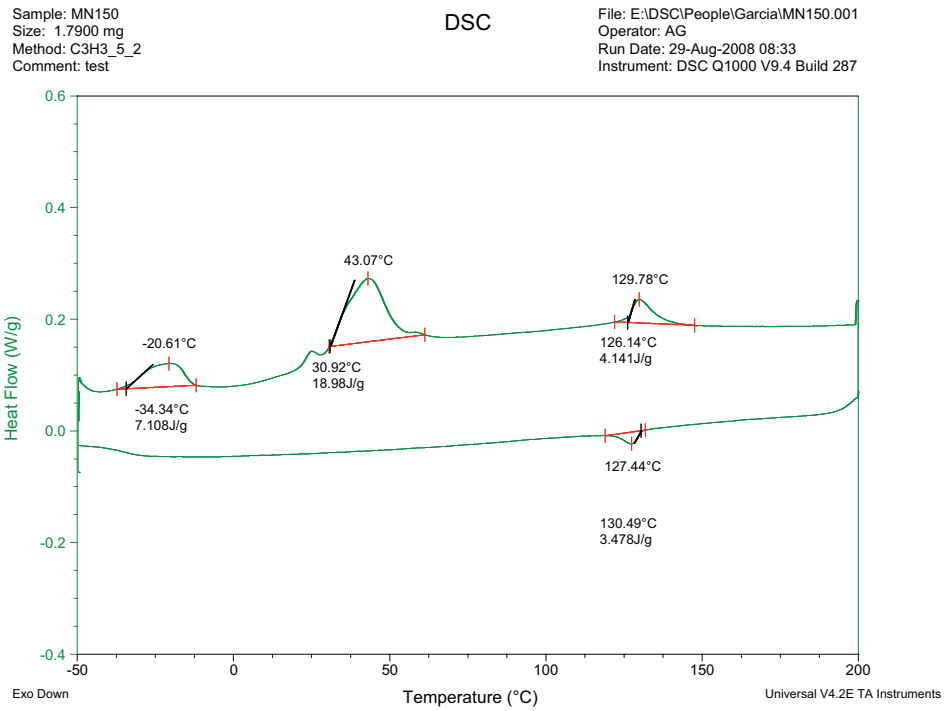

N1/N2 50:50

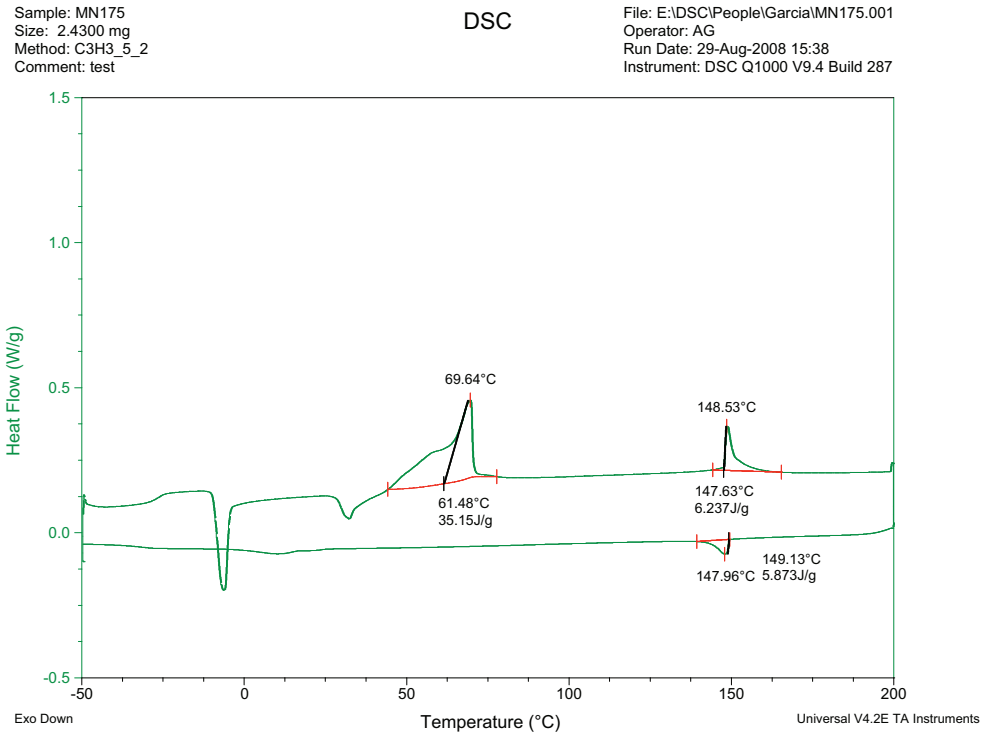

N1/N2 75:25

Trisiloxane Polymers.

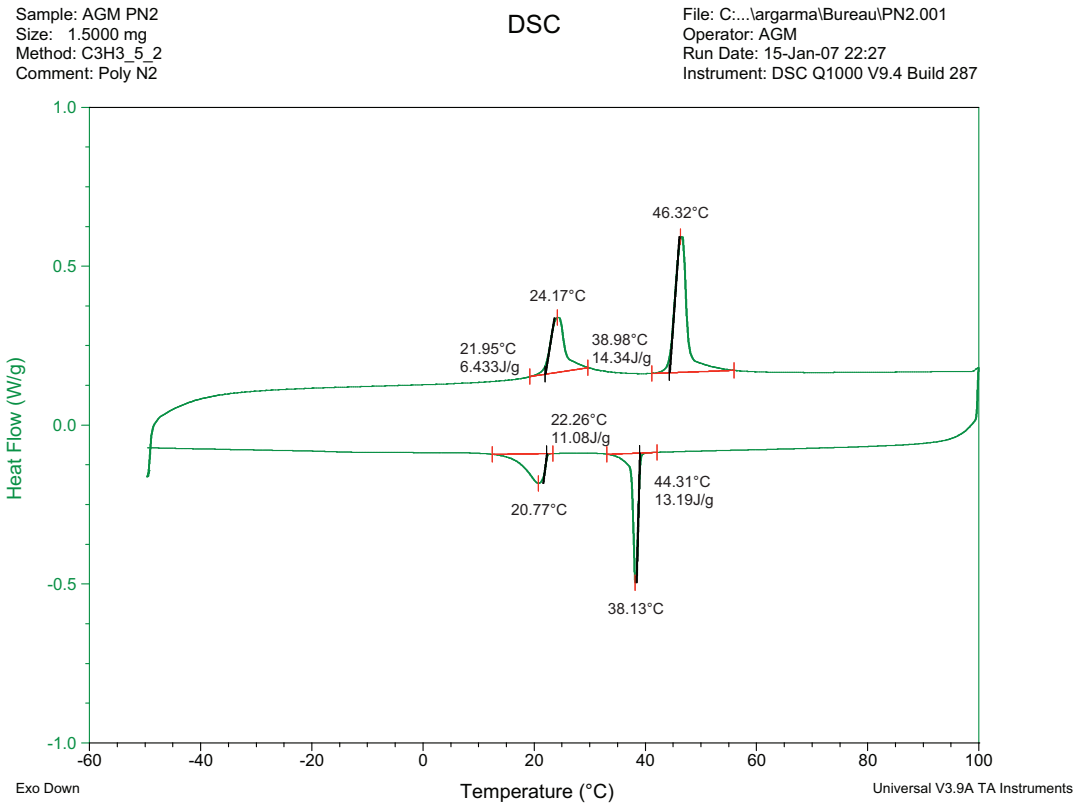

PN2T

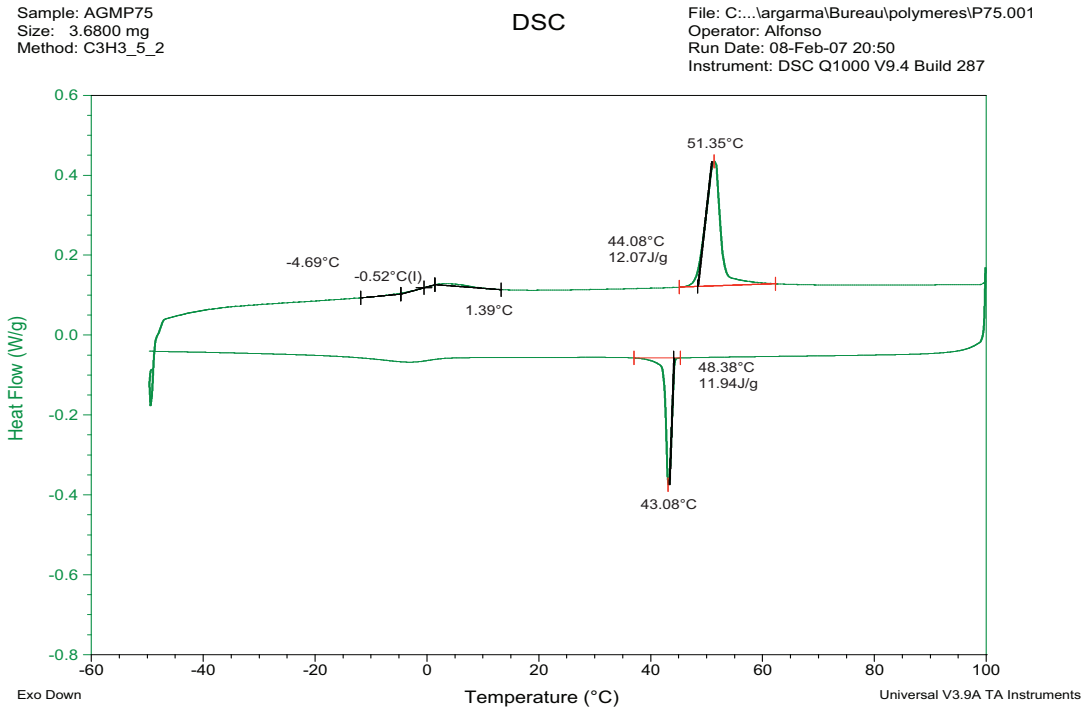

CoP25T

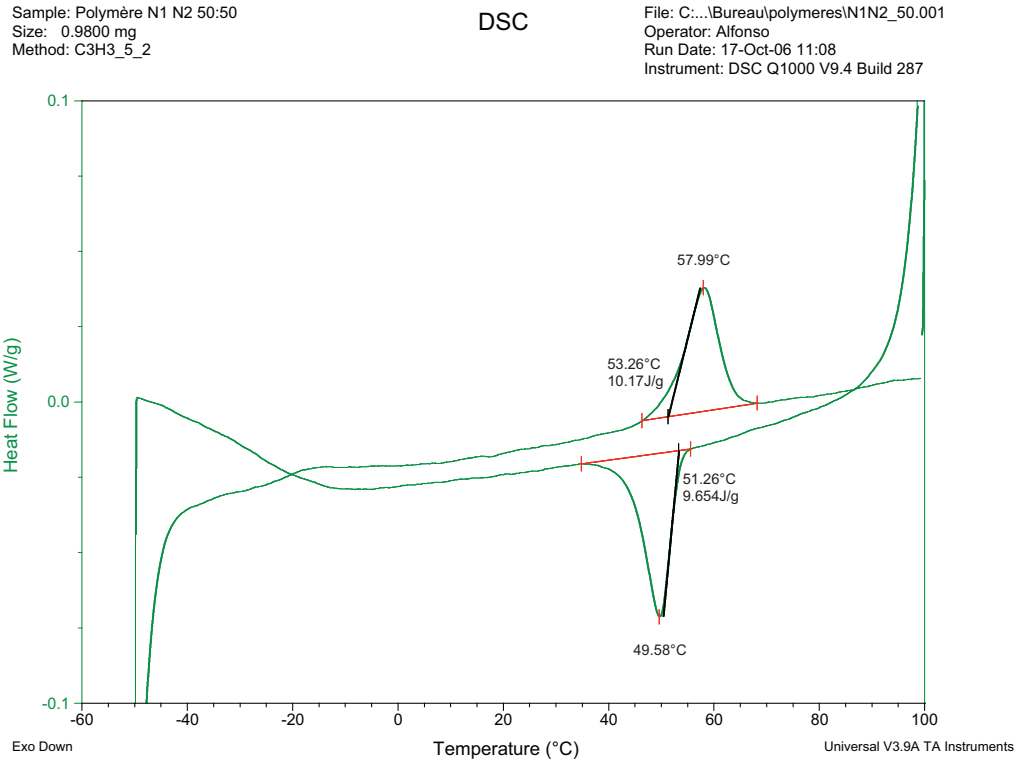

CoP50T

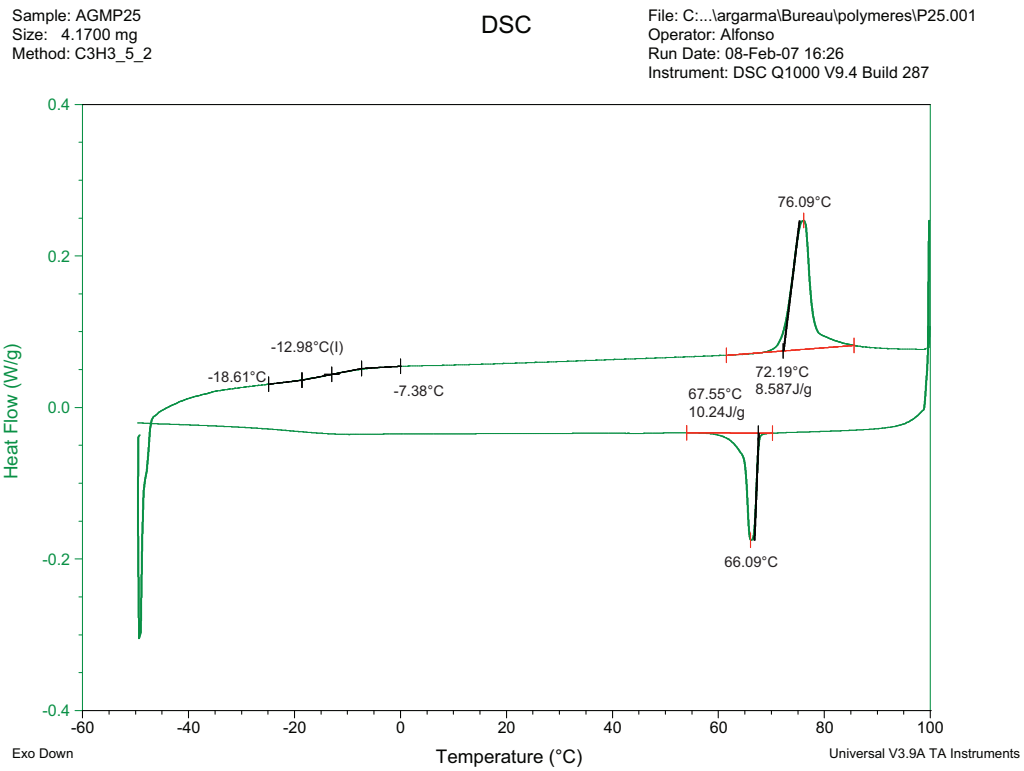

CoP75T

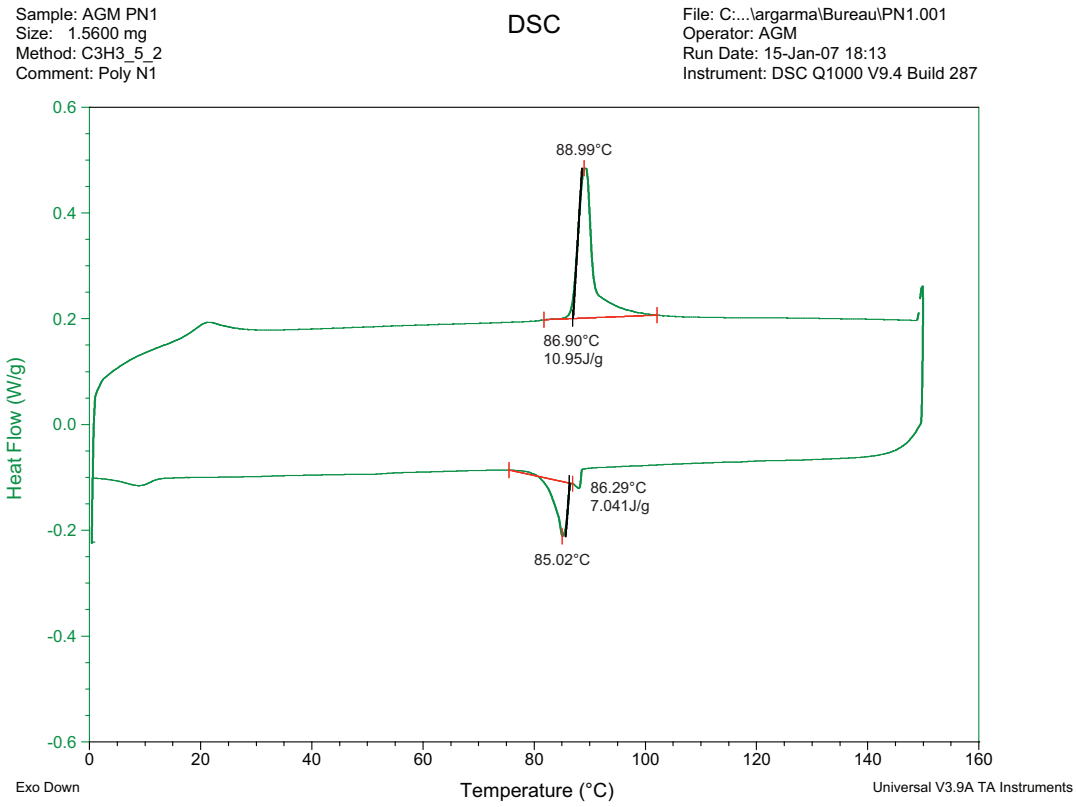
Sample: AGM PN1
Size: 1.5600 mg
Method: C3H3_5_2
Comment: Poly N1
DSC
File: C:...\argarma\Bureau\PN1.001
Operator: AGM
Run Date: 15-Jan-07 18:13
Instrument: DSC Q1000 V9.4 Build 287
88.99°C
86.90°C
10.95J/g
86.29°C
7.041J/g
85.02°C
Heat Flow (W/g)
Temperature (°C)
Exo Down
Universal V3.9A TA Instruments

PN1T

Disiloxane Polymers.

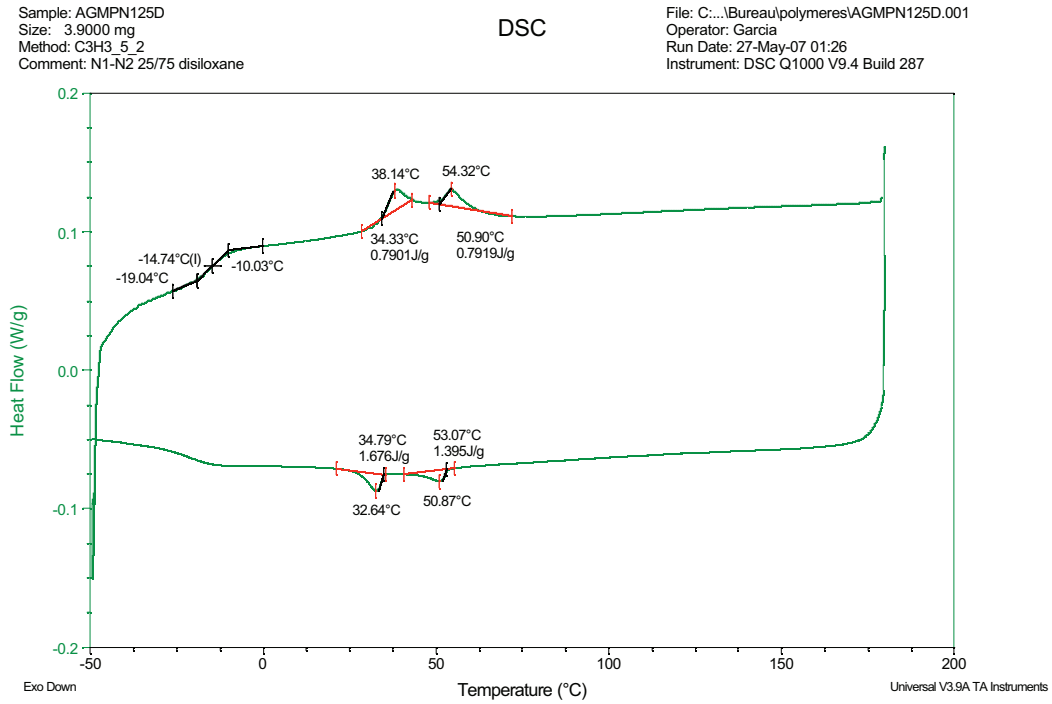

CoP25D

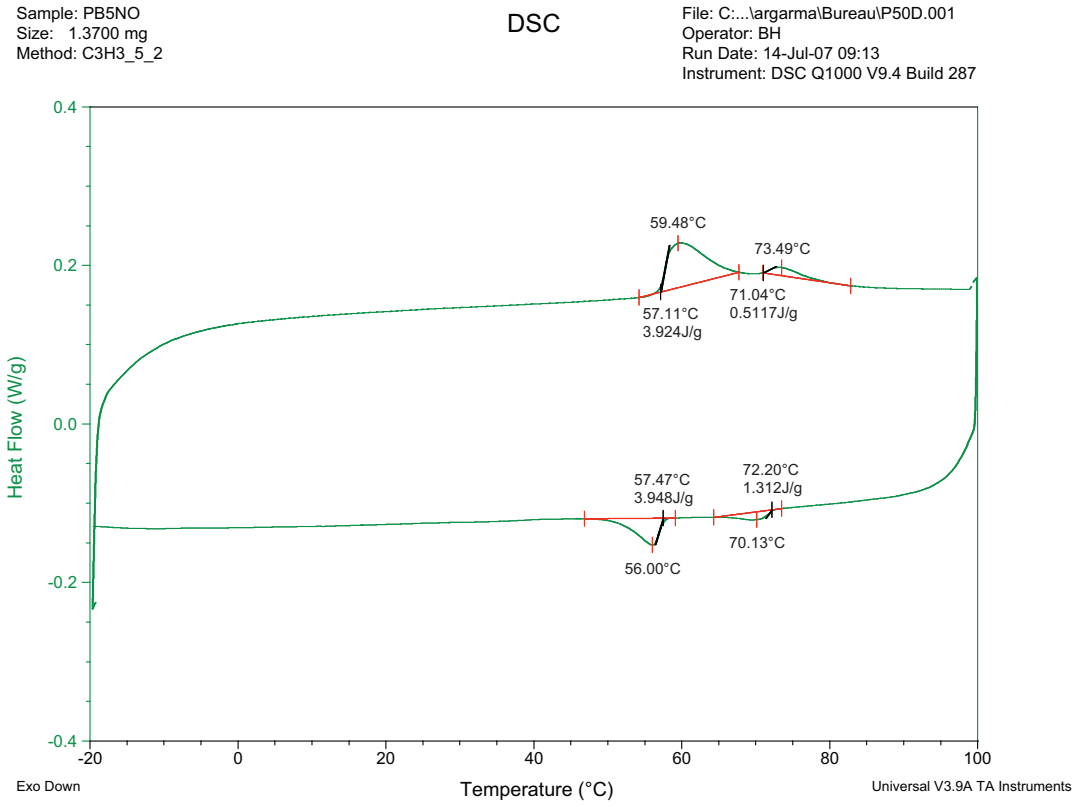

CoP50D

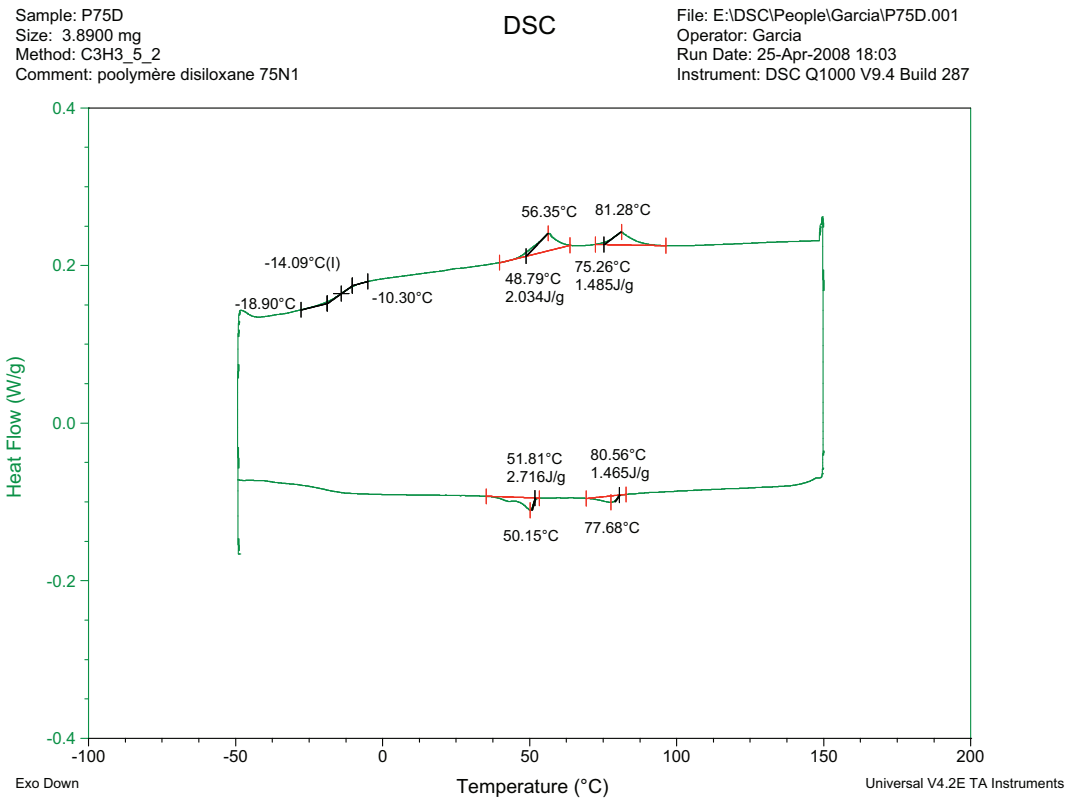
Sample: P75D
Size: 3.8900 mg
Method: C3H3_5_2
Comment: poolymère disiloxane 75N1
DSC
File: E:\DSC\People\Garcia\P75D.001
Operator: Garcia
Run Date: 25-Apr-2008 18:03
Instrument: DSC Q1000 V9.4 Build 287
56.35°C
81.28°C
-14.09°C(I)
-18.90°C
-10.30°C
48.79°C
2.034J/g
75.26°C
1.485J/g
51.81°C
2.716J/g
80.56°C
1.465J/g
50.15°C
77.68°C
Heat Flow (W/g)
Temperature (°C)
Exo Down
Universal V4.2E TA Instruments

CoP75D

Bent-Core Polymers.

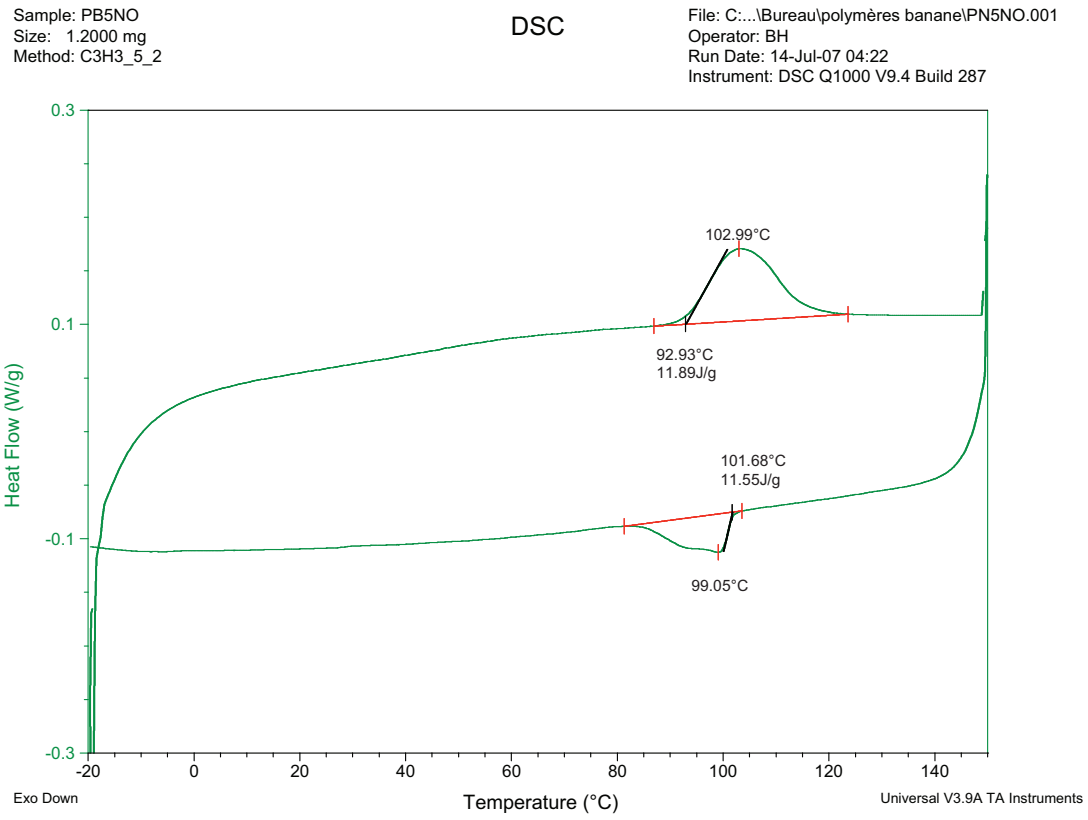

PB1

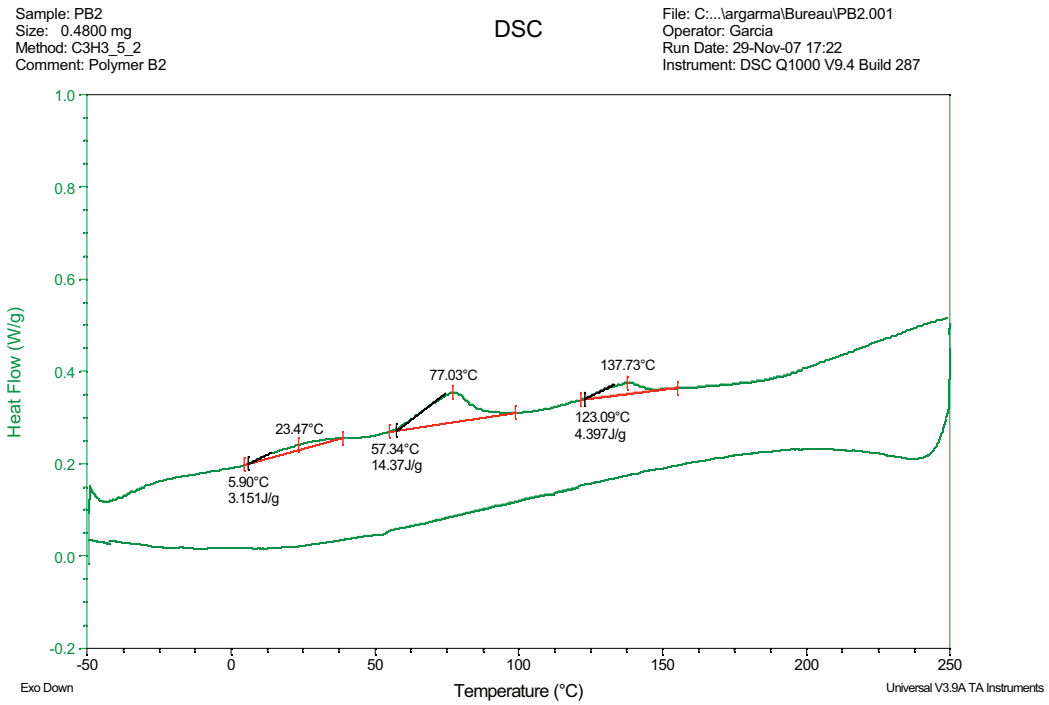

PB2

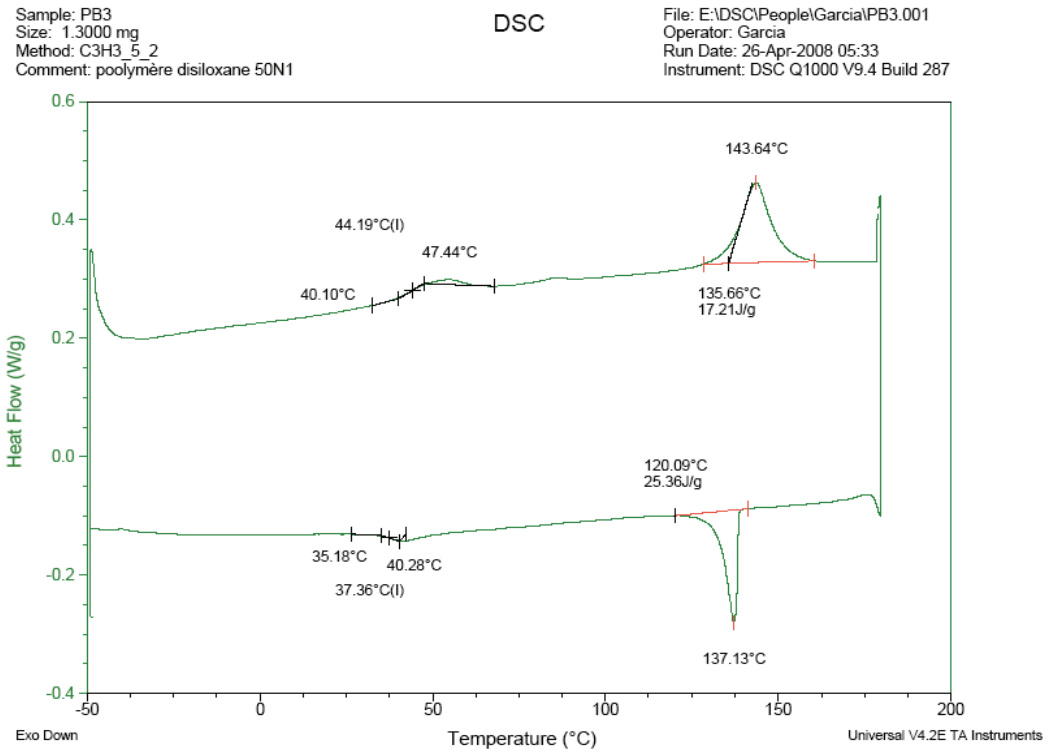
Sample: PB3
Size: 1.3000 mg
Method: C3H3_5_2
Comment: poolymère disiloxane 50N1
DSC
File: E:\DSC\People\Garcia\PB3.001
Operator: Garcia
Run Date: 26-Apr-2008 05:33
Instrument: DSC Q1000 V9.4 Build 287
143.64°C
44.19°C(I)
47.44°C
40.10°C
135.66°C
17.21J/g
120.09°C
25.36J/g
35.18°C
40.28°C
37.36°C(I)
137.13°C
Heat Flow (W/g)
Exo Down
Temperature (°C)
Universal V4.2E TA Instruments

PB3

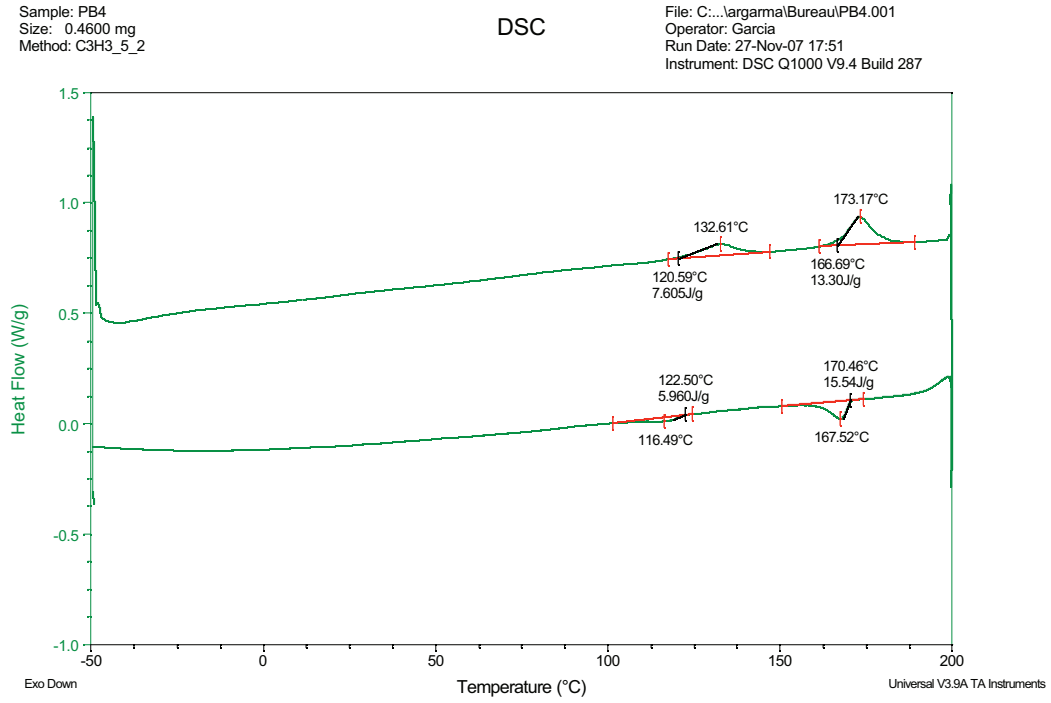
Sample: PB4
Size: 0.4600 mg
Method: C3H3_5_2
DSC
File: C:...\argarma\Bureau\PB4.001
Operator: Garcia
Run Date: 27-Nov-07 17:51
Instrument: DSC Q1000 V9.4 Build 287
173.17°C
132.61°C
120.59°C
7.605J/g
166.69°C
13.30J/g
122.50°C
5.960J/g
170.46°C
15.54J/g
116.49°C
167.52°C
Heat Flow (W/g)
Exo Down
Temperature (°C)
Universal V3.9A TA Instruments

PB4

Trisiloxane elastomers.

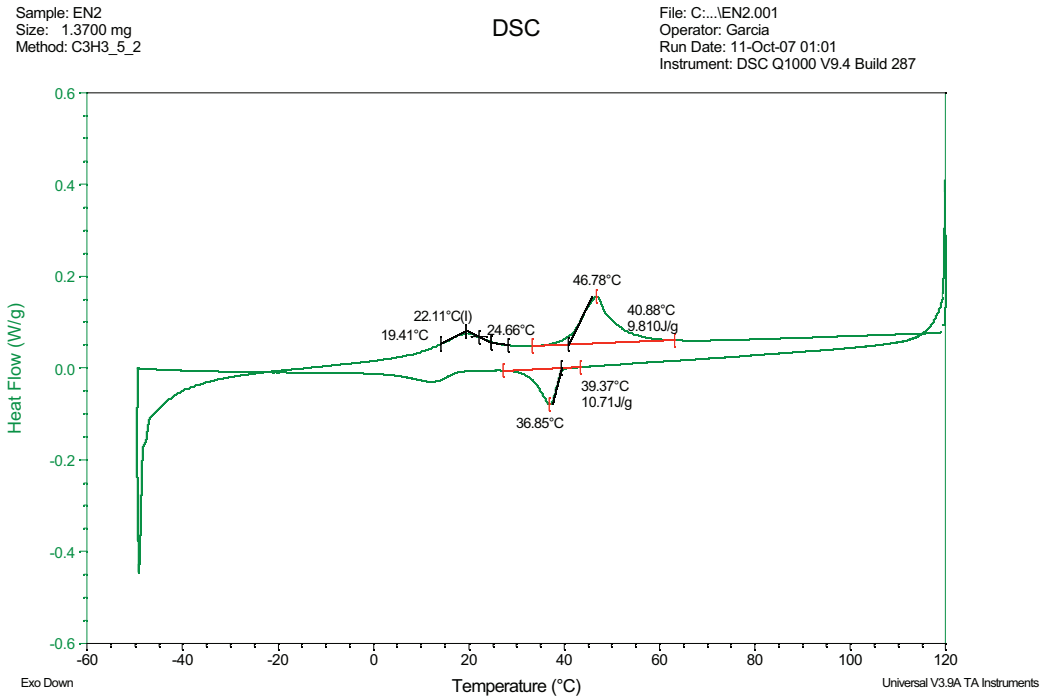

EN2T

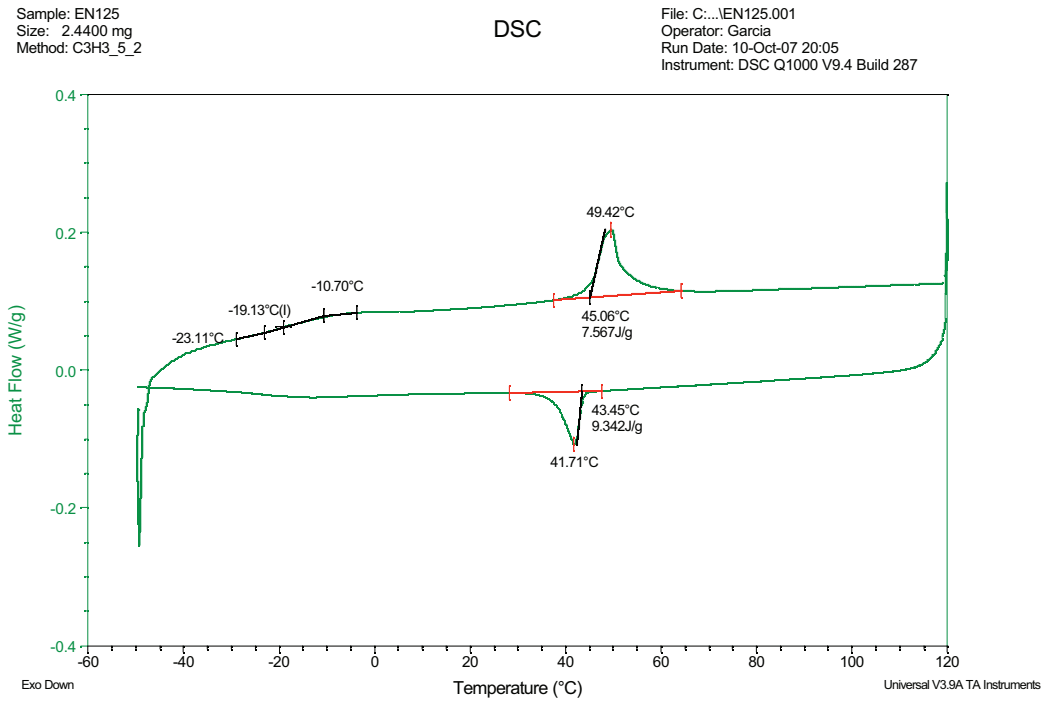

CoE25T

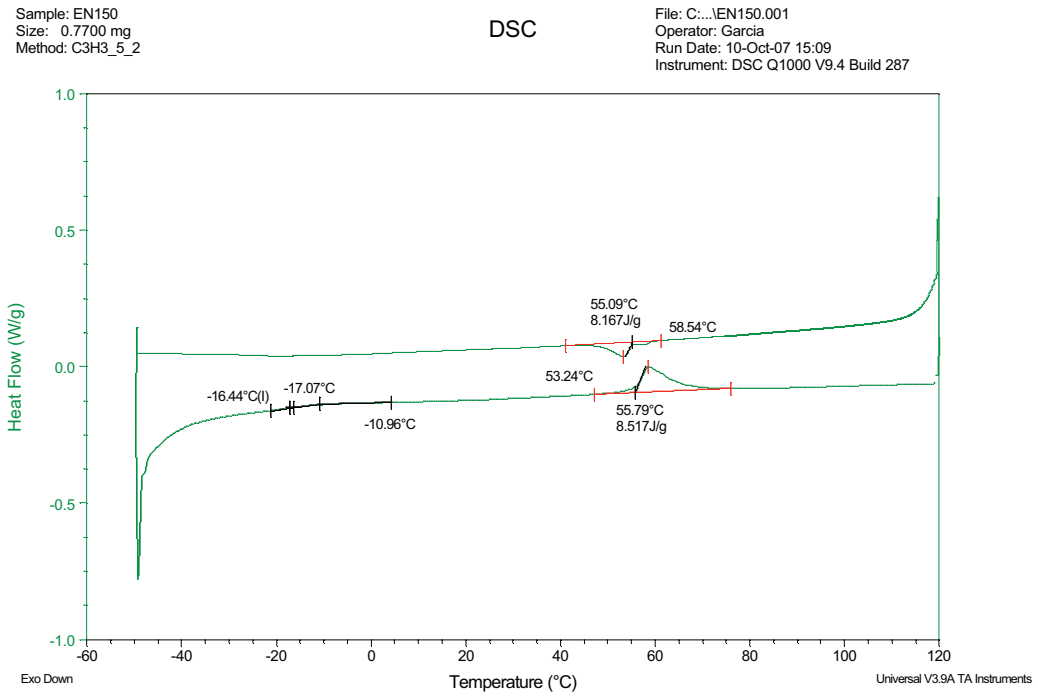

CoE50T

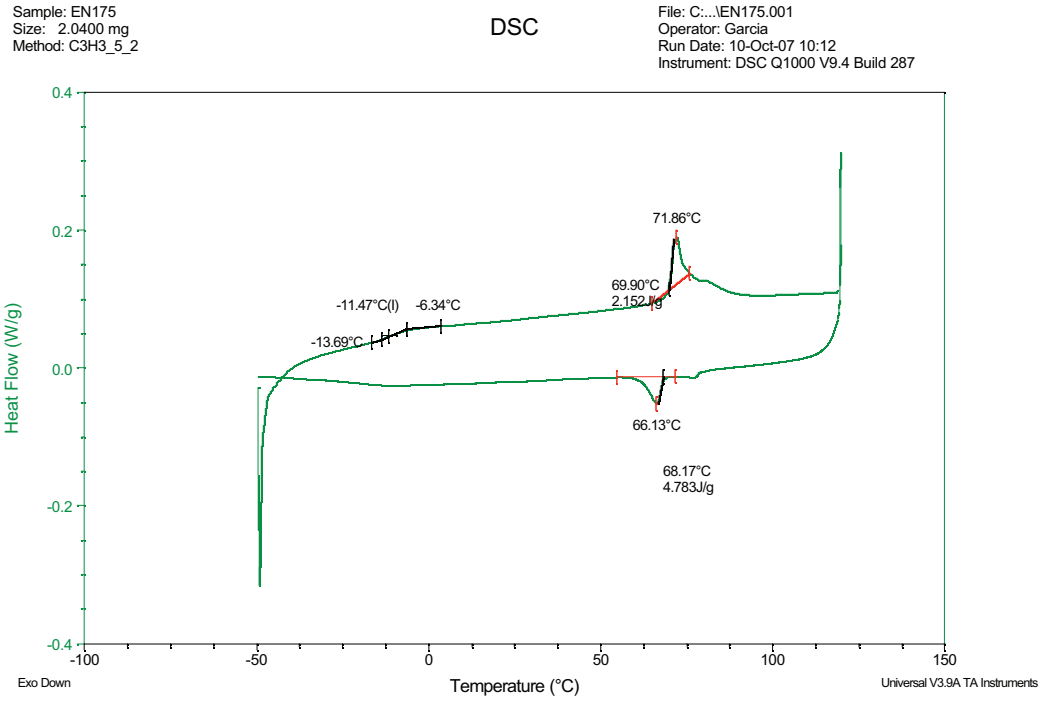

CoE75T

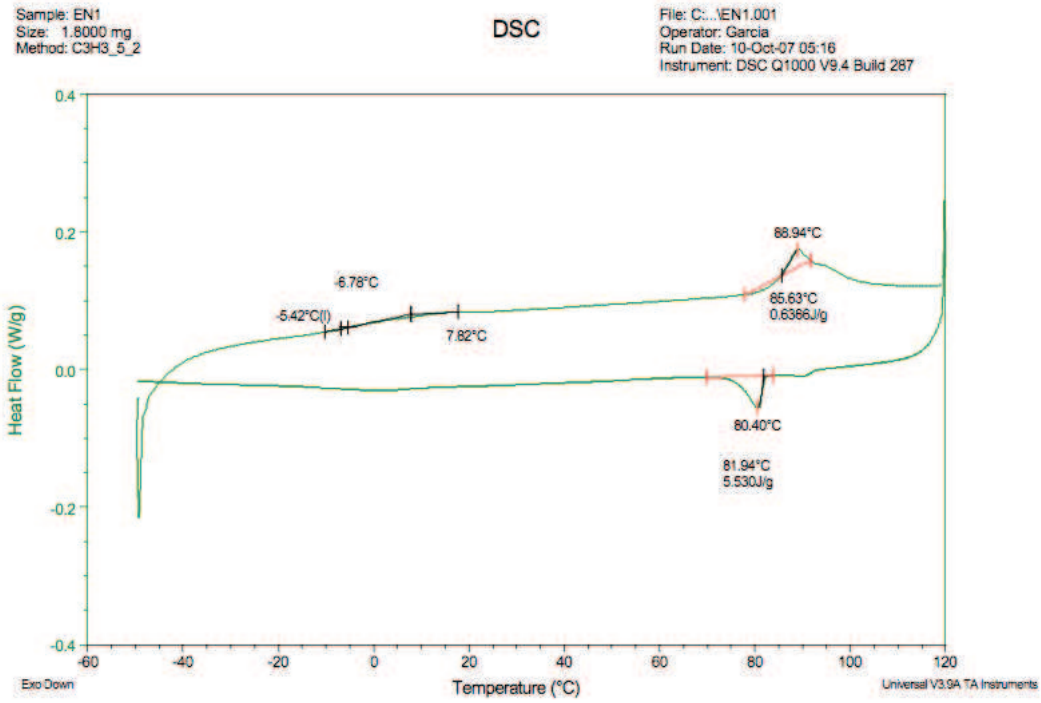
Sample: EN1
Size: 1.8000 mg
Method: C3H3_5_2
DSC
File: C:...\EN1.001
Operator: Garcia
Run Date: 10-Oct-07 05:16
Instrument: DSC Q1000 V9.4 Build 287
Heat Flow (W/g)
0.4
0.2
0.0
-0.2
-0.4
-6.78°C
-5.42°C(I)
7.82°C
88.94°C
85.63°C
0.6366J/g
80.40°C
81.94°C
5.530J/g
-60
-40
-20
0
20
40
60
80
100
120
Exo Down
Temperature (°C)
Universal V3.9A TA Instruments

EN1T

Disiloxane Coelastomers.

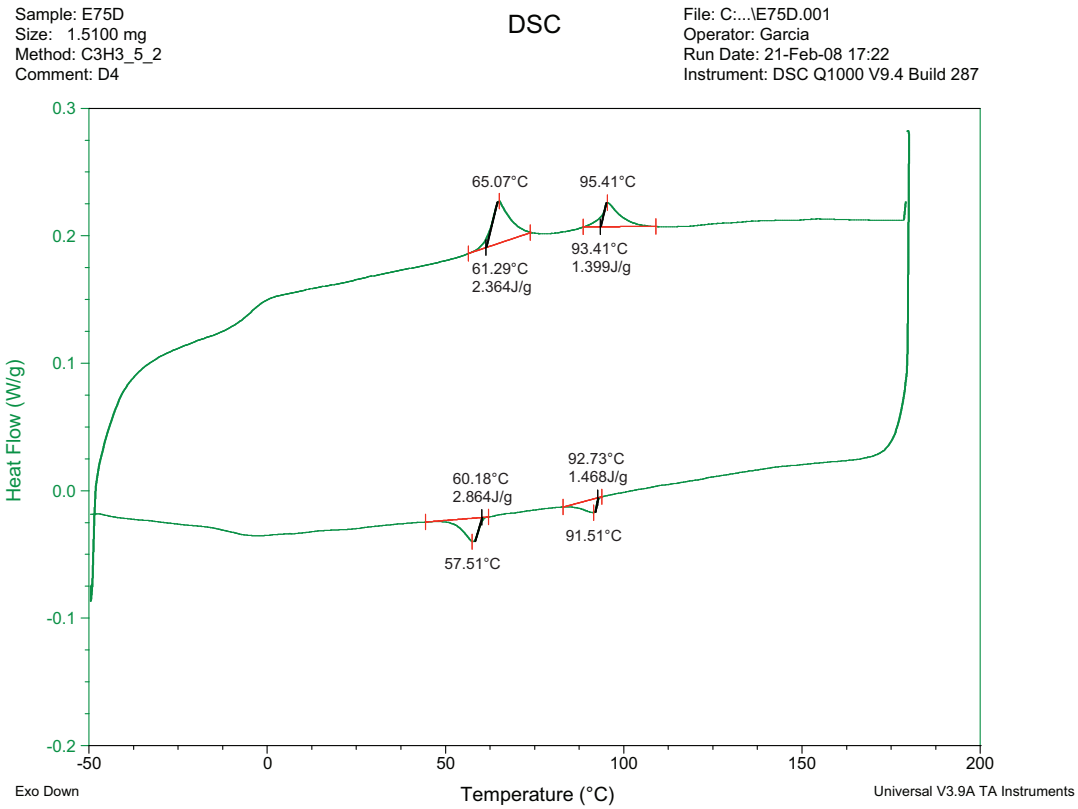

CoE25D

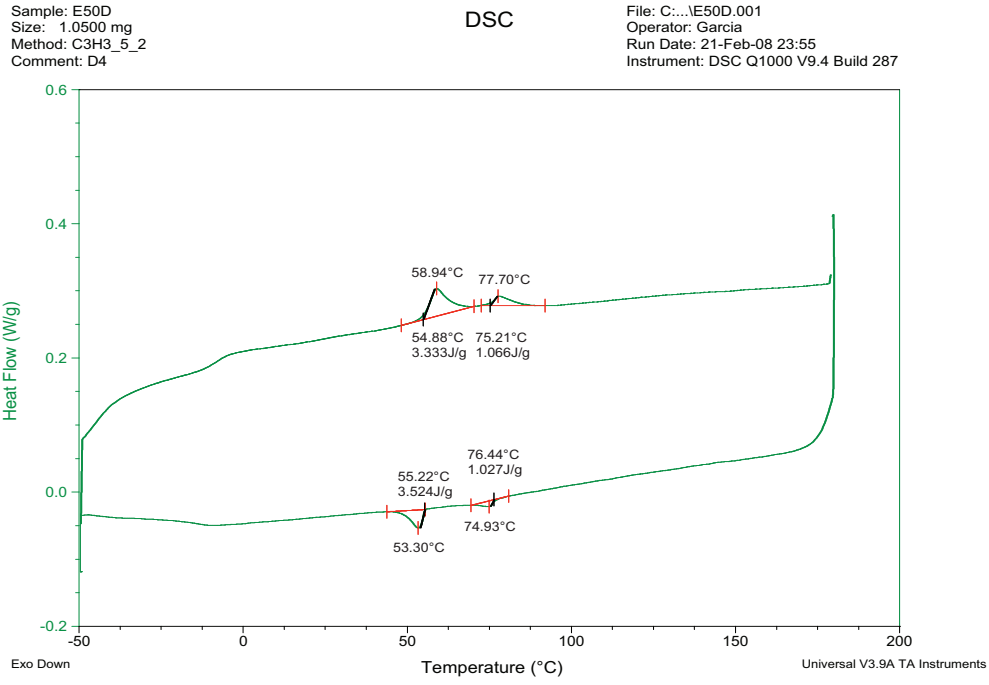

CoE50D

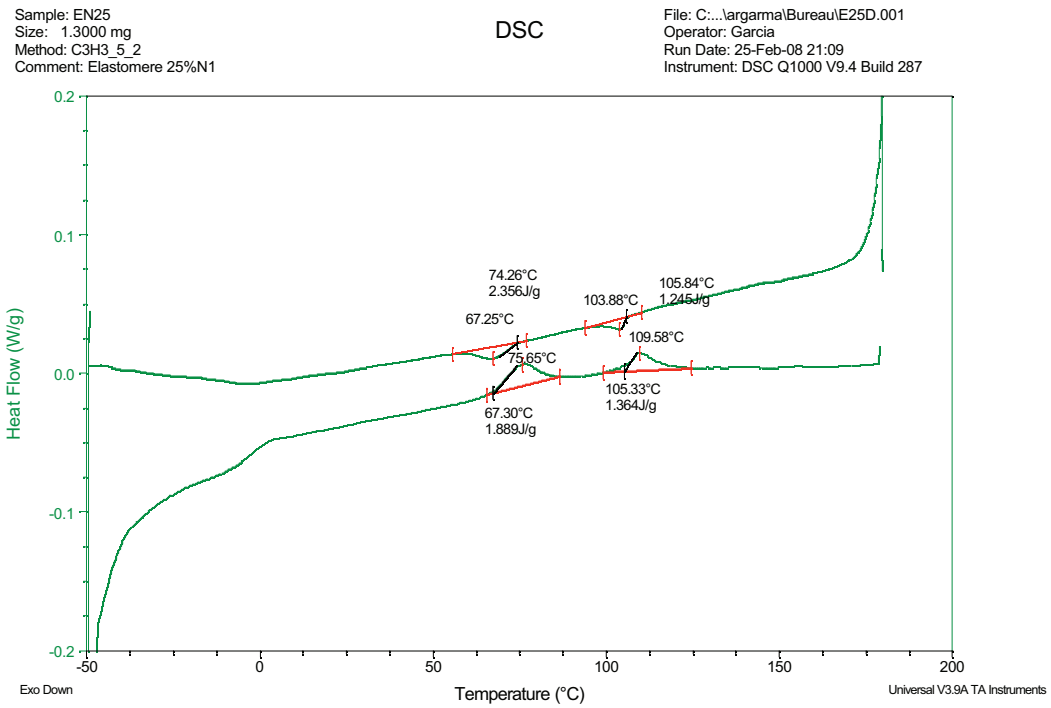
Sample: EN25
Size: 1.3000 mg
Method: C3H3_5_2
Comment: Elastomere 25%N1
DSC
File: C:...\argarma\Bureau\E25D.001
Operator: Garcia
Run Date: 25-Feb-08 21:09
Instrument: DSC Q1000 V9.4 Build 287
Heat Flow (W/g)
0.2
0.1
0.0
-0.1
-0.2
74.26°C
2.356J/g
67.25°C
75.65°C
67.30°C
1.889J/g
103.88°C
105.84°C
1.245J/g
109.58°C
105.33°C
1.364J/g
-50
0
50
100
150
200
Exo Down
Temperature (°C)
Universal V3.9A TA Instruments

CoE75D

Bent-Core/Calamitic Mesogen Liquid Crystalline Coelastomers.

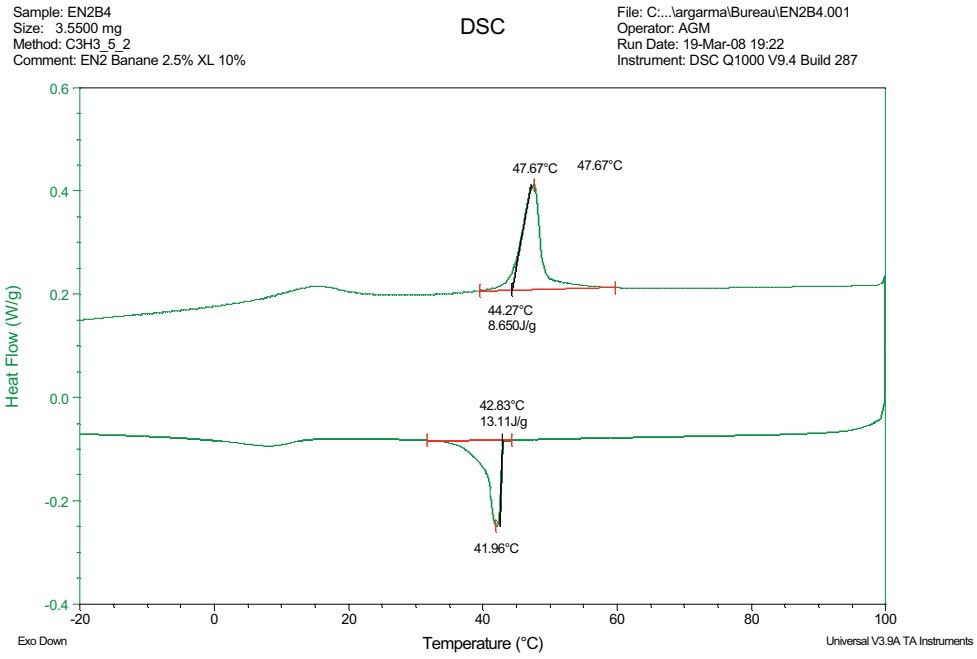

CoEN2B4D 5%

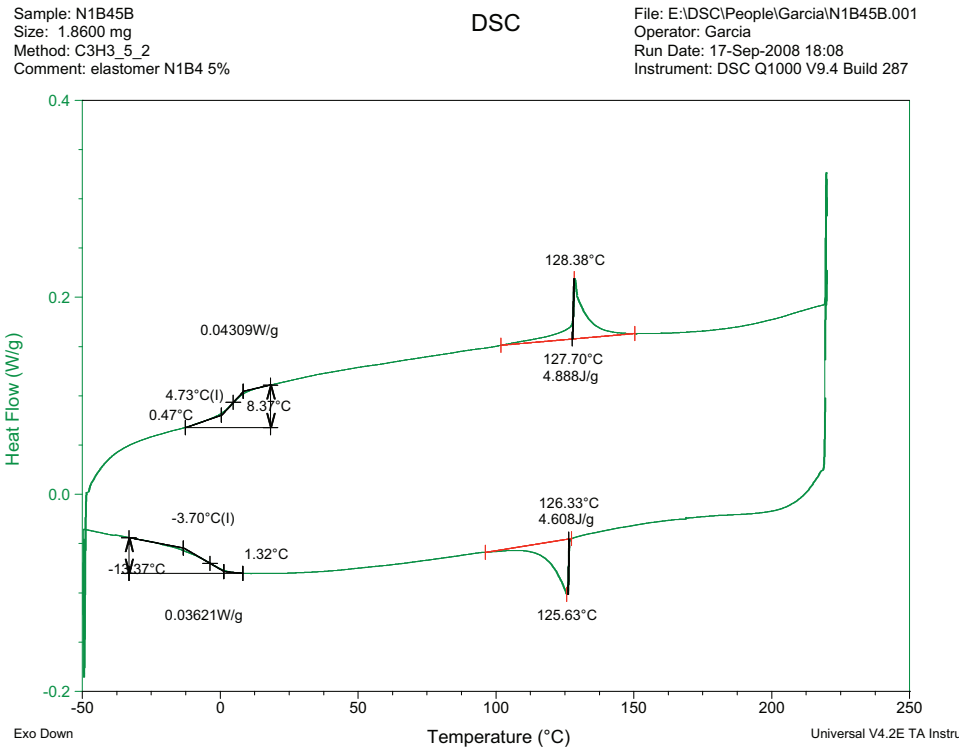

CoEN1B4D 5%

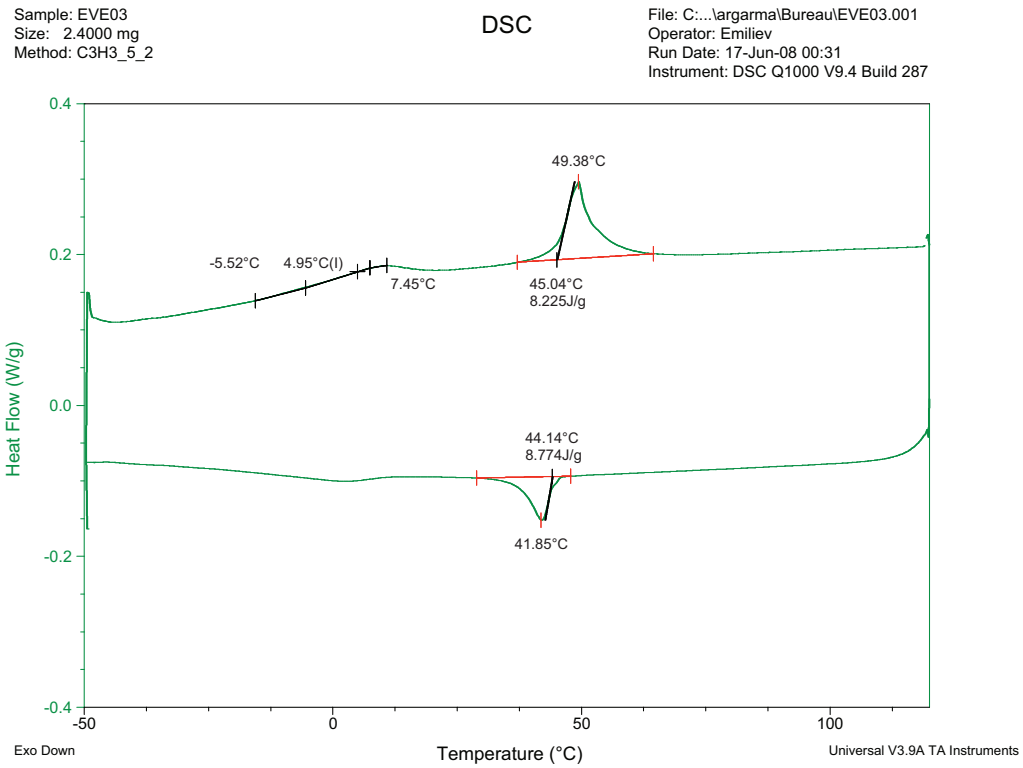

CoEN2B6D 5%

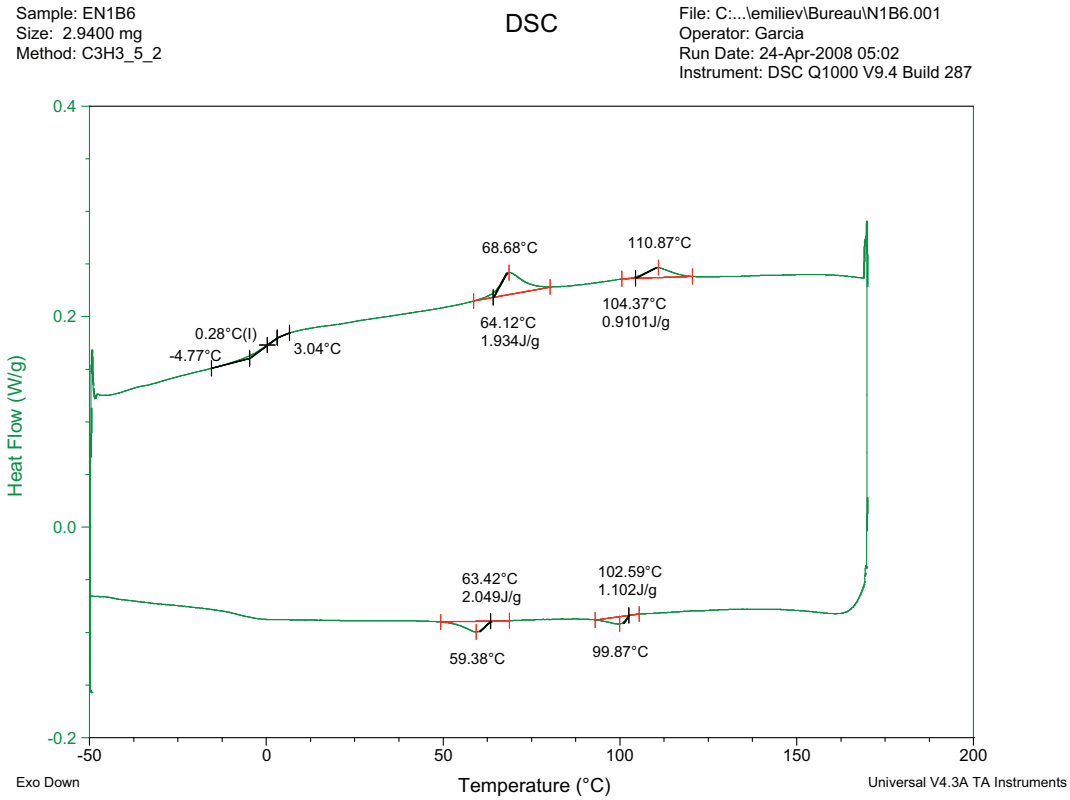

CoEN1B6D 5%

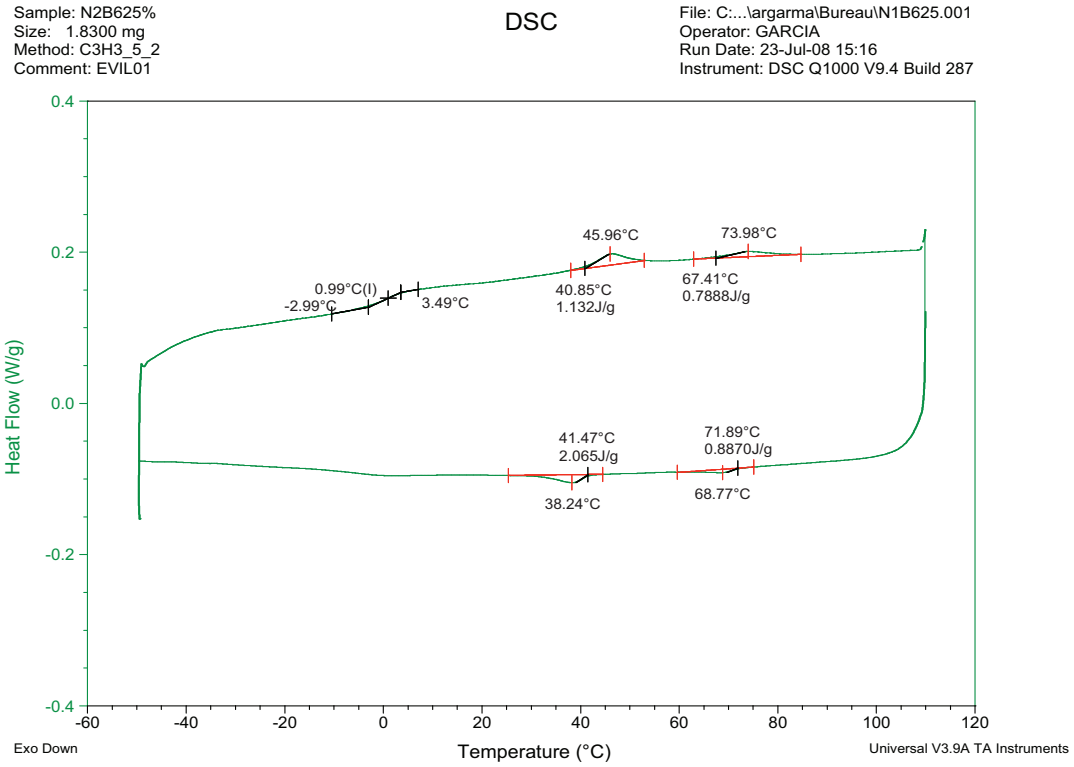

CoEN1B6D 25%

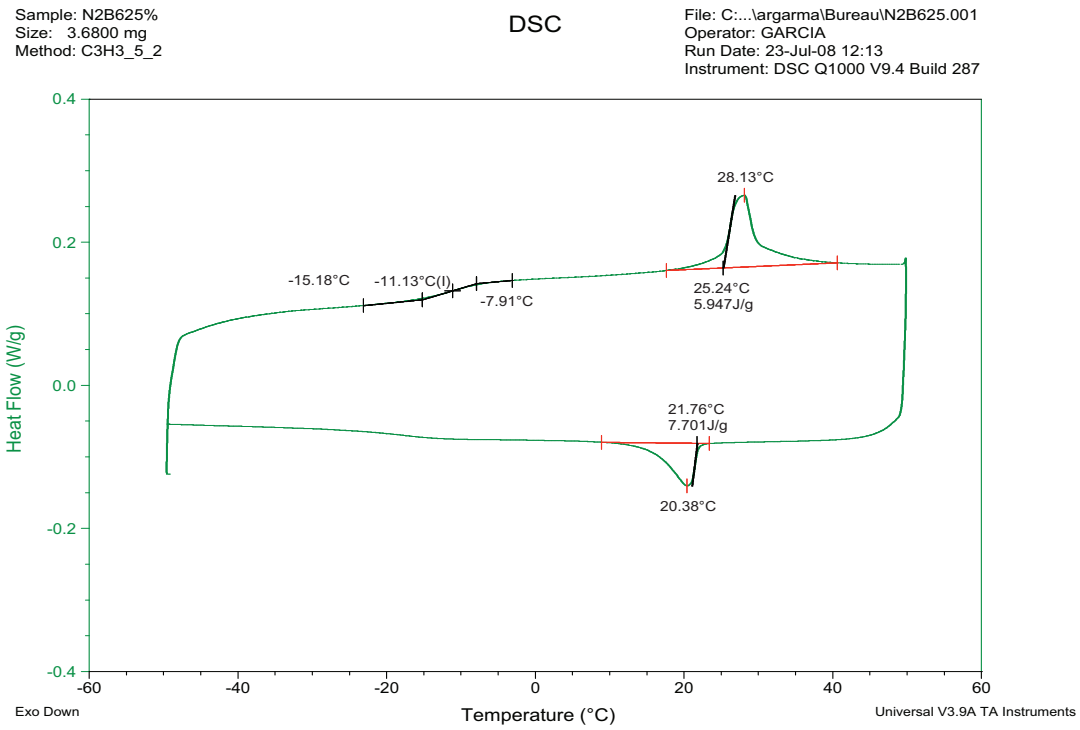

CoEN2B6D 25%

Appendix C

C. Rheological Studies.

C.1. General Considerations.

All the temperature ramp experiments were performed at an oscilating frequency of 1 Hz and a strain of 0.1%.

C.2. Frequency Scan Plots.

C.2.1. *CoE25T*

Frequency scans performed at different temperatures:

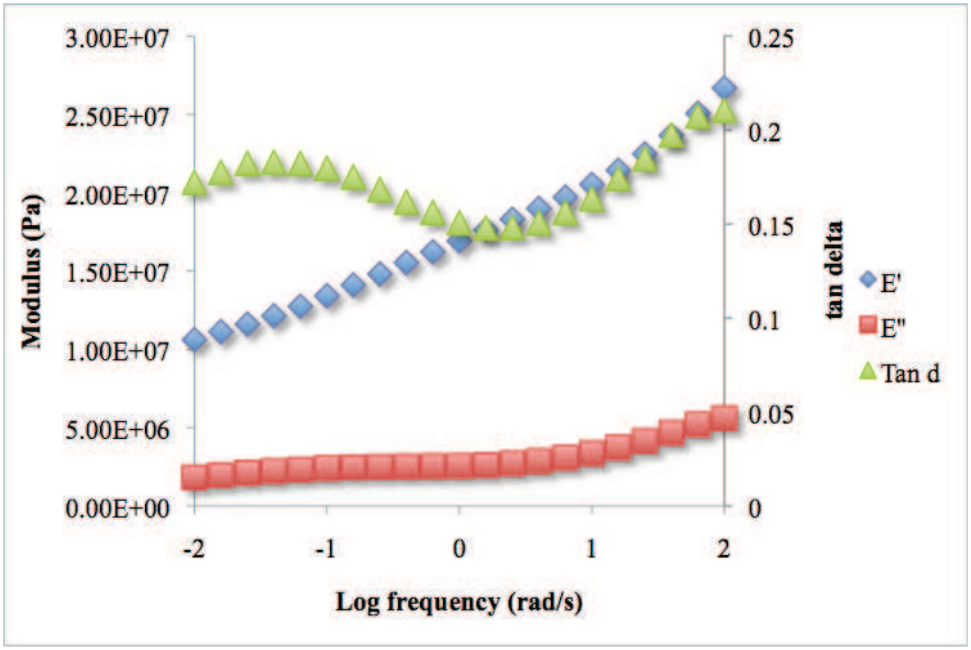

Plot C.I. At 40ºC from 100 to 0.01 rad/s.

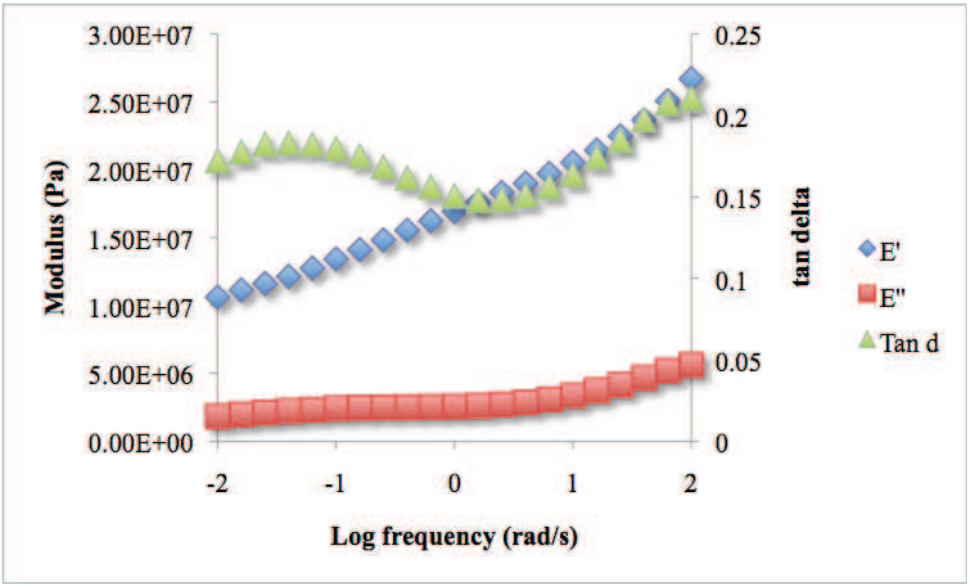

Plot C.II. At 45ºC from 100 to 0.01 rad/s.

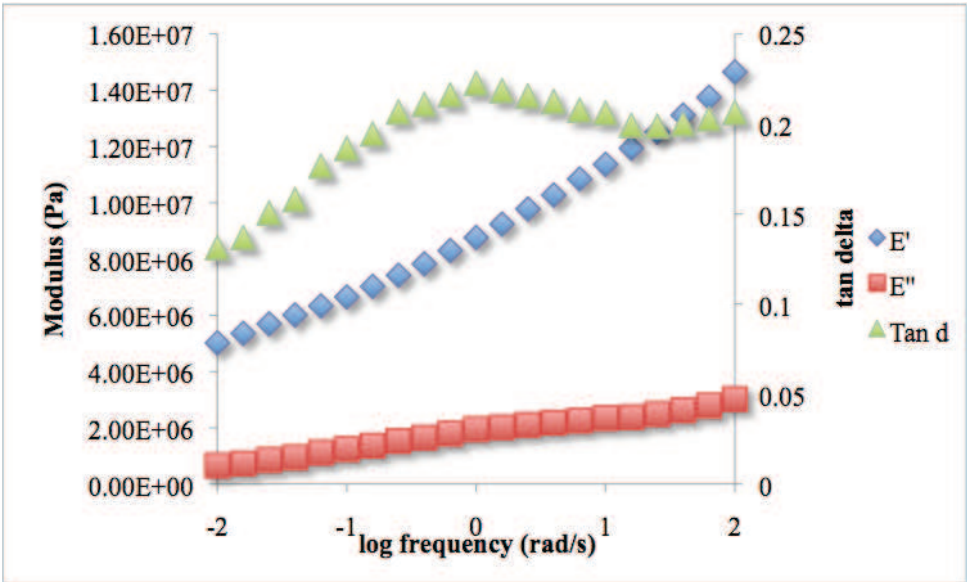

Plot C.III. At 65ºC from 100 to 0.01 rad/s.

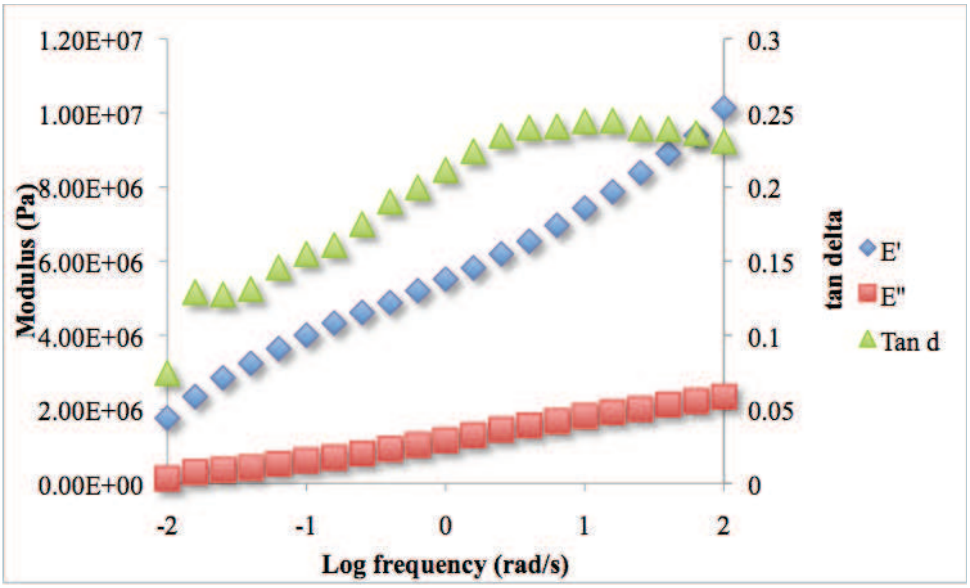

Plot C.IV. At 75ºC from 100 to 0.01 rad/s.

C.2.2. *CoE50T*

Frequency scans performed at different temperatures:

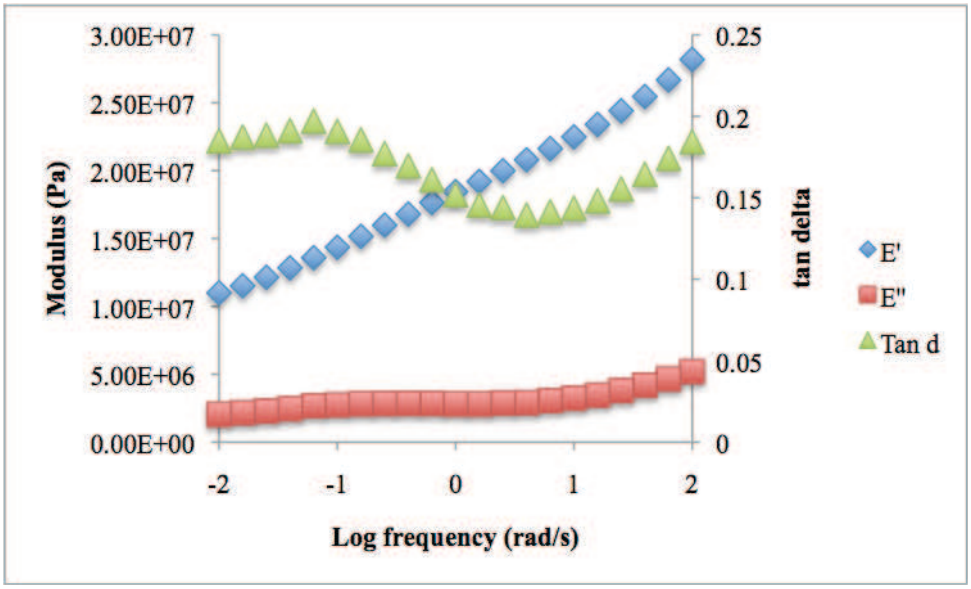

Plot C.V. At 40ºC frequency from 100 to 0.01 rad/s.

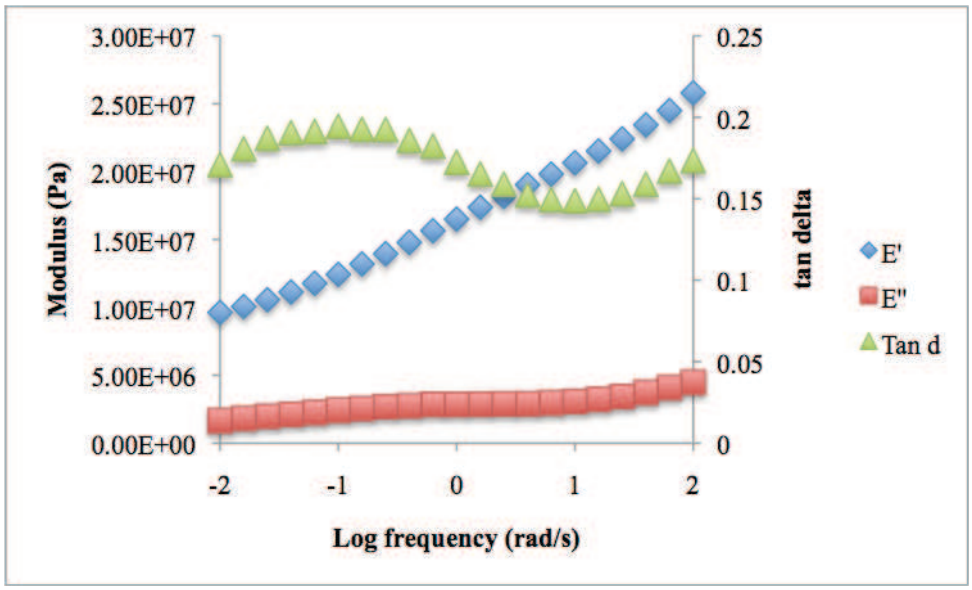

Plot C.VI. At 45ºC frequency from 100 to 0.01 rad/s.

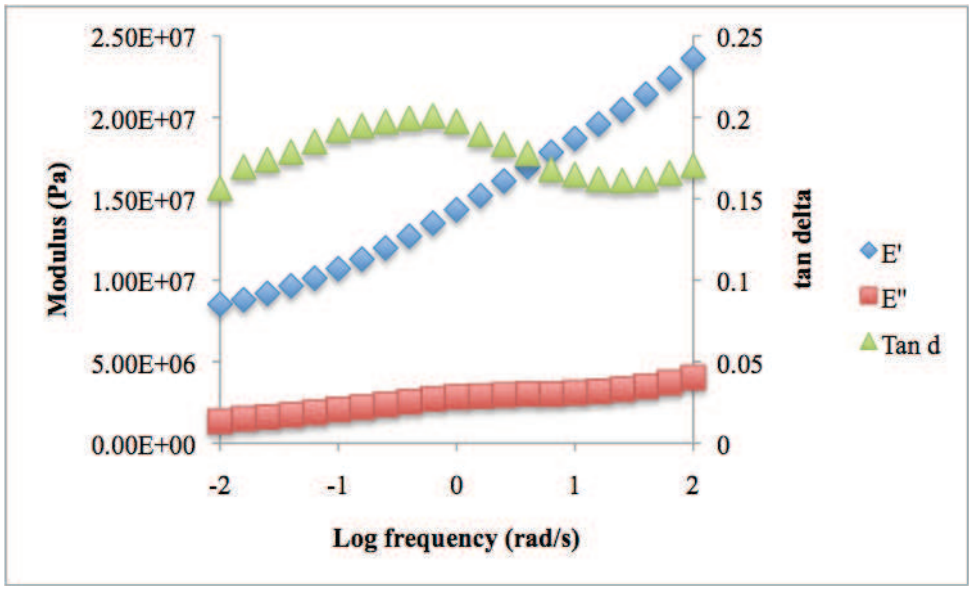

Plot C.VII. At 50ºC frequency from 100 to 0.01 rad/s.

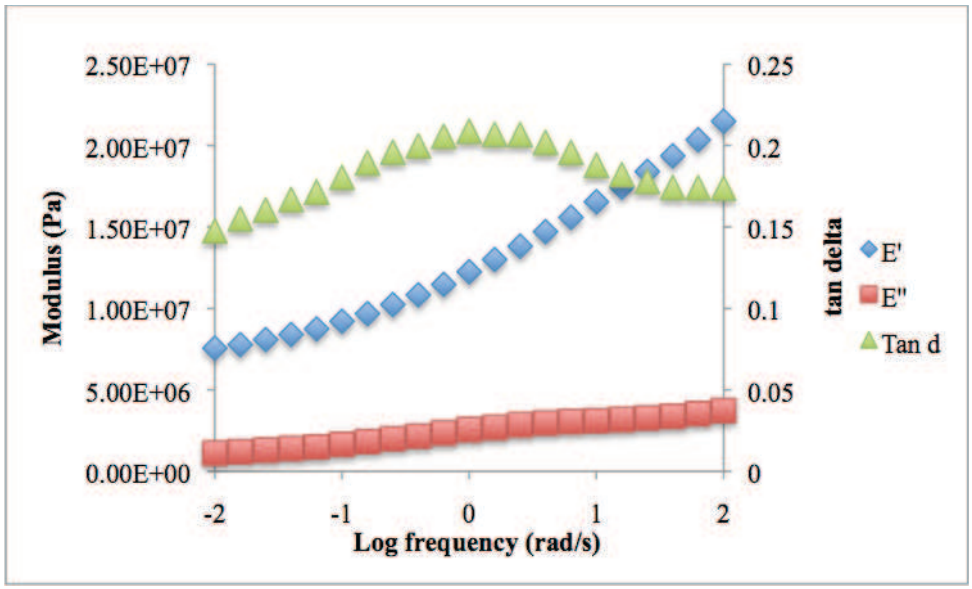

Plot C.VIII. At 55ºC frequency from 100 to 0.01 rad/s.

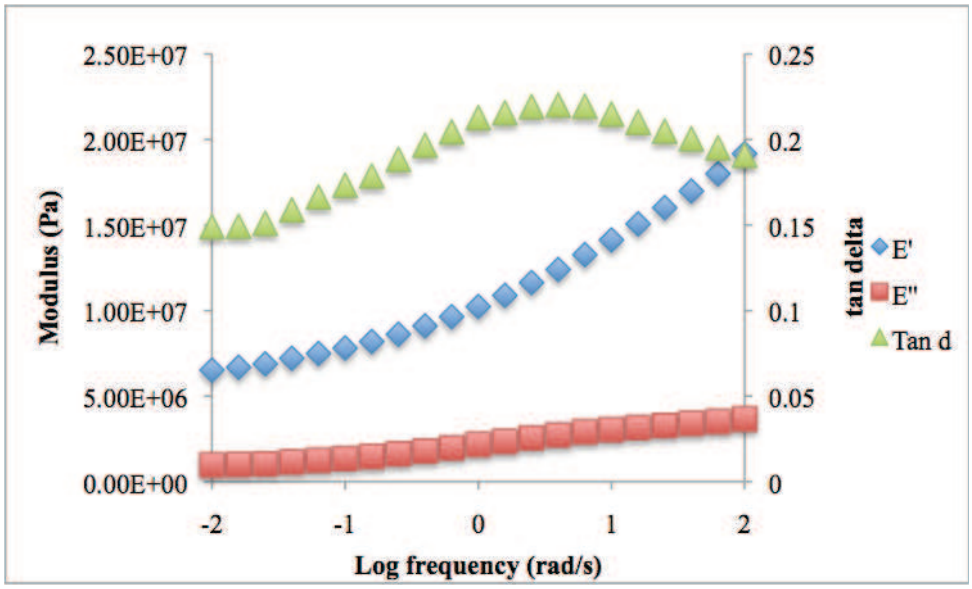

Plot C.IX. At 60ºC frequency from 100 to 0.01 rad/s.

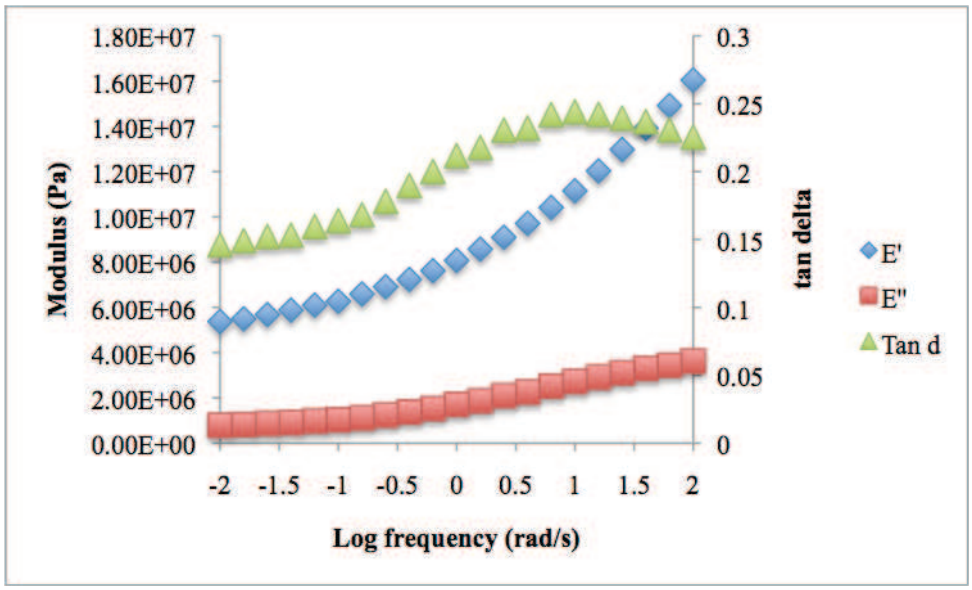

Plot C.X. At 65ºC frequency from 100 to 0.01 rad/s.

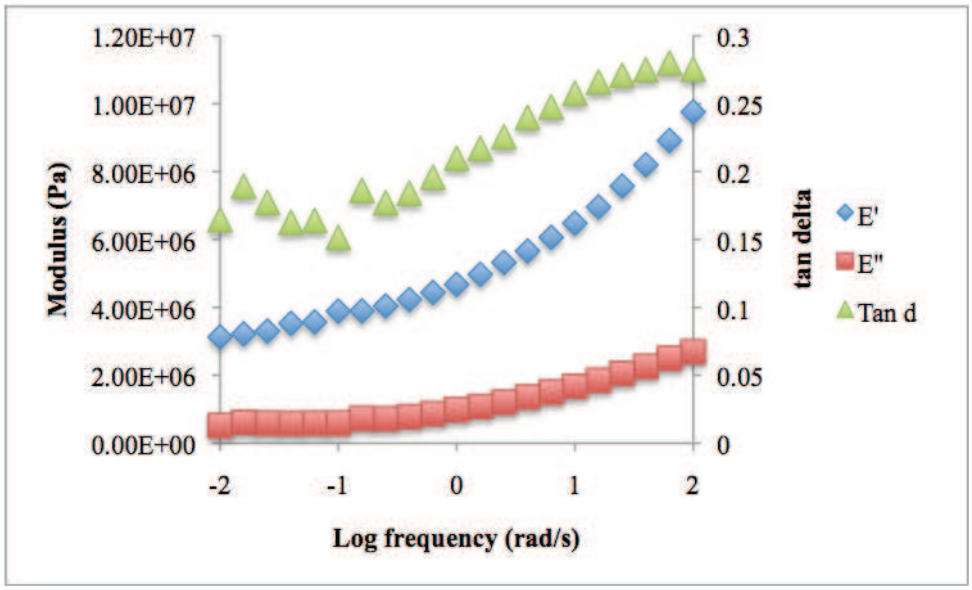

Plot C.XI. At 70ºC frequency from 100 to 0.01 rad/s.

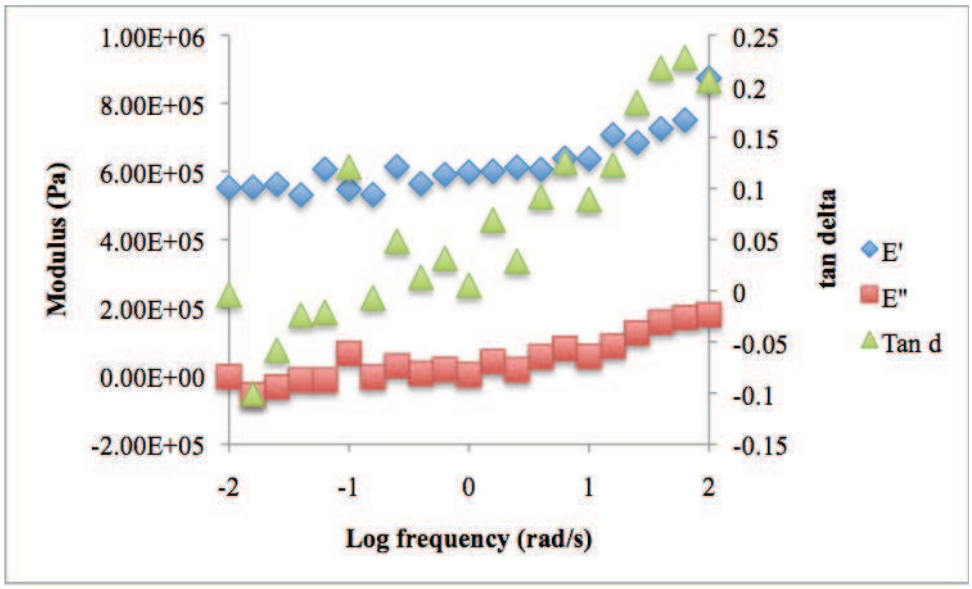

Plot C.XII. At 75ºC frequency from 100 to 0.01 rad/s.

C.2.3. *CoE25D*

Frequency scans performed at different temperatures:

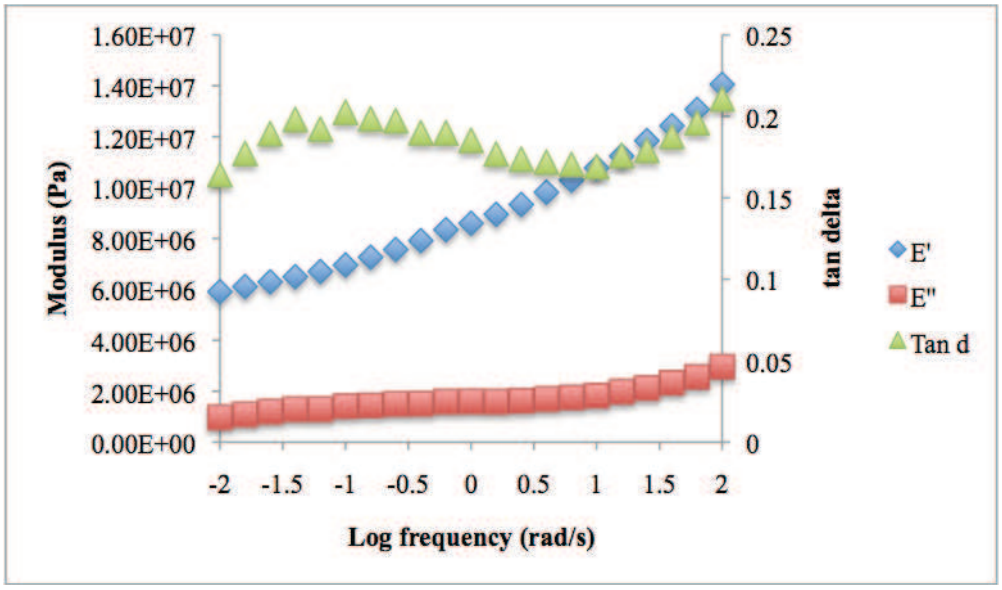

Plot C.XIII. 55ºC frequency from 100 to 0.01 rad/s.

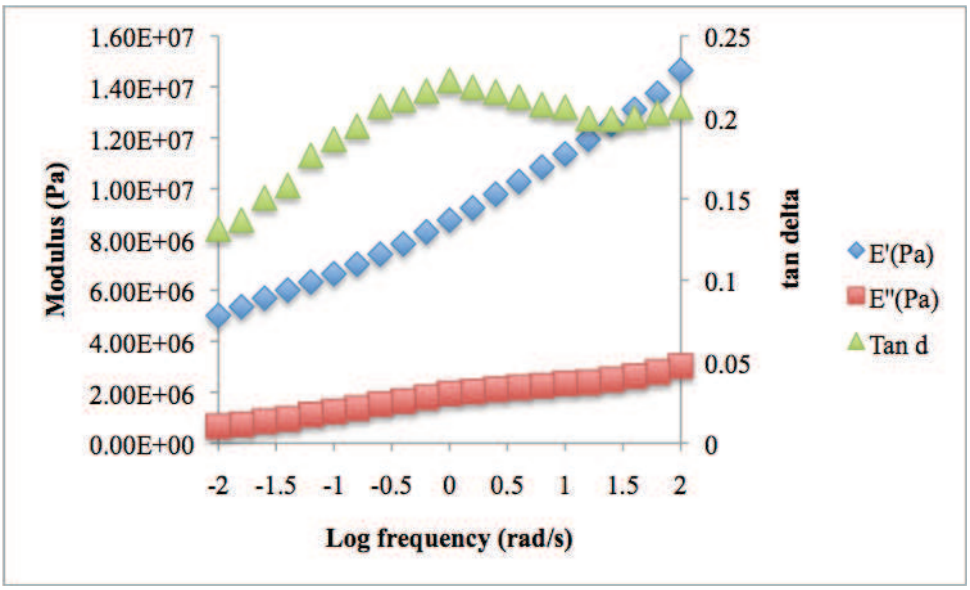

Plot C.XIV. 65ºC frequency from 100 to 0.01 rad/s.

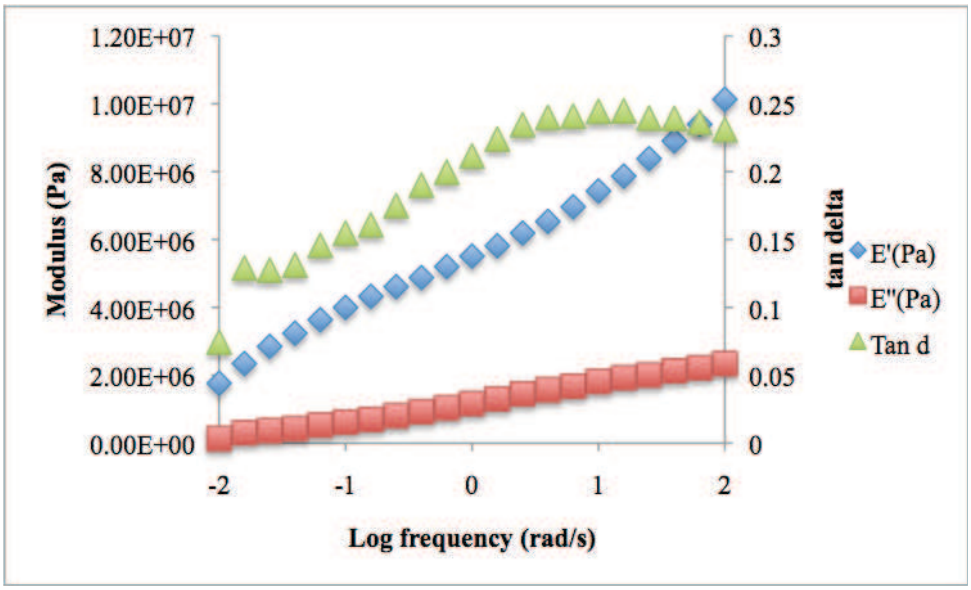

Plot C.XV. 75ºC frequency from 100 to 0.01 rad/s.

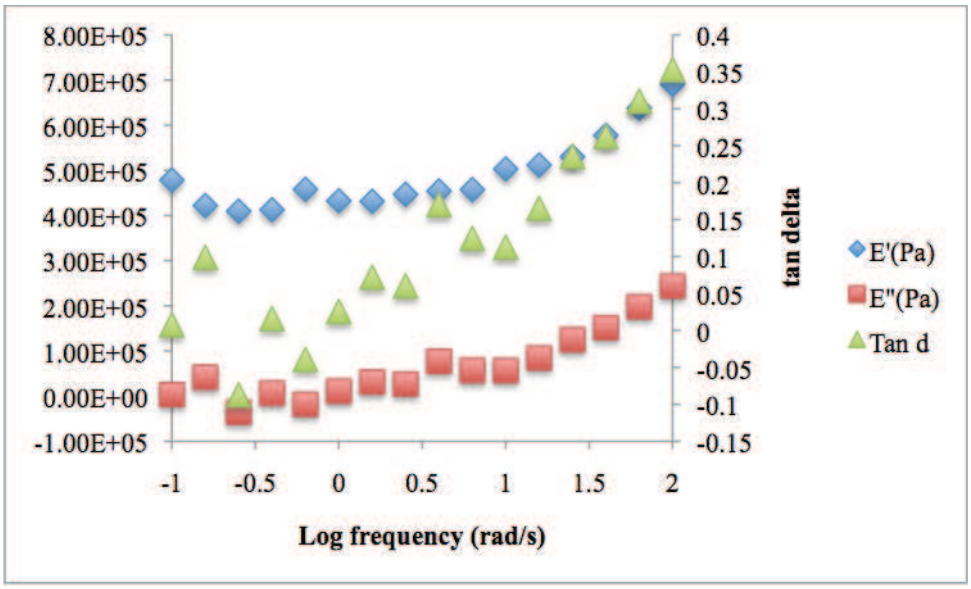

Plot C.XVI. 90ºC frequency from 100 to 0.01 rad/s.

C.2.4. *CoE50D*

Frequency scans performed at different temperatures:

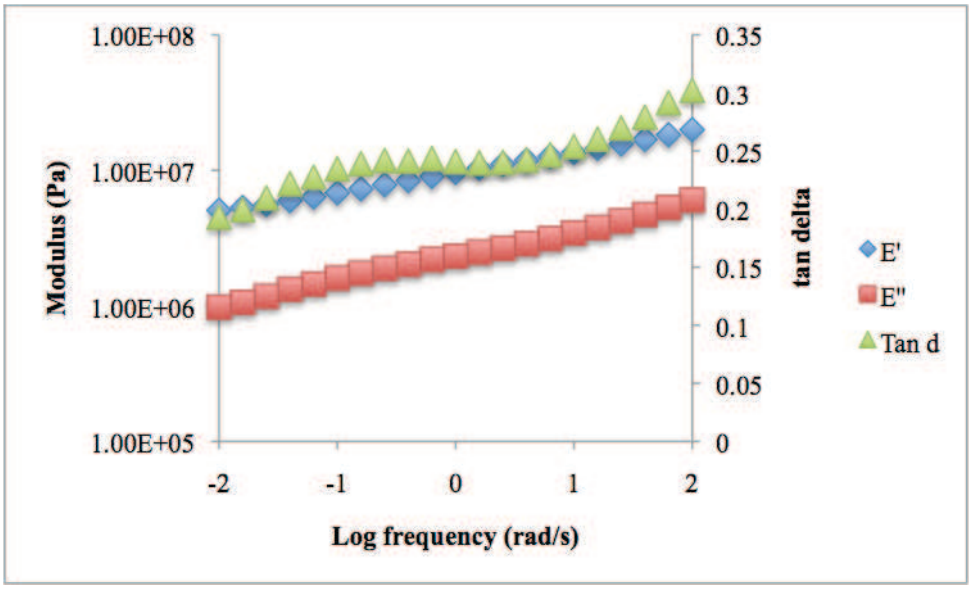

Plot C.XVII. At 40ºC frequency from 100 to 0.01 rad/s.

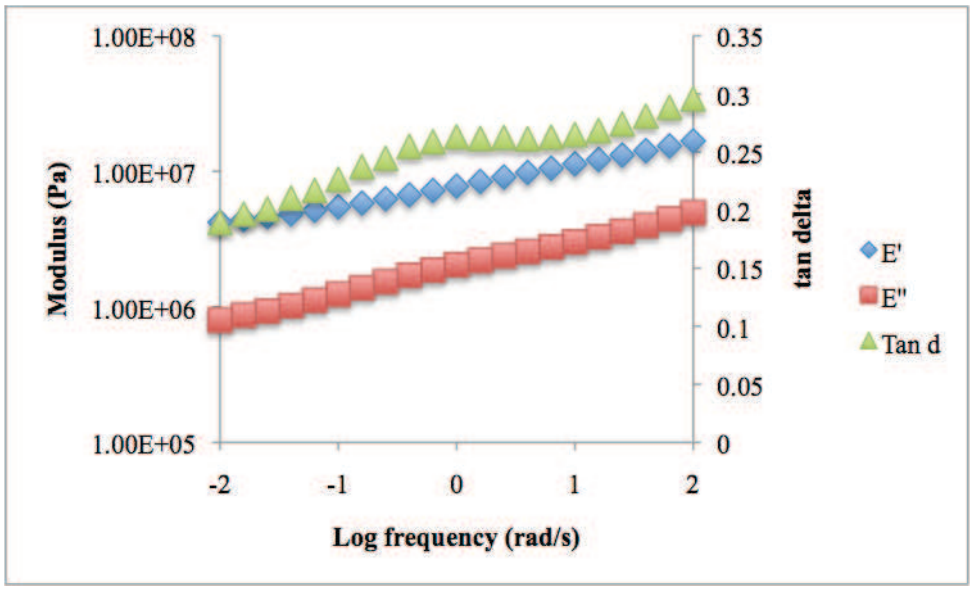

Plot C.XVIII. At 45ºC frequency from 100 to 0.01 rad/s.

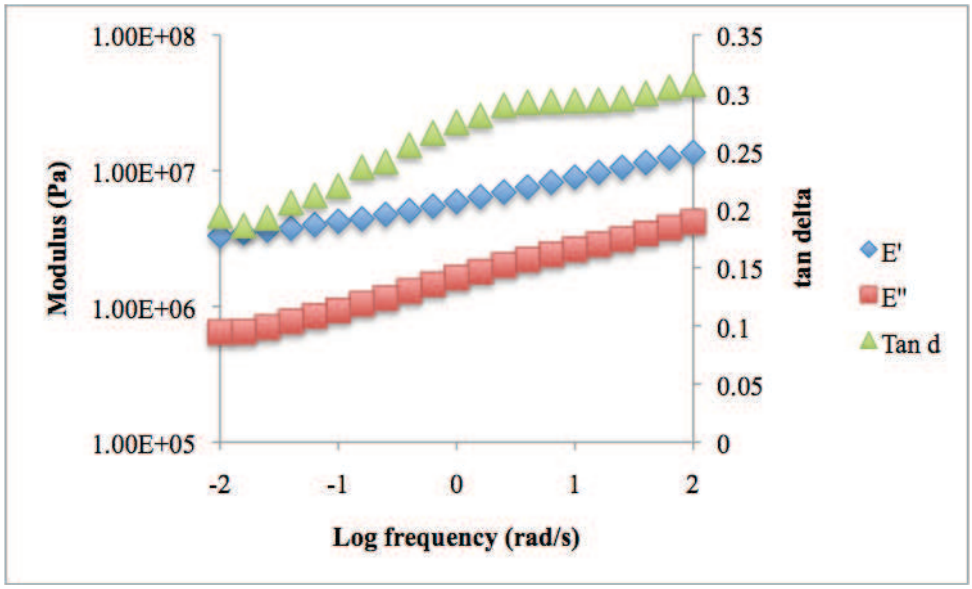

Plot C.XIX. At 50ºC frequency from 100 to 0.01 rad/s.

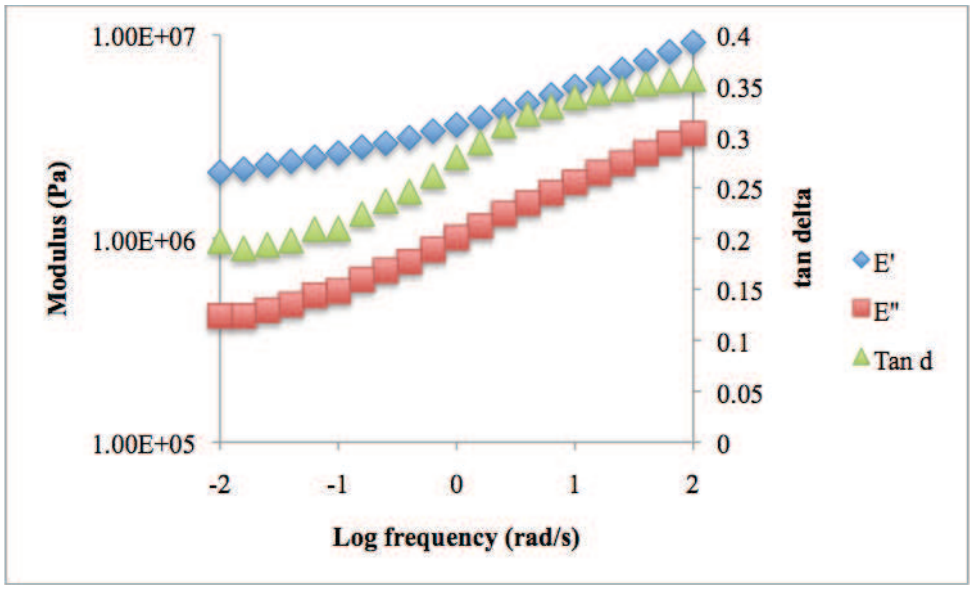

Plot C.XX. At 55ºC frequency from 100 to 0.01 rad/s.

C.3. Comparative Plots.

C.3.1. *Comparative study of trisiloxane series.*

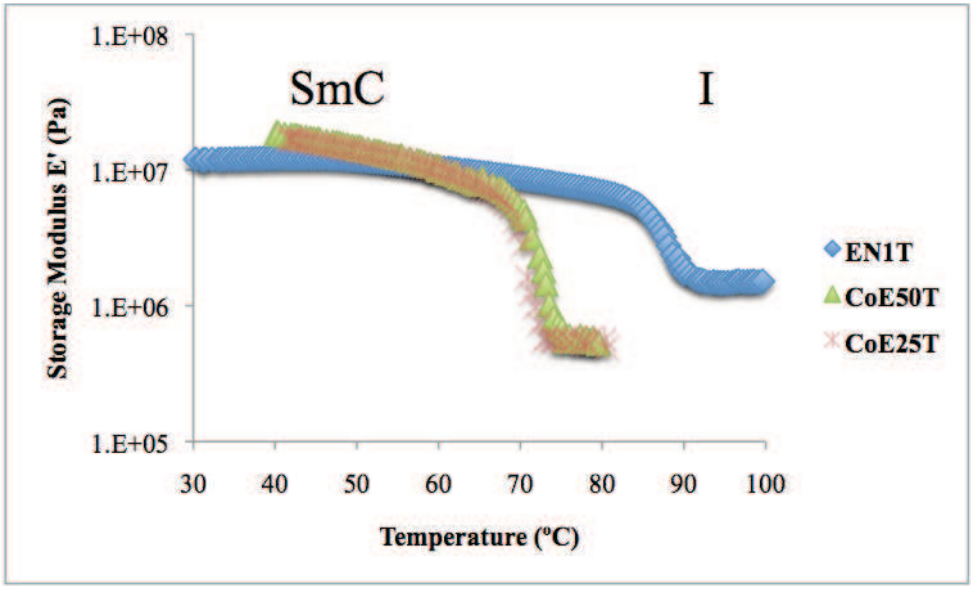

Plot C.XXI. Temperature ramp of trisiloxane temperatures.

C.3.2. *Comparative study of disiloxane coelastomers*

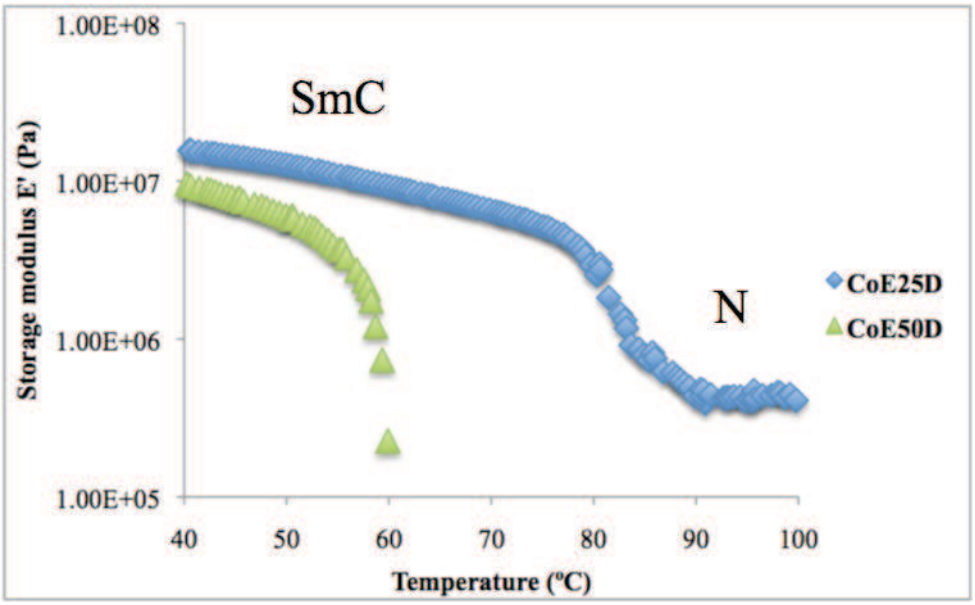

Plot C.XXII. Temperature ramp of disiloxane elastomers.

C.3.3. *Comparative study between disiloxane and trisiloxane analogues*

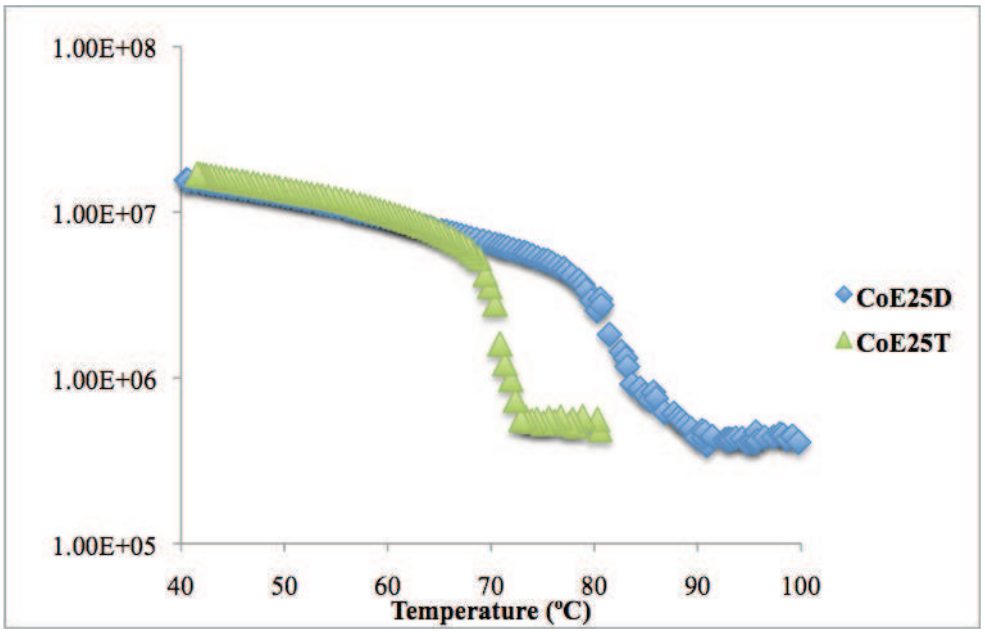

Plot C.XXIII. Temperature ramp of **CoE25** coelastomers.

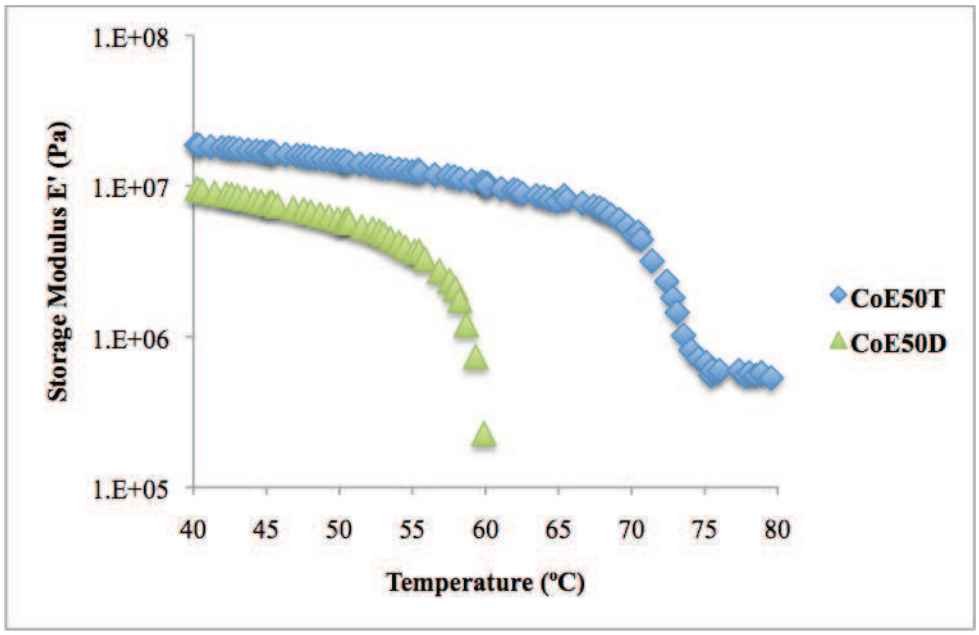

Plot C.XXIV. Ramp temperature for **CoE50** analogues.

C.3.4. *Comparative study of E' at relative temperatures for trisiloxane samples*

Since comparing the results of LCE that present different transition temperatures between them is not optimal, we recurred to perform a temperature approach that allows to estimate values at the same equivalent point of every sample.

Relative temperature approach consists by fixing a given point along the temperature Plot. In our case it was the isotropization temperature (critical point at phase transition interval) of each coelastomer.

$$T_{red} = \frac{T - T_{iso}}{T_{iso}} \qquad \text{(C.1)}$$

With this temperature value we can obtain a ratio of temperatures in which the rate for case will reach 1 (equation C.1). So, all the sample data will converge at T_{red}=0. Thus by taking a given point of relative temperature we can compare now values at the "same range".

The Plot in terms of relative temperatures is shown below.

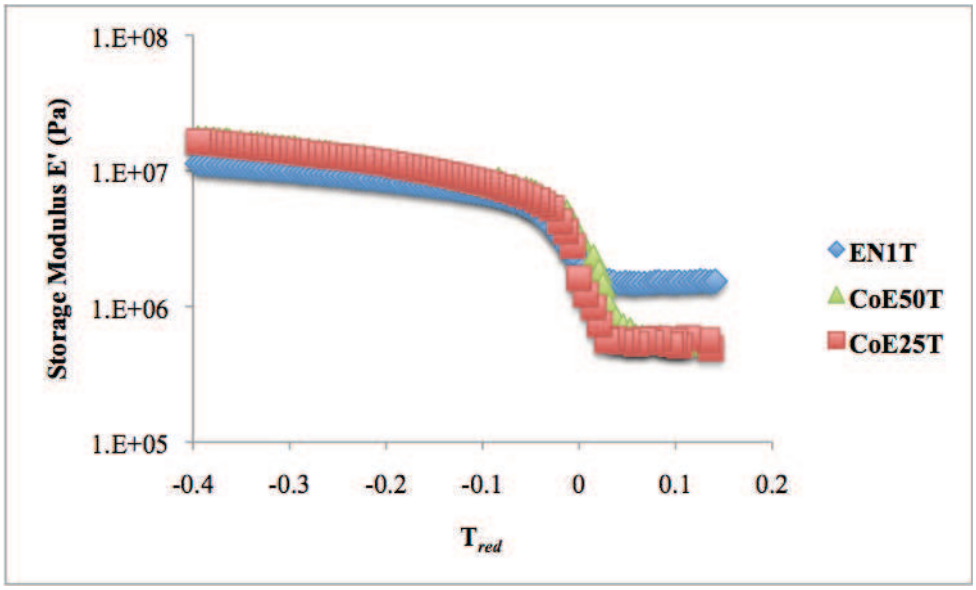

Plot C.XXV. Relative temperature Plot of trisiloxane elastomers. Tiso for CoE25T was 70.86ºC; CoE50T: 71.34ºC and EN1T: 89.32ºC.

C.3.5. *Comparative Study of Calamitic MC LCCoE*

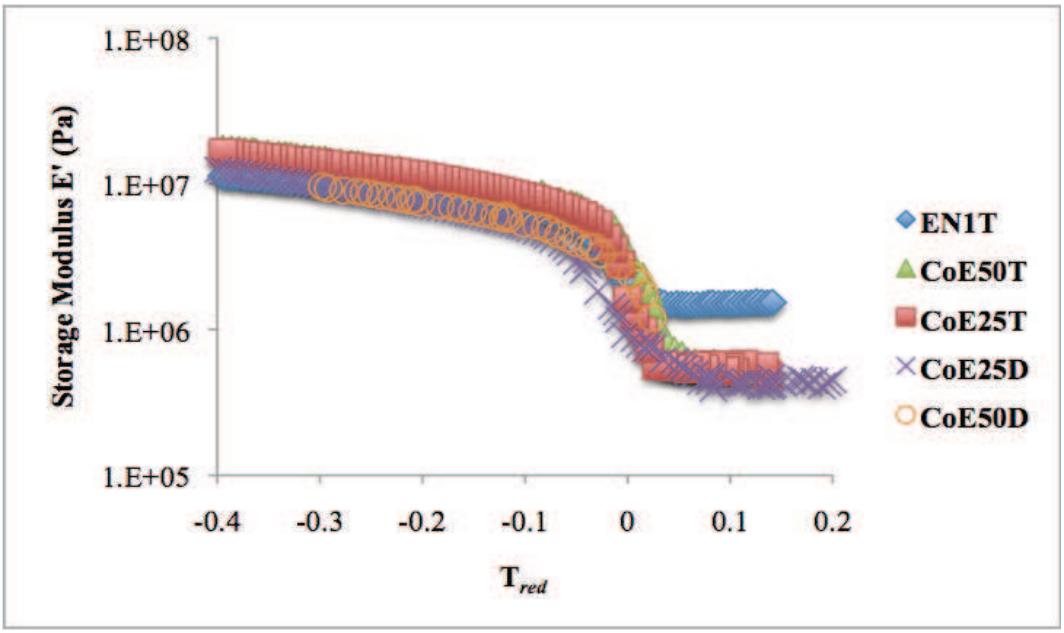

Plot C.XXVI. E' vs Reduced temperature plot of calamitic MC LCEs, critical temperatures (t_0) were: EN1T=89.3ºC; CoE50T=71.3ºC; CoE25T=70.9ºC; CoE25D=83.88ºC; CoE50D=57.33ºC.

Ce travail comprend la synthèse, caractérisation et mésomorphisme de divers monomères, polymères et élastomères cristaux liquides à propriétés modulables. Dans une première partie, divers polymères, copolymères, élastomères et coelastomères cristaux liquides on été conçus a l'aide d'une stratégie de paire de monomères mesogéniques pour contrôler les températures d'isotropization et de transition vitreuse ainsi que les propriétés mésomorphes. Dans un deuxième temps, un autre group de systèmes a été synthétisé en utilisant une mélange contenant un des mésogènes calamitiques et un possédant une structure «coudée » pour étudier la perturbation que ce dernier type de monomère provoque dans l'ordonnement du matériau final. Un échantillonnage choisi a été aussi soumis aux études de rhéologie et thermoelasticité pour observer leur comportement en fonction de la mésophase. Finalement de façon exploratoire, plusieurs réseaux portant des molécules inorganiques magnétiques sont décrits.

Mots-clés : cristaux liquides, élastomère, actionneurs, matériaux hybrides, thermotropes.

« Synthesis and Characterization of Elastomers and Functional Networks »

This research describes the synthesis, characterization and mesomorphism of various liquid crystalline monomers, polymers and elastomers with tailoring properties. The first part comprehends the study of various liquid crystalline polymers, copolymers, elastomers and coelastomers by using a pair of mesogenic monomer approach. This strategy allowed to control the isotropization and the glass transition temperatures as well as their mesophases. In a second term, another group of systems was synthesized in an analogous way by using one of the previously employed monomers and and another one with a "bent-core"shape to study the perturbations induced by this kind of molecule. Rheological and thermoelastic studies were performed to some of these systems to study their behavior as a function of the mesophase. Finally, a description of various hybrid networks containing inorganic moieties with magnetic properties is presented.

Specialité: Chimie des Matériaux

Institut de Physique et de Chimie des Matériaux de Strasbourg IPCMS UMR 7504
23 rue du Loess BP 43, 67034 Strasbourg, FRANCE